Crosstalk between redox regulatory pathways and epigenetic processes in tissue and cell culture models of cardiovascular complications

JG|U

JOHANNES GUTENBERG UNIVERSITÄT MAINZ

Dissertation

zur Erlangung des Grades

Doktor der Naturwissenschaften

am Fachbereich Biologie

der Johannes Gutenberg-Universität Mainz

Vorgelegt von

Alina Hanf (geb. Weber)

geboren am 28.11.1987

in Karlsruhe, Deutschland

Mainz, April 2019

Dekan:

1. Berichterstatter:

2. Berichterstatter:

Tag der mündlichen Prüfung: 27.05.2019

...Für meinen Ehemann Benjamin...

Inhalt

1 Introduction

1.1 Oxidative stress

Utilization of molecular oxygen by aerobic organisms inevitably leads to the formation of reactive oxygen species (ROS) as a byproduct of oxygen metabolism. ROS are derived from both endogenous sources (i.e. mitochondria, peroxisomes, endoplasmic reticulum, phagocytic cells) and exogenous sources (i.e. pollution, alcohol, tobacco smoke, heavy metals, transition metals, industrial solvents, pesticides, certain drugs and ionizing radiation) [1]. Due to unpaired electrons in their valence shell, these free radicals are very reactive in cellular milieu attacking cell constituents. Antioxidant defense mechanisms have evolved in aerobic organisms including humans to counteract the potential harmful effects of ROS and maintain redox homeostasis. When present at moderate levels, ROS can exert beneficial effects and play a key role in various physiologic functions and signaling pathways [2]. However, at higher concentrations, ROS induce oxidative stress. The term "oxidative stress" refers to an imbalance between the production of ROS and the neutralization of these species by antioxidant systems, leading to a disruption of redox signaling [3]. This imbalance can be caused by either increased ROS formation or decreased activity of antioxidants, or both, as well as by insufficient repair of oxidative damage. Aberrant levels of ROS can affect many biological pathways as they readily react with proteins, lipids or DNA, ultimately resulting in pathological consequences. In humans, oxidative damage has been implicated in the pathogenesis of a variety of disorders, including neurodegenerative diseases, cancer or cardiovascular diseases [4-7].
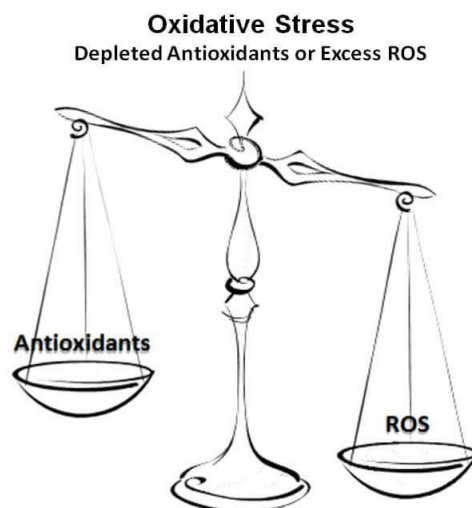
Figure 1 - Oxidative stress is caused by an imbalance between antioxidants and ROS due to antioxidant depletion or excess ROS production and accumulation. *Taken from webpage by Richard G. Godbee.*

1.1.1 Reactive oxygen species – Sources and detoxification

In cellular context, the most common reactive oxygen species are superoxide ($^{\bullet}O_2^-$), hydrogen peroxide (H_2O_2) and hydroxyl radicals ($^{\bullet}OH$).

1.1.1.1 Superoxide

Superoxide can be generated when a single electron is removed from an electron donor (leading to an oxidized metabolite) and transferred to molecular oxygen (O_2), leaving $^{\bullet}O_2^-$ with an unpaired electron in its outer shell. The production of superoxide occurs mostly within the mitochondria of a cell [8]. The mitochondrial electron transport chain is the main source of ATP in the mammalian cell and is thus essential for life. During oxidative phosphorylation, O_2 is an ideal terminal electron acceptor; however, during times of cellular stress the electron transport chain may become dysregulated resulting in superoxide production. Moreover, superoxide can be generated by NADPH oxidases (NOX) in phagosomes as part of the immune defense against microorganisms [9]. NOX are a family of seven members, NOX1-5 and dual oxidase (Duox) 1-2, whose sole function is the production of ROS. Under normal circumstances, most NADPH oxidase isoforms are dormant in resting cells, but are rapidly activated by several stimuli, including bacterial products and cytokines, during respiratory burst [10]. For example, the NADPH oxidase 2 (gp91phox) complex, which is present in neutrophils, macrophages, microglia, but also at lower levels in vascular cells, produces large amounts of superoxide once it is activated [11, 12]. Specifically, NOX catalyze the transfer of an electron from cytosolic NADPH to molecular oxygen via their membrane-bound catalytic NOX or Duox subunit to generate superoxide [13].

$$NADPH + 2\,O_2 \quad \rightarrow \quad NADP^+ + 2\,^{\bullet}O_2^- + H^+$$

NOX4 seems to be an exception since this isoform has an appreciable basal activity and directly generates H_2O_2 that confers important cellular functions [14].

Other enzymes that can produce superoxide include xanthine oxidase (XO), lipoxygenase (LOX), and cyclooxygenase (COX) [15-17]. NOX, XO, COX and LOX can be activated by acute or chronic inflammatory stimuli [18] or by hormones like angiotensin II in hypertension [19, 20].

Physiologically, $^{\bullet}O_2^-$ is rapidly detoxified by superoxide dismutases (SOD) in the mitochondria, the cytosol and the nucleus resulting in the formation of H_2O_2 [21, 22]. To date, three unique and highly compartmentalized isoforms of superoxide dismutases have been biochemically and molecularly characterized in mammals. The first isoform to be identified was the homodimer SOD1 (Cu,Zn-SOD), which contains copper and zinc in its catalytic center and is localized primarily to intracellular

cytoplasmic compartments, but also the nucleus and peroxisomes [23-25]. Another isoform, SOD2 (Mn-SOD), exists as a homotetramer and uses manganese (Mn) as a cofactor [26, 27]. It is localized exclusively to mitochondria and is responsible for the neutralization of mitochondrial-generated ROS from the respiratory chain [27-29]. Extracellular SOD3 (EC-SOD) forms a tetramer and also binds copper and zinc in its active center. It is the most recently discovered and least characterized member of the SOD family. The enzyme contains a signal peptide that directs it to extracellular spaces, where it is anchored to the extracellular matrix (ECM) and cell surfaces through interaction with heparan sulfate proteoglycan and collagen. However, a proteolytically cleaved form of the protein does not interact with the ECM [22, 30]. The expression pattern of SOD3 is highly restricted to specific cell types and tissues where its activity can exceed that of SOD1 and SOD2 [31].

The disproportionation of superoxide catalyzed by different metal-coordinated forms of SOD (M^{n+}-SOD) is depicted in the following equations:

$$M^{(n+1)+}\text{-SOD} + {}^{\bullet}O_2^{-} \quad \rightarrow \quad M^{n+}\text{-SOD} + O_2$$

$$\underline{M^{n+}\text{-SOD} + {}^{\bullet}O_2^{-} + 2H^{+} \quad \rightarrow \quad M^{(n+1)+}\text{-SOD} + H_2O_2}$$

$$2\,{}^{\bullet}O_2^{-} + 2H^{+} \quad \rightarrow \quad O_2 + H_2O_2$$
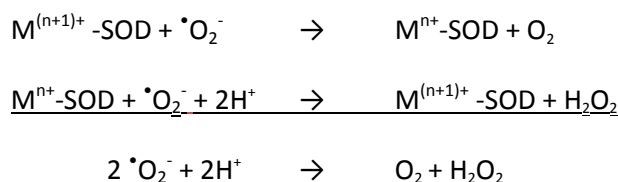
1.1.1.2 *Hydroxyl radical*

The hydroxyl radical (${}^{\bullet}OH$), the neutral form of the hydroxide ion (OH^{-}), is the most toxic free radical species found in biological systems as it is extremely reactive and rapidly oxidizes and damages all types of macromolecules. The main sources of this short-lived radical are the photolysis of ozone or of nitrous acid (HONO), or the decomposition of hydroperoxides (ROOH) [32]. Moreover, ${}^{\bullet}OH$ is formed in a "Fenton reaction", in which H_2O_2 reacts with metal ions (Fe^{2+} or Cu^{2+}) [1, 3, 7]. Under stress conditions, an excess of superoxide releases iron from iron-containing molecules, such as ferritin, making free iron available to participate in the Fenton reaction, resulting in the generation of a hydroxyl radical and hydroxide [33, 34].

Fenton reaction

$$Fe^{2+} + H_2O_2 \quad \rightarrow \quad Fe^{3+} + {}^{\bullet}OH + OH^{-}$$

Similarly, ${}^{\bullet}OH$ is also formed by the reaction between superoxide and H_2O_2 in a reaction called "Haber-Weiss reaction", which partly consists of the Fenton reaction [35]. In contrast to superoxide, which can be neutralized by SODs, the hydroxyl radical cannot be eliminated via an enzymatic reaction.

Haber-Weiss reaction

$$Fe^{3+} + {}^{\bullet}O_2^- \quad \rightarrow \quad Fe^{2+} + O_2$$

$$Fe^{2+} + H_2O_2 \quad \rightarrow \quad Fe^{3+} + {}^{\bullet}OH + OH^-$$

$$\mathbf{{}^{\bullet}O_2^- + H_2O_2 \quad \rightarrow \quad {}^{\bullet}OH + OH^- + O_2}$$
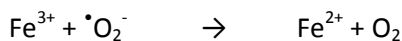
1.1.1.3 Hydrogen peroxide (H_2O_2)

Hydrogen peroxide (H_2O_2) is a non-radical type of ROS that is a weak and relatively stable oxidant. However, it can easily lead to free radical reactions in living organisms, as it can penetrate biological membranes through aquaporins and induce cellular damage by producing hydroxyl radicals (${}^{\bullet}OH$) in the presence of transition metal ions via the Fenton reaction [1, 36]. Formation of H_2O_2 results from superoxide detoxification by SOD or is produced by a number of metabolic enzymes, like the peroxisomal Acyl-CoA oxidase, or through protein oxidation in the ER [37-39]. The major antioxidant enzymes that can detoxify H_2O_2 include catalase (CAT), glutathione peroxidase (GPx) and peroxiredoxins [40, 41]. Catalase exists as a tetramer composed of four identical monomers, which all contain a heme group at the active site that allow the enzyme to react with hydrogen peroxide [42]. CAT is typically located in the peroxisome, a membranous cell organelle involved in catabolism of specific biomolecules, such as fatty acids and amino acids [43]. Catabolic activity in peroxisomes is a major contributor to intracellular H_2O_2 production, explaining the need for high CAT levels in this organelle.

CAT catalyzed reaction

$$2\,H_2O_2 \quad \rightarrow \quad O_2 + 2\,H_2O$$
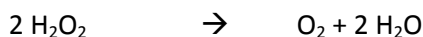
Glutathione peroxidases (GPx) are a family of tetrameric enzymes that contain the unique amino acid selenocysteine within their active sites and use the tripeptide glutathione (GSH) as an obligate cosubstrate/electron donor in the reduction of hydrogen peroxide to water [44]. GPx can also reduce lipid peroxides to their corresponding alcohols. There are four known GPx enzymes, GPx1-4, which are present in cytosol and mitochondria except for GPx3, which resides in the extracellular compartment [42]. The oxidized glutathione disulfide (GSSG) resulting from the GPx-mediated reaction is reduced back to GSH by the enzyme glutathione reductase (GR) which uses NADPH as the electron donor [7].

GPx-catalyzed reaction

$$2\,GSH + H_2O_2 \quad \rightarrow \quad GSSG + 2\,H_2O$$
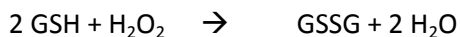
Glutathione reduction by glutathione reductase

GSSG + NADPH + H$^+$ →   2 GSH + NADP$^+$
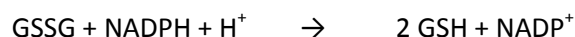
More examples for ROS of the radical kind include the alkoxy radical (RO$^•$) or the peroxyl radical (ROO$^•$), while ROS of the non-radical kind include HOCl, HOBr, ozone (O$_3$), singlet oxygen (^{1}O$_2$), organic peroxides (ROOH), and aldehydes (HCOR) [1].

	Symbol	Half-life
Reactive oxygen species-ROS		
Radicals		
Superoxide	O$_2$$^{•-}$	10^{-6} s
Hydroxyl	OH$^•$	10^{-10} s
Alkoxyl radical	RO$^•$	10^{-6}
Peroxyl Radical	ROO$^•$	17 s
Non radicals		
Hydrogen peroxide	H$_2$O$_2$	Stable
Singlet oxygen	^{1}O$_2$	10^{-6} s
Ozone	O$_3$	s
Organic peroxide	ROOH	Stable
Hypochlorous acid	HOCl	Stable (min)
Hypobromous acid	HOBr	Stable (min)
Reactive nitrogen species-RNS		
Radicals		
Nitric oxide	NO$^•$	s^a
Nitrogen dioxide	NO$_2^•$	s
Non radicals		
Peroxynitrite	ONOO$^-$	10^{-3} s
Nitrosyl cation	NO$^+$	s
Nitroxyl anion	NO$^-$	s
Dinitrogen trioxide	N$_2$O$_3$	s
Dinitrogen tetraoxide	N$_2$O$_4$	s
Nitrous acid	HNO$_2$	s
Peroxynitrous acid	ONOOH	Fairly stable
Nitryl chloride	NO$_2$Cl	s

^{a} The half life of some radicals depends on the environmental medium, for example the half life of NO$^•$ in an air saturated solution may be few minutes. *S* seconds, *min* minutes

Table 1 - List of ROS and RNS produced during metabolism including their half-lives. *Modified from Phaniendra et al. 2015* [1].

1.1.2 Reactive nitrogen species

In addition to ROS, reactive nitrogen species (RNS) are also continuously produced as by-products of aerobic metabolism or in response to stress. ROS and RNS are often collectively referred to as RONS. Cellular stress and damage conferred by RNS is termed nitrosative or nitro-oxidative stress.

1.1.2.1 Nitric oxide

Nitric oxide ($^•$NO) is a free radical with low reactivity generated in tissues by different isoforms of nitric oxide synthases (NOS) or by non-enzymatic pathways. It is an important signaling molecule for both intracellular and extracellular messaging. $^•$NO is both aqueous and lipid soluble and therefore readily diffuses through cytoplasm and plasma membranes to its site of action; in biological systems, it has an estimated half-life of only 3-5 seconds [45]. $^•$NO has been shown to act on a sizeable number of enzymatic targets, one of the most important being soluble guanylate cyclase. Many of nitric oxide's physiological effects are a result of its binding to Fe^{2+} heme groups in the enzyme guanylate cyclase, stimulating enzyme activation and catalysis of cGMP production from GTP [45, 46]. Increased levels of cGMP induce a signaling cascade leading to a decrease in intracellular Ca^{2+} concentration and, ultimately, smooth muscle relaxation [47]. Due to $^•$NOs implication in blood vessel relaxation, it was initially termed "endothelium-derived relaxing factor" (EDRF), before its true identity as well as the $^•$NO/cGMP pathway were fully elucidated [47, 48]. Ever since that, the $^•$NO/cGMP signal transduction pathway has been shown to play major roles in mediating smooth muscle relaxation and blood pressure regulation [49], platelet aggregation [50], and both peripheral and central neurotransmission [49, 51].

Endogenous $^•$NO is derived largely from enzymatic pathways. There are three isoforms of nitric oxide synthases (NOS) that catalyze $^•$NO formation: neuronal NOS (nNOS or NOS1), inducible NOS (iNOS or NOS2) and endothelial NOS (eNOS or NOS3). All three isoforms are homodimers comprising a C-terminal reductase domain and an N-terminal oxygenase domain in each monomer (Figure 2) [52]. The N- and C-terminal domains are linked by a short sequence that binds calmodulin, an allosteric effector that is essential for full NOS activity. NOS use L-arginine as substrate, as well as molecular oxygen and reduced nicotinamide adenine dinucleotide phosphate (NADPH) as cosubstrates. Furthermore, they all require flavin adenine dinucleotide (FAD), flavin mononucleotide (FMN), and (6R-)5,6,7,8-tetrahydrobiopterin (BH_4) as cofactors, as well as binding of heme and calmodulin for the reaction catalysis [52]. The complex reaction involves the transfer of electrons from NADPH via the flavins FAD and FMN in the C-terminal reductase domain of one monomer to the heme in the N-terminal oxygenase domain of the other

monomer, where the substrate L-arginine is oxidized to L-citrulline and $^\bullet$NO (Figure 2A) [53]. The net reaction is:

2 L-arginine + 3 NADPH + 3 H$^+$ + 4 O$_2$ →   2 L-citrulline + 2 $^\bullet$NO + 4 H$_2$O + 3 NADP$^+$

As an overview, the electron flow in this NOS catalysis reaction is as follows:

NADPH → FAD → FMN → heme → O$_2$

The essential NOS cofactor tetrahydrobiopterin (BH$_4$), found in the oxygenase domain, provides an additional electron during the catalytic cycle, which is replaced during turnover. BH$_4$ is biosynthesized from GTP via the GTP-cyclohydrolase-1 (GCH-1) pathway [54].

Figure 2 - Structure and mechanism of NOS enzymes in normal and "uncoupled" state. NOS enzymes act as homodimers, where each monomer contains a reductase and an oxygenase domain. Electrons are donated by reduced NADPH to the reductase domain of the first monomer and transferred through FAD, FMN to the Fe (iron in the heme group) of the oxygenase domain of the second monomer (the subunits are depicted in this fashion for clarity reasons; in their actual conformation, the heme groups (Fe) from the two subunits lie in close proximity). With the help of the cofactor BH$_4$, L-arginine and O$_2$ are converted into $^\bullet$NO and L-citrulline. In the dysfunctional "uncoupled" state (e.g. due to absence of BH$_4$) the electron flow from the reductase domain becomes uncoupled from L-arginine oxidation thereby generating superoxide ($^\bullet$O$_2^-$) instead of $^\bullet$NO. *Taken from Mas 2009 [55].*

nNOS and eNOS are constitutive enzymes, whose catalytic activity is controlled by intracellular free Ca^{2+} levels. Elevated cytosolic Ca^{2+} ions bind to calmodulin (CaM) to form the Ca^{2+}/CaM complex, which subsequently binds to nNOS or eNOS leading to enzyme activation [56]. In contrast, iNOS expression is

Ca^{2+}-independent, as the Ca^{2+}/CaM complex is so tight and stable that Ca^{2+} has no regulatory function for iNOS. In addition, iNOS is inducible at the expression level in response to (pro)inflammatory mediators in macrophages and other tissues [57, 58].

During cellular stress, the NOS-mediated enzymatic reduction of oxygen can become uncoupled from other catalytic function in the oxygenase domain, leading to the formation of superoxide instead of nitric oxide (Figure 2B). This phenomenon is referred to as NOS uncoupling, since superoxide generation mainly occurs when NOS is not coupled with its substrate or cofactors. Whereas L-arginine depletion is the main reason for nNOS or iNOS uncoupling, the most prominent cause of eNOS uncoupling are insufficient levels of the critical cofactor BH_4 due to its oxidation or due to decreased expression of the BH_4 synthesizing enzyme GTP-cyclohydrolase-1 (GCH1) and BH_4 recycling enzyme dihydrofolate reductase (DHFR) [59-62]. However, protein-protein interactions, phosphorylation, S-glutathionylation, and endogenous L-arginine methyl derivatives (e.g. ADMA) may also play key roles in regulating NOS uncoupling.

Non-enzymatic nitric oxide generation involves reduction of inorganic nitrite, particularly under acidic conditions, which mainly occurs in tissues and not blood, as hemoglobin is a very effective $^\bullet$NO-scavenger [63, 64].

$$NO_2^- + e^- + 2H^+ \rightarrow \quad {}^\bullet NO + H_2O$$

In experimental settings, often $^\bullet$NO donors are applied, which are pharmacologically active substances that release a defined amount of $^\bullet$NO molecules *in vivo* or *in vitro*. The most commonly employed $^\bullet$NO donor drugs in clinical use are organic nitrates, which include nitroglycerin, isosorbide dinitrate and isosorbide mononitrate. Indications for these drugs include treatment and prevention of angina attacks, acute coronary syndromes, as well as hypertension and heart failure [65-67]. Another group of $^\bullet$NO donors are diazeniumdiolates (also known as 'NONOates'), such as diethylamine NONOate (DEANO), diethylenetriamine NONOate (DETANO), and spermine NONOate (SPENO). Furthermore, S-nitrosothiols serve as $^\bullet$NO donors, including S-nitroso-glutathione (GSNO), S-nitroso-N-acetylpenicillamine (SNAP), and S-nitroso-N-valerylpenicillamine (SNVP). Other prevalent $^\bullet$NO donors comprise molsidomin (Sin-1), sodium nitroprusside (SNP) or NO hybrid drugs, such as NO aspirin [68].

Since reduced $^\bullet$NO levels have been implicated in the onset and progression of various disease states, especially cardiovascular diseases, pharmacologically active compounds that can release $^\bullet$NO within the body are being used as therapeutic agents; however, their efficacy is limited and further research for the refinement of these drugs is necessary [69].

1.1.2.2 Peroxynitrite

It is important to recognize that the primarily protective effects mediated by nitric oxide require extremely low $^\bullet$NO concentrations (picomolar to nanomolar range). At higher concentrations, properties and cellular targets of $^\bullet$NO are profoundly different, particularly under conditions of oxidative stress, where $^\bullet$NO rapidly reacts with superoxide to form peroxynitrite ($ONOO^-$), a molecule that is itself not a free radical, but is a powerful oxidant [1]. Peroxynitrite is highly cytotoxic, a feature that is exploited by inflammatory cells in response to invading pathogens by expressing an inducible form of NOS (iNOS) in concert with activation of NADPH oxidase to cogenerate $^\bullet$NO and superoxide, forming the highly reactive and cytostatic $ONOO^-$.

$$^\bullet NO \quad + \quad ^\bullet O_2^- \quad \rightarrow \quad ONOO^-$$
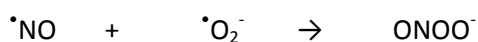
Peroxynitrite can directly react with CO_2 to form other highly reactive nitroso peroxocarboxylate molecules ($ONOOCO_2^-$) or upon protonation peroxynitrous acid (ONOOH). ONOOH is less stable than the peroxynitrite anion and further undergoes homolysis to form both a hydroxyl radical ($^\bullet$OH) and nitrogen dioxide radical ($^\bullet NO_2$), or rearranges and isomerizes to the stable endproduct nitrate (NO_3^-) [70]. Peroxynitrite can cause oxidative damage of biomolecules including proteins, lipids, and DNA. Specifically, it induces lipid peroxidation, (sulf-)oxidation of methionine or cysteine residues and nitration of tyrosine residues in proteins, as well as oxidation of DNA to form 8-nitroguanine and 8-oxoguanine [71-73]. Protein 3-nitrotyrosine (3-NT) residues are considered as a marker of peroxynitrite-induced cellular damage (see 0, Figure 5). Also, lipid hydroperoxides are very unstable and easily decompose to secondary products, such as aldehydes (e.g. 4-hydroxy-2,3-nonenal, 4-HNE) and malondialdehyde (MDA), which are therefore also considered markers of ROS formation and lipid peroxidation (see 0, Figure 6).

When NOS enzymes become uncoupled during cellular stress, they produce superoxide. Consequently, partial uncoupling of NOS activity will lead them to act like peroxynitrite synthases, synthesizing the two precursors of $ONOO^-$, $^\bullet$NO and superoxide [74]. Since peroxynitrite oxidizes the important eNOS cofactor BH_4, it can lead to further eNOS uncoupling, facilitating superoxide production from eNOS and peroxynitrite formation in a vicious cycle [75]. eNOS uncoupling is an emerging therapeutic target in cardiovascular diseases.

1.1.3   Antioxidants

In addition to the previously mentioned major antioxidant enzymes - SOD, GPx and catalase - there are other enzymatic and non-enzymatic antioxidant defense mechanisms that are effective in blocking harmful effects of ROS. For instance, disposal of H_2O_2 is also associated with other redox proteins including thioredoxins (Trx), glutaredoxins (Grx), as well as peroxiredoxins (Prx) [42]. Thioredoxin and glutaredoxin are thiol-disulfide oxidoreductases that control the cellular redox environment. Trx donates electrons to Prx to remove H_2O_2 [41]. After reducing H_2O_2, oxidized thioredoxins are reduced by NADPH-dependent thioredoxin reductases (TrxR), which are dimeric flavoproteins present in all living cells [76, 77]. In contrast, glutaredoxins (Grx) are reduced by glutathione (GSH), the oxidized form of which is GSSG, which is reduced by GSH reductases (GR) [77, 78].
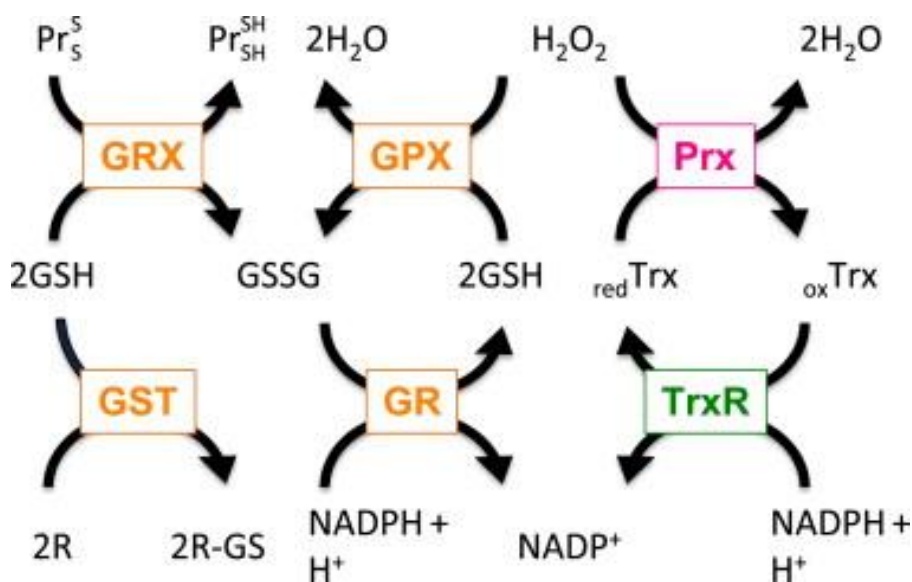
Figure 3 - Interrelation between glutaredoxin, peroxiredoxin, thioredoxin, and glutathione containing antioxidant systems. H_2O_2 can be reduced by peroxiredoxins (Prx) or glutathione peroxidases (GPx), which couple H_2O_2 reduction with oxidation of glutathione (GSH) to glutathione disulfide (GSSG). Oxidized Prx can be reduced by thioredoxins (Trx). The oxidized Trx are then reduced by thioredoxin reductase (TrxR) in a NADPH-dependent manner. Similarly, oxidized glutathione disulfide (GSSG) is reduced by glutathione reductase (GR) in the presence of NADPH. Further, glutaredoxins (Grx) can reduce disulfide (S–S) bonds in proteins (Pr) using GSH. Glutathione S-transferase (GST) conjugates GSH to reactive electrophilic compounds (R), thus detoxifying them. *Taken from Espinosa-Diez et al. 2015 [79].*

Oxidative stress also induces the expression of the cytoprotective stress-response protein heme oxygenase-1 (HO-1). HO-1 catalyzes the oxidative degradation of heme to equimolar amounts of carbon monoxide, biliverdin (subsequently converted to bilirubin), and free ferrous iron [80, 81]. In response to oxidative stress some hemoproteins release cytotoxic free heme, which can produce even more free

radicals through Fenton chemistry [82]. Degradation by HO-1 avoids the pro-oxidant effects of free heme and also subsequent free iron by simultaneous upregulation of ferritin. By-products of the heme degradation (carbon monoxide, biliverdin/bilirubin) also mediate cytoprotective effects [81]. Moreover, HO-1 gets translocated to the nucleus under stress conditions, where it confers protection against oxidative stress and cytotoxicity by up-regulating antioxidant and anti-inflammatory genes [83-85].

Non-enzymatic antioxidants include low-molecular-weight compounds, such as vitamins (vitamins C and E), carotenoids (e.g. beta-carotene, lycopene), uric acid, bilirubin or the tripeptide glutathione (GSH) (Figure 4). The lipid soluble vitamin E (α-tocopherol) scavenges intermediate peroxyl radicals by donating an electron and, therefore, terminates the chain reaction of lipid peroxidation [86]. Similarly, the water soluble vitamin C (ascorbic acid) scavenges oxygen free radicals by electron donation and is also able to convert vitamin E free radicals (tocopheryl radicals) back to vitamin E. Although these antioxidants become new free radicals, they are less active, longer-lived and less dangerous than those radicals they have neutralized due to their aromatic nature, which enables them to delocalize the unpaired electron [87]. Carotenoids, pigments found in plants, primarily scavenge peroxyl radicals by reacting with them to form resonance stabilized carbon-centered radical adducts [86]. Uric acid in plasma is the most abundant aqueous antioxidant found in humans and is an exceptional scavenger of peroxynitrite in the extracellular fluid [88, 89]. GSH works as a cofactor for several detoxifying enzymes by donating an electron, and is indispensable for maintaining the intracellular reducing environment. Furthermore, bioflavonoids (e.g. quercetin, anthocynidine) and hydroxycinnamates (e.g. ferulic acid, caffeic acid) were found to possess strong antioxidant activities [86]. Synthetic antioxidants, based on natural antioxidant structures, are continuously being developed in an attempt to refine reliable targeting and increase the efficiency of the antioxidant defense, in order to diminish the effects of free-radical induced cell damage [90].
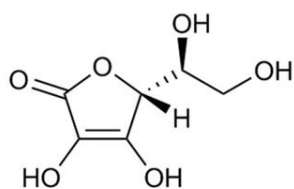
Ascorbic acid (Vit C)   α-tocopherol (Vit E)
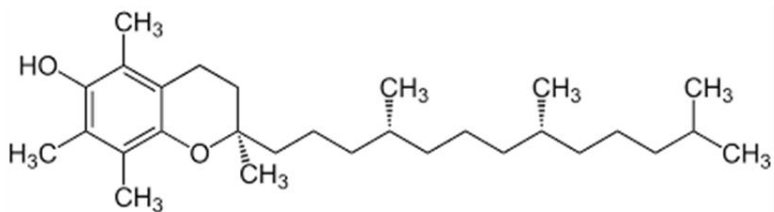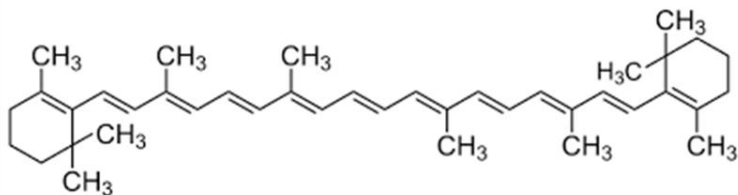
β-carotene
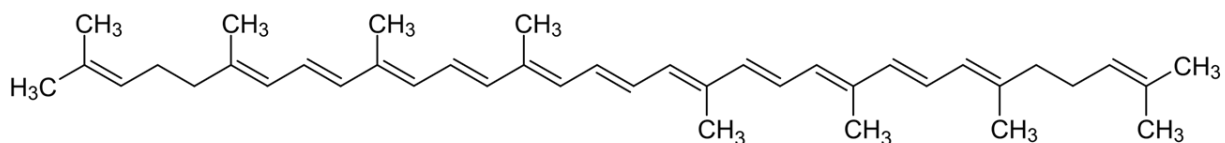
Lycopene
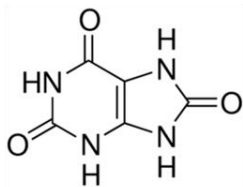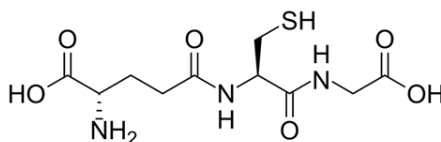
Uric acid   Glutathione   Quercetin
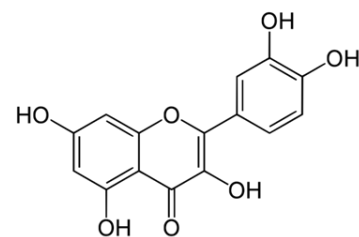
Figure 4 - Examples of antioxidant compounds and their structure.

1.2 Redox-based posttranslational modifications of proteins

Free amino acids and amino acid residues in proteins can easily become oxidized by reactive species, which may cause fragmentation of the peptide chain, alteration of electrical charge of proteins or cross-linking of proteins, ultimately leading to increased susceptibility to proteolysis. Oxidative modifications of enzymes have frequently been shown to inhibit their catalytic activities. In broad terms, peptide oxidative modifications comprise hydroxylation of aromatic groups and aliphatic amino acid side chains, nitration of aromatic amino acid residues, nitrosylation or oxidation of sulfhydryl groups (sulfoxidation), chlorination of aromatic groups and primary amino groups, and the conversion of some amino acid residues to carbonyl derivatives (Figure 5) [91-93].

Protein adduct formation is achieved by reaction of (nucleophilic) amino acid residues in proteins, including lysine, arginine, methionine, tyrosine and histidine, with highly reactive carbonyl groups (ketones, aldehydes) derived from lipid peroxidation products or glycoxidation reactions [93]. Examples of these "Michael additions" are based on lipid peroxidation products such as malondialdehyde (MDA) or 4-hydroxynonenal (4-HNE). Glucose oxidation products, such as glyoxal or methylglyoxal, can react with amino acids to create compounds such as carboxymethyllysine and pentosidine (Figure 6), which are termed "advanced glycation end products" (AGEs) and are implicated in a number of diseases [93, 94]. Protein carbonylation is achieved by reaction of saturated hydrocarbon side chains of amino acids with hydroxyl radical leading to aldehyde or ketone formation (=introduction of a carbonyl group).

Oxidation of aromatic amino acid residues involves the conversion of phenylalanine residues by hydroxyl radicals to ortho- and meta-tyrosine derivatives [92]. Tryptophan residues are oxidized to hydroxytryptophan derivatives, and also to N-formylkynurenine and kynurenine [95]. Oxidation of tyrosine leads to formation of 3,4-dihydroxyphenylalanine (DOPA), or to inter- or intra-molecular dityrosine cross-linking via the generation of tyrosyl radicals [96]. Tyrosine and tryptophan residues also become nitrated by peroxynitrite forming 3-nitrotyrosine and nitrotryptophan, respectively [72, 97, 98].

Chlorination of amino acid residues, mediated by myeloperoxidase-derived HOCl, is another oxidative modification that can occur on proteins, altering their function. HOCl chlorinates tyrosine to form 3-chlorotyrosine. It also forms chloramine derivatives of lysine amino groups, and oxidizes sulfhydryl groups to sulfenic acid derivatives [91, 92].
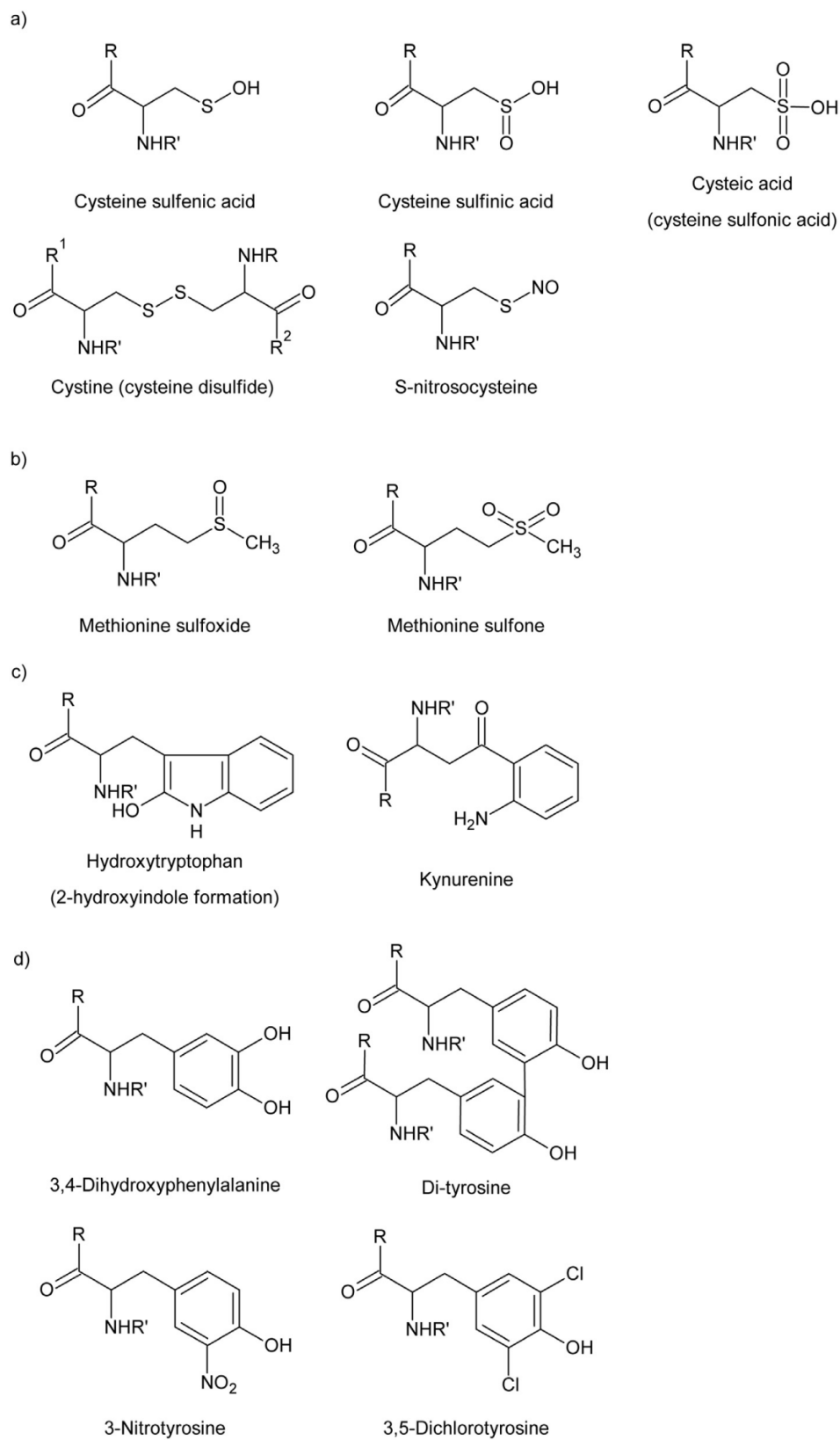
Figure 5 - Examples of oxidative posttranslational modifications on amino acids. *Taken from Ryan et al. 2014 [93].*
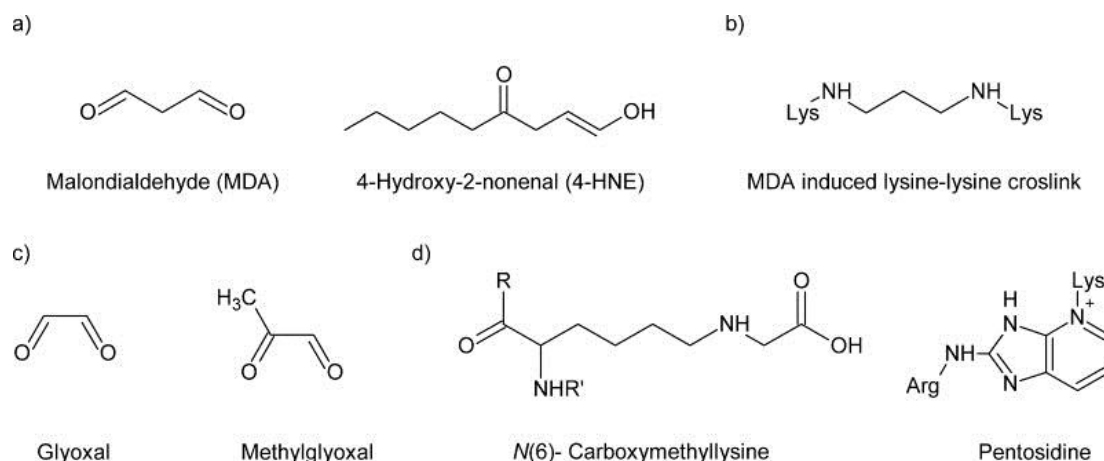
Figure 6 - Examples of lipid and glucose oxidation products and the products formed by their reactions with amino acids. Structures of (a) lipid peroxidation products, MDA and 4-HNE (b) a product of lysine side-chain modification by MDA, (c) structures of the products of glucose oxidation, glyoxal and methylglyoxal, and (d) the AGEs carboxymethyllysine and pentosidine. *Taken from Ryan et al. 2014 [93].*

Surface-exposed cysteine and methionine residues in proteins are particularly sensitive to oxidation due to their free thiol (-SH) group. Under biological conditions, the major product of methionine oxidation is methionine sulfoxide, which can be further oxidized to methionine sulfone [99]. Cysteine may be oxidized to cysteine sulfenic, sulfinic and sulfonic acid derivatives. While sulfenic and sulfinic intermediates are easily reversible by reductases, the sulfonic acid product is quite stable [100, 101]. The free thiol may also be oxidized to form either an inter- or an intra-molecular disulfide bond with another free thiol (−S−S−) [93, 102]. For instance, a protein cysteine thiol group can form an inter-molecular disulfide bond with the thiol group of cysteine in reduced glutathione, a process termed protein S-glutathionylation. Formation of disulfide bonds often alters protein folding and function. Cysteine S-glutathionylation of eNOS, for example, has been shown to be involved in eNOS uncoupling [46]. Cysteine oxidation and disulfide formation in proteins constitutes an important role in the context of cellular signaling, protein-protein interactions, substrate and metal binding, and catalysis.

Importantly, cysteine is also a target of S-nitros(yl)ation. S-nitros(yl)ation is a reversible covalent attachment of a nitroso (-NO) group to the thiol in cysteine residues, forming S-nitrosothiols (SNOs), via redox-mediated reactions. Here, it is differentiated between "nitrosylation", which is the addition of $^\bullet$NO to cysteine thiyl radicals (or metal centers), or "nitrosation", which is the reaction of a nitrosonium ion (NO$^+$) with the nucleophilic thiolate [103]. Both mechanisms are combined in the term "nitros(yl)ation". S-nitros(yl)ation is used by cells to modulate protein function and stability, regulate gene expression, and provide $^\bullet$NO donors. SNO generation, localization, activation, and catabolism are tightly regulated [104]. S-nitros(yl)ated proteins can be denitrosylated through the action of thioredoxin or by glutathione (GSH)

[105]. The hereby formed nitroso-glutathione (GSNO) is a stable and mobile molecule and can therefore serve as a reservoir of $^\bullet$NO bioactivity [104, 106]. Similarly, SNO groups in proteins can serve as intermediates in the cellular metabolism or bioactivity of $^\bullet$NO and their formation represents an important cellular regulatory mechanism [104]. S-nitros(yl)ation plays a key role in many processes ranging from signal transduction, DNA repair, host defense, and blood pressure control to ion channel regulation and neurotransmission [107, 108]. Substrates for S-nitros(yl)ation include protein kinases, phosphatases, ion channels, metabolic and regulatory enzymes, cytoskeletal and structural proteins, transcription factors, oxidoreductases, and respiratory proteins [108].

1.3 ROS detection methods

There are multiple assays to detect specific ROS or cellular oxidative stress in general. There are generally two approaches, which include either ROS trapping and measurement of the levels of trapped molecules, or measuring the levels of the damage done by ROS.

Since ROS often exist in very low concentrations and have a very short half-life, detection probes have to react very rapidly with ROS to compete with antioxidants and produce stable products that can be quantified. Such requirements are met by the spin trapping technique, in which spin trapping agents covalently bind free radicals, forming stable radical adducts that can be detected by electron paramagnetic resonance (EPR) (also known as electron-spin resonance, ESR) [109]. The most commonly used spin trapping molecules are 5,5-dimethyl-1-pyrroline N-oxide (DMPO), N-tert-butyl-α-phenylnitrone (PBN), 3,5-dibromo-4-nitrosobenzenesulfonic acid (DBNBS) or 5-diethoxyphosphoryl-5-methyl-1-pyrroline N-oxide (DEPMPO) [110, 111]. In addition to the very potent EPR technique, alternative approaches can be applied to detect spin trap adducts or their metabolites including high-performance liquid chromatography (HPLC), mass spectroscopy (MS), nuclear magnetic resonance (NMR) and antibody-immune-based detection [111]. An example for the latter is the detection of protein-DMPO adducts by an anti-DMPO antibody developed by Ronald Mason and colleagues in 2004 [112].

ROS can also be detected by chemiluminescent probes, such as lucigenin and luminol. These probes undergo a chemical reaction with ROS that releases energy in the form of light. Lucigenin- or luminol-enhanced chemiluminescence measurement is mostly applied to detect ROS in activated phagocytes, but is also being used in other cell types. The luminol analogue L-012 has been reported to be even more sensitive than luminol or lucigenin for the detection of ROS, although lucigenin-enhanced chemiluminescence is most specific for superoxide detection [113].

Specific detection of superoxide can be done by dihydroethidium (DHE). Upon oxidation by $^\bullet O_2^-$, DHE is converted to the fluorescent 2-hydroxyethidium (2-HE), that can be detected via HPLC or fluorescent microscopy at Ex. 480 nm/Em. 580 nm [114]. A second unspecific oxidation product, ethidium (E$^+$), is also formed, but usually disregarded during quantification. A modified DHE analog that is targeted to mitochondria, referred to as mitoSOX, is commonly used for detection of mitochondrial $^\bullet O_2^-$. Analogous to DHE, mitoSOX reacts with $^\bullet O_2^-$ to form 2-hydroxy-mito-ethidium (Mito-HE) [115].

Extracellular hydrogen peroxide can be detected by the reagent N-acetyl-3,7-dihydroxyphenoxazine (Amplex Red) [116]. Catalyzed by horseradish peroxidase (HRP), the colorless non-fluorescent Amplex Red reacts in a 1:1 stoichiometry with H_2O_2 to produce highly fluorescent resorufin [117]. Since Amplex Red is cell-impermeable, only extracellular H_2O_2 is measured [117, 118]. Resorufin emits light at 590 nm when excited at 570 nm, which can be measured by HPLC-mediated fluorescence detection, a fluorescence plate reader or other fluorescence detection systems.

Detection of intracellular H_2O_2 can be achieved by the fluorescent sensor HyPer, which can be introduced into the cell genome via plasmids or adenoviruses [119]. The expressed HyPer protein is based on the properties of OxyR, a prokaryotic H_2O_2 sensing protein. HyPer has an extremely high affinity to H_2O_2 and can be targeted to different cell compartments for detection of fast changes of H_2O_2 concentrations under various physiological and pathological conditions [120].

General cellular oxidative stress can be measured by analyzing ROS-induced damage. For instance, tissue and plasma concentrations of lipid peroxidation products, such as lipid hydroperoxides or unsaturated aldehydes, can be assessed by HPLC [111, 121]. Furthermore, proteins modified by lipid peroxidation-derived aldehydes such as 4-HNE, MDA, and acrolein, are commonly detected by several immune-based assays with suitable antibodies. Generally, all oxidative posttranslational modifications of proteins, as described in 0, can be detected via immunological assays, if a corresponding antibody is available. For instance, 3-nitrotyrosine antibodies are used as a strong marker for RNS stress.

The biological redox status of a cell or tissue is often reflected by the balance of GSH/GSSG, NAD$^+$/NADH, and NADP$^+$/NADPH. Several kits for fluorometric assessment of these redox couples are commercially available.

There is a great variety of ROS detection methods with different specificities and limitations that are not covered here, but are elaborately reviewed elsewhere [110, 111, 122].

Increasing evidence shows that ROS/RNS influence epigenetic pathways by affecting the function or expression of epigenetic modulators, such as histone and DNA modifying enzymes, as well as the regulation of miRNAs and chromatin remodeling complexes [123-127] (see 1.5). Adverse redox regulation of epigenetic processes may induce changes in gene expression and ultimately result in pathological consequences. Conversely, epigenetic alterations may affect redox signaling by influencing the expression of oxidative stress-associated enzymes [11, 125, 128]. In order to be able to understand the crosstalk between redox regulatory pathways and epigenetic processes, the major epigenetic mechanisms will be introduced in the following chapters.

1.4 Epigenetics

Epigenetics commonly refers to alterations in gene expression that are mitotically and/or meiotically heritable and that do not involve changes in the DNA sequence [129]. Epigenetic alterations generally involve DNA methylation, histone posttranslational modifications, ATP-dependent chromatin remodeling, and non-coding RNA transcripts (Figure 7). By altering DNA accessibility and chromatin structure, epigenetic processes regulate patterns of gene expression, which is crucial to normal development and differentiation of distinct cell lineages in an organism. Specifically, epigenetic modifications allow variable expression of the identical genetic information in each cell of an organism by activation or repression of gene transcription, thus resulting in specific expression patterns and therefore different cellular or physiological phenotypes [130]. These effects can be due to internal cues as part of the normal developmental program or occur in response to environmental factors, such as diet, smoking or drug abuse. It has been shown that epigenetic mechanisms or disturbance thereof (e.g. by mentioned exogenous influences) are involved in the pathogenesis of many diseases.
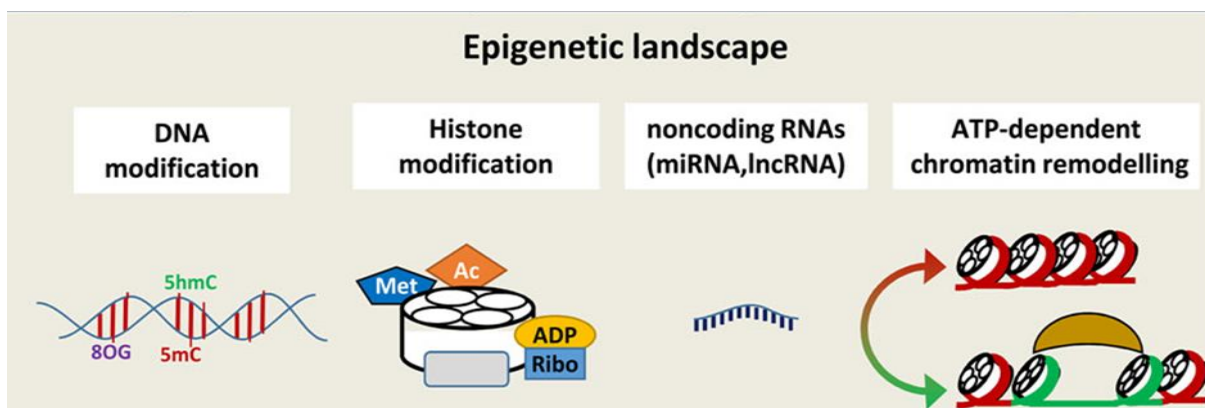
Figure 7 - Epigenetic mechanisms for gene regulation involve DNA modification, histone posttranslational modification, non-coding RNAs, and ATP-dependent chromatin remodeling. *Taken from Kietzmann et al. 2017 [125].*

1.4.1 DNA methylation

The main epigenetic DNA modification in mammals is methylation of cytosine, producing 5-methylcytosine (5mC). Methylation occurs mostly on cytosines in CpG islands, which are sequences of repeating CpG dinucleotides (meaning each cytosine nucleotide is followed by a guanine nucleotide, *5'—C—phosphate—G—3'*). In mammals, about 70-80% of CpG cytosines are methylated [131]. Hypermethylation of CpG islands, often located near promoter sites, is associated with epigenetic gene silencing [132, 133]. CpG methylation can suppress transcription by several mechanisms. The presence of the methyl group can directly interfere with DNA recognition and binding of transcription factors. Similarly, specialized methyl-DNA binding proteins can be recruited and block DNA accessibility for transcription factors. In other cases, methylation of cytosine may induce gene silencing by attracting mediators of chromatin remodeling, such as histone modifying enzymes or other repressors of gene expression [128, 134].
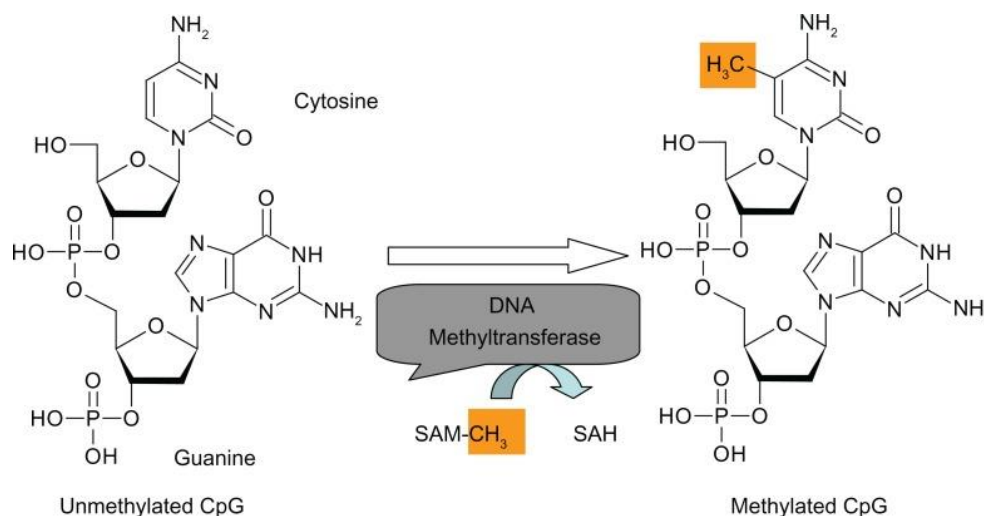
Figure 8 - DNA methylation of cytosine in a CpG dinucleotide catalyzed by DNA methyltransferase. DNA methyltransferase transfers a methyl group from S-adenosyl methionine (SAM-CH$_3$) to the 5-carbon of cytosine yielding S-adenosyl homocysteine (SAH) and 5-methylcytosine. *Taken from Ahmed 2010 [135].*

The covalent attachment of a methyl group to the C5 position of cytosine residues is catalyzed by DNA methyltransferases (DNMTs). The ubiquitously expressed DNMT1 is responsible for maintaining cellular DNA methylation and occurs simultaneously with DNA replication, thereby passing on established methylation patterns to daughter cells [136]. DNMT3A and DNMT3B mediate de novo methylation during embryogenesis [137]. DNMT enzymes share a basic common mechanism using S-adenosyl methionine (SAM) as methyl donor. The methyl group is transferred to the 5'-carbon of cytosine yielding S-adenosyl homocysteine (SAH) and 5mC (Figure 8). DNA demethylation can occur via the action of ten

eleven translocation (TET) proteins, which are 2-oxoglutarate (2-OG) and Fe(II)-dependent dioxygenases that actively oxidize 5mC to 5-hydroxymethylcytosine (5hmC). Further, TET proteins can generate 5-formylcytosine (5fC) and 5-carboxylcytosine (5caC) from 5hmC [138]. These cytosine derivatives can then undergo thymine-DNA glycosylase (TDG)-mediated base excision and subsequent DNA base excision repair (BER) resulting in DNA demethylation (Figure 9) [139, 140].
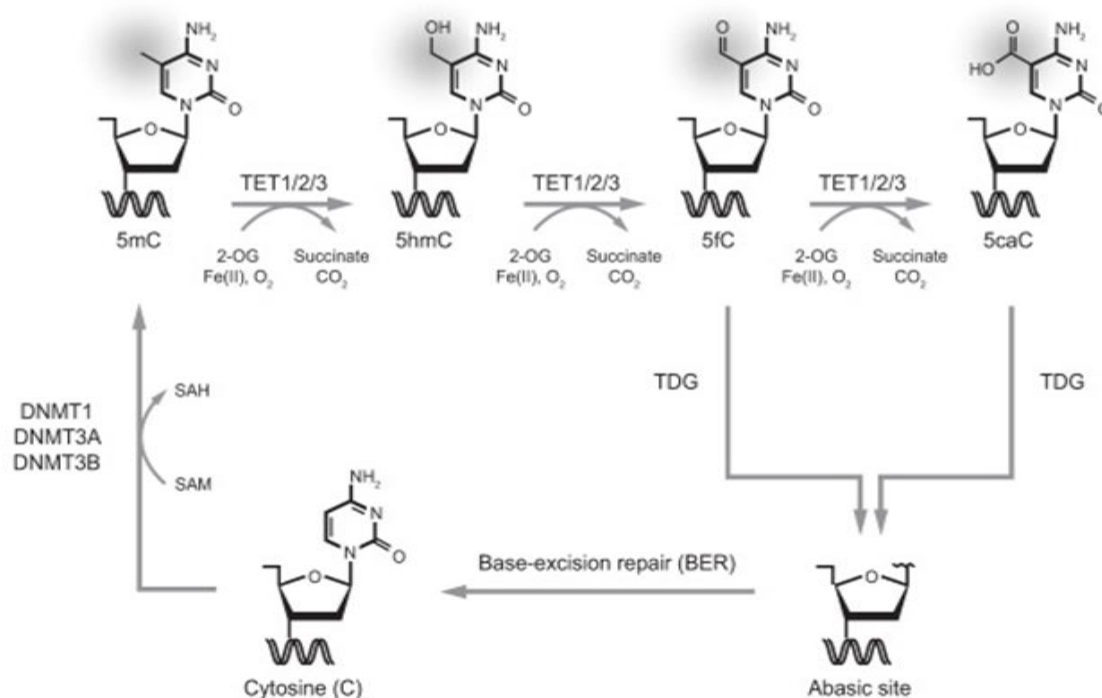
Figure 9 - Pathways of DNA methylation by DNMTs and demethylation mediated by TET enzymes. A cytosine residue can be methylated by DNMTs forming 5mC, which can then successively be oxidized by TET enzymes to produce 5hmC, 5fC, and 5caC. Thymine-DNA glycosylase (TDG) then recognizes 5fC and 5caC, and the oxidized cytosine base is excised. This results in an abasic site that is repaired by BER leading to restoration of the unmodified cytosine state. Taken *from Rasmussen & Helin 2016 [140].*

Also, other DNA modifications may have an impact on DNA methylation. For instance, in presence of 8-oxo-2'-deoxyguanosine (8-oxo-dG), the oxidation product of guanosine, adjacent cytosines cannot be methylated anymore, resulting in hypomethylation and, thus, transcriptional activation [125, 141].

1.4.2 Histone modifications

Eukaryotic chromatin is highly organized and packaged in the nucleus. When chromatin is packed very tightly ("condensed"), it is referred to as heterochromatin. Since accessibility for transcription factors is difficult under these conditions, heterochromatin is associated with transcriptional repression. On the other hand, euchromatin is the term for unwound and accessible chromatin, which is associated with

active transcription. The key building blocks for chromatin packaging are nucleosomes, which consist of a histone protein octamer core that is wrapped by 147 bp of DNA in ~1.65 superhelical turns (Figure 10) [129, 142]. Specifically, the octamer is composed of the four canonical histones (H2A, H2B, H3 and H4), which are arranged in a H3-H4 histone tetramer surrounded by two H2A-H2B dimers [143]. Nucleosome cores are connected by linker DNA, which varies in length (~20-90 bp) and is usually bound to histone H1 [144]. This architecture of nucleosome assembly on DNA is often referred to as beads on a string, which can be observed under the microscope. In heterochromatin multiple nucleosomes assemble into a 30 nm fiber and further supercoiling of these fibers results in a metaphase chromosome (Figure 11).
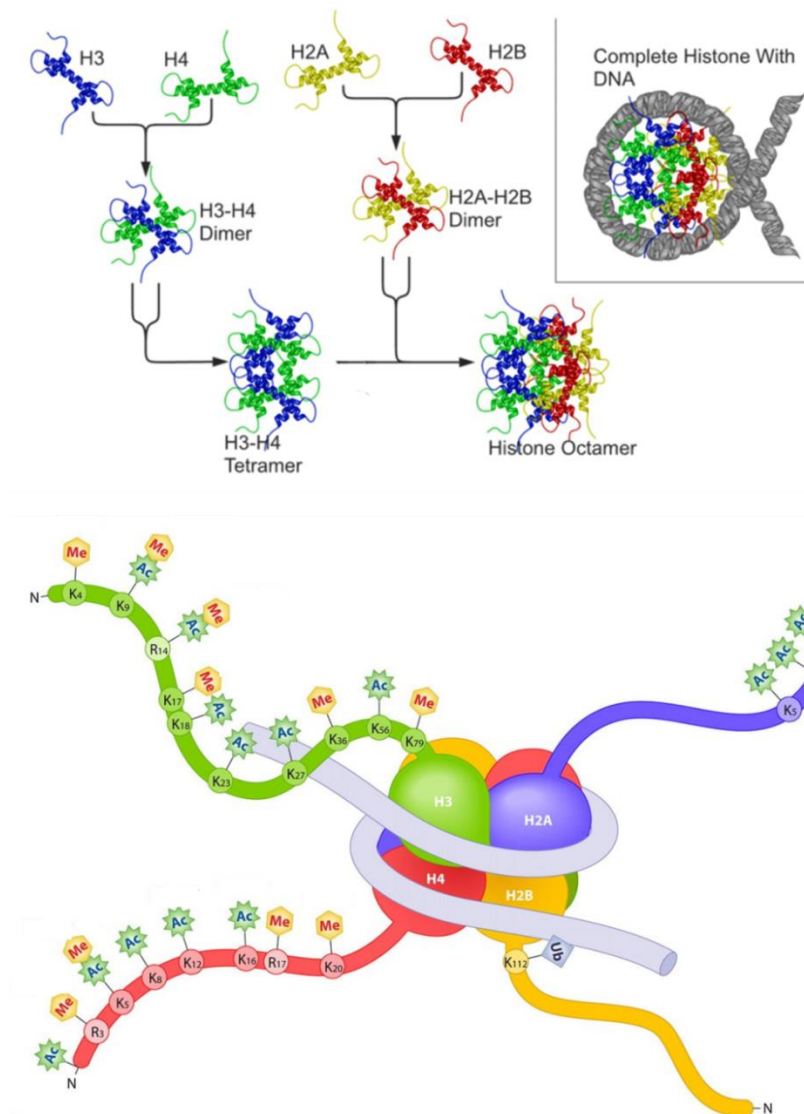
Figure 10 - Nucleosome structure and organization. DNA wraps in ~1.65 turns around a histone octamer composed of a H3-H4 histone tetramer and two H2A-H2B dimers. Protruding N-terminal histone tails are subjected to posttranslational modifications, mainly acetylation and methylation on lysine and arginine residues. *Taken from Wikipedia (Nucleosome structure, **Top**) and adjusted from amsbio webpage (**Bottom**).*
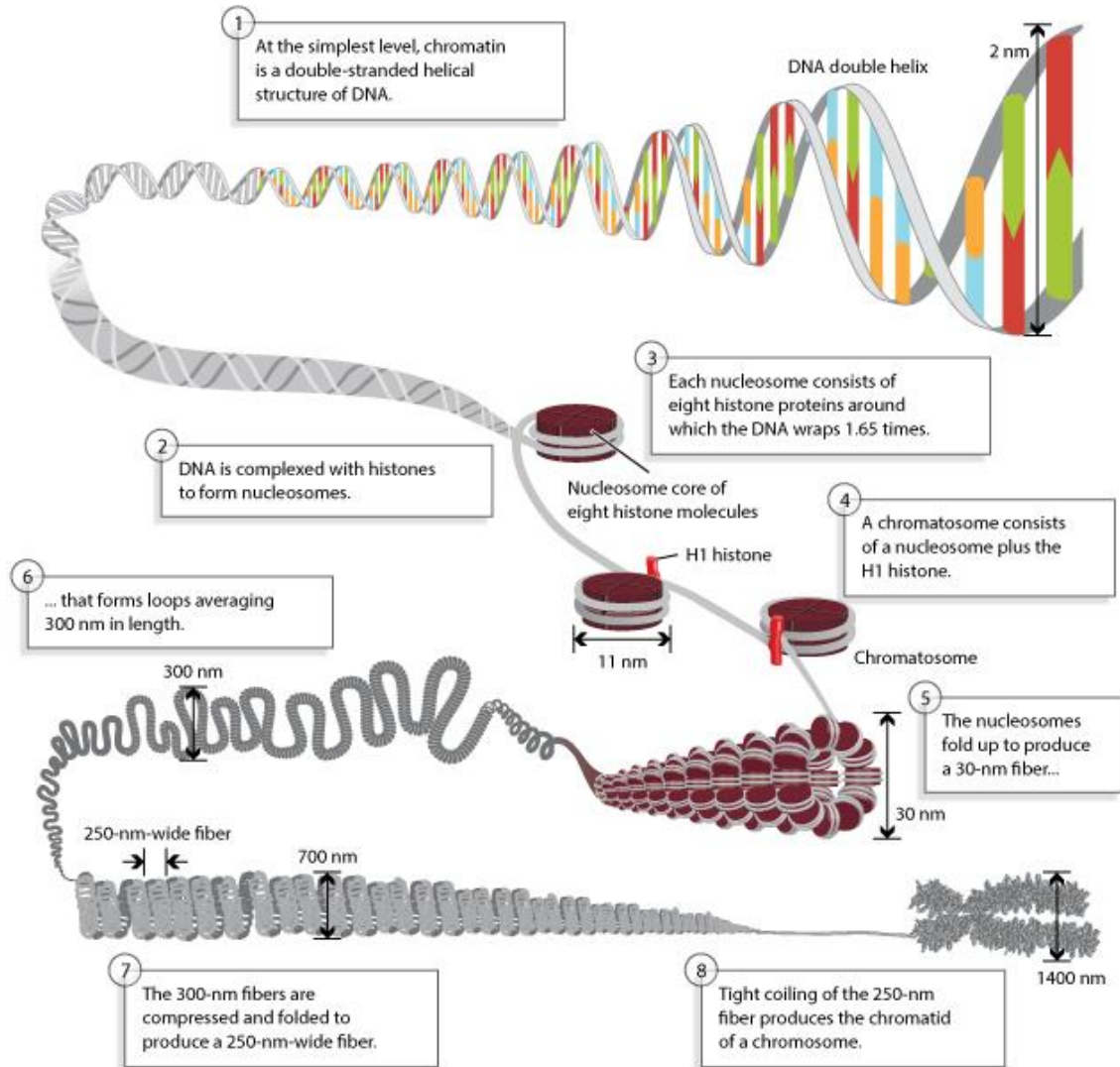
Figure 11 - Chromatin packaging. DNA is wrapped around a histone octamer to form a nucleosome. Nucleosomes are connected by stretches of linker DNA. This basic nucleosome structure is folded into a fiber-like structure of about 30 nm in diameter. These 30-nm fibers are further compacted into higher-order structures. *Taken from Annunziato, A. (2008) DNA Packaging: Nucleosomes and Chromatin. Nature Education 1(1):26.*

Histones are relatively small (102-135 amino acids) and are among the most highly conserved eukaryotic proteins [145]. All core histones have a long N-terminal amino acid tail containing many basic lysine and arginine residues. These highly positively charged N-terminal tails extend out from the nucleosome core into the nuclear lumen and are subject to various posttranslational modifications (PTMs) that can affect chromatin conformation and DNA accessibility (Figure 10). Such modifications include methylation, acetylation, phosphorylation, ubiquitination, ADP-ribosylation, and SUMOylation primarily on specific lysine, arginine and serine residues [146, 147]. The correlation of specific histone modifications with

transcriptional regulation led to the "histone code hypothesis" that suggests that different combinations of histone marks may epigenetically regulate chromatin structure and transcriptional status [148, 149].

To date, the best characterized modifications are acetylation and methylation of lysine residues on histones H3 and H4.

1.4.2.1 *Histone acetylation/deacetylation*

Histone acetylation occurs at the ε-amino group of lysine residues in H3 and H4 tails and is most consistently associated with transcriptional activation. The addition of acetyl groups to the lysine residues neutralizes their positive charge, thereby reducing the electrostatic attraction between the histone and the negatively charged phosphate groups of the DNA backbone. This leads to decompaction of the nucleosomes and a relaxation of the chromatin structure [150]. Consequently, the DNA is more accessible for transcription factors and RNA polymerases, promoting gene transcription. Accordingly, acetylation is mostly found at transcription start sites and/or enhancers of active genes [151]. In principle, all histone lysine residues can be acetylated, but the major acetylation sites described are H3K9, H3K14, H3K18, H3K23, H3K27, H4K5, H4K8, H4K12, and H4K16 [129, 152]. Histone acetylation is a dynamic process that is mediated by the antagonistic actions of two large families of enzymes - the histone acetyltransferases (HATs) and the histone deacetylases (HDACs) (Figure 12). By regulating the balance between acetylation and deacetylation these enzymes play a central role in the epigenetic regulation of gene expression and therefore in numerous developmental processes and disease states.
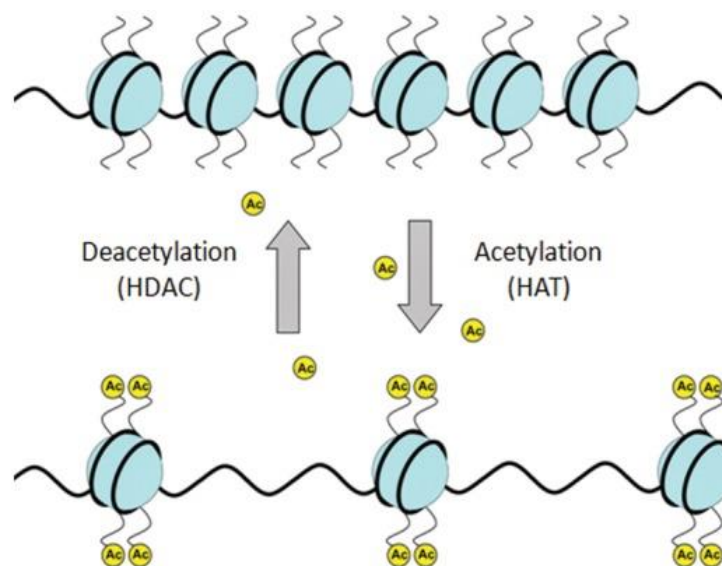
Figure 12 - Histone acetylation and deacetylation. Histone acetyltransferases (HATs) add acetyl groups to lysine residues of histones in nucleosomes. This results in chromatin unwinding and transcriptional activation. Histone deacetylases (HDACs) remove acetyl groups inducing a closed chromatin structure and transcription repression. *Taken from Eslaminejad et al. 2013 [153].*

1.4.2.2 Histone acetyltransferases (HATs)

Histone acetyltransferases (HATs) catalyze the transfer of an acetyl group from acetyl coenzyme A (acetyl-CoA) to lysine residues in histone tails. There are two different types of HATs: type A HATs are located in the nucleus and type B HATs in the cytoplasm. Type A HATs can be classified into five families GNAT1, MYST, SRC, p300/CBP, and a group of other acetyltransferases that cannot clearly be categorized based on defining features of the first four classes [154]. These nuclear HATs acetylate nucleosomal histones and other chromatin-associated proteins and are thus involved in the regulation of gene expression. Cytoplasmic type B HATs acetylate newly synthesized free histones, which is important for their deposition into chromatin but has no direct impact on transcription [155]. Acetyl-CoA is produced through glycolysis as well as other catabolic pathways and is used as a substrate for the citric acid cycle and as a precursor in synthesis of fatty acids. Since HATs are dependent on the availability of acetyl-CoA, the extent of histone acetylation is influenced by the cellular metabolic state [156].
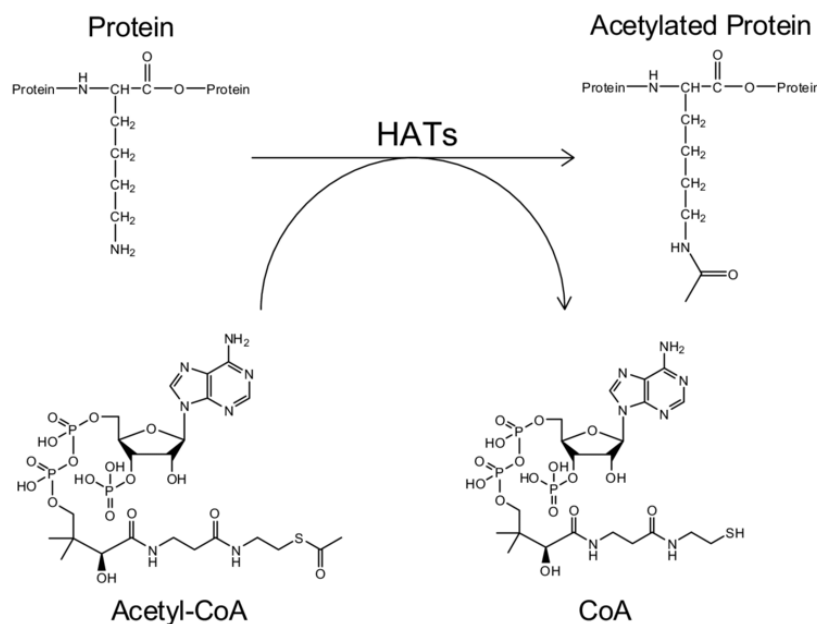
Figure 13 - Reaction mechanism of protein lysine acetylation by histone acetyltransferases (HATs). HATs catalyze the transfer of an acetyl group from acetyl coenzyme A (acetyl-CoA) to a lysine residue yielding the acetylated protein and a CoA molecule. *Taken from Rye et al. 2011 [157].*

1.4.2.3 Histone deacetylases (HDACs)

Histone lysine acetylation is highly reversible. The removal of acetyl groups from histone lysine residues is catalyzed by histone deacetylases (HDACs). There are four major classes of HDACs described in mammals, which are classified based on structure, catalytic mechanism, and sequence homology to the enzymes originally discovered in *S. cerevisiae*. Class I comprises HDAC1, -2, -4 and -8, which are

predominantly localized in the nucleus and ubiquitously expressed in most tissues and cell lines. Class II is subdivided into class IIA containing HDAC4, -5, -7, and -9, and class IIB, which includes HDAC6 and HDAC10. Class II HDACs are expressed in a tissue-specific manner and their nuclear or cytoplasmic localization is regulated by signal-dependent phosphorylation. The sole member of class IV is HDAC11. Class I, II and IV HDACs require Zn^{2+} ions as cofactors for their deacetylation mechanism. Class III HDACs are known as sirtuins and differ from the other HDAC classes in that they possess a highly conserved zinc tetra-thiolate motif within their catalytic pocket and require nicotinamide adenine dinucleotide (NAD^+) as cofactor for their catalytic activity. While the mechanism of class I, II and IV HDACs yields the deacetylated substrate and free acetate, the sirtuin-mediated deacetylation reaction results in O-acetyl-ADP-ribose, the deacetylated substrate and nicotinamide (Figure 14) [150, 158, 159].
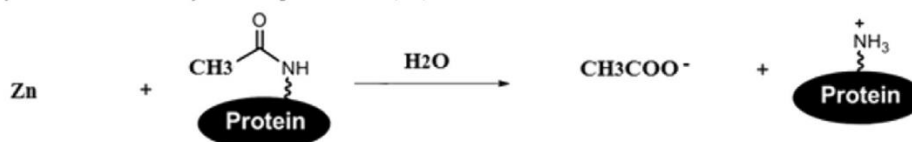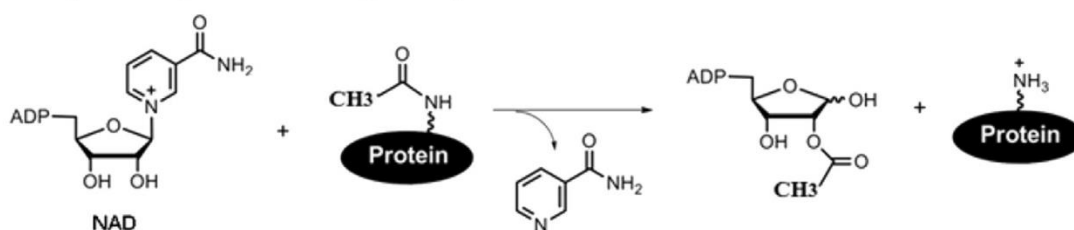
Figure 14 - Two catalytic mechanisms of Histone Deacetylases. Class I/II/IV HDACs require Zn ions as cofactors for catalysis and yield free acetate and the deacetylated substrate. Class III HDACs (sirtuins) use NAD^+ as cofactor to which they transfer the acetyl group producing O-acetyl-ADP-ribose and nicotinamide, as well as the deacetylated substrate. *Taken from Li et al. 2015 [160].*

Generally, HDACs have relatively low substrate specificity, as a single enzyme is mostly capable of deacetylating multiple sites within a histone. Due to their major role in transcription regulation, HDACs constitute a promising therapeutic target in many diseases including cancer, inflammation, and neurological diseases. Therefore, much effort is put into the development of effective HDAC inhibitors with minimal side effects.

1.4.2.3.1 Sirt1

The highly conserved sirtuin family consists of seven members, Sirt1-7, that differ in their localization, enzymatic activity, tissue specificity, and functions. Their name derives from their sequence similarity to

the yeast progenitor sirtuin "silent information regulator 2" (Sir2), which is a transcriptional repressor [161, 162]. Sirtuins can be further discriminated by their subcellular localization. Sirt1, -6 and -7 are localized in the nucleus, whereas Sirt2 is mainly cytosolic but can shuttle to the nucleus during mitosis. Sirt3, -4 and -5 are generally found in the mitochondria [163, 164]. Sirtuins do not only act as transcriptional effectors by mediating histone deacetylation, but also serve as energy sensors due to their dependency on NAD$^+$ [162, 165]. Sirtuins are widely expressed and have a broad range of biological functions including the regulation of cellular metabolism, stress response, genomic stability, and aging [166-169]. The nuclear deacetylase Sirt1 is the most evolutionarily conserved mammalian sirtuin with highest homology to Sir2. It deacetylates and regulates histones as well as a broad range of non-histone substrates, such as p53, stress response-associated forkhead (Fox) transcription factors, mitochondrial biogenesis regulator PGC1-α, and others. Through either direct modulation or by influencing gene expression, Sirt1 is implicated in a variety of cellular processes including cell cycle, response to DNA damage, metabolism, apoptosis and autophagy [29].

1.4.2.3.2 HDAC2

The class I HDAC2 is ubiquitously expressed in all tissues and predominantly localized in the nuclear compartment of the cell. HDAC2 acts via the formation of a large multiprotein complex that interacts with transcription factors and is recruited to target genes to mediate repression. Complexes that include HDAC2 as a catalytic subunit are the Sin3, NuRD and CoREST complexes. In the late S-phase of DNA-replication, HDAC2 is also found in a DNMT1-containing transcriptional repressor complex [29, 163, 170-172]. HDAC2 has crucial roles in many cellular processes such as proliferation, cell cycle, differentiation and apoptosis. Physiologically, HDAC2 is a key regulator of the transcription of genes implicated in hematopoiesis, epithelial cell differentiation, heart development and neurogenesis [150, 173-177].

1.4.2.4 *Histone methylation/demethylation*

Unlike histone acetylation, the effects of histone lysine methylation patterns on transcription are more complex, since some methylation sites are associated with active transcription (euchromatin), while some are repressive, promoting heterochromatin formation. Generally, the methylation of H3K9, H3K27 and H4K20 are associated with gene silencing, whereas H3K4, H3K36 and H3K79 methylation states are transcriptionally permissive modifications [129]. Methylation marks lead to recruitment of effector proteins ("readers") (e.g. heterochromatin protein 1 (HP1) or TATA-Box Binding Protein Associated Factor 3 (TAF3)), that bind to the methylated residue and initiate downstream effects altering chromatin structure or affecting transcription directly [178, 179]. In addition, the ε-amino group of lysine can be

mono-, di-, or tri-methylated, since each hydrogen of the NH_3^+ group can be replaced by a methyl group. Those different extents of methylation may have different effects on transcription due to high sensitivity of reader proteins containing methyl-binding domains that recognize the methylation status [180]. For instance, while H3K4me3 modifications mark active promoters, H3K4me1 marks are found in enhancer regions [181]. Histone methylation also occurs on basic arginine residues, which can be monomethylated, symmetrically dimethylated or asymmetrically dimethylated on their guanidinyl group [180]. Sites of arginine (R) methylation include H3R2, H3R8, H3R17, H3R26 and H4R3. Histone arginine methylation also plays a, yet less described, role in transcription regulation, as it was shown to promote or prevent the docking of key transcriptional effector molecules [182].

Histone lysine methylation is catalyzed by S-adenosylmethionine (SAM)-dependent lysine methyltransferases (KMTs). However, methyl groups can be removed by flavin-dependent or JumonjiC (JmjC) domain-containing lysine demethylases (KDMs) [183]. A family of nine protein arginine methyltransferases (PRMT1-9) catalyzes the methylation of arginine, which can be reversed by a subset of JmjC demethylases [182, 184].

1.4.2.5 Histone lysine methyltransferases (HMTs)

Histone lysine methyltransferases can be grouped into SET domain-containing enzymes and the non-SET domain-containing enzyme DOT1-like protein (DOT1L). DOT1L is responsible for mono-, di-, and trimethylation of the ε-amino group on H3K79 and is the only methyl-transferase with this target known so far [185]. H3K79 is an activating mark that, unlike most other histone marks, resides in the globular core and not the tail of the histone. The majority of histone lysine methyltransferases contain a conserved catalytic SET (suppressor of variegation, enhancer of zeste, trithorax) homology domain [180]. These methyltransferases can methylate histone lysine residues, but also non-histone substrates [186]. SET methyltransferases can again be grouped into four families based on the sequence similarity in their SET domain and in adjacent protein regions: SET1, SET2, SUV39, and RIZ [187]. Also, there are other additional SET domain-containing methyltransferases that have not been assigned to a certain group, like SET7 (SET7/9), SET8, SUV4-20H1, and SUV4-20H2.

All HMTs use S-adenosylmethionine (SAM) as methyl donor. To date more than 50 human lysine methyltransferases (KMTs) have been reported [188]. All these enzymes are highly selective regarding their target lysine residue, as well as the degree of methylation they confer.

1.4.2.5.1 Set7

Set7 (SET7) is a 41 kDa SET domain-containing histone lysine methyltransferase that is also known by the names SET7/9 or SETD7. Set7 specifically monomethylates lysine 4 of histone 3 (H3K4me1) and thereby plays a role in transcriptional activation of genes including insulin or collagenase [189-191]. Involvement of Set7 in di- or trimethylation of histones was disproved [192, 193]. Set7 is also able to catalyze methylation of non-histone proteins, such as p53, TAF10, SOX2, SIRT1, and DNMT1 [194]. It is suggested that Set7 plays an important role in development and skeletal muscle differentiation [189, 195].

1.4.2.5.2 SMYD1

The SMYD family proteins belong to the SET2 class of SET domain-containing methyltransferases and comprise five proteins (SMYD1-5) [188, 196]. Their catalytic SET domain is split into two segments by a MYND domain, followed by a cysteine-rich post-SET domain, hence the name SET and MYND domain-containing protein (SMYD). While the SET domain is responsible for the methylation of lysine residues, the zinc-finger motif-containing MYND domain facilitates protein-protein interactions that may underlie methylation specificity [197]. SMYD1, also known as BOP, is a nuclear and cytoplasmic protein that is expressed specifically in cardiac and skeletal muscle [198]. It was shown by Tan *et al.* that SMYD1 catalyzes methylation of histone 3 on lysine 4 (H3K4), a mark of transcriptional activation [199]. However, further studies have shown that SMYD1 also methylates multiple non-histone proteins, such as the muscle-specific transcription factor skNAC [200, 201]. Interestingly, SMYD1 can also function as transcriptional repressor due to interaction with histone deacetylases. Specifically, the MYND domain recruits and directly binds to class I and class II HDACs, whose catalytic activity induces transcriptional silencing [198]. The highly dynamic function of SMYD1 plays a key role in cardiac and skeletal muscle development and related pathology [202].

1.4.2.6 Histone lysine demethylases (KDMs)

It was long believed that histone methylation is irreversible, since the half-life of histone methylation marks was approximately the same as histone turnover [203]. However, in 2004 Shi *et al.* identified an amine oxidase, lysine-specific demethylase 1 (LSD1 or KDM1A), that specifically removes methyl groups from histone 3 lysine 4 (H3K4) in a FAD-dependent reaction limited to mono- and dimethylated substrates [204]. Not much later, the family of JumonjiC (JmjC) domain-containing histone demethylases (JHDMs) was discovered, which can be divided into seven subfamilies (KDM2-8) based on the JmjC domain homology [205, 206]. JmjC domain-containing histone demethylases are iron- and

2-oxoglutarate (2-OG)-dependent and are able to remove methyl groups from all three methyl lysine states.

1.4.2.6.1 LSD1

The histone lysine demethylase LSD1 (KDM1A) is a flavin adenine dinucleotide (FAD)-dependent amine oxidase that generally demethylates monomethylated and dimethylated lysine 4 of histone 3 (H3K4me1/2). In the demethylation reaction an iminium cation intermediate is generated from the methylated amino group of lysine, which is further hydrolyzed to a carbinolamine that spontaneously dissociates yielding the demethylated amine and formaldehyde (Figure 15) [207]. During the reaction the cofactor FAD is reduced to $FADH_2$, which is recycled through oxidation by molecular oxygen thereby forming hydrogen peroxide as a byproduct. The LSD1-mediated demethylation reaction is limited to di- and monomethylated lysines, as it requires a free electron pair on the lysine ε-nitrogen atom to initiate demethylation [188, 207].
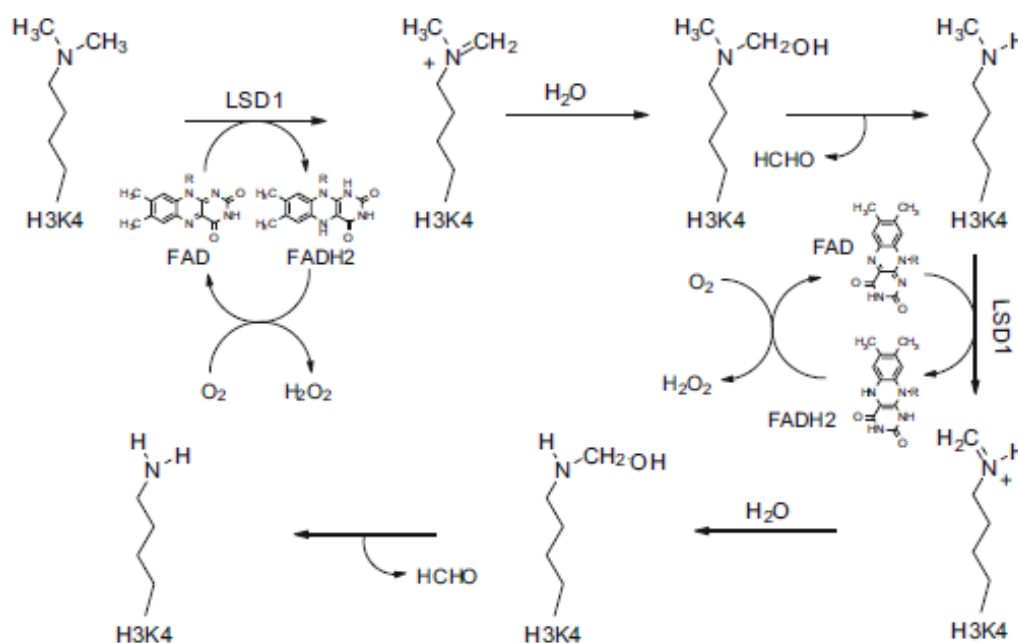
Figure 15 – Mechanism of action of LSD1. LSD1 uses FAD as cofactor to generate an iminium cation intermediate from dimethylated lysine. The intermediate is then hydrolyzed to a carbinolamine that spontaneously degrades to the demethylated amine, thereby releasing formaldehyde. This reaction is then repeated until the lysine residue is completely demethylated. *Taken from Rotili et al. 2011 [207].*

By demethylating H3K4 LSD1 acts as a transcriptional repressor; however, LSD1 is also associated with transcriptional activation due to its dual substrate specificity. When bound to androgen receptor (e.g in

prostate cancer cells), LSD1 changes its substrate target to H3K9me1/2. By demethylation of the repressive H3K9me1/2, LSD1 induces the activation of androgen receptor target genes [208].

Of note, generation of H_2O_2 during the catalytic activity of LSD1 is associated with DNA base oxidation, thereby triggering the recruitment of the base excision repair (BER) machinery to the gene promoter and regulatory response sites [209-211]. Effective coupling of BER to LSD1-mediated histone demethylation is critical for efficient transcriptional regulation. The toxic formaldehyde released during lysine demethylation is possibly scavenged by tetrahydrofolate (THF), as it was shown that LSD1 contains a THF binding site that binds THF with high affinity [212]. Bound THF was shown to accept the formaldehyde generated in the course of histone demethylation to form 5,10-methylene-THF [213, 214].

LSD1 plays a critical role in development, especially differentiation and maintenance of embryonic stem cells. It has also been shown to be involved in the control of hematopoiesis, the DNA damage response, the circadian cycle and the regulation of cellular energy metabolism [206, 215, 216].

1.4.2.6.2 KDM3A

KDM3A (also JHDM2A, JMJD1A) belongs to the family of JumonjiC domain-containing histone lysine demethylases (JHDMs). These enzymes are mononuclear iron-dependent dioxygenases that use 2-oxoglutarate (2-OG) and molecular oxygen (O_2) as cosubstrates for oxidative demethylation of histones. All JHDMs share a common conserved structural motif, namely a 2-histidine-1-carboxylate facial triad, that coordinates a non-heme Fe(II) at the catalytic center (Figure 16) [207, 217]. The demethylation reaction involves an initial step of 2-OG and oxygen binding to the catalytic center, resulting in release of CO_2 and formation of a highly reactive oxo-ferryl intermediate that reacts with the methylated lysine substrate. Subsequent hydroxylation produces succinate and an unstable hemiaminal intermediate that rapidly breaks down, leading to the release of formaldehyde and the demethylated lysine residue (Figure 16) [183, 207]. In general, JHDMs are able to remove methyl groups from all three methyl lysine states; however, KDM3A preferentially demethylates mono- and dimethylated H3K9, while it has weak or no activity on trimethylated H3K9 [218]. Despite producing toxic formaldehyde as a byproduct, the reason for the absence of damage to this class of histone demethylases is yet unknown.
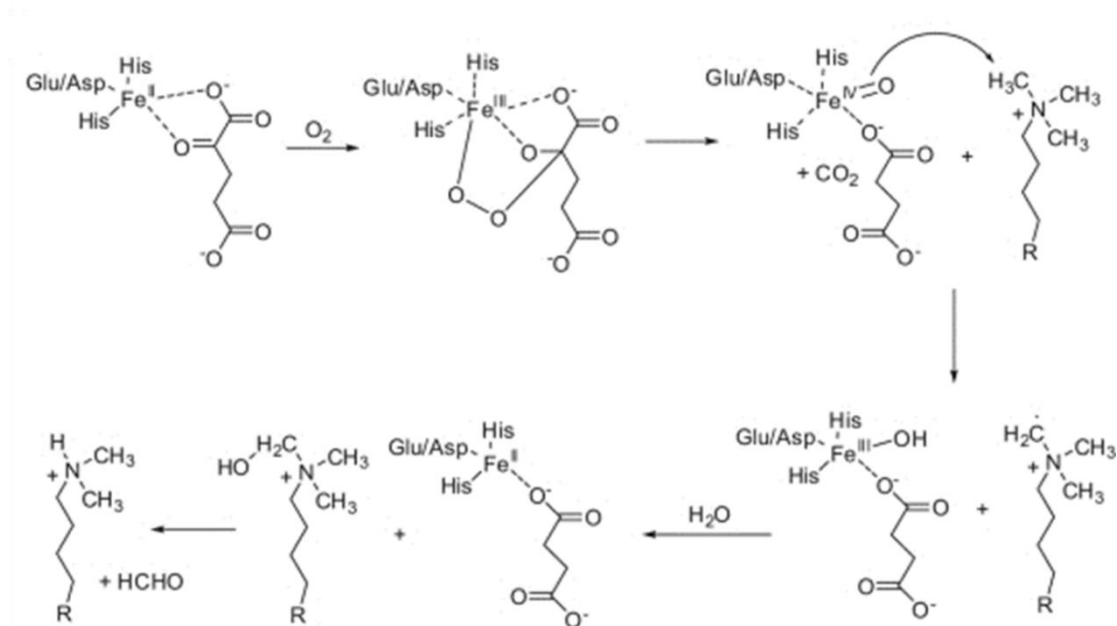
Figure 16 - Mechanism of action of KDM3A. 2-oxoglutarate and oxygen bind to the 2-histidine-1-carboxylate facial triad in the catalytic center of KDM3A. The resulting oxo-ferryl (Fe(IV)-oxo) intermediate reacts with the methylated lysine substrate. This leads to hydroxylation of lysine to a hemiaminal intermediate and release of succinate. The hydroxylated lysine degrades into formaldehyde and a demethylated lysine residue. *Taken from Rotili et al.2011 [207].*

KDM3A was shown to play an important role in germ cell development, as it is highly expressed during spermatogenesis, while KDM3A-KO mice are infertile [206, 207, 219]. In addition, KDM3A has been implicated in the transcriptional control of metabolic genes in muscle and adipose tissues, as demonstrated by development of adult obesity phenotype in KO mice [220, 221].

1.4.3 ATP-dependent chromatin remodeling

In addition to DNA and histone modification, ATP-dependent chromatin remodeling complexes play an important role in epigenetic processes due to their ability to enable transcriptional access to DNA by altering the structure, composition or positioning of nucleosomes [222]. Those chromatin remodelers are large multi-subunit complexes that contain a highly conserved ATPase catalytic domain, as they require the energy from ATP hydrolysis for their remodeling functions. These functions include the dissociation of DNA-histone contacts in nucleosomes (looping), translocation of the nucleosome along the DNA (sliding) or even eviction of nucleosomes from the DNA, thereby increasing DNA accessibility (Figure 17). Furthermore, nucleosomal histone subunits including their specific posttranslational modifications can be exchanged by remodeling complexes [223].

There are five known families of chromatin remodeling complexes in eukaryotes: SWItch/Sucrose Non-Fermentable (SWI/SNF), Imitation SWItch (ISWI), NURD/Mi-2/CHD (a complex including a nucleosome

remodeling deacetylase and chromodomain-helicase-DNA-binding protein), as well as the complexes INO80 and SWR1 [222, 224]. The unique protein subunit composition of each complex (like presence of a helicase or bromodomain etc.) specify its function and biological role (e.g. in apoptosis, DNA repair etc.). For instance, ISWI-complexes are implicated in chromatin assembly after DNA replication, while remodelers of the families INO80 and SWI/SNF participate in DNA double-strand break (DSB) repair and nucleotide-excision repair (NER) [223]. The dynamic remodeling of the fundamental nucleosomal structure, organization and localization through remodeling complexes plays a key role in the epigenetic regulation of gene expression underlying many fundamental cellular processes.

Figure 17 - Mechanisms of ATP-dependent chromatin remodeling. The energy from ATP hydrolysis is used for changes in nucleosomal assembly and structure. These changes include translocation of the nucleosome along DNA (sliding), nucleosome eviction, dissociation of DNA-histone contacts (unwrapping/looping), and exchange or ejection of nucleosomal subunits (dimer replacement). *Taken from Chen et al. 2017 [225].*

1.4.4   Non-coding RNAs

About 90% of the human genome is transcribed into RNA, but only 1-2% of the transcripts actually encode proteins [226]. The generated non-coding RNA (ncRNA) transcripts are functional RNA molecules that are either involved in "housekeeping" processes for translation (e.g. transfer RNAs or ribosomal RNAs) or can modulate gene expression and therefore play a role as epigenetic modifiers (Figure 18) [227]. Epigenetic-related ncRNAs can further be divided into two groups; short ncRNAs are less than 200 nucleotides in length, while long ncRNAs (lncRNAs) include all larger transcripts [228].
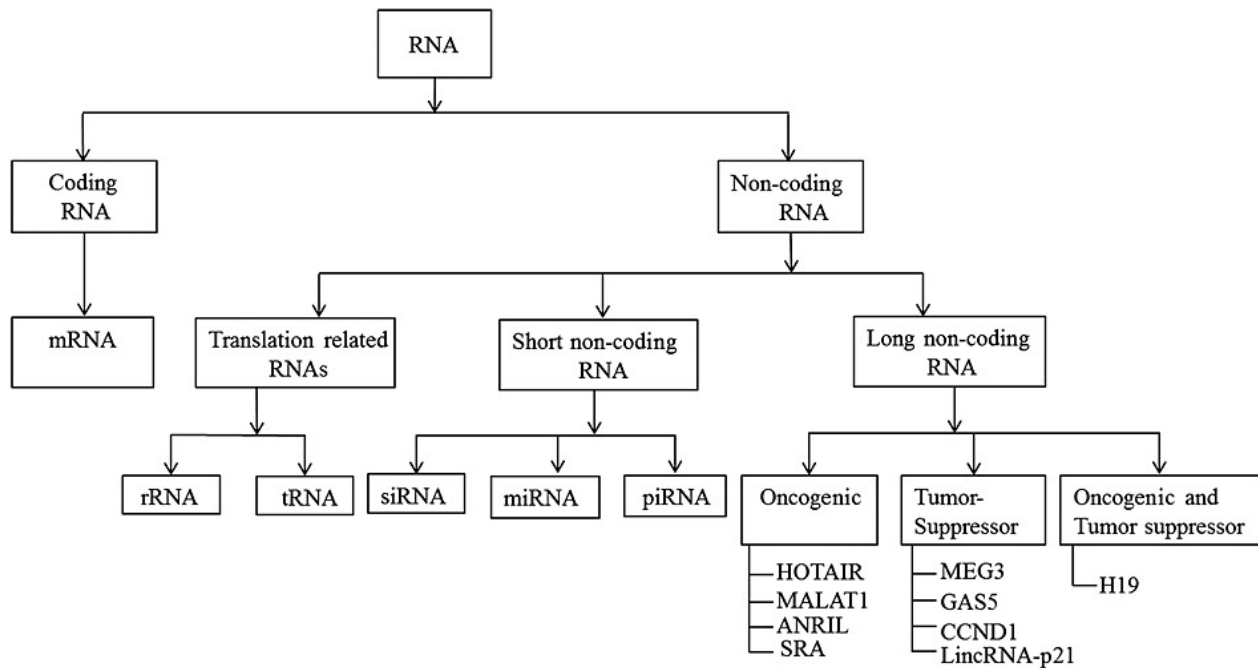
Figure 18 - Classification of different RNA types, divided into coding and non-coding RNA subscripts. Non-coding RNAs comprise translation-related RNAs and two groups of epigenetic-related RNAs, short ncRNA and long ncRNA. *Taken from Santosh et al. 2015 [229].*

Long non-coding RNAs comprise the majority of non-coding RNA transcripts and are highly diverse in structure and function. They can influence gene expression by serving as a scaffold for or complexing with chromatin-modifying proteins and recruiting their catalytic activity to specific sites in the genome [230]. For instance, the lncRNA HOTAIR (for HOX transcript antisense RNA) can silence Hox genes by recruiting polycomb-group proteins, which are chromatin remodeling complexes that induce formation of repressive heterochromatin [231]. In addition, lncRNAs can also suppress transcription by obstructing promoter association of transcription factors or by recruitment of RNA-binding proteins that interfere with histone deacetylation [230].

Short non-coding RNAs can be further divided into three major classes: microRNAs (miRNAs), short interfering RNAs (siRNAs), and piwi-interacting RNAs (piRNAs). Micro-RNAs are about 17-25 nucleotides in length and regulate messenger RNA (mRNA) expression. Specifically, miRNAs target and bind complementary 2-7 nt long seed regions of mRNAs, ultimately resulting in mRNA cleavage and therefore suppression of translation in a process termed RNA interference [227, 228]. In some cases, miRNAs can even target the gene promoter on the DNA itself and thereby act as transcriptional repressor [232]. Another way, in which miRNAs may affect epigenetic pathways is the regulation of translation of epigenetic enzymes, such as DNMTs or histone modifiers [227]. The microRNA miR-34a, for instance, was shown to repress the expression of the histone deacetylase Sirt1 [233]. Short interfering RNAs (siRNAs) work in a similar way as miRNAs, inducing gene silencing by mRNA degradation [234]. However, in contrast to miRNAs, siRNAs are perfectly complementary to their mRNA sequence target and therefore highly specific for transcriptional suppression [235]. Synthetic siRNAs are widely used to achieve targeted and effective silencing of genes. The class of Piwi-interacting RNAs (piRNAs) interacts with piwi family proteins in order to mediate gene silencing. piRNAs are restricted to the germline and germline bordering somatic cells and their primary function involves chromatin regulation and suppression of transposon activity [229, 236].

1.5 The interrelation of oxidative stress and epigenetics

Increasing evidence shows that ROS/RNS influence epigenetic pathways by affecting the function or expression of histone and DNA modifying enzymes [123-125]. Adverse redox regulation of epigenetic processes may ultimately result in pathological consequences.

Overall, increased oxidative stress is associated with global DNA hypomethylation [125, 128]. ROS can induce changes in DNA methylation patterns by directly reacting with DNA bases. Hydroxyl radicals can oxidize 5-methylcytosine (5mC) to 5-hydroxymethylcytosine (5hmC), which may interfere with the activity of the maintenance DNA methyltransferase DNMT1 or, upon further oxidation, be subjected to base excision repair (as described in 1.4.1, p.20), ultimately leading to demethylation [125, 139, 237]. Also, in conditions of oxidative stress the availability of DNMT cofactor S-adenosyl-methionine (SAM) is reduced, restricting DNMT activity and therefore leading to decreased DNA methylation [125, 128, 238].

Oxidative stress is also associated with dysregulation of histone acetylation. Many studies have reported an increase in histone acetylation upon increased ROS; however, opposing results have also been described (Figure 19) [239-241]. Increased acetylation levels can be caused by reduced expression or activity of class I HDACs due to ROS-induced PTMs or by ROS-mediated nuclear export of oxidized class II

HDACs [239, 242-245]. In addition, ROS can decrease the activity of sirtuins by decreasing the availability of the cofactor NAD^+ or by generating inhibitory PTMs, thereby contributing to increased histone acetylation [240, 246, 247]. Sirtuin expression upon oxidative stress, on the other hand, can either be increased, dependent on the redox-sensitive transcription factor HIF1α [248, 249], or decreased due to transcriptional or miRNA-mediated repression conditions [250].
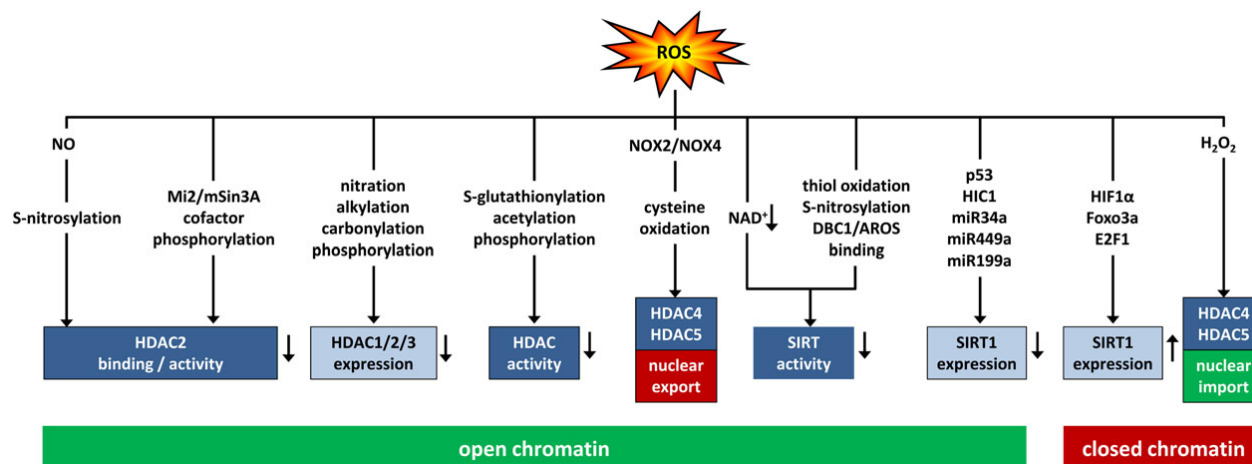
Figure 19 - ROS affect histone acetylation by modulating histone deacetylases. *Taken from Kietzmann et al.2017 [125].*

Histone methylation marks have also been reported to be modulated by ROS, mainly by ROS-induced alteration of the activity or expression of HMTs or KDMs (Figure 20). In order to catalyze histone methylation, HMTs, like DNMTs, depend on the cofactor SAM, which is reduced during oxidative stress, thus decreasing HMT activity [125]. Furthermore, it has been shown that ROS can inhibit JmjC KDM activity by oxidizing or binding the non-heme Fe(II) at the catalytic center [124, 125, 217]. Increased expression of several JmjC KDMs was also observed during oxidative stress in a HIF1α-dependent manner [251].

Additionally, various miRNAs have been shown to be regulated by ROS [126, 127] and there is increasing evidence that ROS can also affect ATP-dependent chromatin remodeling complexes [125, 252].

On the other hand, it is also possible that epigenetic alterations affect redox signaling by directly or indirectly regulating the function or expression of ROS-producing enzymes or antioxidant enzymes. For instance, epigenetic silencing of NOX enzymes via promoter hypermethylation has been shown in diseases such as lung cancer or hepatocellular carcinoma [11, 253-255]. Furthermore, class I HDACs were shown to be involved in the transcriptional activation of NOXs in endothelial and smooth muscle cells [256-259]. Epigenetic silencing of SOD2 via histone modifications or DNA hypermethylation was found in in several disorders including cancer, diabetes and hypertension [260-263].
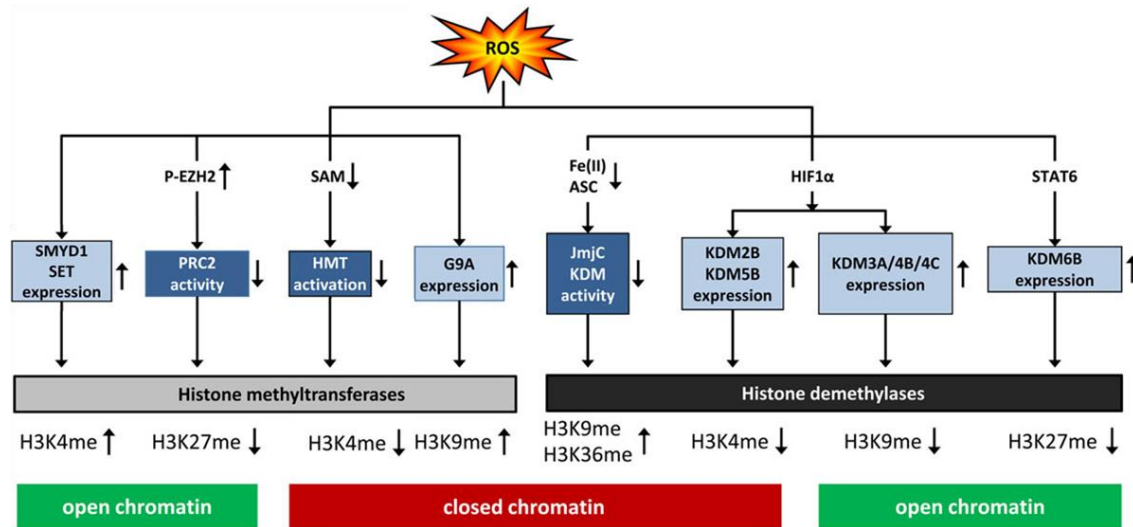
Figure 20 - ROS affect histone methylation by modulating histone methyltransferases or histone demethylases. *Taken from Kietzmann et al. 2017 [125]. Edited for accuracy.*

In summary, disruption of epigenetic regulation by ROS may induce changes in gene expression with potential pathological consequences. Or conversely, epigenetic alterations may affect the expression of energy expenditure, antioxidant or inflammatory genes leading to dysfunctional energy metabolism or inflammation, inducing oxidative stress. Oxidative stress-associated enzymes may therefore play a dual role serving as target and/or source of epigenetic remodeling.

The effect of ROS on epigenetic regulation, including mechanisms and consequences, was reviewed in detail by Kietzmann *et al.* 2017 [125], Kreuz & Fischle 2016 [36], Mikhed *et al.* 2015 [211], and Cyr & Domann 2011 [128].

1.6 Implications of oxidative stress and epigenetics in cardiovascular diseases

Cardiovascular diseases (CVDs) are the leading cause of death worldwide and not only cause a public health issue but also account for trillions of dollars of global healthcare expenditure [264-266]. CVDs are multifactorial disorders of the heart or blood vessels and include stroke, heart failure, hypertension, coronary artery diseases, cardiomyopathy, atherosclerosis, arrhythmia, diabetic vascular disease, and more [264]. Multiple genetic and environmental risk factors are associated with the development of CVDs, e.g. genetic predisposition, aging, smoking, diet, pollution, circadian rhythm or socioeconomic status [264, 267, 268]. In order to develop more efficient and cost-effective therapy it is necessary to gain a thorough understanding of the interplay of these factors and the underlying molecular pathways that ultimately result in CVDs. Epigenetic gene regulation is increasingly recognized as playing a causative role in CVDs and is also emerging as a key target for therapeutic treatment [152, 227, 269-275]. In short,

some known epigenetic changes involved in CVD include DNA hypomethylation in proliferating vascular smooth muscle cells in atherosclerosis, changes in estrogen receptor-α/β promoter methylation in vascular disease, as well as changes in global histone H3K4 and H3K9 trimethylation in congestive heart failure [134, 276-280]. Furthermore, it is well established that increased ROS formation is involved in the pathogenesis of cardiovascular diseases [5, 75, 281-285]. There is now increasing data showing a link between epigenetic pathways and ROS signaling in CVDs. For instance, it was demonstrated that oxidative stress caused aberrant DNA methylation in atherosclerosis by altering the binding of DNMTs to chromatin [276, 286-288]. Furthermore, in pulmonary arterial hypertension epigenetic silencing of superoxide dismutase 2 (SOD2) by selective promoter hypermethylation impaired redox signaling and promoted vascular smooth muscle cell (SMC) proliferation [134, 263, 289, 290]. In addition, oxidation of HDAC4 mediated by NOX4 has been shown to induce cardiac hypertrophy [291]. Interestingly, in turn, it was demonstrated that HDACs play a key role in transcriptional regulation of NOX4 in human endothelial and smooth muscle cells and are therefore implicated in vascular pathophysiology [256, 258]. A global decrease in H3K9 acetylation and increased global H3K9 methylation across different cells has been observed in hypoxia due to HDAC and HMT upregulation, respectively [292, 293]. A key feature of CVDs is endothelial dysfunction, which can be caused by several factors including downregulation of eNOS expression and activity, eNOS uncoupling, or nitric oxide scavenging by free radicals [294, 295]. The restriction of eNOS expression to vascular endothelium was shown to be regulated by DNA methylation and histone modifications. In contrast to non-expressing cells, endothelial cells are demethylated at the eNOS promoter along with a local enrichment of acetylated H3 and H4 histones promoting transcriptional activation [152, 296]. Under hypoxic conditions eNOS expression is reduced due to a decrease in H3/H4 acetylation of eNOS proximal promoter histones, thus fostering endothelial dysfunction [297]. In line with that, it has been proposed that HDAC1 inhibition may represent a method to prevent endothelial dysfunction [298].

With the increasing evidence of involvement of epigenetic regulation in the development and progression of cardiovascular disorders, it is becoming more and more important to investigate the interplay of redox signaling and epigenetic regulation in this context.

1.6.1 The role of oxidative stress and epigenetics in diabetes

Diabetes mellitus (DM) is a globally growing health problem with increased mortality due to its consequential complications. Diabetes is characterized by a relative or absolute lack of insulin, resulting in elevated blood glucose levels (hyperglycemia). Type 1 diabetes mellitus (T1DM), previously known as insulin-dependent DM, is caused by an autoimmune-mediated loss of insulin-producing beta-cells in the pancreas, resulting in insulin deficiency [299]. Type 2 diabetes mellitus (T2DM), previously known as non-insulin-dependent or adult-onset DM, is the most common type of diabetes. It is characterized by insulin resistance meaning insulin receptors are desensitized and do not respond to insulin, ultimately decreasing glucose uptake into cells and elevation of blood glucose. This condition is often accompanied by obesity and dyslipidemia [284, 300]. Hyperglycemia in diabetes is a major risk factor for the development of cardiovascular diseases, as it is associated with inflammation and increased oxidative stress, leading to vascular dysfunction. Vascular diabetic complications include retinopathy, cardiomyopathy, and nephropathy [6, 301-304].

It is well established that generation of ROS is highly increased in diabetes and that the onset of diabetes is closely associated with oxidative stress [305-307]. Hyperglycemia can induce oxidative stress via several mechanisms including glucose autoxidation, increased formation of advanced glycation end-products (AGEs), and activation of the polyol pathway [284, 308].

Glucose autoxidation leads to increased levels of NADH and FAD, resulting in disruption of the electron transport chain and production of superoxide [309-311].

AGEs are formed by the non-enzymatic reaction of reducing sugars with proteins, lipids, and nucleic acids with subsequent structural rearrangement [94, 312, 313]. Binding of AGEs to their receptor RAGE ("receptor for advanced glycation end-products") induces a broad proinflammatory response and production of ROS via NOXs [314-316]. Furthermore, by crosslinking with macromolecules AGEs can impair antioxidant systems [304]. In turn, increased oxidative stress promotes new formation of AGEs and RAGE upregulation, leading to a vicious cycle [312, 317, 318]. Thus, increased AGE accumulation may be both a cause and effect of diabetes.

The polyol pathway is a two-step process that converts glucose to sorbitol and then to fructose. Under hyperglycemic conditions this pathway is excessively activated, thereby increasing intracellular and extracellular sorbitol concentrations, reducing NADPH availability, and decreasing levels of nitric oxide and GSH. This decreases the overall reducing capability of the cell, ultimately increasing free ROS levels [284, 309, 319]. Independent of glucose, additional sources of ROS in diabetes can be elevated

circulating factors such as free fatty acids or leptin [320-323]. This increase in ROS formation/levels induces the activation of several transcription factors and signaling pathways involved in the pathogenesis of chronic complications, including protein kinase C (PKC), c-Jun N-terminal kinase (JNK), p38 mitogen-activated protein kinase (MAPK), and nuclear factor kappa-B (NFkB) [6, 324]. Especially endothelial cells are major targets of oxidative damage causing endothelial dysfunction in the target organs.

Increasing evidence demonstrates key roles of epigenetic pathways in the pathogenesis of diabetes [325-329]. Alterations of histone modifications as well as changes in the function or expression of the relevant histone modifiers have been demonstrated in vascular cells under diabetic conditions and in experimental models of diabetes [262, 330-332]. Since these changes persisted in those models even after their removal from the diabetic milieu, epigenetic mechanisms were implicated in the "metabolic memory" (also called "glycemic memory") phenomenon, which refers to the sustained proinflammatory states and increased risk for vascular complications observed in some diabetes patients even long time after intensive glycemic control is instituted [327, 328, 333, 334]. Epigenetic processes in diabetes have repeatedly been reported to appear in a vital crosstalk with oxidative stress [6, 304]. It has been found that the histone acetyltransferase p300 is overexpressed in models of diabetes via pathways that are activated in response to oxidative stress [335, 336]. In comparison, reduced protein levels of the histone deacetylase Sirt1 were observed in diabetic patients or experimental models along with increased global oxidation, reduced GSH levels and accumulation of lipid oxidation products [337, 338]. Therefore, the balance between histone acetylation and deacetylation is altered, increasing the expression of various vasoactive factors and ECM proteins involved in the development and progression of chronic diabetic complications, such as vascular endothelial growth factor (VEGF), endothelin 1 (ET-1), fibronectin (FN), collagen (COL), or transforming growth factor-β (TGF-β) [6, 335-342]. Histone hyperacetylation and transcriptional activation was also observed at inflammation-related gene promoters such as tumor necrosis factor-α (TNF-α) and cyclooxygenase-2 (COX2) [326, 343-345]. Moreover, the repressive mark H3K9me3 was found to be decreased at promoters of inflammatory genes, promoting their expression in diabetic models [331, 346]. In addition, overexpression of growth factors and inflammatory mediators was also observed due to loss of transcription repression in response to downregulation of certain miRNAs in diabetes (e.g. miR-15a, miR-103, miR-107, miR-143, and miRNA-146a) [6, 347]. Decreased levels of miRNA-25 in diabetic nephropathy have been associated with increased NOX4 expression contributing to ROS formation [348]. Alternatively, some miRNAs are found overexpressed in diabetes, such as miR-377, which silences SOD2 and, thus, impairs the antioxidant defense [349]. The oxidative

stress-responsive microRNA miR-195 was shown to mediate Sirt1 downregulation [350]. DNA methylation is also affected by ROS, cytokines or other metabolites in diabetes [351-353] and, conversely, altered DNA methylation patterns can also lead to increased ROS formation. For instance, in diabetic retinopathy active promoter demethylation of the NOX2 subunit Rac1 leads to transcription activation and consequently NOX2-mediated elevation of cytosolic ROS levels [303].

Many more changes in epigenetic mechanisms have been described contributing to the pathogenesis of diabetes [304, 326, 334, 354-357]. Implication of ROS in these effects is very likely, however remains to be investigated in detail.

1.6.1.1 *The SGLT2 inhibitor empagliflozin as a potential treatment for type 2 diabetes*

Glucotoxicity resulting from hyperglycemia is a major risk factor for the development of cardiovascular diseases in diabetes. Therefore, controlling blood glucose is of paramount importance in the prevention of vascular complications. To date, the first-line therapy for T2DM management is the oral medication metformin, which decreases glucose production by the liver and improves insulin sensitivity of body tissues [358]. However, if metformin is contraindicated, poorly tolerated, or inadequately effective, many therapeutic alternatives are available, such as sulfonylureas, thiazolidinediones (TZDs), dipeptidyl-peptidase-4 (DPP-4) inhibitors, or glucagon-like peptide-1 (GLP-1) analogs [359]. Despite the availability of a wide variety of medications, numerous patients with diabetes still fail to achieve acceptable glycemic control, underlining the necessity of more effective medications [360]. A new class of anti-hyperglycemic medications, the gliflozins, have entered the market in 2013. Canagliflozin, dapagliflozin and empagliflozin were approved by the FDA for the treatment of T2DM in subsequent order [361-363]. Gliflozins are inhibitors of the sodium-glucose co-transporter 2 (SGLT2), which is a low-affinity, high-capacity transporter found almost exclusively in the proximal tubules of nephronic components in the kidney (Figure 21) [364]. Under normal circumstances, the adult kidney filters ~180 g of glucose per day and SGLT2 is responsible for the renal reabsorption of >90% of glucose from primary urine into the blood [365, 366]. Inhibitors of SGLT2 (SGLT2i) block the reabsorption of filtered glucose leading to increased urinary glucose excretion (glucosuria). As a result plasma glucose levels are reduced preventing hyperglycemia and glucotoxicity in diabetic patients [367, 368]. Of the gliflozins, empagliflozin (Jardiance®) is the most selective for SGLT2 [369, 370]. In 2015, the EMPA-REG OUTCOME® trial demonstrated that empagliflozin could reduce major adverse cardiovascular events, cardiovascular mortality, hospitalization for heart failure, and overall mortality when given in addition to standard care in T2DM patients at high cardiovascular risk [371, 372]. Ever since, the potential mechanisms underlying cardiovascular benefits of empagliflozin have been subject to extensive research.
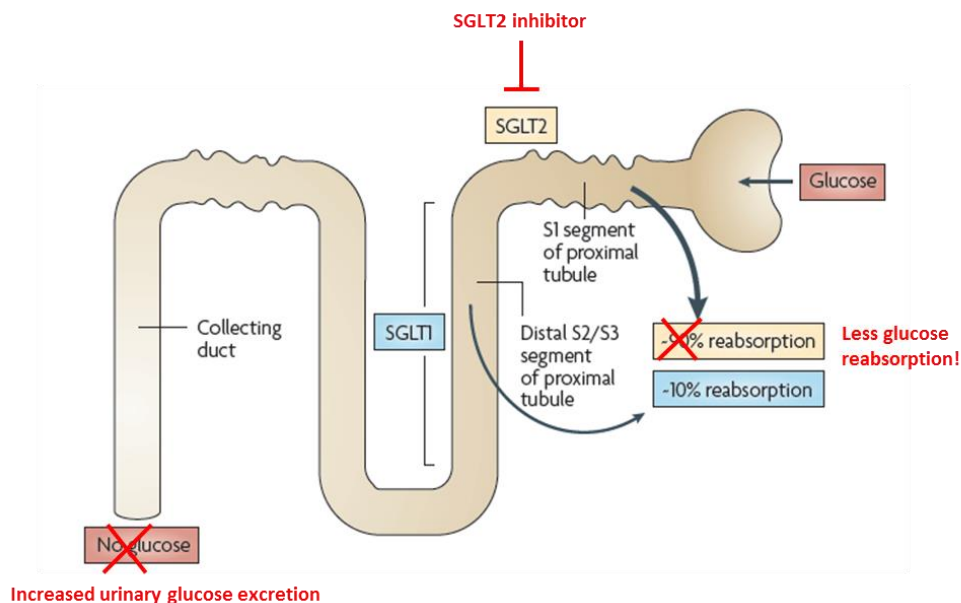
Figure 21 - Mechanism of SGLT2 inhibitors. The sodium-glucose co-transporter 2 (SGLT2) is located in the proximal tubules in the kidney, where it normally mediates reabsorption of ~90% of glucose into the blood (SGLT1 is responsible for reabsorption of the remaining 10%). SGLT2 inhibitors block SGLT2-mediated glucose reabsorption leading to increased urinary glucose excretion lowering blood glucose levels. *Taken and modified from Sushruta Diabetes and Endocrinology Research Trust webpage.*

1.6.2 The role of oxidative stress and epigenetics in response to doxorubicin therapy

The anthracycline doxorubicin (Dox) is a chemotherapeutic agent effective in the treatment of a variety of adult and pediatric cancers [373-376]. However, the benefit of doxorubicin in the clinic is compromised by the risk of development of severe cardiotoxicity. It has been reported repeatedly that patients treated with doxorubicin or its derivatives develop cardiac complications even up to 10-15 years after termination of chemotherapy [375-377]. The probability of developing cardiomyopathy is primarily related to the dosage and duration of treatment, but may also occur at low doses due to increased individual susceptibility (risk factors being age, gender or chronic conditions) [375, 378, 379]. Doxorubicin cardiotoxicity can be acute, occurring within 2-3 days after administration, or chronic, where it is usually evident within 30 days after the last dose, but may occur even 10-15 years after its administration [376]. The incidence of acute cardiotoxicity (manifested as arrhythmias, hypotension etc.) is approximately 11%, but is generally reversible and clinically manageable [376, 379, 380]. However, the incidence of chronic doxorubicin cardiotoxicity, leading to congestive heart failure (CHF), is highly dose-dependent with a documented prevalence of CHF in 5%, 26%, and 48% in patients treated with a cumulative dose of 400, 550 and 700 mg/m^2 doxorubicin, respectively [381]. The prognosis of patients who develop congestive heart failure is poor with a mortality rate of ~50% in 1 year [376, 382, 383].

While doxorubicin acts via a range of different mechanisms in order to combat cancer cells, it is well established that the primary cause of doxorubicin-induced cardiomyopathy is increased cardiac oxidative stress, as evidenced by ROS-induced damage such as lipid peroxidation, along with reduced levels of antioxidants and sulfhydryl groups in respective cell and animal models [375, 384-388]. Elevated ROS levels in response to doxorubicin treatment may result from different mechanisms, such as disruption of the mitochondrial electron transport chain (METC) by doxorubicin either directly through its quinone ring structure, which reacts with mitochondrial enzymes (e.g. NADH dehydrogenase) to undergo redox cycling between quinone and semiquinone states (Figure 22) [380, 389-391], or indirectly via compromising the mitochondrial genome and, thus, mitochondrial biogenesis [392, 393]. Additional to causing mitochondrial dysfunction through ROS formation, doxorubicin also interferes with the mitochondrial membrane phospholipid cardiolipin, further altering mitochondrial bioenergetics [394].
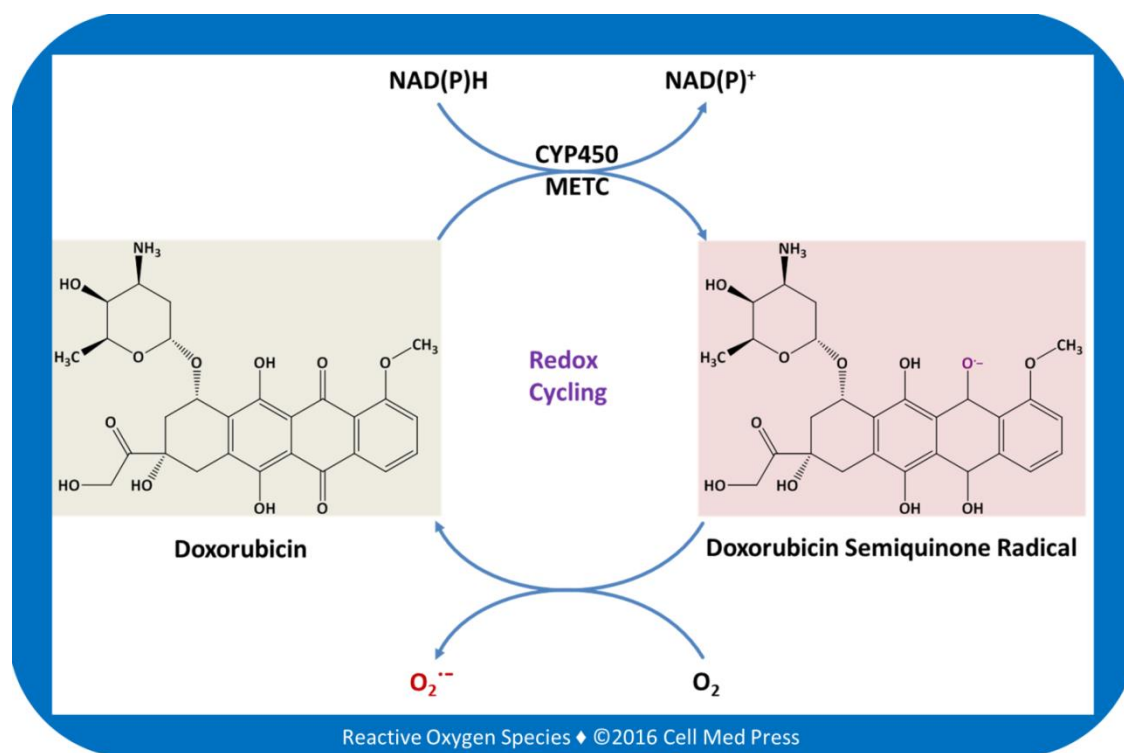
Figure 22 - Doxorubicin redox cycling catalyzed by the cytochrome P450 system (CYP450) and mitochondrial electron transport chain (METC). *Taken from Zhu et al. 2016 [389].*

Cardiac oxidative stress can also be attributed to doxorubicin-mediated activation of ROS-generating enzymes, including NOX2 and its activating subunit Rac1. In animals with disrupted NOX2 activity and in cell models treated with inhibitors of NAD(P)H activity, superoxide generation and cardiotoxic effects in response to chronic doxorubicin treatment were shown to be decreased [395-399]. Another mechanism by which doxorubicin may cause elevated ROS levels is through dysregulation of antioxidant enzymes,

such as glutathione peroxidase-1 (GPx-1), an important hydrogen peroxide degrading enzyme. It has been reported that GPx-1 is readily inactivated upon exposure to doxorubicin in cardiac tissue [400, 401], while GPx-1 deficiency in mice was shown to increase the susceptibility to doxorubicin-induced cardiotoxicity [402]. In line with that, overexpression of GPx-1 was demonstrated to protect mice hearts against doxorubicin-induced cardiotoxicity and prevented impairment of mitochondrial respiration [403]. In addition, it has been demonstrated that up-regulation of the mitochondrial antioxidant enzyme SOD2 counteracted cardiotoxic effects induced by doxorubicin exposure [404-406], whereas deficiency in mitochondrial aldehyde dehydrogenase 2 (ALDH-2), which removes toxic aldehydes resulting from lipid peroxidation, rendered mice more susceptible to doxorubicin-induced cardiac and vascular damage [407].

While it is established that the generation of ROS plays a major role in doxorubicin-induced cardiotoxicity, less is known about the role of epigenetics in this field. Long-term persistence of doxorubicin toxicity suggests an involvement of epigenetic mechanisms that promote the development of cardiac complications even long after cessation of doxorubicin chemotherapy. As it causes mitochondrial dysfunction, it has been proposed that doxorubicin initially disturbs the mitochondrial-dependent production of important cofactors of epigenetic modulators, such as the main acetyl and methyl donors (acetyl-CoA and SAM, respectively), thereby imprinting a long lasting toxic epigenetic memory that manifests itself through an aberrant metabolic transcriptome and metabolome [408]. Epigenetic changes associated to acute doxorubicin toxicity are usually attributable to doxorubicin-induced ROS formation, affecting epigenetic pathways as described in 1.5.

2 Aim

The aim of this thesis was to investigate the crosstalk between redox regulatory pathways and epigenetic processes. It was of interest to investigate ROS-induced epigenetic changes in oxidative stress-related cardiovascular complications. For this purpose suitable models with increased ROS formation had to be established and confirmed. The focus was on detecting changes in expression or activity of epigenetic modifiers, such as HMTs, HDMs, HATs or HDACs, or altered histone methylation and acetylation patterns in response to oxidative stress. Another objective was to establish assays to determine whether exposure to ROS causes redox modifications, such as nitros(yl)ation, nitration or sulfoxidation, within epigenetic enzymes with potential impact on enzyme activity. In addition, specific target genes affected by alterations in epigenetic regulation were supposed to be identified (i.e. by ChIP) and their role in pathological progression to be analyzed.

The ultimate goal was to gain more thorough mechanistic insights into the interplay of oxidative stress and epigenetics in the context of cardiovascular diseases and complications.

3 Materials

3.1 Chemicals and Consumables

Product	Company	Catalog No.
100 µm Meshfilter	Greiner, EASYstrainer	542 000
2-Mercaptoethanol (β-ME)	Sigma	M6250
40% Acrylamide/Bis sol. 29:1	BioRad	1610146
5,5-Dimethyl-1-Pyrroline N-Oxide (DMPO)	Sigma	D5766
Accutase	PromoCell	C41310
Acetonitrile	Promochem	SO-9128-B025
Acrylamide bis solution 40% 29:1	BioRad	1610146
Albumin Fraktion V (BSA)	Roth	8076.3
Aldehyde dehydrogenase (ALDH)	Roche	10171832001
Amersham Protran 0,45µm Nitrocellulose Blotting membrane	GE Healthcare	GE10600002
Ammonium persulfate (APS)	Sigma	A9164
AmplexRed	Molecular Probes	A12222
BenchMark Unstained Protein Ladder	Life technologies	
Bovine Serum Albumin Standard Ampules	Thermo Scientific	23209
Cell culture flasks	Greiner	Various
Cell Culture Multiwell Plates for Adherent Cell Cultures	Greiner	Various
Copper(II)-sulfate (CuSO$_4$)	Roth	P023.1
D(+)-Glucose	Sigma	G8270
Dihydroethidium 95% (DHE)	Sigma	37291
Dimethyl pimelimidate (DMP)	Sigma	21667
Dimethylsulfoxide 99,5%	Sigma	41639
Dithiothreitol (DTT)	Sigma	D0632
DNA LoBind Tubes 1,5ml	Eppendorf	0030108051
Doxorubicin hydrochloride	Tocris	2252
Dynabeads™ M-280 Sheep Anti-Mouse IgG	Thermo Scientific	11201D
Dynabeads™ M-280 Sheep Anti-Rabbit IgG	Thermo Scientific	11203D
Empagliflozin (SGLT2 inhibitor)	Boehringer Ingelheim Pharma GmbH & Co KG	Gift
Ethylene glycol-bis(2-aminoethylether)-N,N,N',N'-tetraacetic acid (EGTA)	Sigma	E4378
Ethylenediaminetetraacetic acid (EDTA)	Sigma	E9884
Fetal bovine serum (FBS)	Gibco	10270-106
Glutathione (GSH)	Sigma	G4251
Glycerol	Roth	3783.1
Hemoglobin from bovine blood	Sigma	08449
Hydrochloric acid	Merck	109057
Interleukin-1β (IL-1β)	Peprotech	200-01B
Isocitrate dehydrogenase type I	Sigma	I1877
Isopropanol	Sigma	34959
L-012 (8-amino-5-chloro-7-phenylpyrido[3,4-d] pyridazine-1,4-(2H,3H)dione sodium salt)	WAKO Chemicals	120-04891
Lysozyme	Sigma	L6876
Methanol 99,8%	Sigma	322415
Milk powder	Roth	T145.2

MNase (Micrococcal Nuclease)	NEB	M0247S
Paraquat (dichloride hydrate)	Riedel de Haen	36541
PBS Dulbecco's Phosphate Buffered Saline	Sigma	D8537
Penicillin-Streptomycin (PenStrep)	Sigma	P0781
PerfeCTa SYBR Green FastMix ROX	Quanta	95073-012
Phenylmethanesulfonyl fluoride (PMSF)	Sigma	P7626
Phosphatase Inhibitor Cocktail	Sigma	P2850
Pierce™ ECL Western Blotting Substrate	Thermo Scientific	32106
Ponceau S / Ponceau Red	Sigma	P5288
Potassium chloride	Sigma	P4504
Potassium dihydrogenphosphate (KH_2PO_4)	Roth	P018.2
Potassium hydrogencarbonate ($KHCO_3$)	Merck	104854
Potassium hydrogenphosphate (K_2HPO_4)	Roth	P749.2
Potassium nitrite (KNO_2)	Merck	1050670250
Precision Plus Protein Standards	BioRad	161-0374
Protease Inhibitor Cocktail	Sigma	P8340
Protein G Magnetic Beads (PureProteome Protein G Magnetic Beads)	Millipore	LSKMAGG02
Protein Kinase Inhibitor	Sigma	P0300
QIAQuick PCR Purification Kit	Qiagen	28104
RAGE Antagonist, FPS-ZM1	Merck	553030
Rat Negative Control Primer Set 1	Active motif	71024
Roche Complete Mini Protease Inhibitor Cocktail	Sigma	04693124001
Roti®-Quant	Roth	K015.1
Simple CHIP Rat GAPDH Promoter Primers	Cell Signaling	7964
SIN-1 chloride	Cayman Chemical	82220
S-Nitrosoglutathione (GSNO)	Sigma	N4148
Sodium butyrate	Sigma	B5887
Sodium chloride	Roth	3957.1
Sodium dodecyl sulfate	Merck	822050
Sodium hydrogenphosphate (Na_2HPO_4)	AppliChem	A1046
Sodium hydroxide solution	Merck	109137
Sodium phosphate monobasic dihydrate	Sigma	71505
Spermine NONOate	Cayman Chemical	82150
Sucrose	Sigma	S9378
SuperSignal™ West Femto Maximum Sensitivity Substrate	Thermo Scientific	34095
Triethanolamine	Sigma	T1502
Tris(hydroxymethyl)-aminomethane (Tris-base)	Sigma	252859
Tris-hydrochlorid (Tris-HCl)	Roth	9090.2
TritonX -100	Sigma	93420
Tween 20	Sigma	P2287

3.2 Antibodies

Product	Dilution	Washing buffer	Blocking buffer	Species	Company	Catalog No.
Anti-4-Hydroxynonenal antibody	1:3000	TBS-T	5% BSA/TBS-T	rabbit	Abcam	ab46545
Anti-acetyl-Histone H3 antibody	1:2500	TBS-T	5% BSA/TBS-T	rabbit	Millipore	06-599
Anti-Actin antibody	1:2500	TBS-T	5% BSA/TBS-T	rabbit	Sigma	A5060
Anti-AGE antibody	1:500	PBS-T	5% BSA/PBS	mouse	Transgenic inc.	KH001
Anti-alpha-Actinin antibody	1:2500	TBS-T	5% BSA/TBS-T	mouse	Sigma	A5044
Anti-beta Tubulin antibody (BT7R)	1:2000	TBS-T	5% BSA/TBS-T	mouse	Thermo Fisher	MA5-16308
Anti-Dityrosine antibody	1:1000	TBS-T	5% Milk/TBS-T	mouse	JaICA	MDT-020P
Anti-DMPO [N1664A] antibody	1:1000	TBS-T	5% Milk/TBS-T	mouse	Stress Marq Bioscience Inc.	SMC-189-D
Anti-GAPDH antibody	1:1000	TBS-T	5% BSA/TBS-T	rabbit	Cell Signaling	2118
Anti-Glutathione Peroxidase 1 antibody	1:1000	PBS-T	5% BSA/PBS-T	rabbit	Abcam	ab22604
Anti-HDAC2 antibody [EPR5001]	1:10000	TBS-T	5% BSA/TBS-T	rabbit	Abcam	ab124974
Anti-Histone H3 (di methyl K9) antibody	1:1000	TBS-T	5% Milk/TBS-T	mouse	Abcam	ab1220
Anti-Histone H3 (di methyl K9) antibody [Y49]	1:1000	TBS-T	5% Milk/TBS-T	rabbit	Abcam	ab32521
Anti-Histone H3 (mono methyl K9) antibody	1:1000	TBS-T	5% BSA/TBS-T	rabbit	Abcam	ab9045
Anti-Histone H3 (tri methyl K4) antibody	1:1000	TBS-T	5% BSA/TBS-T	rabbit	Abcam	ab8580
Anti-Histone H3 (tri methyl K9) antibody	1:1000	TBS-T	5% BSA/TBS-T	rabbit	Abcam	ab8898
Anti-Histone H3 antibody	1:1000	TBS-T	5% Milk/TBS-T	mouse	Active motif	39763
Anti-Histone H3 antibody	1:2000	TBS-T	5% BSA/TBS-T	rabbit	Abcam	ab1791
Anti-Histone H4 antibody	1:1000	TBS-T	5% BSA/TBS-T	mouse	Abcam	ab31830
Anti-KDM1 / LSD1 antibody [EPR6825]	1:10000	TBS-T	5% BSA/TBS-T	rabbit	Abcam	ab129195
Anti-KDM3A / JMJD1A antibody	1:5000	TBS-T	5% BSA/TBS-T	rabbit	Novus Biologicals	NBP1-49601
Anti-Malondialdehyde antibody	1:2000	PBS-T	5% Milk/PBS	rabbit	Abcam	ab27642
Anti-NFkB p65 (D14E12) antibody	1:1000	TBS-T	5% BSA/TBS-T	rabbit	Cell Signaling	8242
Anti-Nitrotyrosine antibody	1:2000	PBS-T	1% Hemoglobin/ PBS-TT	rabbit	Millipore	06-284
Anti-Nitrotyrosine antibody	1:1000	PBS-T	5% Milk/PBS	mouse	Millipore	05-233
Anti-RAGE antibody	1:1000	PBS-T	5% BSA/PBS-T	rabbit	Cell Signaling	4679S
Anti-SETD7 antibody [EPR5574]	1:5000	TBS-T	5% BSA/TBS-T	rabbit	Abcam	ab124708
Anti-SirT1 (1F3) antibody	1:1000	TBS-T	5% Milk/TBS-T	mouse	Cell Signaling	8469
Anti-SMYD1 antibody	1:5000	TBS-T	5% BSA/TBS-T	rabbit	Thermo Fisher	PA5-31482
Anti-S-Nitrosocysteine	1:2000	TBS-T	5% Milk/TBS-T	mouse	A.G. Scientific	N-1078
Anti-S-nitrosocysteine	1:1000	TBS-T	5% Milk/TBS-T	rabbit	Abcam	ab50185
Anti-Trimethyl-Histone H3 (Lys4) antibody	1:2000	TBS-T	5% BSA/TBS-T	rabbit	Millipore	17-614
Anti-Trimethyl-Histone H3 (Lys4) antibody	1:5000	TBS-T	5% BSA/TBS-T	rabbit	Millipore	07-473
Anti-Caspase 3 antibody	1:1000	TBS-T	5% Milk/TBS-T	rabbit	Cell Signaling	9662S
Anti-SOD2 (Mn-SOD) Antibody	1:1000	TBS-T	5% BSA/TBS-T	rabbit	Millipore	06-984
Anti-Fractin antibody	1:1000	TBS-T	5% BSA/TBS-T	rabbit	Millipore	ab3150
Goat F(ab) Anti-Mouse IgG H&L	1:5000	*Same conditions as primary antibody*		goat	Abcam	ab6823
Peroxidase labeled anti mouse made in horse	1:10000	*Same conditions as primary antibody*		horse	Vektor	PI-2000
Peroxidase labeled anti rabbit made in goat	1:10000	*Same conditions as primary antibody*		goat	Vektor	PI-1000

3.3   Media

EA.hy926 culture medium

DMEM (1x) + GlutaMAX™	Gibco	21885-025
10 % FBS	Gibco	10270-106
0.5 % PenStrep	Sigma	P0781

H9c2 culture medium

DMEM High Glucose with L-Glutamine	ATTC	ATTC® 30-2002
10 % FBS	Gibco	10270-106
0.5 % PenStrep	Sigma	P0781

3.4   Buffers

Potassium phosphate buffer

K_2HPO_4 x 3 H_2O	40 mM
KH_2PO_4	10 mM
pH 7.5	

Homogenization buffer

Tris-HCl	20 mM
Sucrose	250 mM
EGTA	3 mM
EDTA	20 mM
Protease inhibitor cocktail	1%
Phosphatase inhibitor cocktail	1%
PMSF	0.5%
TritonX-100	1%

Laemmli buffer (3x)

Tris-HCl (pH 6.8)	0,188 mol (157,6 g/mol)
SDS	60 mmol (288,5 g/mol)
Glycerol	30%
Bromophenol blue	0,01% (669,96 g/mol)
β-Mercaptoethanol	1,5%

SDS-PAGE stacking gel buffer

Tris-HCl	0.5 M
pH 6.8	

SDS-PAGE separation gel buffer

Tris-HCl	1.5 M
pH 8.8	

SDS-PAGE running buffer (10x)

Tris base	250 mM
Glycin	192 mM
SDS	35 mM

Western blot transfer buffer (10x)

Tris base	250 mM
Glycin	192 mM
Methanol	25%

ChIP cell lysis buffer

Saccharose	500 mM
Tris-HCl (pH 7.6)	15 mM
KCl	60 mM
EDTA	0.25 mM
EGTA	0.125 mM
DTT	1 mM
TritonX-100	1%
Protease inhibitor cocktail	1%

ChIP nuclear lysis buffer

Hepes (pH 7.6)	20 mM
NaCl	150 mM
EDTA	1 mM
EGTA	0.5 mM
TritonX-100	1%
SDS	0.15%

ChIP MNase buffer

Tris-HCl (pH 7.6)	20 mM
NaCl	70 mM
KCl	20 mM
$MgCl_2*6H_2O$	5 mM
$CaCl_2*2H_2O$	3 mM

3.5 Cell lines

EA.hy926	*Gift from C.-J. S. Edgell (University of North Carolina, Chapel Hill, USA)*	Immortalized human umbilical vein endothelial cells
H9c2(2-1)	*ATCC® CRL-1446™*	Rat myoblasts

3.6 ChIP Primers

DHFR (promoter): forward GGCCTTCGCTATGACAAATAG, reverse CGCCGCGCATCCTATT;

DHFR (promoter-5'-UTR): forward GGGCCTTCGCTATGACAA, reverse GCTGAGTACCACTAAGGCAGC;

DHFR (intron1): forward AAAGCACCAACACCACCTCC, reverse TCATGTGTGTGCTCAGGCTC;

eNOS: forward CTGGCCCACACTCTTCAAGT, reverse CCTAAGGAAAAGGCCAGGAC;

HO-1: forward CAGAGTTTCCGCCTCCAAC, reverse GTAGTCGCTTGCCTGTCGAG;

IFNγ (promoter): forward GCCCAAGGAGTCGAAAGGAA, reverse AGATAGGTGGCGGGAGCTTA;

IFNγ (intron3): forward AATCGGGCTCTGAGGAGACT, reverse TGAGCTGCATAGCACGAGAG;

NOS2 (promoter-5'-UTR): forward CTGTCAGGGCCACAGCTTTA, reverse TCACCAAGGTGGCTGAGAAG;

NOS2 (intron 2.1): forward TGGGAGTGGTCTAGTGAAGCA, reverse TTTATGGCGGCAGAAGTTGG;

NOS2 (intron 2.2): forward AGGTCGCCAGTCGCGT, reverse AAGTTCCTTGGTGCAGAATCC;

RAGE (promoter): forward GCTGGACCATGCTGCCTAAT, reverse CATTTCCTTCAGCCCACCGA;

RAGE (promoter-5'-UTR): forward TGGGACAAGATGGCAGTTGG, reverse CAGGCTCCTGGTTCTGTCTG.

Control primers

GAPDH:	Simple CHIP Rat GAPDH Promoter Primers	(Cell Signaling 7964)
Gene desert:	Rat Negative Control Primer Set 1	(Active motif 71024)

3.7   Technical Devices

Device	Company
ChemiLux Imager (CsX-1400 M)	Intas
HPLC-column C18-Nucleosil	Macherey & Nagel
HPLC-System	Jasco
ECL plate reader Centro	Berthold Technologies
Magnetic rack (Magna GrIP Rack, 8well)	Millipore
MRX II microplate reader	Dynex Technologies
NanoDrop 2000 UV-Vis spectrophotometer	Thermo Fisher Scientific
NeoLab-Sunlab Rotator	NeoLab
PCR-device StepOnePlus™	Thermo Fisher Scientific
StepOnePlus Real-Time PCR Systems	Thermo Fisher Scientific (Applied Biosystems)
TissueLyser LT	Qiagen
Whatman Minifold I vacuum dot-blot system device	Whatman, GE Healthcare

3.8   Software

Gel-Pro Analyzer, Media Cybernetics

GraphPad Prism 5

PyMol, Version EduPyMOL-v1.7.4.4, Schrödinger

Revelation, Dynex Technologies

StepOne Software v2.3, Applied Biosystems

4 Methods

4.1 Cell culture

4.1.1 Cell maintenance

For general cell maintenance, culture medium was aspirated and cells washed with 0.9% NaCl + 1% penicillin-streptomycin (Sigma P0781). Cells were detached by addition of accutase (PromoCell C41310) followed by a short incubation time at 37°C. Cells were then transferred to a falcon and centrifuged at 100 g for 5 min at RT. Subsequently, the supernatant was removed and the cell pellet resuspended in culture medium. An appropriate amount of cells was transferred to a new culture flask and placed at 37°C.

For experiments, cells were counted manually using a Neubauer chamber and seeded at assay-dependent densities in plates or flasks.

4.1.2 EA.hy926 cell cultivation and induction of hyperglycemia

The human endothelial cell line EA.hy926 was a kind gift from C.-J. S. Edgell (University of North Carolina at Chapel Hill, USA). EA.hy926 cells were grown at 37°C and 10% CO_2 in Dulbecco's Modified Eagle's Medium (DMEM) + GlutaMAX (Gibco 21885-025) supplemented with 10% fetal bovine serum (FBS, Gibco 10270-106) and 0.5% penicillin-streptomycin (Sigma P0781).

For hyperglycemia experiments, EA.hy926 cells were seeded in 6-well plates ($0.2x10^6$ cells/well) or in 96-well plates ($0.1x10^5$ cells/well) and grown until reaching complete adhesion and semi confluence. Semi-confluent EA.hy926 cells were then incubated with medium containing either 5 mM or 35 mM D-glucose (Sigma G8270) and grown for 5 days with daily renewal of medium. Similarly, to induce hyperglycemia and inflammation, semi-confluent EA.hy926 cells were incubated with either 5 mM D-glucose, 25 ng/ml IL-1β (Peprotech 200-01B) or a combination of IL-1β and 35 mM D-glucose for 48 h. Culture and hyperglycemia conditions were previously published by Karbach *et al*. [409], whereas the hyperglycemia/inflammation protocol was modified from a publication by Deshwal *et al.* [410].

4.1.3 HUVEC cultivation and induction of hyperglycemia

Human umbilical vein endothelial cells (HUVECs) were obtained from Academic Teaching Hospital in Frankfurt am Main/Höchst and Katholisches Klinikum Mainz St. Vincenz- und Elisabeth-Hospital. Isolation of HUVECs was conducted by Angelica Karpi. HUVECs were isolated by collagenase digestion as described by Baudin *et al.* [411] and cultured in endothelial cell growth medium (ECGM, Promocell C22110) mixed

1:1 with M199 (Sigma M4530) containing 20% FBS (Gibco 10270-106), 0.5% penicillin-streptomycin (Sigma P0781) and 1% L-glutamine (Sigma G7513) at 37 °C and 5% CO_2.

For hyperglycemia experiments, the cells were seeded into 6-well plates (0.6×10^6 cells/well) and grown until confluency was reached. On "day 0" the experiment was started by changing the medium to M199 only containing 10% FBS (Gibco 10270-106), 0.5% penicillin-streptomycin (Sigma P0781) and 1% L-glutamine (Sigma G7513). Cells in one plate were cultured under normoglycemic (NG) conditions (5 mM glucose) and cells in 6 other plates were grown under hyperglycemic (HG) conditions (30 mM glucose). On "day 3" of normo- and hyperglycemic conditions the treatment with the SGLT2i empagliflozin, the dipeptidyl peptidase-4 inhibitor sitagliptin or the RAGE inhibitor FPS-ZM1 was started at concentrations of 1 µM or 10 µM (each stock in DMSO prepared for 1:1000 dilution) for another 2 or 3 days. The medium containing the different drugs or the solvent was changed daily. Cells were photographed each day until "day 6" and living cells were manually counted using the Cell B software (Olympus).

In order to measure nitrite formation in hyperglycemic HUVEC cells, on "day 6" the cells were stimulated with 1 µM acetylcholine for 30 min at 37 °C and the supernatant was subjected to HPLC analysis of nitrite (see 4.10).

4.1.4 H9c2 cell cultivation and doxorubicin treatment

Rat myoblast H9c2 cells were acquired from ATCC (CRL-1446™). H9c2 cells were grown at 5% CO_2 in ATTC High Glucose DMEM (ATTC 30-2002) supplemented with 10% fetal bovine serum (Gibco 10270-106) and 0.5% penicillin-streptomycin (Sigma P0781), according to supplier's (ATCC) instructions.

Special care had to be taken when cultivating H9c2 cells, as they start differentiating from myoblasts to cardiomyocytes upon confluency and therefore stop dividing. To avoid loss of the myoblastic population, it was necessary to subculture the cells before they became confluent (at around 70-80% confluency).

For doxorubicin treatment H9c2 cells were seeded in six T75 culture flasks (75 cm^2 growth area) at 0.75×10^6 cells per flask and grown for 7 days until a multinucleated, elongated phenotype was observed (differentiation into cardiomyocytes/myotubes). Medium was renewed twice during this time. On day 7 medium was exchanged to either untreated medium or medium containing 1 µM or 5 µM doxorubicin (Tocris 2252). Cells were then incubated for 24 h and 48 h before being lysed and subjected to further investigation. Of note, also detached apoptotic cells from the medium supernatant (SN) were included in the analyses. Figure 23 shows the preparation of H9c2 cell pellets for the purpose of subsequent lysis

and protein extraction. Due to its red color, the amount of doxorubicin-uptake in the cells is clearly visible.
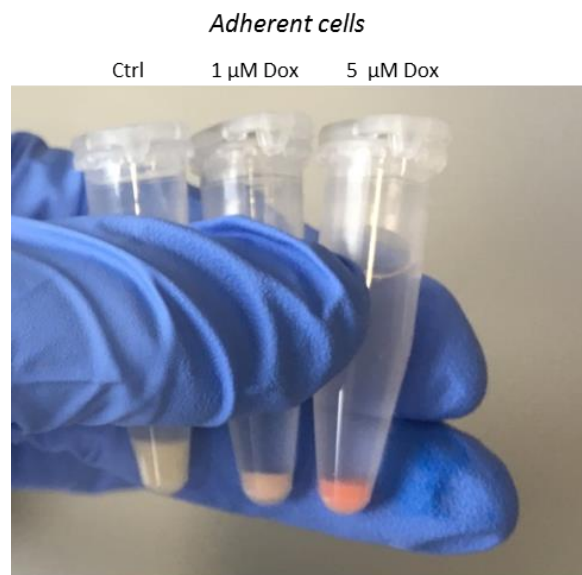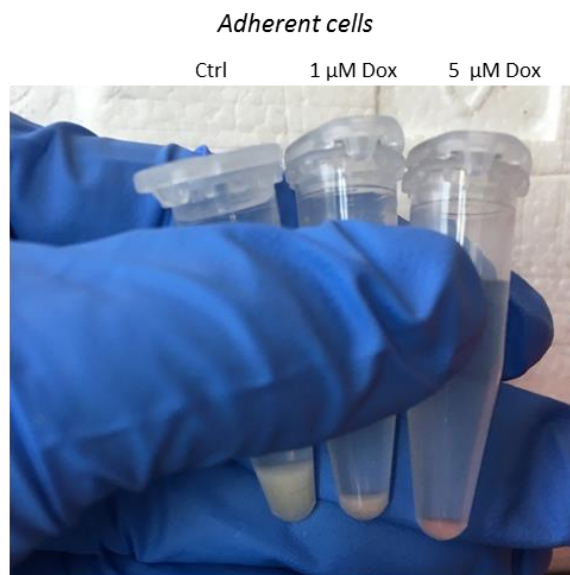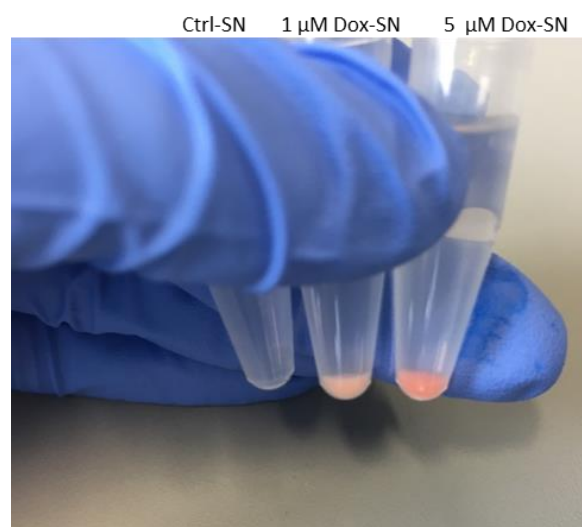
Figure 23 - H9c2 cell pellets were prepared for subsequent lysis and protein extraction. After 24 h (left) or 48 h (right) of incubation with doxorubicin adherent cells were stripped from the flasks using accutase. Floating apoptotic cells were collected from the medium. All fractions were washed and pelleted by centrifugation. The red color visualizes the amount of doxorubicin-uptake in the cells.

4.2 In vivo treatment of ZDF T2DM animal model

Animal treatment was performed by Matthias Oelze and Sebastian Steven as published by Steven *et al.* [412]: All animals were treated in accordance with the Guide for the Care and Use of Laboratory Animals as adopted by the U.S. National Institutes of Health and approval was granted by the Ethics Committee of the University Hospital Mainz and the Landesuntersuchungsamt Rheinland-Pfalz (Koblenz, Germany; permit number: 23 177-07/G 12- 1-025). As a model of T2DM Zucker Diabetic Fatty (ZDF) rats were used.

A total number of 35 diabetic ZDF rats (ZDF-Lepr$^{fa/fa}$) and respective 16 lean controls (ZDF-Lepr$^{+/+}$) were directly ordered from Charles River at an age of 16±1 weeks. Rats were fed with Purina 5008 chow and divided into 4 treatment groups: lean control rats (ZDF-Lepr$^{+/+}$, Ctr), type 2 diabetic rats (ZDF-Lepr$^{fa/fa}$, ZDF), type 2 diabetic rats on SGLT2i low dose (10 mg/kg/d p.o.) or SGLT2i high dose (30 mg/kg/d p.o.) treatment via drinking water. After 6 weeks of treatment duration, animals were killed under isoflurane anesthesia by transection of the diaphragm and removal of the heart and thoracic aorta. Hyperglycemia as a marker for type 2 diabetes was assessed by glucose levels and glycosylated hemoglobin (HbA1c) in whole blood using the ACCUCHEK Sensor system from Roche Diagnostics GmbH (Mannheim, Germany) and A1C Now^{+} system from Bayer HealthCare Diabetes Care (Basel, Switzerland), respectively.

4.3 Tissue homogenization/ Cell lysis

Frozen tissue from experimental animals was pulverized using a liquid nitrogen-cooled ceramic mortar and pestle and transferred to Eppendorf tubes kept on liquid nitrogen. Subsequently, an estimated equal volume of homogenization buffer was added to the amount of tissue powder present in each Eppendorf tube and vortexed vigorously. Similarly, cultivated cells were washed, detached by addition of accutase and pelleted by centrifugation. Pellets were then resuspended in cold homogenization buffer and vortexed vigorously. Resulting homogenates were incubated on ice for 1 h to allow cell swelling and membrane disruption. Afterwards, samples were centrifuged for 15 min at 10000 g at 4°C. The supernatants containing the protein were transferred into new Eppendorf tubes and stored at -20°C until further use. The obtained pellets made up of cell debris and DNA were kept for subsequent histone acid extraction in cases needed.

4.4 Histone acid extraction

Remaining pellets from tissue/cell lysis were resuspended in 0.2 M HCl, using roughly half the volume that had been used previously for lysis. Samples were then rotated over night at 4°C for acidic extraction of histones. Thereupon, samples were centrifuged at 6500 g for 10 min at 4°C. The supernatant, which contained the histone fraction, was saved and transferred into a new Eppendorf tube. HCl was neutralized with 2 M NaOH at 1/10 of the volume of the supernatant. Samples were kept at -20°C until further analysis. This protocol was modified from the histone extraction protocol provided by Abcam.

4.5 Quantitative protein determination by Bradford assay

All protein concentration measurements were compared to a standard curve generated from dilutions of bovine serum albumin (BSA) at 0, 1, 5, 10, 20 and 30 µg/ml in H_2O. Lysates were diluted in H_2O (1:200 dilution for cells, 1:600 dilution for tissue) and 80 µl of each sample was transferred to a 96-well plate in quadruplicates. Subsequently, 200 µl of the reagent Roti® Quant (Roth K015.1) were added to each well and thoroughly mixed, before absorption values of the plate were measured by a MRX II plate reader (Dynex Technologies) at 595 nm. The results were assessed using the associated application program Revelation (Dynex Technologies).

This protocol is based on the method described by Bradford in 1976 [413].

4.6 Western blot analysis

Protein expression or modification was assessed by Western blot analysis. Proteins were denatured by incubation with Laemmli buffer for 5 min at 95°C. Equal amounts of total protein were loaded onto polyacrylamide gels and electrophoresis was conducted in SDS-PAGE running buffer at 120 V until the desired separation of proteins was reached, as was observed using Western blot protein markers. Subsequently, proteins were transferred from each gel onto a Protran BA85 (0.45 mm) nitrocellulose membrane by tank-blotting in ice-cold transfer buffer for 135 min at 250 mA. Afterwards, loading and transfer were controlled by staining with Ponceau S dye. Washed membranes were then blocked with suitable blocking buffer for 90 min at RT before being incubated with primary antibodies at their appropriate dilution in blocking buffer over night at 4°C. The next day, following three washing steps (5 min each) with correspondent buffers, membranes were incubated with horseradish peroxidase (HRP)-conjugated secondary antibodies (diluted in the same blocking buffer as the primary antibody) for 90 min at RT. Afterwards, membranes were again washed three times for 5 min with correspondent buffers. For visualization Pierce™ ECL Western Blotting Substrate was applied and antibody-specific

chemiluminescent bands on the membranes were captured with ChemiLux Imager (CsX-1400 M, Intas). Densitometric quantification was performed using Gel-Pro Analyzer software (Media Cybernetics).

Western blot analysis was performed according to an established protocol previously published by Oelze *et al.* [414-416] with minor modifications. All antibodies, dilutions and buffers that were applied are listed in the Materials section (3.2, p.47).
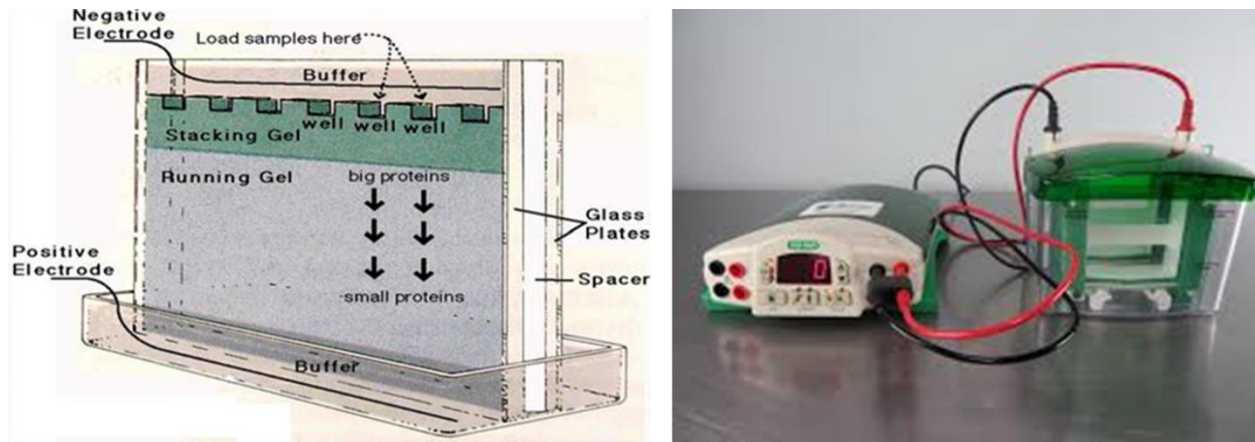
Figure 24 - Illustration of an apparatus used for SDS PAGE. (Left) Scheme of a SDS gel electrophoresis chamber composition and sample application. *Image taken from Roy and Kumar 2012 [417].* **(Right)** Bio-Rad PowerPac Basic Mini Electrophoresis System.

4.7   Dot blot analysis

Analysis of total protein content was performed by dot blot. For this, equal amounts (usually ~20 µg) of protein homogenates were diluted in PBS and each sample was applied to a buffer-soaked nitrocellulose membrane using a Minifold I vacuum dot-blot system device (Whatman, GE Healthcare) with a 96-well top frame (see Figure 25). Vacuum was generated by connecting the dot blot device to a water pump jet. This allowed the aspiration to the membrane of samples in each well. Subsequently, the membrane was removed from the dot blot device and dried for 1 h at 60°C to immobilize proteins on the membrane surface. Equal loading of protein amounts per well/dot was then verified by staining the membrane with Ponceau S. Blots were then blocked with suitable blocking buffer for 90 min at RT before being incubated with primary antibodies at their appropriate dilution in blocking buffer over night at 4°C. The next day, following three washing steps (5 min each) with correspondent buffers, membranes were incubated with horseradish peroxidase (HRP)-conjugated secondary antibodies (diluted in the same blocking buffer as the primary antibody) for 90 min at RT. Afterwards, membranes were again washed three times for 5 min with correspondent buffers. For visualization Pierce™ ECL Western Blotting Substrate was applied

and antibody-specific chemiluminescent dots on the membranes were captured with ChemiLux Imager (CsX-1400 M, Intas). Densitometric quantification was performed using Gel-Pro Analyzer software (Media Cybernetics).

Dot blot analysis was performed according to an established protocol previously published by Oelze *et al.* [414-416] with minor modifications. All antibodies, dilutions and buffers that were applied are listed in the Materials section (3.2, p.47).
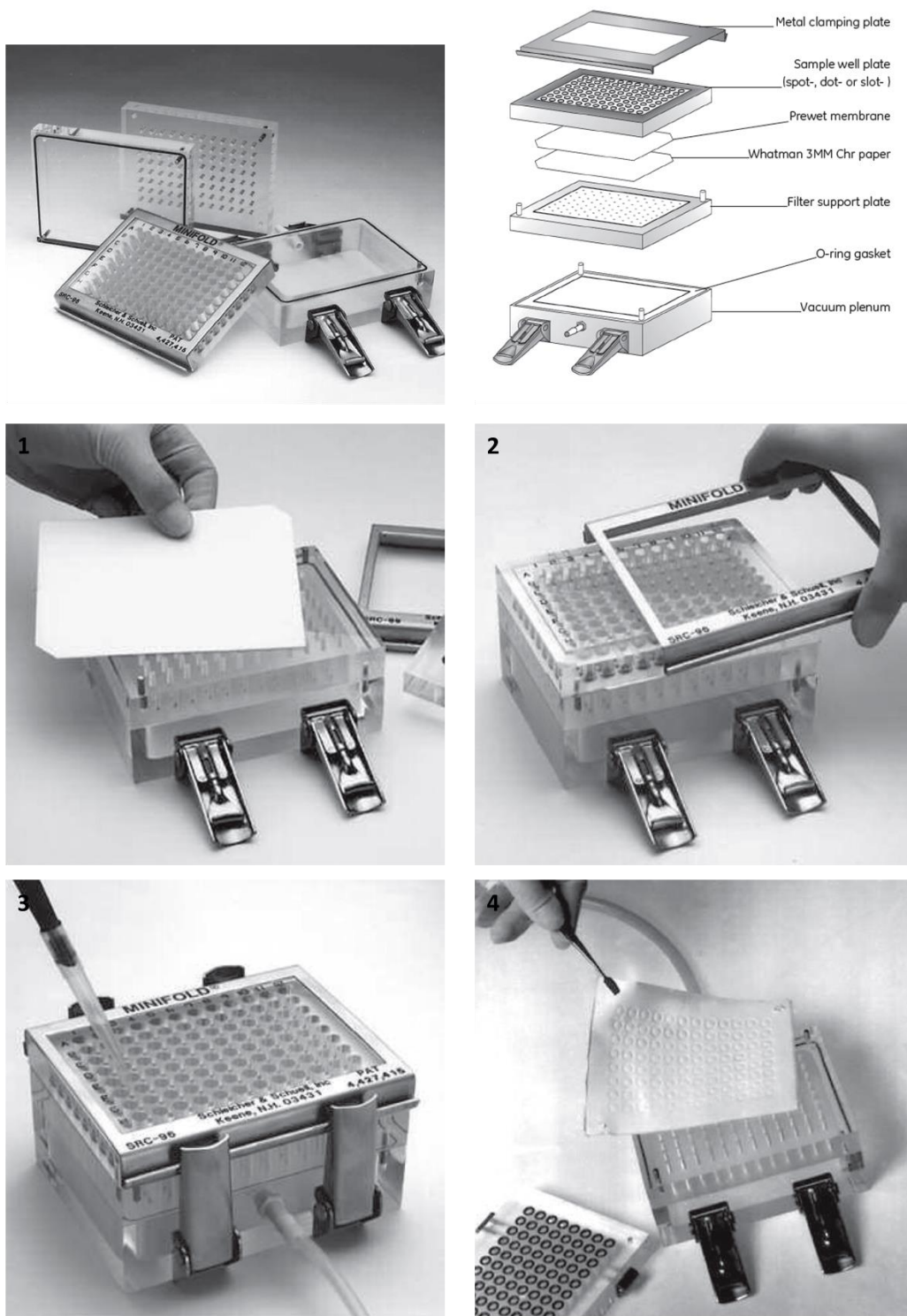
Figure 25 - **Dot blot system set-up and procedure. (Top)** Components of the Minifold I vacuum dot-blot system device and assembly. **(1)** Placement of prewet membrane and filter paper on the filter support plate on top of the vacuum plenum. **(2)** Tightening by placing the clamping plate on top of the sample well plate and clamping with adjustable stainless steel latches. **(3)** Application of samples into wells during vaccum generation **(4)** Removal of membrane and filter papers. *Images taken from the Minifold I System set-up protocol provided by GE Healthcare.*

4.8   Protein S-nitrosylation and DMPO-spin trapping

Aldehyde dehydrogenase or isocitrate dehydrogenase were diluted in potassium phosphate buffer (pH 7.5) and 1 mg protein loaded per Eppendorf tube. Nitrosylation agents were each added 1:100 from stock solutions resulting in final concentrations of 1 µM SPENO/1 µM Sin-1, 10 µM SPENO/10 µM Sin-1, 100 µM SPENO/100 µM Sin-1, 1 mM SPENO and 20 mM KNO_2 (in 0.2 M HCl). The high concentration of SPENO (1 mM), as well as 20 mM acidic KNO_2 both served as positive controls. Samples were then incubated at 37°C for 90 min to enable the formation of S-nitroso groups on the reactive cysteines of the proteins.
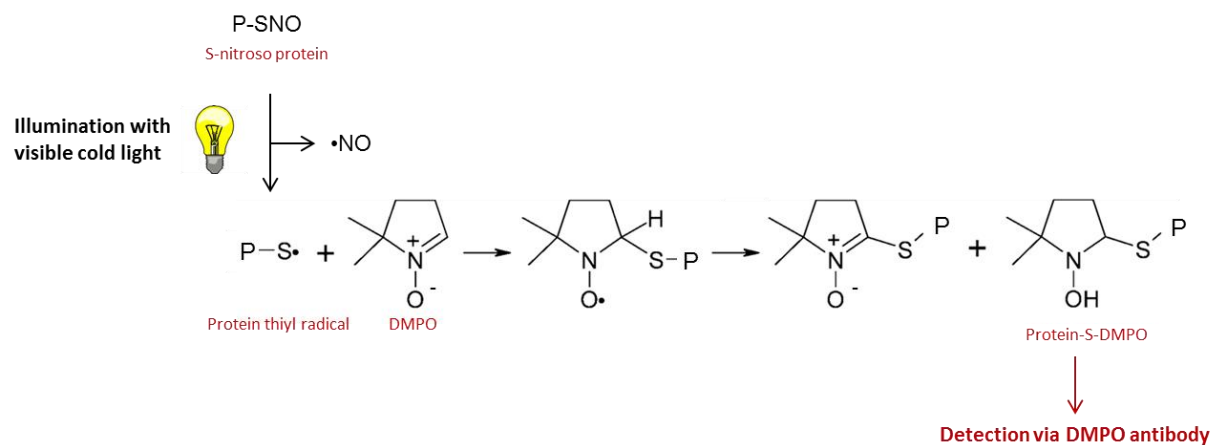
Figure 26 - (Top) Spin-trapping of protein thiyl radical by DMPO. *Edited graph from Sengupta et al.2009 [418].* **(Bottom) Photograph of Eppendorf tubes containing nitros(yl)ated protein being illuminated.**

After incubation, each sample was treated with 20 mM DMPO and illuminated with visible light with a wavelength of >420 nm for 30 min. It has been shown that upon irradiation with visible light, protein-S-nitrosothiols undergo photolytic homolysis to $^{\bullet}$NO and protein thiyl radicals, which can be spin trapped by DMPO forming a thioether and upon rearrangement a stable thionitrone product (Figure 26) [418]. The formation of protein-DMPO adducts is representative for S-nitros(yl)ation. To quantify protein S-nitros(yl)ation, samples were subjected to dot blot analysis using a DMPO-specific antibody.

4.9   HPLC analysis of ROS formation

Cellular ROS formation was measured by HPLC-based fluorescence detection of 2-hydroxyethidium (2-HE) or resorufin via HPLC. Fluorescent 2-HE is formed upon oxidation of non-fluorescent dihydroethidium (DHE) and is specific for the detection of superoxide, whereas resorufin is an indicator for hydrogen peroxide formation as it is formed from the reaction of Amplex Red with H_2O_2 in presence of horseradish peroxidase (Figure 27). Cells were treated either with 50 µM DHE or with 100 µM Amplex Red/0.1 µM HRP in PBS and incubated for 60 min at 37°C. To measure oxidation of Amplex Red by extracellular H_2O_2, 200 µl of cell supernatant were directly transferred to an HPLC vial and resorufin fluorescence was measured. For extraction of DHE oxidation products an equal volume of acetonitrile was added to the cells, inducing protein precipitation and therefore cell lysis. Cells were scraped from the culture wells, transferred to an Eppendorf tube and centrifuged at 20000 g for 15 min at 4°C. 200 µl of the supernatant were transferred to a vial and subjected to HPLC analysis.

The HPLC system consisted of a control unit, two pumps, mixer, detectors, column oven, degasser, and an autosampler (AS-2057 plus) from Jasco and a C18-Nucleosil 100-3 (125×4) column from Macherey &Nagel. A high pressure gradient was applied with the organic solvent acetonitrile (90 vv% acetonitrile/10 vv% water) and 25 mM citrate buffer, pH 2.2, as mobile phases.

2-hydroxyethidium and ethidium levels were measured using the following percentages of the organic solvent: 0min, 36%; 7 min, 40%; 8-12 min, 95%; 13min, 36%. The flow was 1 ml/min and DHE was detected by its absorption at 355 nm, whereas 2-HE and ethidium were detected by fluorescence (Ex. 480 nm/Em. 580 nm) (Figure 28 A). Typical retention time of 2-HE was 3.5 min. The signal was normalized to a 1.25 µM 2-HE standard.
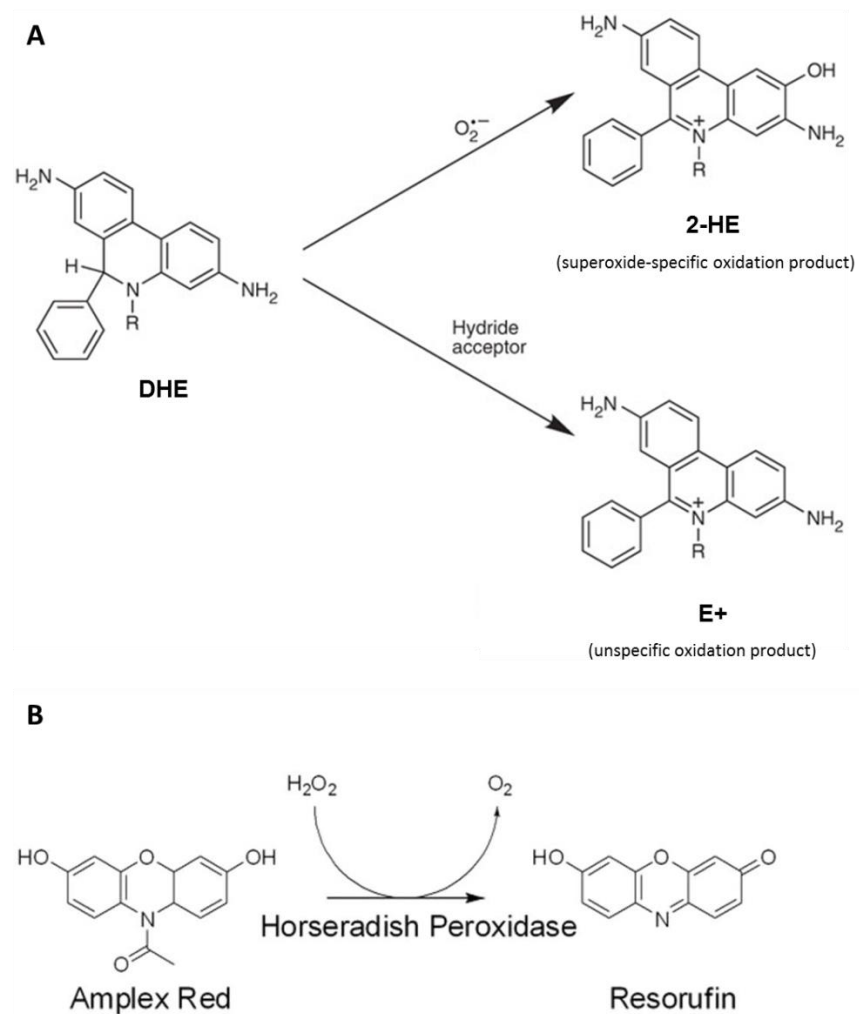
Figure 27 - Reaction scheme of (A) DHE oxidation by superoxide resulting in the fluorescent products 2-hydroxyethidium (2-HE) and the unspecific oxidation product ethidium (E$^+$), and (B) Amplex Red oxidation by H$_2$O$_2$ resulting in fluorescent resorufin.

Resorufin levels were measured using the following percentages of the organic solvent: 0 min, 41%; 7 min, 45%; 8-9 min, 100%; 10–12 min, 41%. The flow was 1 ml/min, compounds were detected by their absorption at 300 nm, and resorufin was also detected by fluorescence (Ex. 570 nm/Em. 590 nm) (Figure 28 B). Typical retention time of resorufin was 2.8 min. The signal was normalized to a 5 µM resorufin standard.

HPLC analysis of 2-HE and resorufin was performed according to a previously published method [419, 420].
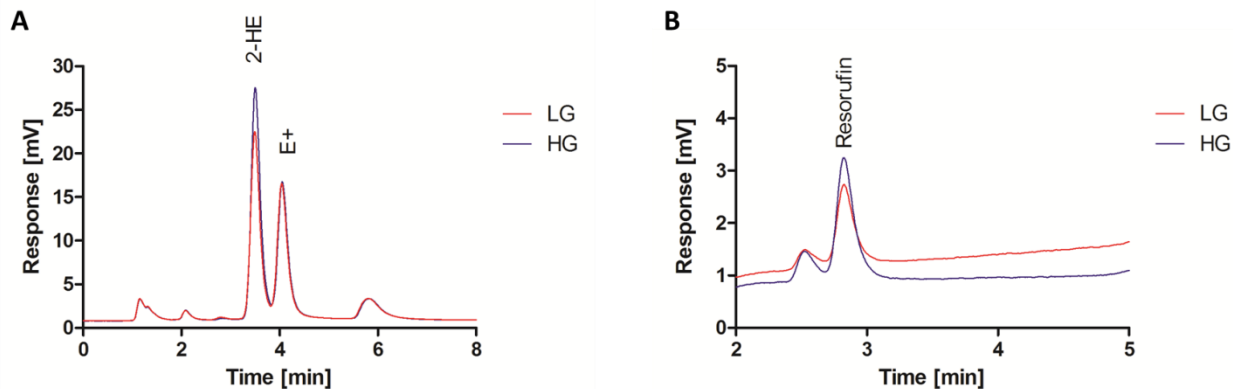
Figure 28 - Representative chromatograms of HPLC-mediated fluorescence detection of (A) 2-hydroxyethidium (2-HE) and ethidium (E[+]) and (B) resorufin. *Graphs are derived from data of EA.hy hyperglycemia experiments.*

4.10 HPLC analysis of nitrite formation

Nitrite formation in response to stimulation with acetylcholine was determined in HUVECs. For this purpose, the cells were stimulated with 1 µM acetylcholine for 30 min at 37 °C. Subsequently, the supernatant medium containing the produced nitrite was mixed 1:1 with 1 M HCl containing 200 µM 2,3-diaminonaphthalene and incubated for 10 min at 37 °C. Under acidic conditions nitrite will form a highly fluorescent triazol product with 2,3-diaminonaphthalene. 50 µl of the supernatant were subjected to HPLC analysis.

The system consisted of a control unit, two pumps, a mixer, detectors, a column oven, a degasser, an autosampler (AS-2057 plus) from Jasco (Groß-Umstadt, Germany), and a C18-Nucleosil 100-3 (125 × 4) column from Macherey & Nagel (Düren, Germany). A high-pressure gradient was employed with solvent B (acetonitrile/water 90:10 v/v%) and solvent A (25 mM citrate buffer pH 2.2) as mobile phases with the following percentages of the organic solvent B: 0 min, 30%; 8 min, 65%; 8.5‑9 min, 100%; and 9.5 min, 30%. The flow was 1 ml/min, and the triazol product was detected by its fluorescence (Ex. 375 nm/Em. 415 nm). Nitrite concentrations were quantified by external standards. The background nitrite signal of the culture medium was subtracted from the determined nitrite values.

4.11 L-012 measurement of cellular ROS formation

The dye L-012 (8-amino-5-chloro-7-phenyl-pyrido[3,4-d]pyridazine-1,4(2H,3H)dione), a luminol analogue, is a highly sensitive chemiluminescent probe, which detects a variety of intracellular or extracellular ROS or RNS (Figure 29). In order to measure cellular ROS formation, treated EA.hy cells grown in 96-well plates were washed with NaCl before addition of 100 µl NaCl per well. Subsequently, 100 µl of PBS buffer

containing 200 µM L-012 was added yielding a final concentration of 100 µM L-012. The chemiluminescence was monitored at intervals of 10min over 40 min with an ECL plate reader Centro (Berthold Technologies, Bad Wildbad, Germany), and the signal at 10 min was expressed as counts/s.

L-012 measurement was modified from a previously published protocol by Daiber or Oelze et al. [113, 414, 421]
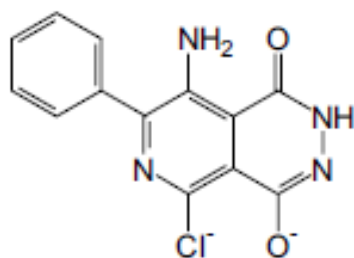
Figure 29 - Structure of L-012. Taken from Halliwell *et al. 2004* [122].

4.12 Immunoprecipitation with magnetic beads

Magnetic beads (anti-rabbit or anti-mouse, Thermo Scientific) in an Eppendorf tube were washed three times with PBS/0.1% BSA using a magnetic rack. In this procedure beads are first resuspended in buffer, then the magnetic force assembles the beads in one spot and the fluid can be removed without touching the beads (Figure 30, bottom). Subsequently, the relevant antibody was added to the beads in a volume recommended by the manufacturer. This suspension was then rotated over night at 4°C to allow antibody binding to the beads. On the next day, the antibody was crosslinked to the beads. For this the antibody-loaded beads were washed twice with triethanolamine (TEA, pH 8.2), thereby removing any unbound antibodies. Then the beads were resuspended in 20 mM dimethyl pimelimidate (DMP) diluted in TEA and rotated for 30 min at RT. Afterwards, beads were resuspended in 50 mM Tris (pH 7.5) and rotated for 15 min at RT, followed by three washing steps with PBS/0.1% BSA. Next, precipitation was induced by adding the protein homogenate in an assay-dependent concentration to the beads and incubating the mixture for 2 h at 4°C while rotating. Subsequently, beads were washed three times for 5 min each with PBS/0.2% Triton-X and a final time with PBS for 5 min at RT under rotation in order to remove any unbound material. Finally, 1x concentrated Laemmli buffer containing β-mercaptoethanol was added to the beads, vortexed and incubated at 95°C for 5 min to denature the antibody-antigen link. To rid the precipitated protein completely from the antibody-crosslinked beads, the mix was transferred

to the magnetic rack and the supernatant containing the precipitate removed into a new tube. The remaining beads were then discarded.

The protocol was modified from the immunoprecipitation protocol provided by the magnetic bead manufacturer (Thermo Scientific).
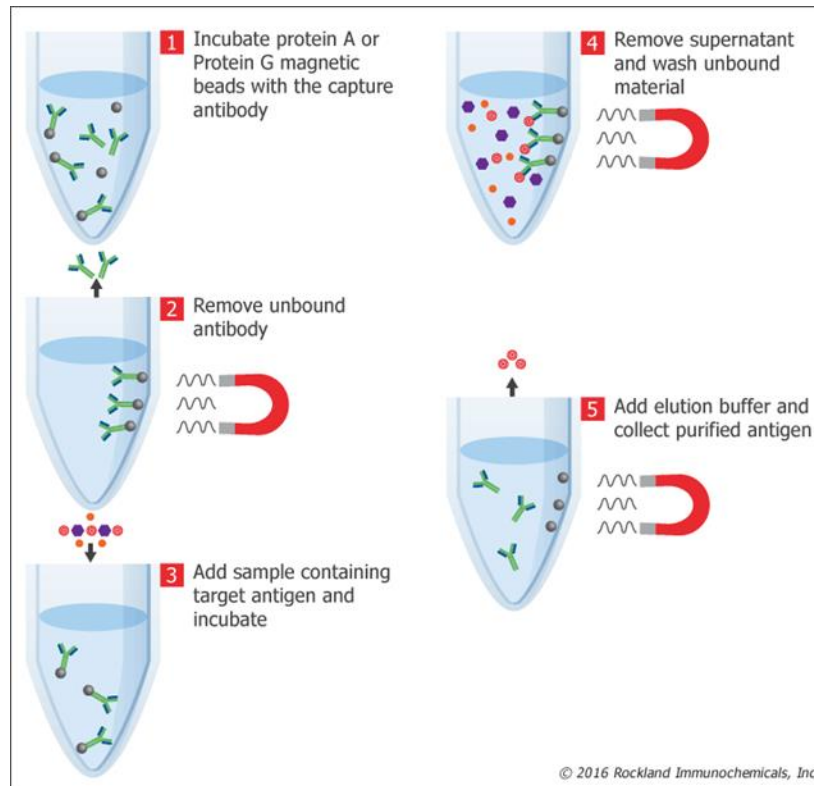
Figure 30 - (Top) Scheme of immunoprecipitation procedure. (Bottom) Representative image of a magnetic rack, as well as sample purification by bead assembly at the magnet and removal of supernatant. *Images taken and compiled from websites of Rockland Immunochemicals, Cell Signaling and Fisher Scientific.*

4.13 Native chromatin immunoprecipitation (ChIP)

Rat kidney samples were homogenized in liquid nitrogen and 50 mg of pulverized kidney was used per ChIP experiment. Samples were resuspended in PBS supplemented with protease inhibitors and further comminuted in a TissueLyser LT (Qiagen) for 3 min at 50 Hz. Single cells were obtained by filtering the suspension through a 100 µm mesh filter (Greiner). The cells were then pelleted by low-speed centrifugation (3000 g, 4 min) and lysed in ChIP cell lysis buffer containing protease inhibitors. DNA was fragmented using Micrococcal Nuclease (NEB, 2000 gel units) to an average DNA fragment size of 300-400 bp. The nuclear membrane was broken using ChIP nuclear lysis buffer containing TritonX and SDS. Ten µg of DNA was used for each ChIP experiment and 1% (0.1 µg) DNA was retained as input control. Immunoprecipitations were performed by overnight incubation of the chromatin samples with protein G magnetic beads (Millipore) and 3 µg of the respective antibodies. Antibodies used were Anti-Histone H3 (tri-methyl K9) antibody (abcam ab8898) and Anti-Histone H3 (trimethyl K4) antibody (Millipore 07-473). After removal of the beads, the eluate was purified with the QIAQuick PCR Purification Kit (Qiagen 28104). Immunoprecipitated DNA was subjected to qPCR analysis using specifically designed primers for HO-1, eNOS, DHFR, IFNγ, iNOS, and RAGE (HO-1 and eNOS primers were a kind gift from Prof. Li). Chip data were calculated relative to DNA input. Primer sequences for ChIP-qPCR are listed in the Materials section (3.6).

In order to test successful extraction of DNA containing the corresponding histone marks (H3K4me3 or H3K9me3), each ChIP precipitate was validated by qPCR-based quantification of the constitutively active gene GAPDH, as well as a genomic region that is devoid of protein-coding genes ("gene desert"). For this purpose commercial ChIP primers were applied: Simple CHIP Rat GAPDH Promoter Primers (Cell Signaling 7964) and Rat Negative Control Primer Set 1 (Active motif 71024). A ChIP was considered valid when high levels of GAPDH and low levels of gene desert were detected by qPCR in chromatin derived from H3K4me3-mediated ChIP, while H3K9me3-mediated ChIP resulted in low levels of GAPDH and high levels of gene desert, in relative terms.

Of note: As histones are closely wrapped around DNA and are therefore naturally linked, it is not necessary to perform a cross-linking step between chromatin and protein. Native chromatin is applied in the assay, hence the term "native ChIP".
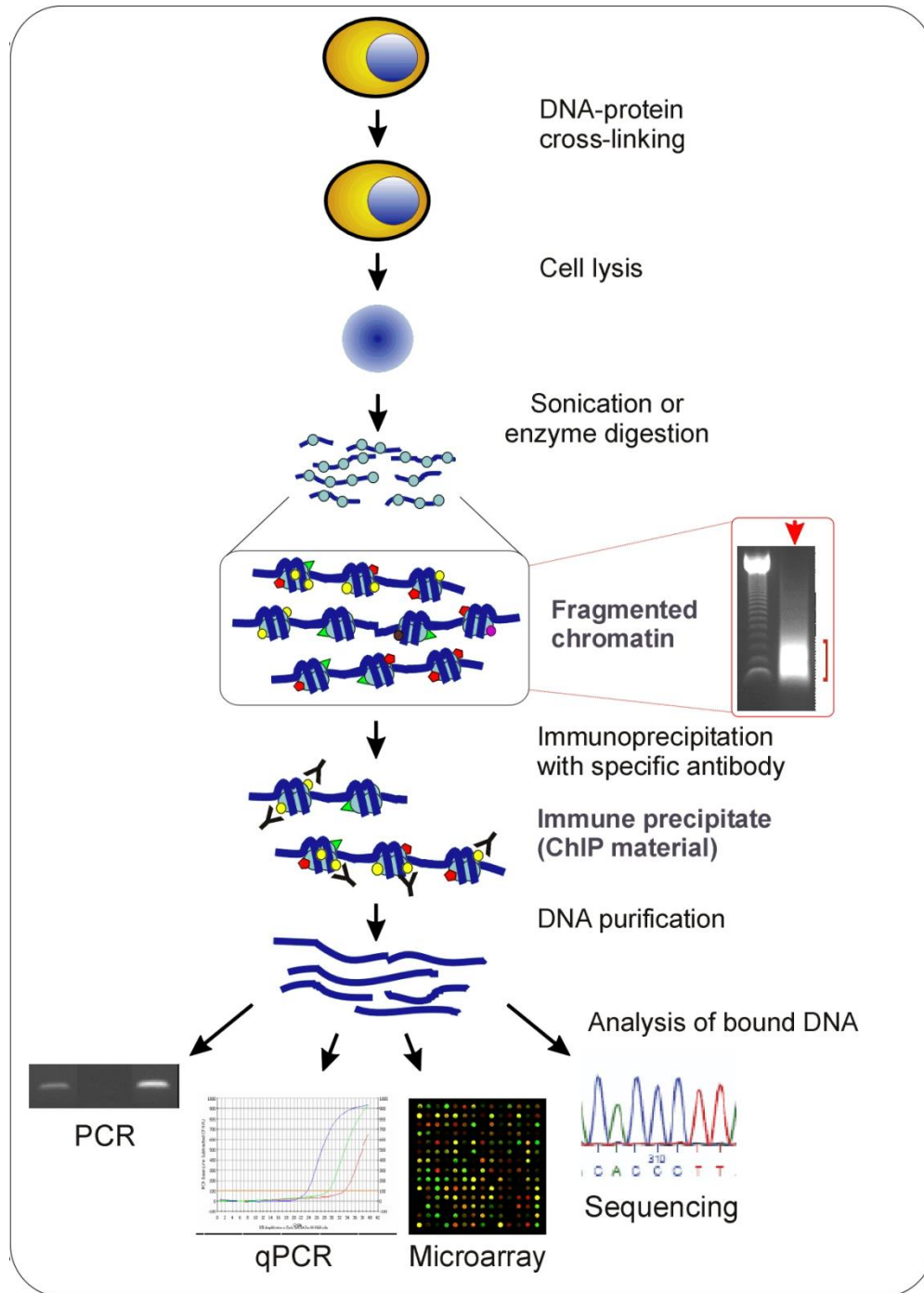
Figure 31 - ChIP assay procedure. *Taken from Collas & Dahl 2008 [422].*

4.14 ChIP primer design

Since there is no ChIP primer repository/database available thus far, several steps were devised in order to develop optimal qPCR primers for the genes DHFR, eNOS (NOS3), HO-1 (HMOX1) (C), interferon-γ (IFNG), NOS2 and RAGE (AGER). At first, data about the respective gene was collected using UCSC genome browser (Figure 32). Here, data of genomic histone mark distribution of human H3K4me1/3 and H3K27Ac is available, however not for other histone modifications such as H3K9me3. In general, H3K4me3 is mostly enriched within promoter regions, but can also be found in regulatory regions promoting transcription enhancement [151, 423, 424]. The region around the transcription start site (TSS) is usually nucleosome-depleted, thus free from any histone modifications. Also, H3K4me3 marks often appear in proximity to CpG islands. Unfortunately, no such database is offered for mouse or rat yet. Therefore, genomic regions, where high accumulation of H3K4me3 signal was indicated in the human database, were zoomed in to base level in the UCSC browser table (Figure 33 A, B). Base sequences were visually monitored for short stretches that were conserved between human and rat. The complete rat genomic sequence of each gene, including 1000 bases upstream of the TSS, constituting the promoter region, as well as the 5'-untranslated region (5'-UTR) and the intron sequences were exported into a word file. The defined short conserved sequences were identified in the rat genomic sequence as reference point to where H3K4me3 was found enriched in the respective human gene. Genomic regions of around 200-500 bp containing at least one or more of these short conserved sequences were then checked for possible primers using NCBI Primer-BLAST (Figure 33 C). Furthermore, specificity of the suggested primers was surveyed using NCBI Nucleotide Blast, IDT OligoAnalyzer and the UCSC tools "BLAT" and "In-Silico PCR". There are some important parameters to consider when designing ChIP primers. Amplification products should not be longer than 150 bp. Since MNase cuts at the linker DNA between nucleosomes during DNA digestion, the smallest generated fragment is 146 bp. Longer amplification products should therefore be avoided, as the amplification efficiency may be substantially lower. Furthermore, like for normal qPCR, primers should be 20 to 30 bases long with a melting temperature of 60°C ± 2°C. GC content should be 50% on average (35-65%) and runs of an identical nucleotide (such as 'CCCC'), especially 'G's, should be avoided. Formation of self- or hetero-dimers should be prevented (ΔG > -9 kcal/mol) and the melting temperature of hairpin structures should be around 30°C. Using UCSC "BLAT" it can be inquired if the amplified region is unique in the genome and with "In-Silico PCR" it is possible to visualize where the amplicon is in relation to the gene of interest (Figure 33 D).
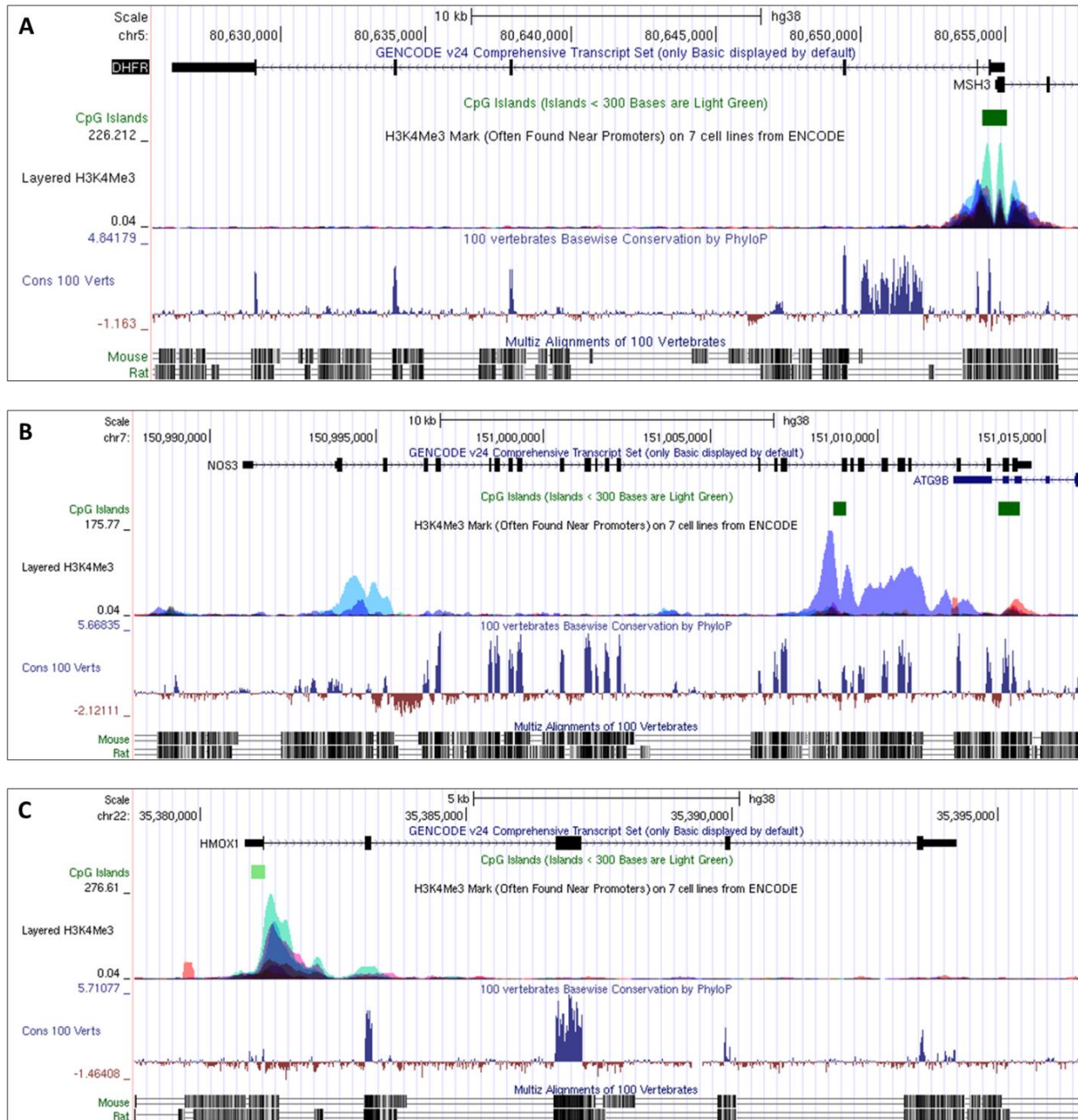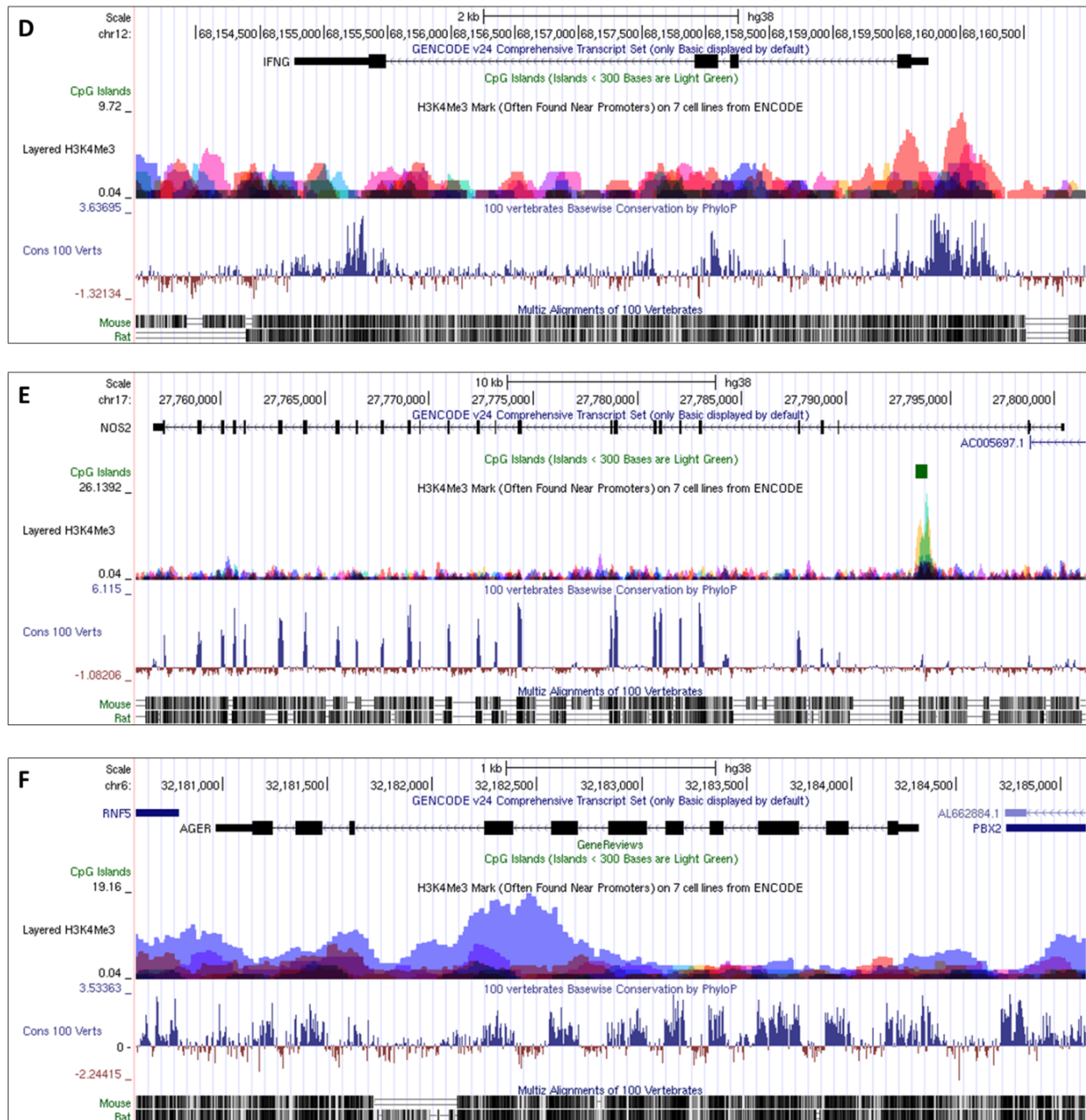
Figure 32 - Representative genome browser assembly from the UCSC database (https://genome.ucsc.edu/) for the human genes DHFR (A), eNOS (NOS3) (B), HO-1 (HMOX1) (C), interferon-γ (IFNG) (D), NOS2 (E) and RAGE (AGER) (F). Gene reading direction is from right to left in A, D, E, F and from left to right in B and C. The browser is set to show at least 500 bp of the promoter region, as well as the 5'-UTR, exons and introns. CpG islands are indicated in green and genomic H3K4me3 distribution is displayed as a transparent overlay of available cell line data. DNA sequence conservation between human, mouse and rat is indicated by data from basewise conservation and multiple alignments.

A **Human NOS2 – H3K4me3 enrichment in intron 2**

B **Zoom to base level in human NOS2 intron 2**
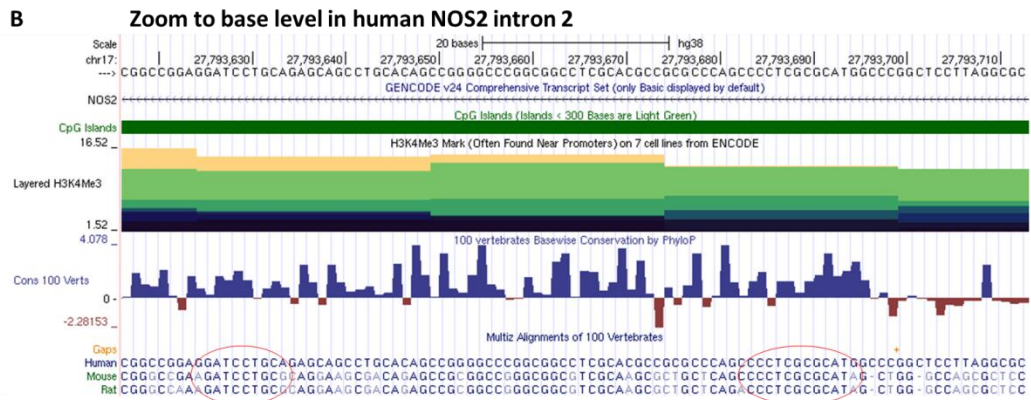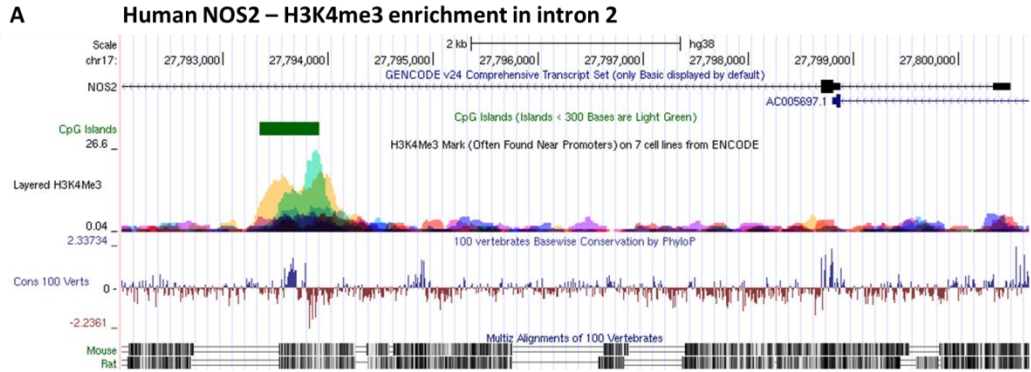
C **Primer search with NCBI Primer-BLAST within sequence in rat intron 2**
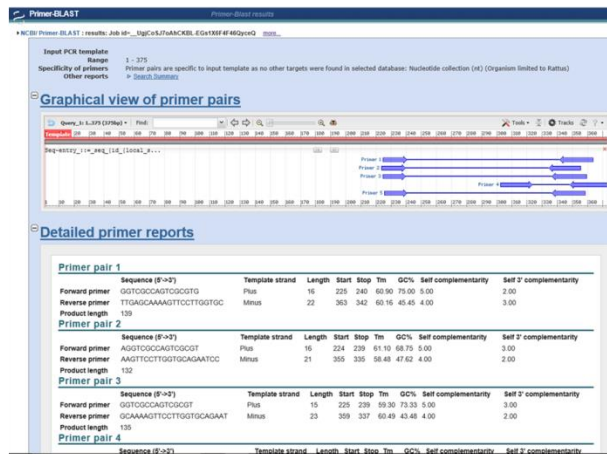
D **UCSC In-silico PCR with selected rat primer pair**
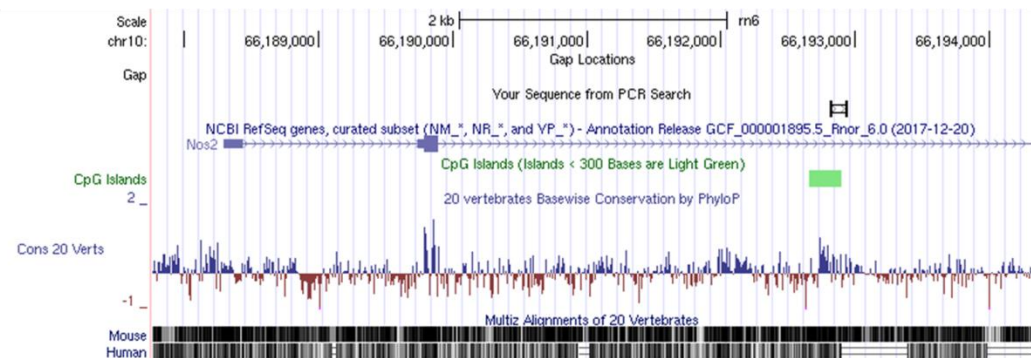
Figure 33 - Representative overview of ChIP primer design in rat. (A) Strong enrichment of H3K4me3 was found in intron 2 of human NOS2 in the UCSC database (see also Figure 32 E). (B) The H3K4me3-rich intron 2 region was zoomed in to base level and base sequences monitored for short human-rat conserved stretches. (C) Rat NOS2 intron 2 regions of around 200-500 bp containing at least one or more of short conserved sequences were checked for possible primers using NCBI Primer-BLAST. Several primer pairs were suggested and analyzed for specificity with other programs. (D) The selected primer pair's uniqueness and position within the rat genome was assessed through UCSC In-silico PCR.

Ten primers spanning promoter and intron regions of each selected gene were designed using this developed protocol, i.e. DHFR (Promoter), DHFR (Promoter-5'UTR), DHFR (Intron1), interferon-γ (Promoter), interferon-γ (Intron3), NOS2 (Promoter-5'UTR), NOS2 (Intron2.1), NOS2 (Intron2.2), RAGE (Promoter), and RAGE (Promoter-5'UTR). HO-1 and eNOS primers were a kind gift of Prof. Li.

Ultimately, the devised primers were ordered and tested in a qPCR for their efficacy and specificity. MNase-digested genomic DNA was serially diluted in 1:10 steps and run in a qPCR with 200 nM primer. Ideally, the number of molecules of the target sequence should double during each replication cycle, therefore the Ct value should decrease by $\log_2(10)=3.3219$ every cycle, corresponding to a 100% amplification efficiency. To calculate primer specificity the obtained Ct values were plotted on a logarithmic scale along with corresponding concentrations. Then a linear regression curve through the data points was generated and the slope of the trend line was calculated (Figure 34, Figure 35). Finally, the primer efficiency was calculated using the equation: E = -1+10(-1/slope). Typically, desired amplification efficiencies range from 90% to 110%.

In addition, the melting curves were examined to check that the primers are generating a specific PCR product and there is no non-specific amplification (Figure 34, Figure 35). Additional peaks may stem from nonspecific amplification, such as primer-dimers.

In the end the primers DHFR (promoter) and DHFR (promoter-5'UTR) were excluded from further analysis due to indeterminate efficiency and lack of specificity (Figure 34, top left). All other primers displayed satisfactory results and were therefore applied in the ChIP assays.
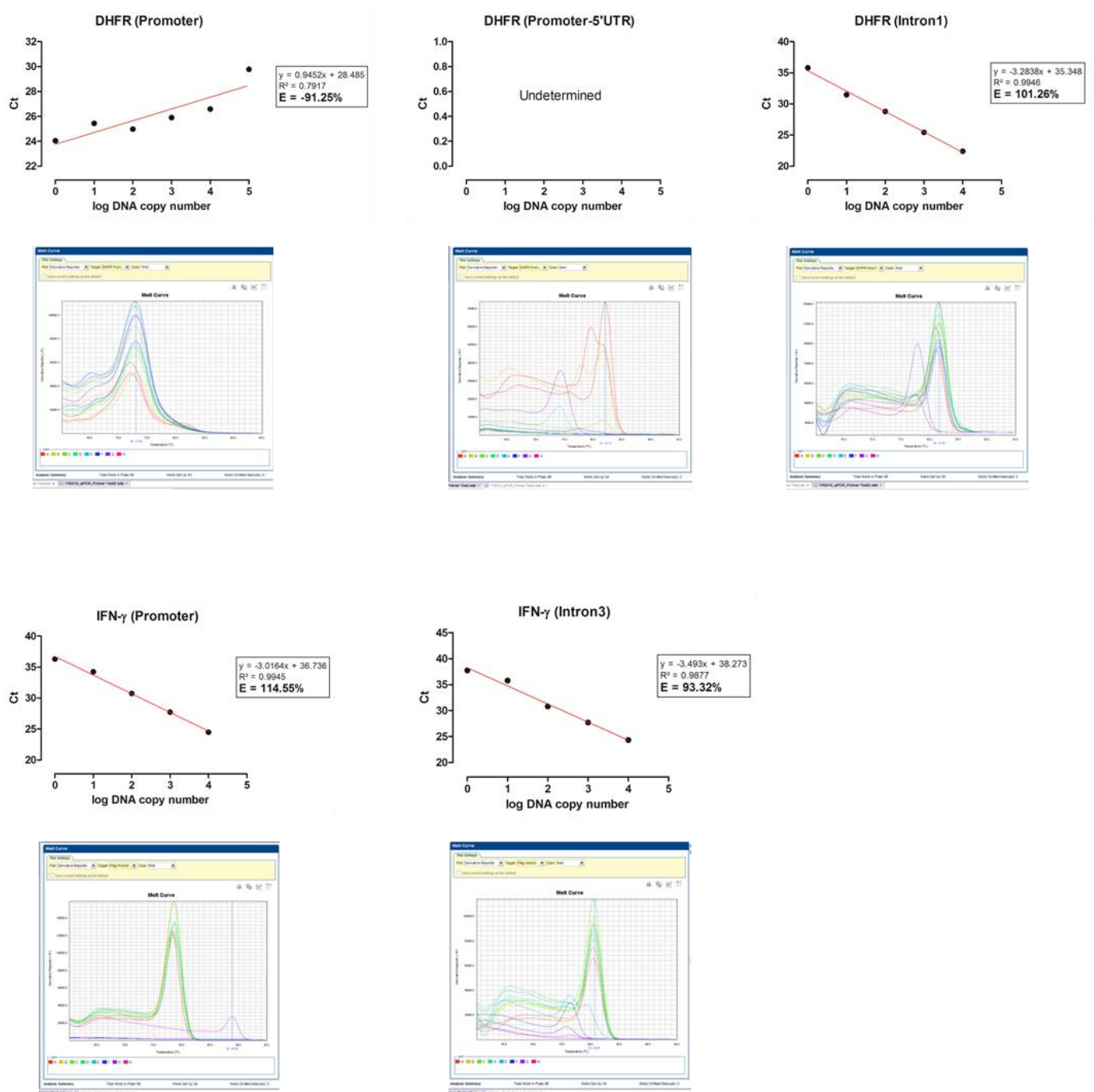
Figure 34 - Analysis of primer efficacy and specificity. Self-designed primers were tested in a qPCR using genomic DNA serially diluted in 1:10 steps. A decrease by $\Delta Ct = \log_2(10) = 3.3219$ corresponds to a 100% amplification efficiency. Linear regression curves of DHFR and IFN-γ primers are shown along with their calculated efficiencies and melting curves.
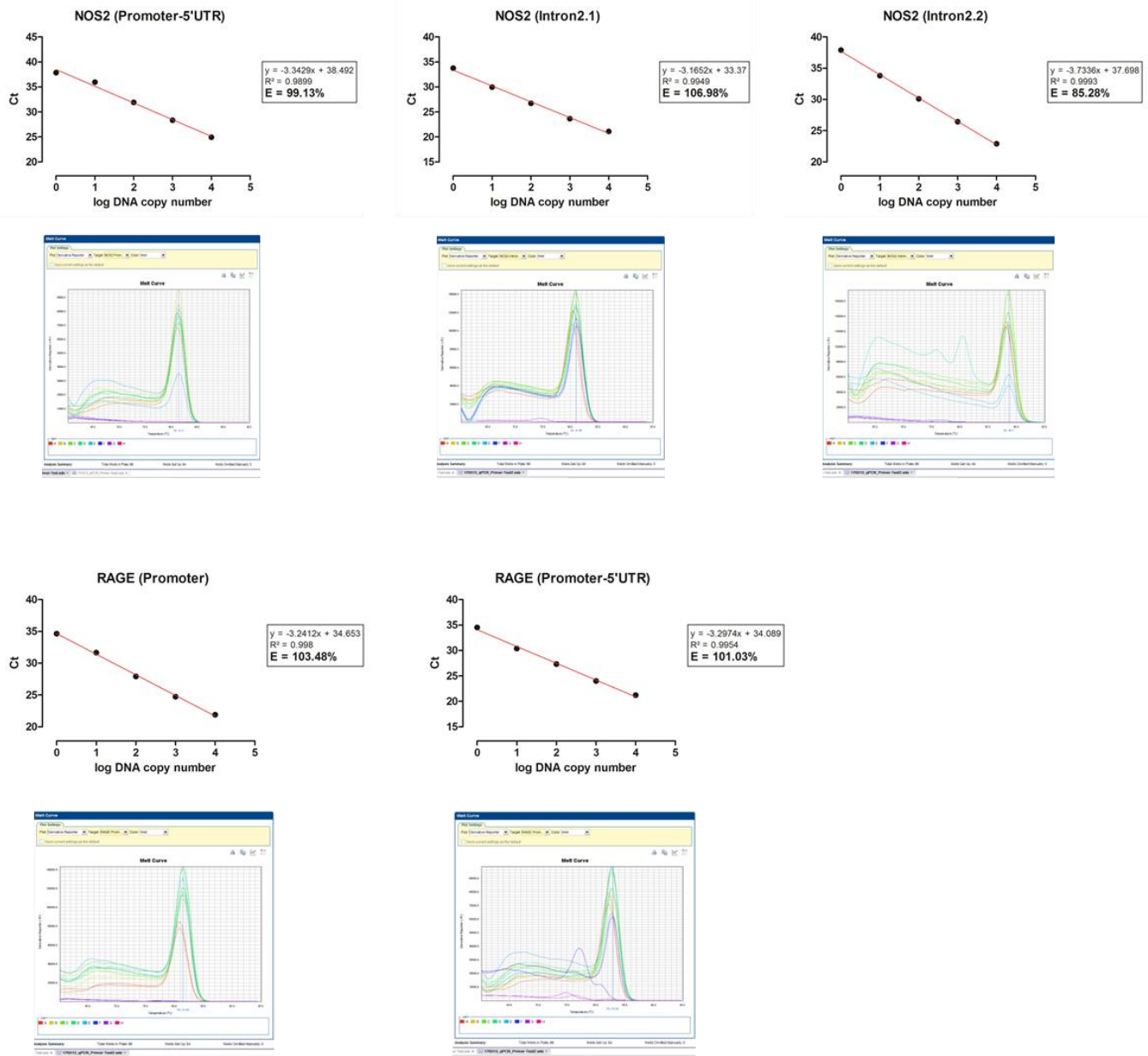
Figure 35 - Analysis of primer efficacy and specificity. Self-designed primers were tested in a qPCR using genomic DNA serially diluted in 1:10 steps. A decrease by ΔCt = $\log_2(10)=3.3219$ corresponds to a 100% amplification efficiency. Linear regression curves of NOS2 and RAGE primers are shown along with their calculated efficiencies and melting curves.

4.15 Quantitative real-time PCR (qPCR)

Quantification of chromatin-immunoprecipitated DNA fragments was performed by qPCR analysis using the described primers. The 2x concentrated reaction cocktail "PerfeCTa SYBR Green FastMix ROX" (Quanta) was diluted to a 1x mix containing 200 nM primer (forward/reverse) and 2 µl of isolated genomic DNA fragments. The reaction mix was pipetted into a 96-well PCR plate, which was sealed, gently vortexed and then briefly centrifuged to collect components at the bottom of the plate. Templates were amplified using the thermal cycler "StepOnePlus Real-Time PCR Systems". The initial denaturation phase was set to 2 min at 94°C, followed by 40 cycles of 15 sec denaturation at 94°C and 1 min of primer annealing and nucleotide extension at 60°C. Amplification was recorded by the device by reading the fluorescence emission intensity of the dsDNA dye SYBR green (contained in the reaction mix) and subsequently evaluated using the StepOne software. The fluorophore ROX (carboxy-X-rhodamine) (contained in the reaction mix) was used as a passive reference dye. Resulting data were normalized to the amount of input chromatin.

4.16 Statistics

Results are expressed as means ± SEM. One-way ANOVA with Bonferroni's or Tukey's correction was used between different groups for comparisons of multiple means for RONS detection, protein expression and modification, as well as ChIP data. One-way ANOVA with Dunnett's correction was used for comparisons against control group. Gaussian distribution of datasets was determined by SigmaStat for Windows (version 3.2, Systat Software Inc.). When normality test failed an equivalent non-parametric test (Kruskal-Wallis/ Dunn's multiple comparison) was applied. P-values <0.05 were considered statistically significant. Software used for calculations were Microsoft Excel and GraphPad Prism (version 5.02, GraphPad Software Inc).

5 Results

In the course of this PhD thesis several projects were conducted that are briefly summarized here before detailed description of all results.

First of all, a detection assay for the formation of S-nitrosocysteine was developed using the spin trapping agent 5,5-dimethyl-1-pyrroline N-oxide (DMPO). S-nitros(yl)ation of isolated protein was induced with various nitros(yl)ation agents and resulting S-nitroso-proteins were transformed into protein-DMPO adducts by light-induced homolysis and spin trapping. These adducts were quantitatively detectable by a DMPO-specific antibody.

In order to investigate epigenetic changes induced by ROS, an attempt was made to establish a previously described model system of hyperglycemia-induced oxidative stress in the endothelial cell line EA.hy926. But ultimately, there was no substantial and reproducible effect on ROS formation under hyperglycemic conditions detected. Similarly, assay approaches using a combination of hyperglycemia and interleukin-1β, or treatment of EA.hy cells with redox cycling agents (paraquat, rotenone) were also not convincingly successful in generating increased oxidative stress. Concomitantly, there were also no changes in histone methylation and acetylation patterns observed in these cells.

Samples from an animal model with already defined oxidative-stress related complications were then chosen for epigenetic investigation. Mice deficient in the antioxidant protein glutathione peroxidase-1 (GPx-1) have already been shown to have enhanced ROS/RNS formation, which was further potentiated during the aging process [416]. Indications were found that led to the hypothesis of potential dityrosine cross-linking between histone 3 and histone 4 accompanied by enhanced histone 3 lysine 9 dimethylation (H3K9me2) upon increased oxidative stress. However, upon further investigation this assumption was revealed to be false.

In a published study by our group it was demonstrated that empagliflozin, a selective sodium-glucose co-transporter 2 inhibitor (SGLT2i), reduced glucotoxicity and thereby prevented the development of endothelial dysfunction, reduced oxidative stress and exhibited anti-inflammatory effects in ZDF rats, an animal model of type 2 diabetes mellitus (T2DM) [412]. Investigation of involved epigenetic mechanisms by ChIP analysis revealed an effect of empagliflozin on expression of glucotoxicity and inflammation markers in diabetic animals via altered histone methylation patterns.

Furthermore, the interplay of increased ROS formation and epigenetic regulation was studied in the context of a doxorubicin-induced cardiotoxic phenotype in H9c2 cardiomyocytes. It was discovered that

doxorubicin treatment affected the expression of certain epigenetic modulators in correlation with increased oxidative stress markers. However, the exact interaction between redox signaling and epigenetic modulation or clear identification of specific ROS-producing enzymes as causative factors of epigenetic changes in this model remain to be analyzed.

5.1 Detection of protein S-nitros(yl)ation by immuno-spin trapping

In the first part of this project, a readout assay was established for the detection of protein S-nitros(yl)ation, which is the covalent attachment of a nitroso ("NO") group to the thiol group in cysteine. For this purpose an *in vitro* approach was set up to identify S-nitros(yl)ation by immuno-spin trapping using 5,5-dimethyl-1-pyrroline N-oxide (DMPO) and subsequent Western blotting against DMPO-positive proteins. Upon irradiation with visible light, protein S-nitrosothiols undergo photolytic homolysis to $^\bullet$NO and protein thiyl radicals, which can be spin trapped by DMPO forming a thioether and upon rearrangement a stable thionitrone product (see Methods 4.8, p.60) [418]. These protein-DMPO adducts can then be analyzed by Western blot or dot blot using a DMPO-specific antibody.

Experiments for the establishment of a detection assay for S-nitrosocysteine-positive proteins were first conducted in an *in vitro* fashion using the enzymes aldehyde dehydrogenase (ALDH) and isocitrate dehydrogenase (ICDH), since they contain reactive cysteine residues (with partial thiolate character, $-S^-$) as potential targets for S-nitros(yl)ation (see Figure 70 in Discussion 6.1, p.125).

S-nitros(yl)ation of aldehyde dehydrogenase or isocitrate dehydrogenase was induced by addition of increasing equimolar concentrations of the nitric oxide ($^\bullet$NO) donor spermine-NONOate (SPENO) and the peroxynitrite-generating compound 3-morpholinosydnonimine hydrochloride (Sin-1), resulting in the stoichiometric release of $^\bullet$NO and $^\bullet O_2^-$ in a ratio of 3:1. Prof Daiber and colleagues had previously shown in a study that this is the optimal ratio for nitros(yl)ation while mimicking low physiological fluxes [103]. Furthermore, high concentrations of SPENO, as well as acidic potassium nitrite solution (KNO_2) served as positive controls. After incubation, samples were exposed to DMPO and illuminated using visible light with a wavelength >420 nm to form a stable DMPO-protein adduct, the latter being the spin trapping step. Nitros(yl)ation was then assessed by dot blot using an antibody against protein-DMPO adducts.

In six independent experiments aldehyde dehydrogenase showed a significant increase in DMPO signals representing nitros(yl)ation upon treatment with 20 mM KNO_2, as well as a substantial increase at 1 mM SPENO, indicating effective ALDH nitrosylation by these agents (Figure 36 A). ALDH treatment with the combination SPENO/Sin-1 resulted in a significant ~3-fold increase of DMPO-adduct detection compared to control only at 100 µM SPENO/Sin-1 but showed no major effects at concentrations below.

Likewise, for isocitrate dehydrogenase a significant intensification of DMPO staining was detected when treated with 20 mM KNO_2, and was also considerably elevated at 1 mM SPENO treatment (Figure 36 B). Compared to untreated samples, there was also a concentration dependent increase in S-nitros(yl)ation upon incubation with the combination of SPENO/Sin-1, reaching significance upon treatment with 100 µM SPENO/Sin-1. It is noteworthy, however, that there were inconsistencies between ICDH-S-nitros(yl)ation experiments accounting for the high error bars.

In both cases the specificity of DMPO-adduct formation as a result of ˙NO abstraction from a SNO group in response to irradiation with visible light was tested by incubating samples with DMPO with or without illumination. It was observed that indeed the absence of light resulted in no detectable DMPO staining signal.

As a marginal note, also two different anti-S-nitrosocysteine antibodies (A.G. Scientific N-1078 and Abcam ab50185) were tested on nitros(yl)ated protein in several experiments but they turned out to be highly unspecific (data not shown).

Figure 36 - Protein-S-nitros(yl)ation analysis by dot blot using DMPO-antibody upon light-induced homolysis and spin trapping of resulting thiyl radicals. Chemiluminescence of DMPO as a result of nitros(yl)ation of aldehyde dehydrogenase **(A)** or isocitrate dehydrogenase **(B)** was quantified using Gel Pro analyzer. Representative dot blots are shown below. Data are mean ± SEM of n=6 independent experiments. *, $p < 0.05$ vs. control.

5.2 Hyperglycemia and oxidative stress in the endothelial cell line EA.hy926

It has been shown previously that hyperglycemia induces the formation of reactive oxygen species (ROS) in endothelial cells. In a 2012 publication by Karbach *et al.* it was demonstrated that induction of hyperglycemia in the immortalized human endothelial cell line EA.hy926 by five-day exposure to 35 mM D-glucose increases ROS formation in these cells in comparison to control cells incubated under normoglycemic conditions with 5 mM D-glucose [409]. Besides data from our own group, also other groups reported that hyperglycemia increases intra- and extracellular superoxide and ROS formation in EA.hy926 cells [425, 426], total protein kinase C (PKC) activity and expression, as well as endothelin-1 (ET-1) signaling [427, 428]. Based on these previous data, the use of this cellular model system seemed to be suitable to investigate epigenetic changes induced by ROS, with focus on alterations in histone methylation or acetylation patterns upon increased oxidative stress in these cells.

Semi-confluent EA.hy926 cells were incubated with either 5 mM (low glucose, LG) or 35 mM D-glucose (high glucose, HG)-containing medium and grown for 5 days with daily renewal of medium. There were no evident differences in shape and viability between the two groups during the treatment. Cellular ROS formation was measured by fluorescence detection of 2-hydroxyethidium (2-HE) or resorufin via HPLC, as well as by L-012 chemiluminescence detection. In addition, cell protein content was analyzed by dot blot using specific antibodies to determine the presence of oxidative stress markers, such as 3-nitrotyrosine (3-NT), 4-hydroxynonenal (4-HNE) or malondialdehyde (MDA).

Unfortunately, the previous results by Karbach *et al.* could not be fully reproduced, as the observed increases in ROS formation under hyperglycemic conditions were significantly less pronounced. In seven independent experiments 2-HE or resorufin detection via HPLC only showed an average increase by 12% of intracellular superoxide formation and an increase by 21% of extracellular hydrogen peroxide (Figure 37 A, B) (for comparison, in the original paper by Karbach *et al*. ROS formation was more than doubled [409]). Measurement of ROS formation by the L-012 chemiluminescence-based assay showed no effect on oxidative stress in hyperglycemic cells. There was also no increase in signal intensity of oxidative stress markers detected by dot blot (data not shown).

Several adjustments to assay conditions were made trying to improve the model, such as application of different batches of D-glucose or FCS, or starving cells prior to or during the treatment. Also, a time course was conducted with ROS measurements after 2, 4, 5 and 6 days of incubation with high glucose, showing no considerable differences in ROS formation between the groups at any given time point.

Following a suggestion from Prof. Di Lisa´s lab, who use a combination of hyperglycemia and the pro-inflammatory and pro-oxidant cytokine interleukin-1β (IL-1β) to induce oxidative stress in primary cardiomyocytes [410], these conditions were applied on EA.hy926 cells. Semi-confluent EA.hy926 cells were incubated with either 5 mM (LG), 25 ng/ml IL-1β or a combination of IL-1β and 35 mM D-Glucose for 48 h. ROS formation was measured by fluorescence detection of 2-HE or resorufin via HPLC. In four independent experiments an average increase by only 16% of intracellular superoxide formation and 9% of hydrogen peroxide formation was detected in response to hyperglycemia in presence of IL-1β (Figure 37 C, D). Treatment with IL-1β alone did not result in any effect.
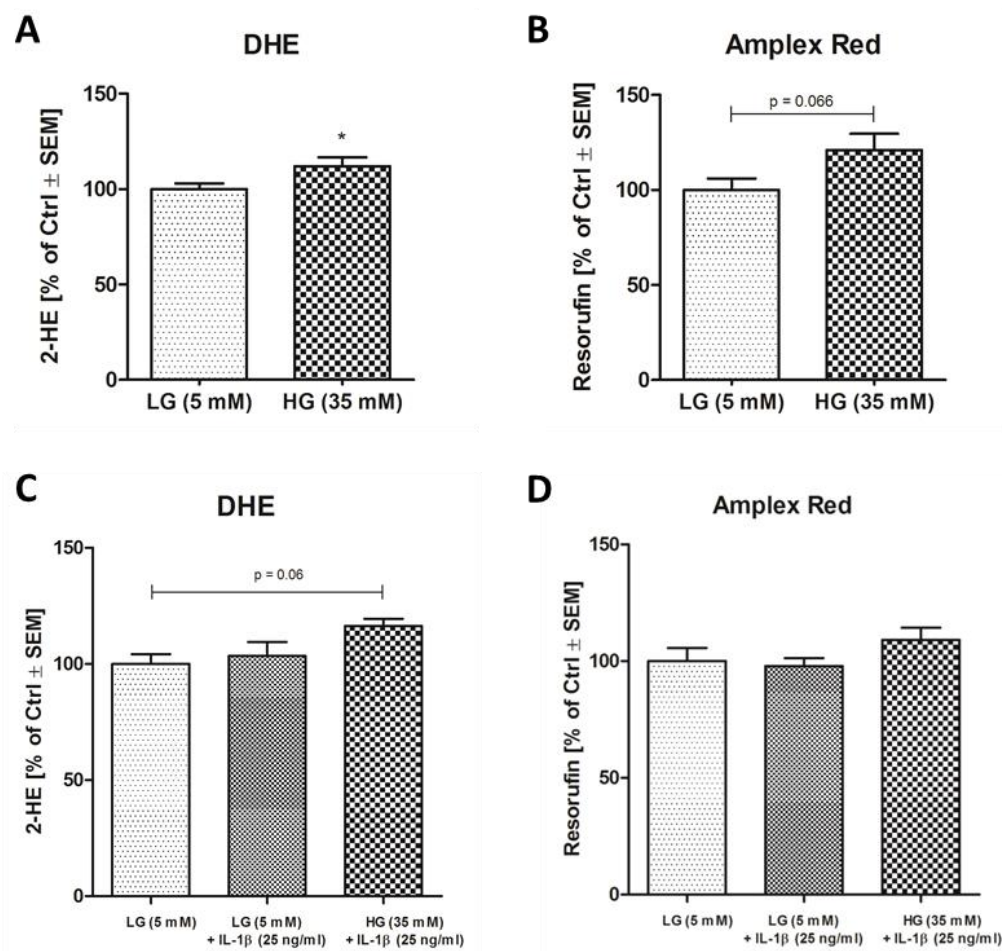
Figure 37 - (A+B) Effects of hyperglycemia on ROS formation in EA.hy926 cells. Superoxide and hydrogen peroxide formation was determined by HPLC-based quantification of 2-HE and resorufin, respectively. The data are mean ± SEM of 7 independent experiments. **(C+D) Effects of IL-1β and hyperglycemia on ROS formation in EA.hy926 cells.** Superoxide and hydrogen peroxide formation was determined by HPLC-based quantification of 2-HE and resorufin. The data are mean ± SEM of 4 (C) and 2 (D) independent experiments.

Also, it was attempted to increase ROS formation in EA.hy926 cells through treatment with the redox cycling agent paraquat. The herbicide paraquat induces superoxide formation upon its reduction by

complex 1 of the mitochondrial respiratory chain [429]. Several experiments were made using different concentrations of paraquat and incubation times of 1 h or 24 h, but not more than 15% increase in ROS formation was obtained compared to untreated cells. There was also no increase in signal intensity of oxidative stress markers detected by dot blot analysis (data not shown).

In all of the previously described settings cellular histone methylation and acetylation patterns were analyzed alongside. Focus was on the marks H3K9me1/2/3, H3K4me3, H3K27me3, H3Ac (pan), which were detected via Western blot with the respective antibodies. There were no major epigenetic changes observed (data not shown).

Since the goal to establish an oxidative stress model to investigate ROS-induced effects on epigenetic modulation could not be achieved, the utilization of EA.hy926 as cellular model was discontinued in favor of other oxidative stress models.

5.3 ROS formation and epigenetic investigation in the setting of glutathione peroxidase-1 deficiency and aging

In order to analyze ROS-induced epigenetic alterations in a model with clinical relevance, tissue samples from an animal model with already defined oxidative stress-related complications were used for further investigation.

It was shown previously by Oelze *et al.* that ablation of the antioxidant protein glutathione peroxidase-1 (GPx-1) potentiates age-dependent vascular dysfunction and ROS/RNS formation in mice [416]. The authors demonstrated that aging itself caused endothelial NO synthase (eNOS) dysfunction and uncoupling via adverse eNOS phosphorylation and S-glutathionylation, an effect that was further potentiated in aged GPx-1 deficient (GPx-1$^{-/-}$) mice.

Here, ROS formation and histone mark changes were analyzed in young (2 months) and aged (12 months) mice with GPx-1 deficiency. For this purpose, stored frozen heart and kidney samples (kept at -80 °C) from above-mentioned study from 2013 were lysed and used for further investigations. The tissue had been isolated from GPx-1$^{-/-}$ mice on a C57 black 6 (C57BL/6) background and C57BL/6 control mice at 2 and 12 months of age (≥ 3 animals per group). GPx-1 knockout was confirmed by Western blot as depicted in Figure 38.
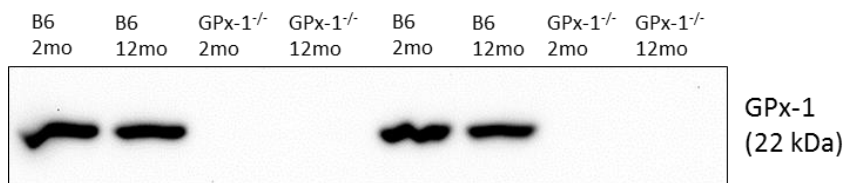
Figure 38 - Western blot confirming loss of glutathione peroxidase-1 expression in GPx-1-deficient mice. Blot is representative for n=1 independent experiments.

Dot blot analysis of oxidative stress markers indicated increased levels of 3-nitrotyrosine (3-NT)-modified proteins in heart and kidney tissue lysates of aged mice, but even more profoundly in aged GPx-1$^{-/-}$ mice (Figure 39 A).
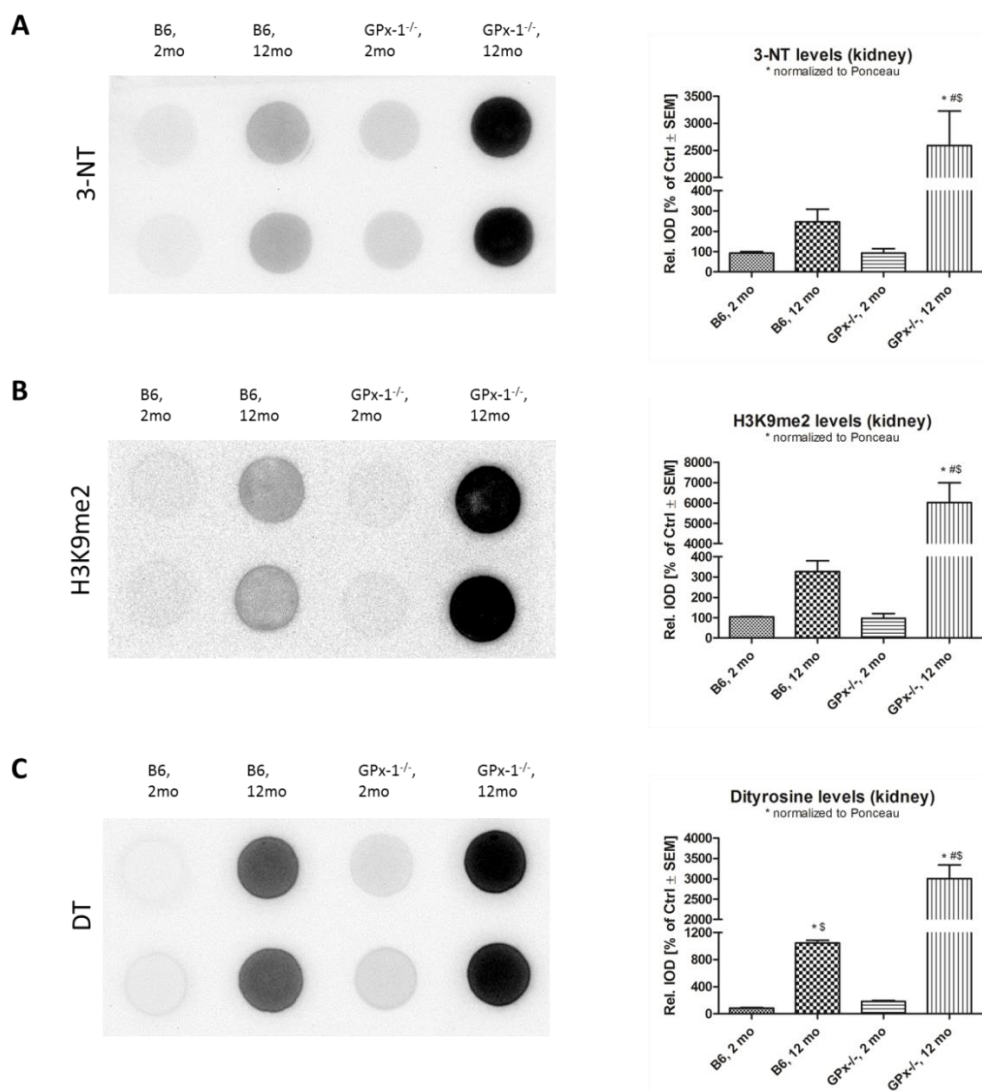
Figure 39 - Representative dot blots analyzing kidney tissue lysates of control and GPx-1$^{-/-}$ mice at 2 and 12 months of age with antibodies against (A) 3-NT, (B) global H3K9me2 and (C) dityrosine-modified proteins. Densitometric quantification combines data of ≥ 3 independent experiments with pooled tissues from at least 4 animals/group. IOD of each dot was normalized to IOD of Ponceau staining. *, $p < 0.05$ vs. B6 (2 mo); #, $p < 0.05$ vs. B6 (12 mo); $ $p < 0.05$ vs. GPx-1$^{-/-}$ (2 mo).

Furthermore, changes in histone marks were assessed via Western blot and dot blot using specific antibodies in whole protein lysates or in histone extracts that were specially prepared by acid extraction. While there were no changes observed for the histone modifications H3K9me1/3, H3K27me3 or H3Ac, analysis by dot blot revealed a gradual increase of global histone 3 K9 dimethylation (H3K9me2) in heart and kidney of the aged mice (Figure 39 B). The signal intensity correlated with 3-NT formation in the respective groups. Furthermore, during Western blot examination the H3K9me2 antibody recognized a non-reducible ~26-27 kDa band and a weaker band between 50-60 kDa (~53 kDa) in protein lysates, as well as in histone acidic extracts from the same lysates (Figure 40 + Figure 41 A). These bands were more pronounced in the aged groups. This was an interesting finding since the highly conserved histone 3 has a molecular weight of 15.404 kDa and typically runs at ~17 kDa in SDS-PAGE.
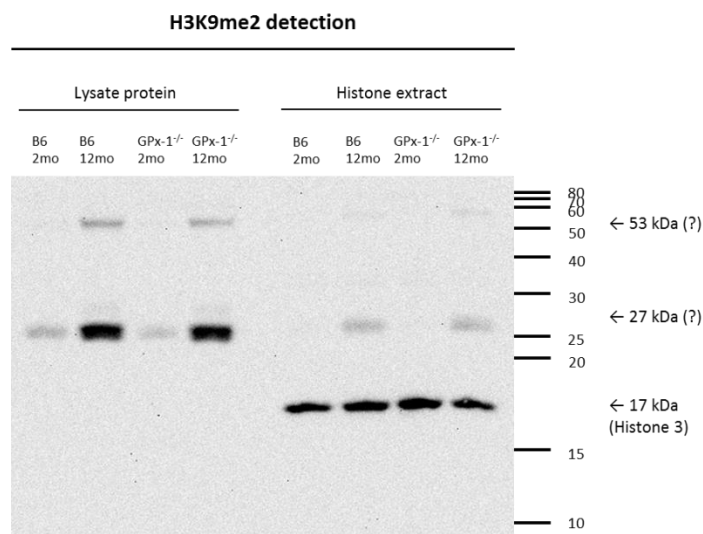
Figure 40 - Western blots of kidney tissue lysates and their histone extracts from control and GPx-1$^{-/-}$ mice at 2 and 12 months of age using a H3K9me2-antibody. The H3K9me2 antibody recognized a non-reducible ~27 kDa band and a weaker band at ~53 kDa in lysates, as well as in histone extracts. Actual histone 3 monomer at 17 kDa was only detected in the histone extract. Blot is representative for n=8 independent experiments.

Speculation that this increase in molecular weight was due to monoubiquitination (addition of an 8 kDa ubiquitin residue) of histone 3 was ruled out by testing samples with a ubiquitin-specific antibody (data not shown).

The next hypothesis was that the additional bands may represent oligomerization of histones, specifically a H3-H4 dimer and (H3-H4)$_2$ tetramer with the calculated sizes of ~26.7 kDa and ~53.4 kDa, respectively. Western blots using antibodies against H3 and H4 confirmed presence of bands of these sizes in the tissue lysates (Figure 41 B, C), therefore promoting the hypothesis of H3-H4 oligomers.
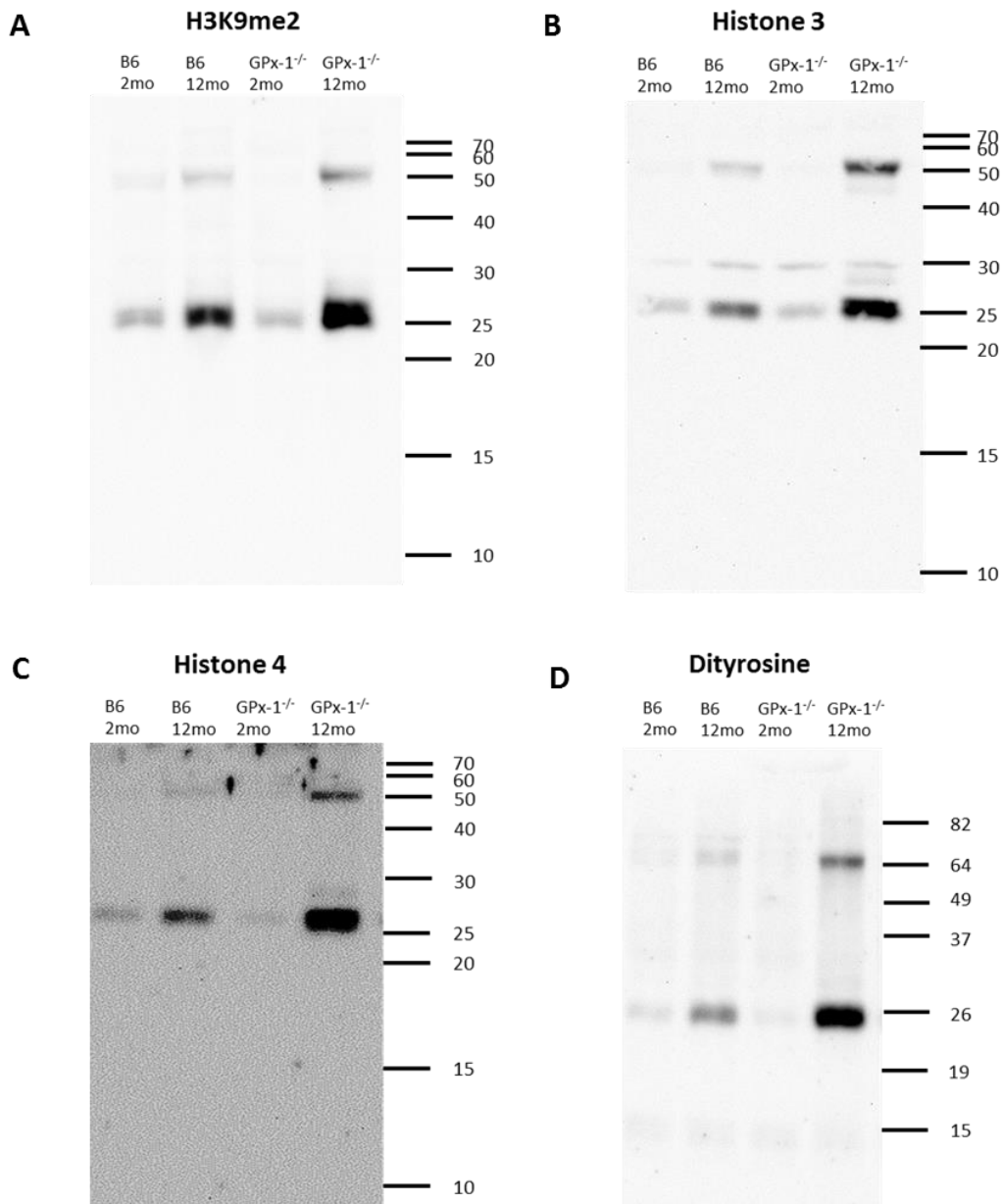
Figure 41 - Western blots of kidney tissue lysates from control and GPx-1^{-/-} mice at 2 and 12 months of age using a (A) H3K9me2-, (B) H3-, (C) H4-, and (D) dityrosine-antibody. A non-reducible ~27 kDa band and a weaker band at ~53 kDa were detected in aged animals by each antibody. Blots are representative for n=4-8 independent experiments.

It is known that histone 3 contains two cysteines, which can get oxidized leading to H3 dimer formation through formation of disulfide bridges [430]. However, this effect is reversible by reducing agents like β-mercaptoethanol (β-ME) or dithiothreitol (DTT). Since there are no cysteine residues in histone 4 and, moreover, sample reduction did not abolish the presence of the bands, it was assumed that the potential oligomer formation was due to a more stable covalent linkage of the histone proteins.

It has previously been shown that exposure to peroxynitrite induces dityrosine formation in histone H2A, H2B and H3, leading to intramolecular (but not intermolecular) cross-linking [431-433]. Like cysteine, tyrosine is one of the amino acids that are most susceptible to oxidation. Various tyrosine derivatives such as nitrotyrosine, dityrosine and halogenated tyrosine can be formed upon exposure to free radicals. Dityrosine (DT) is a tyrosine dimer derived from tyrosyl radicals and can be formed by ROS, metal-catalyzed oxidation, ultraviolet irradiation, and peroxidases [434, 435].
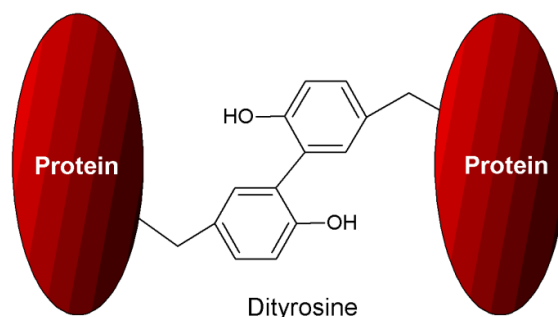
Figure 42 - Intermolecular cross-link between two proteins via dityrosine. *Adapted from Correia et al. 2012 [436].*

H3 contains three and H4 four tyrosine residues (see sequences in Appendix, p.192), therefore oligomerization may have been a result of intermolecular dityrosine cross-linking (Figure 42). Western blot detection using a dityrosine-specific antibody revealed DT-positive bands of the size predicted for H3-H4 dimers and (H3-H4)$_2$ tetramers (Figure 41 D), with signal intensities correlating with the pattern seen before for H3K9me2, H3 and H4. Furthermore, dot blot also showed increased dityrosine levels in the aged groups, where DT signal intensity correlated nicely with observed levels of 3-NT and H3K9me2 (Figure 39 C).

In order to confirm the existence of an intermolecular H3-H4 dityrosine cross-link, samples were analyzed by mass spectrometry. For this purpose, dityrosine-modified proteins or histone 3 were precipitated from kidney lysates of young and old GPx-1$^{-/-}$ mice using the respective antibodies, and subsequently run on SDS-PAGE. The alleged dimer and tetramer bands at 27 kDa and 53 kDa were cut out, trypsin-digested and subjected to mass spectrometry (MS) analysis (collaboration with AG Tenzer, MS platform laboratory). Unfortunately, no histone masses could be detected in these measurements (except for traces in the 27 kDa band of young GPx-1$^{-/-}$ mice) and no indication of a covalent dityrosine cross-link was found (Table 2 + Appendix p. 193). Instead, a big amount of contaminations was detected, especially mouse immunoglobulins. In another approach, not IP precipitates from whole protein lysates, but specifically histone extracts from these lysates were analyzed by MS. Here, histone masses were found at 17 kDa,

27 kDa and 53 kDa, but there were no indications found by MS that pointed to a dityrosine cross-link between H3 and H4 (Table 2 + Appendix p. 195). The histones found in the higher molecular weight bands may still account for histone dimers or tetramers, but their presence may not be due to a covalent link between single histones but rather due to insufficient denaturation and therefore remaining histone folding, as is present in nucleosome assembly. However, higher molecular weight of histones may also be due to posttranslational modifications.

Mass spectrometry analysis

H3-IP precipitates

Sample	Band size	Observed histone type
GPx-1$^{-/-}$, 2 mo	27 kDa	H2A, H2B, H4
GPx-1$^{-/-}$, 2 mo	53 kDa	None
GPx-1$^{-/-}$, 12 mo	27 kDa	none
GPx-1$^{-/-}$, 12 mo	53 kDa	none

Histone extracts

Sample	Band size	Observed histone type
GPx-1$^{-/-}$, 2 mo	17 kDa	H1, H2A, H2B, H3
GPx-1$^{-/-}$, 2 mo	27 kDa	H1, H2A, H2B, H3, H4
GPx-1$^{-/-}$, 2 mo	53 kDa	H1, H2A, H2B, H3, H4
GPx-1$^{-/-}$, 12 mo	17 kDa	H1, H2A, H2B, H3
GPx-1$^{-/-}$, 12 mo	27 kDa	H1, H2A, H2B
GPx-1$^{-/-}$, 12 mo	53 kDa	H1, H2A, H2B, H3, H4

Table 2 – Results of mass spectrometry analysis. Histone 3 was precipitated from kidney lysates of young and old GPx-1$^{-/-}$ mice and 27 kDa and 53 kDa bands subjected to MS. Also, 17 kDa, 27 kDa and 53 kDa bands from histone extracts from kidney lysates were analyzed by MS. See appendix for details.

In an attempt to prove that the bands detected after immunoprecipitation were actual precipitates and not the light and heavy chain of the H3 mouse IgG antibody used for the IP (which have similar masses, approx. 25 kDa and 50 kDa), blots of IP precipitates and whole lysates were incubated only with anti-mouse IgG secondary antibody (without primary antibody). Unfortunately, the same pattern of bands appeared as were also detected with H3K9me2 or dityrosine primary antibodies (Figure 43). This indicated that, in fact, the mouse IgG heavy and light chains were detected. Since the anti-mouse secondary antibody also detected mouse IgGs not only in the IP-precipitates but also in the whole protein lysate, it was concluded that the observed effect originated from endogenous mouse immunoglobulins. These immunoglobulins were increased in the aged groups due to increased inflammation and infiltration of immune cells in the examined mouse heart and kidney tissues. Also, in parallel, an IP with a new rabbit anti-H3 antibody was performed and, in accordance with the other findings, these precipitates did not show any bands for dityrosine, histone 4 or H3K9me2.

All previous discoveries were therefore interpreted falsely due to the recognition of tissue-intrinsic mouse immunoglobulins by the anti-mouse secondary antibody that was used in conjunction with the primary mouse monoclonal H3-, H4-, H3K9me2- and dityrosine antibodies.
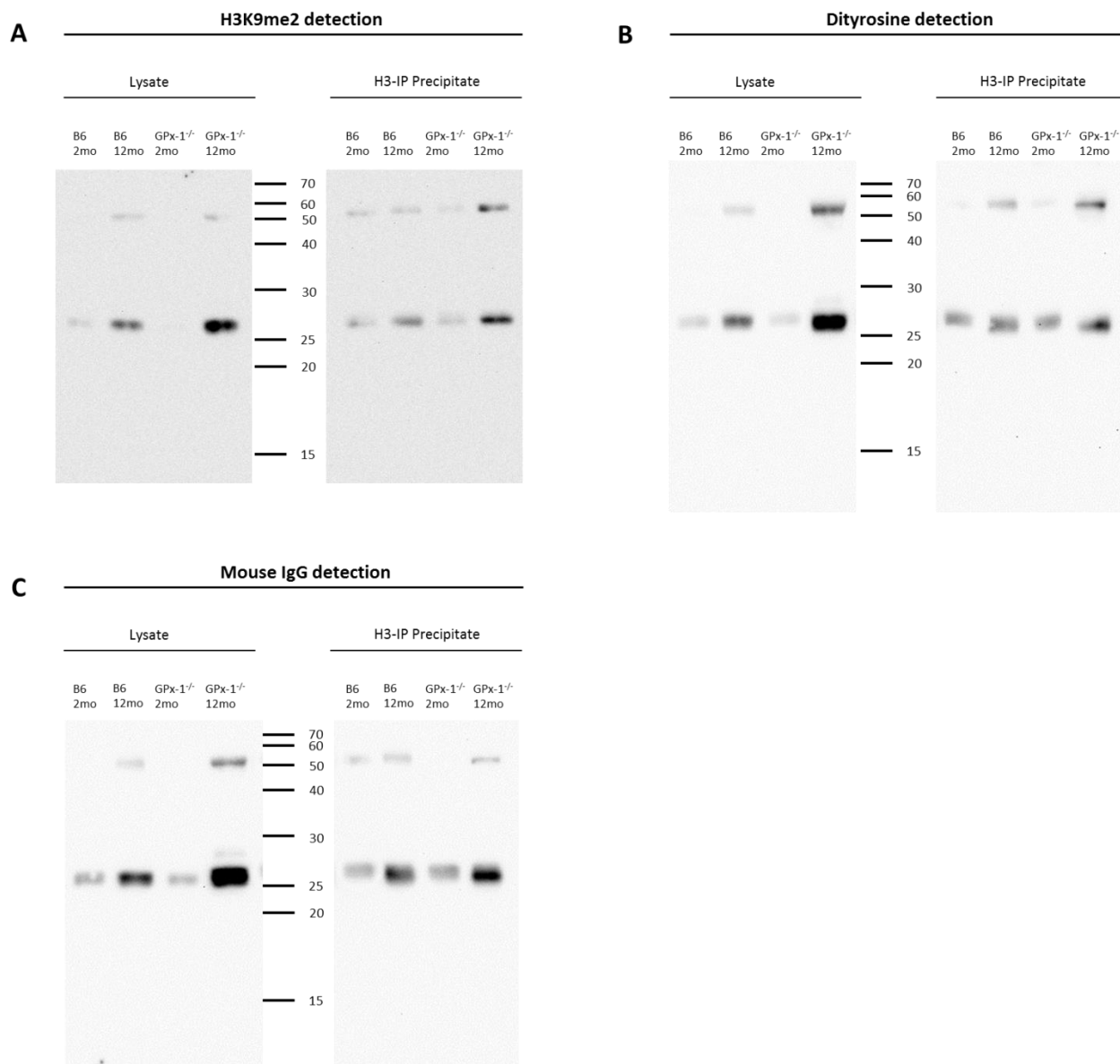
Figure 43 - Western blot analysis of kidney tissue lysates and their H3-IP precipitates from control and GPx-1$^{-/-}$ mice at 2 and 12 months of age using a (A) H3K9me2 or (B) dityrosine mouse primary antibody in conjunction with an anti-mouse IgG secondary antibody or (C) no primary antibody, only anti-mouse IgG secondary antibody. Blots are representative for n=2 (A, B) and n=1 (C) independent experiments.

In another approach to investigate possible dityrosine cross-linking between histones, recombinant human histone 3 and histone 4 were directly treated with oxidizing agents to provoke formation of oxidative modifications. A mix of 2 µg histone 3 and 2 µg histone 4, or histone 3 and 4 each individually were either incubated with hydrogen peroxide catalyzed by copper or horse radish peroxidase (HRP), or with the peroxynitrite-generating compound Sin-1.

Of note, in a previous experiment the specificity of the dityrosine antibody had been tested on isolated protein (hemoglobin, BSA, or lysozyme) that had been oxidized under the mentioned conditions and, at least, treatment with H_2O_2/Cu^{2+} resulted in extensive dityrosine formation (Figure 44).

Dityrosine detection in controls

1) untreated, over night @ 37°C
2) + 5 mM H_2O_2 + 50 µM CuSO$_4$, over night @ 37 °C
3) + 5 mM H_2O_2 + 50 µM FeSO$_4$, over night @ 37 °C
4) + 5 mM H_2O_2 + 1 µM HRP, 90 min @ 37 °C
5) + 1 mM sin-1, 90 min @ 37 °C
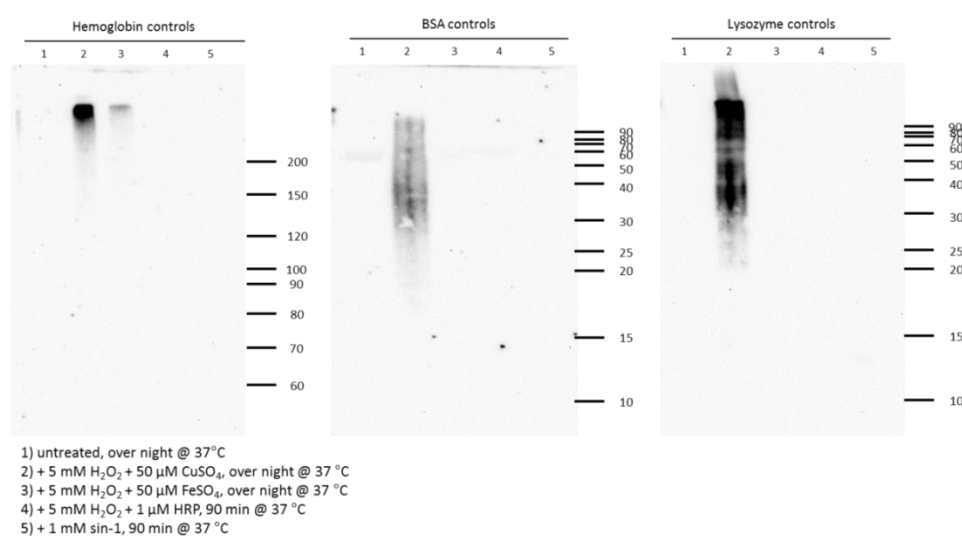
Figure 44 – Generation of positive controls for dityrosine formation by oxidation of isolated protein (hemoglobin, BSA, lysozyme) and detection via Western blot with a dityrosine antibody. 250 µg of the proteins hemoglobin, BSA and lysozyme were incubated over night at 37°C with the following oxidizing agents: 2) 5 mM H_2O_2 + 50 µM CuSO$_4$, 3) 5 mM H_2O_2 + 50 µM FeSO$_4$, or for 90 min at 37°C with 4) 5 mM H_2O_2 + 1 µM HRP or 5) 1 mM Sin-1. Formation of a dityrosine-modification on the respective protein was analyzed using a dityrosine antibody in WB. Blots are representative for n=1 independent experiments.

There was no H3-H4 dimer formation observed by Western blot, but a strong band was detected between 30-40 kDa in the fractions containing histone 3 (Figure 45). This is because H3 contains two cysteines, which can get oxidized leading to H3 dimer formation by forming disulfide bridges, as mentioned previously. Dityrosine staining did not result in any signal, neither in the histone fraction nor in the lysozyme controls that had been oxidized simultaneously. Nevertheless, it is possible that oxidation affected the structure of these proteins in such a way that they did not enter the gel, since they appeared neither on the blot nor in the Ponceau red staining.

In summary, there was no solid confirmation found that histone 3 and 4 oligomerize by forming dityrosine cross-links under oxidative conditions.

Ctrl) untreated, over night @ 37°C
1) + 5 mM H_2O_2 + 50 µM $CuSO_4$, over night @ 37 °C
2) + 5 mM H_2O_2 + 1 µM HRP, over night @ 37 °C
3) + 1 mM sin-1, over night @ 37 °C
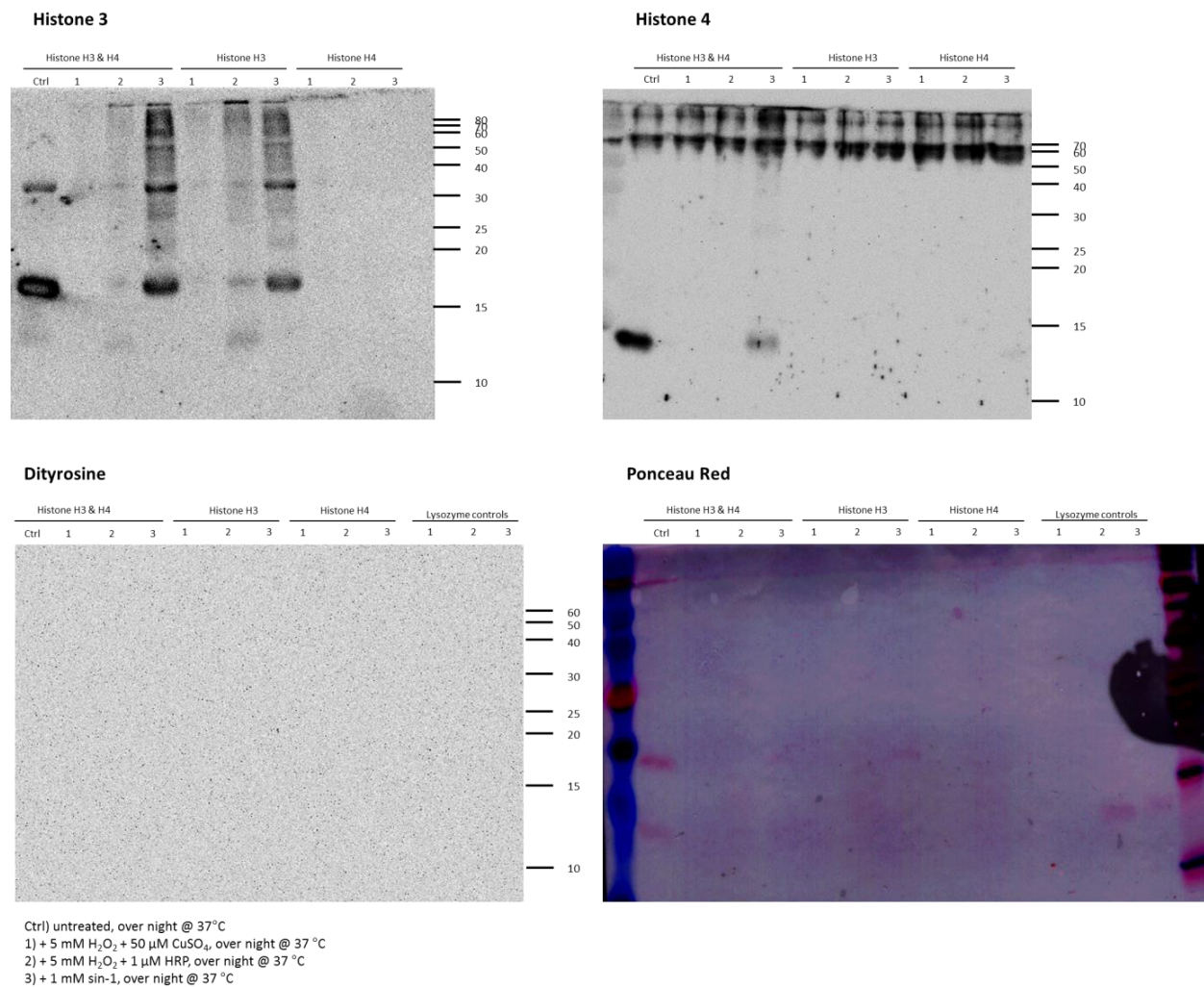
Figure 45 – Western blot analysis of histone 3/ histone 4 oxidation. Recombinant human histone 3 and histone 4 were incubated over night at 37°C with the following oxidizing agents: 1) 5 mM H_2O_2 + 50 µM $CuSO_4$, 2) 5 mM H_2O_2 + 1 µM HRP, 3) 1 mM Sin-1. Potential oligomerization of histones 3 and 4 or formation of dityrosine were detected by Western blotting using the respective antibodies. Protein loading and transfer was monitored by Ponceau Red staining. Blots are representative for n=1 independent experiments.

5.4 Epigenetic investigation of diabetic complications in ZDF rats and effect of the SGLT2 inhibitor empagliflozin

The sodium-glucose co-transporter 2 (SGLT2) is responsible for the renal reabsorption of >90% of glucose from primary urine [437]. Inhibitors of SGLT2 (SGLT2i) increase urinary excretion of glucose, thus preventing hyperglycemia as well as resulting glucotoxicity in diabetic animals and individuals.

In our recently published paper "The SGLT2 inhibitor empagliflozin improves the primary diabetic complications in ZDF rats" [412] it was demonstrated that the drug empagliflozin reduces glucotoxicity and thereby prevents the development of endothelial dysfunction, reduces oxidative stress and exhibits anti-inflammatory effects in Zucker diabetic fatty (ZDF) rats, a model of type 2 diabetes (T2DM) (see Discussion 6.4, Figure 76, p.141).

Male rats at the age of 16 ± 1 weeks were used in the study. In total, 35 diabetic ZDF-Lepr[fa/fa] and 16 respective lean controls ZDF-Lepr^{+/+} were examined. Empagliflozin (SGLT2i: 10 and 30 mg/kg/d, considered as low and high dose, respectively) was administered via drinking water for 6 weeks.
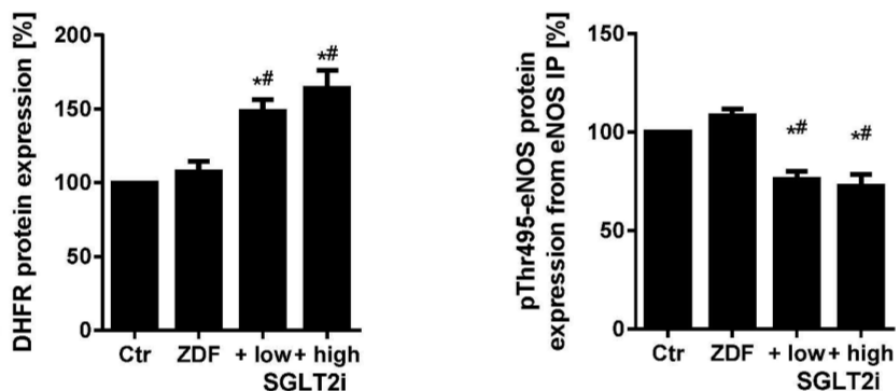
Figure 46 - Effects of SGLT2i treatment on vascular parameters in ZDF rats. Protein expression of DHFR, as well as phosphorylation of eNOS at Thr495 (in immunoprecipitated eNOS) as surrogate parameters for the integrity of vascular •NO/cGMP signaling was determined by Western blot analysis. Data are the means ± SEM from at least 4 independent experiments with pooled tissues from at least 8 animals/group. *, p<0.05 vs. control and #, p<0.05 vs. ZDF group. *Data was collected by co-authors. Graphs were taken from our publication Steven et al. 2017 [412].*

In the study it was shown that low and high doses of empagliflozin prevented endothelial dysfunction as measured by endothelium-dependent relaxation by the vasodilator acetylcholine (ACh) in aortic rings (see publication [412] and Figure 74 in the Discussion 6.4 for further detail). Furthermore, surrogate parameters for the functional state of endothelial nitric oxide synthase (eNOS) and integrity of the vascular •NO/cGMP signaling pathway were analyzed, which indicated that empagliflozin treatment rescued ZDF rats from endothelial dysfunction. For instance, the expression of dihydrofolate reductase

(DHFR), which is responsible for ensuring the availability of the eNOS cofactor tetrahydrobiopterin (BH_4) by reducing oxidized BH_2 back to BH_4, and is therefore essential for eNOS function, was increased by SGLT2i treatment. In addition, the inhibitory phosphorylation of eNOS at Thr495, conferred by protein kinase C, was diminished by SGLT2i treatment (Figure 46).
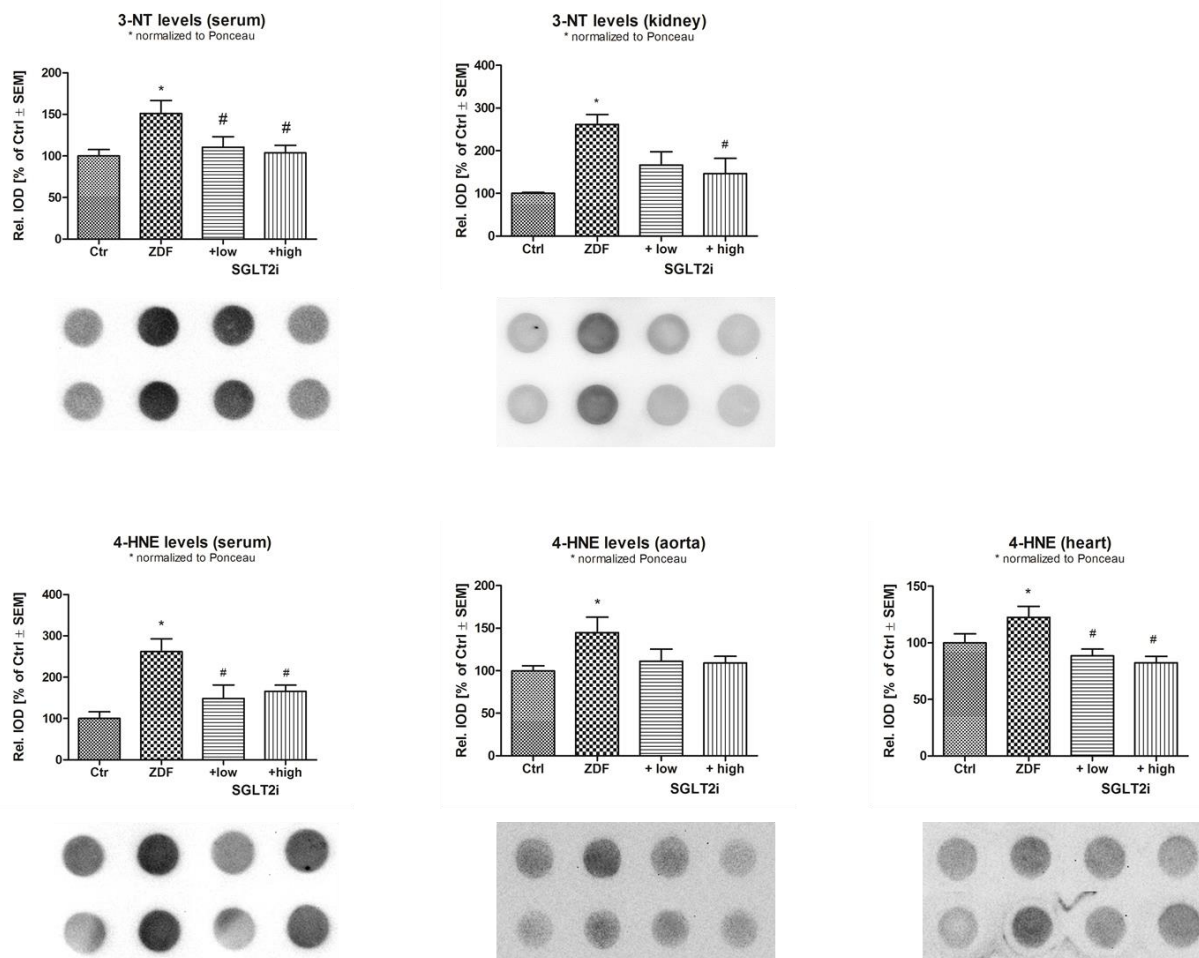
Figure 47 - Effects of SGLT2i treatment on ROS-induced protein modifications in serum, kidney, aortic and cardiac tissue of ZDF rats. 3-nitrotyrosine (3-NT)-positive and 4-hydroxynonenal (HNE)-positive proteins were measured by dot blot analysis in serum, as well as in kidney, aortic and cardiac tissue. IOD was evaluated and normalized to Ponceau S staining. Representative blots are shown below the densitometric quantification. Data are the means ± SEM from 4-8 animals/group. *, $p < 0.05$ vs. control and #, $p < 0.05$ vs. ZDF group. *Graphs were published in modified form in Steven et al. 2017 [412].*

Empagliflozin also reduced oxidative stress in ZDF rats, which was shown by chemiluminescent measurement of zymosan A-induced oxidative burst in whole blood, as well as HPLC measurement of 2-hydroxyethidium (2-HE) of cardiac tissue and DHE fluorescence microtopography in aorta (see publication [412] and Figure 74 in the Discussion 6.4 for further detail).

Additionally, oxidative stress was measured by dot blot analysis of 3-nitrotyrosine (3-NT)- and 4-hydroxynonenal (4-HNE)-modified proteins, which represent surrogate parameters for ROS formation.

Levels of 3-NT and 4-HNE were found to be elevated in serum, kidney, aortic or cardiac tissue of ZDF rats and were decreased upon SGLT2i treatments (Figure 47).

Western blot analysis of the NADPH oxidase isoform NOX2 and heme oxygenase 1 (HO-1) revealed increased expression of these proteins, which are involved in oxidative stress and antioxidant defense, in aorta of ZDF rats (Figure 48). This effect was not observed in ZDF rats treated with the SGLT2 inhibitor empagliflozin. Furthermore, SGLT2i treatment reduced levels of RAGE (receptor for advanced glycation end products), a protein associated with glucotoxicity, in ZDF rats.

Additionally, it was found that aortic mRNA levels of the inflammatory markers interferon-γ (IFN- γ), cyclooxygenase-2 (COX2) and inducible nitric oxide synthase (NOS2), which were increased in diabetic ZDF rats, decreased upon SGLT2i treatment (Figure 49).
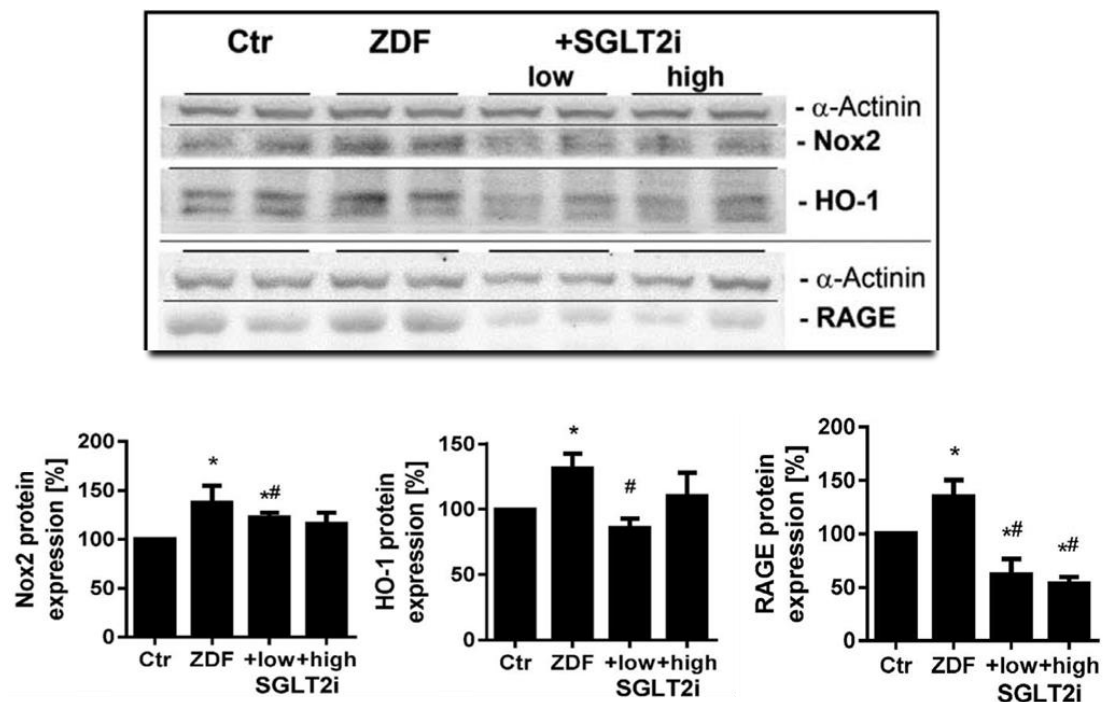
Figure 48 - Effects of SGLT2i treatment on aortic protein expression involved in oxidative stress, antioxidant defense and glucotoxicity pathways in ZDF rats. Aortic protein expression of the NADPH oxidase isoform Nox2, the antioxidant stress-response-enzyme heme oxygenase-1 (HO-1) and the receptor for advanced glycation end products (RAGE) was assessed by Western blot analysis using specific antibodies. Representative blots for all proteins are shown along with the densitometric quantification. Data are the means ± SEM from 4-6 animals/group. *, p<0.05 vs. control and #, p<0.05 vs. ZDF group. *Data was collected by co-authors.Graphs were taken from our publication Steven et al. 2017 [412].*
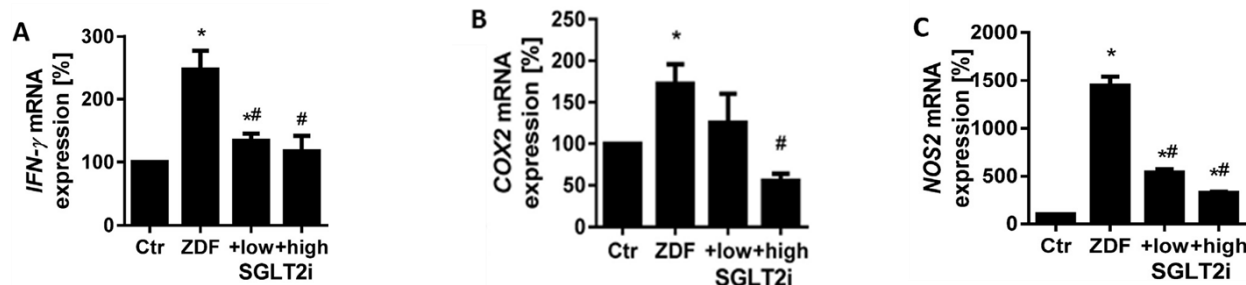
Figure 49 - Effects of empagliflozin treatment on aortic mRNA expression of pro-inflammatory genes in ZDF rats. mRNA expression of inflammatory genes (A): interferon-γ (IFN-γ), (B): cyclooxygenase-2 (COX-2), (C): inducible NO synthase (NOS2) was assessed by quantitative RT-PCR. The data are expressed as % of control and are the means ± SEM from at least 3 animals/group.*, p<0.05 vs. control and #, p<0.05 vs. ZDF group. *Data was collected by co-authors.Graphs were taken from our publication Steven et al. 2017 [412].*

Certain genes involved in oxidative stress, glycemic control or inflammation, which had been shown to be affected in ZDF rats by Western blot or mRNA expression (Figure 48, Figure 49), were selected to be analyzed by chromatin immunoprecipitation (ChIP), i.e. HO-1, RAGE, IFN-γ and NOS2, as well as eNOS and DHFR. The intention was to examine if changes in gene expression, as observed in ZDF rats, were caused by epigenetic regulation through histone modifications and if SGLT2i treatment could antagonize these effects. Native ChIP assays were performed analyzing the transcription-activating histone mark H3K4me3 (trimethylation of lysine 4 in histone 3) and the repressive mark H3K9me3 (trimethylation of lysine 9 in histone 3) in mentioned genes using rat kidney tissue.

It has been shown previously that global differences in H3K4 trimethylation are associated with overweight and type 2 diabetes [438]. Furthermore, it has also been shown that H3K9 trimethylation is involved in metabolic memory and is decreased at the promoters of key inflammatory genes in type 2 diabetic mice [331].

A reliable protocol for the ChIP assay was set up with the help of Prof. Wojnowski's group. 50 mg of rat kidney tissue were used per ChIP. Chromatin was precipitated using either H3K4me3- or H3K9me3-specific antibodies. Specific qPCR primers suitable for ChIP-obtained rat DNA were designed using data from the UCSC genome browser. Since there is no ChIP primer repository/database available thus far, a protocol was developed to design optimal qPCR primers, which is described in detail in the Methods section (4.14, p.68).The primers used for HO-1 and eNOS quantification were a kind gift of Prof. Li.
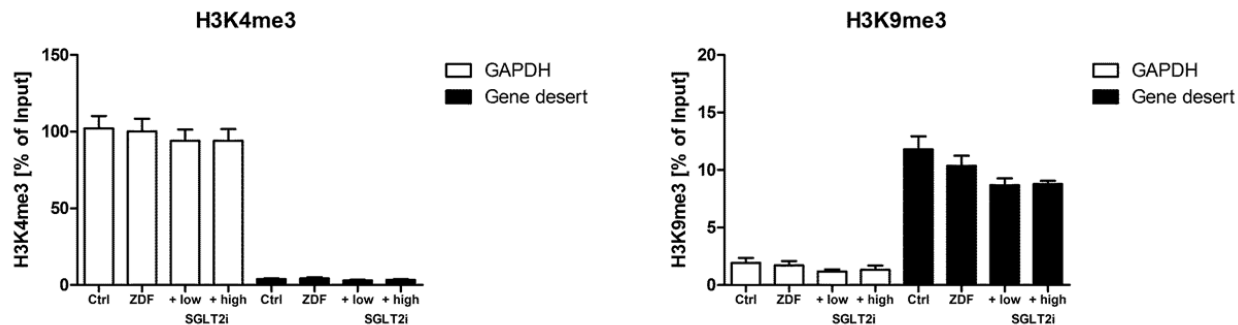
Figure 50 – Validation of ChIP assay. Successful performance of each ChIP was confirmed by qPCR-based quantification of the constitutively active gene GAPDH and a gene desert, a genomic region devoid of protein-coding genes and therefore suppressed transcription. Data from 16 H3K4me3- and 10 H3K9me3-ChIP experiments were combined. Data are expressed as % of input and are the means ± SEM from 10 animals/group.

To validate each ChIP experiment, DNA precipitates were subjected to qPCR-based quantification of the constitutively active gene GAPDH, as well as a genomic region that is devoid of protein-coding genes ("gene desert"). The GAPDH gene is actively transcribed in all cell types and its promoter is highly enriched in histone modifications associated with active transcription, such as histone H3K4 trimethylation and general histone acetylation. This gene promoter shows very low levels of histone modifications associated with transcription repression, such as histone H3K9 or H3K27 trimethylation. On the other hand, a gene desert on rat chromosome 3 was targeted, because this region contains high levels of histone marks associated with heterochromatin, such as H3K9me3. As there is only non-coding DNA, no transcription-activating histone marks can be found. Thus, a ChIP was considered valid when high levels of GAPDH and low levels of gene desert were detected by qPCR in chromatin derived from H3K4me3-mediated ChIP, while H3K9me3-mediated ChIP resulted in low levels of GAPDH and high levels of gene desert, in relative terms. Figure 50 shows the results of GAPDH and gene desert quantification from all H3K4me3- and H3K9me3-ChIP experiments combined. Results were always calculated as percentage of input DNA. Transcription activating H3K4 trimethylation was found to be present at 94-100% of GAPDH promoters, whereas in the gene desert only 3-4% was modified. In contrast, transcription suppressing H3K9me3 levels at GAPDH promoters ranged between 1-2% of input, but made up 9-12% in the gene desert.

In general, H3K9me3-induced ChIP analysis of the selected genes yielded very low percentages of H3K9me3-modified genes, ranging from 1-7%, thus questioning the relevance of epigenetic regulation by H3K9me3 in the correspondent genes. Therefore, as an additional control, a subsidiary normalization method was applied, subtracting the background signals. The background was defined as levels of

repressive mark H3K9me3 at the active gene GAPDH and, on the other hand, activating mark H3K4me3 at the transcriptionally repressed gene desert.

No significant changes were detected between the groups for activating H3K4me3 marks in regulatory regions of heme oxygenase-1 (HO-1) and dihydrofolate reductase (DHFR) (Figure 51 A, Figure 52 A). However, H3K9me3 levels were slightly decreased in SGLT2i-treated rats, which could explain part of the upregulation of HO-1 and DHFR by SGLT2i therapy, although the physiological relevance of these changes in H3K9me3 levels may be limited by the generally low signal (Figure 51 B, Figure 52 B).
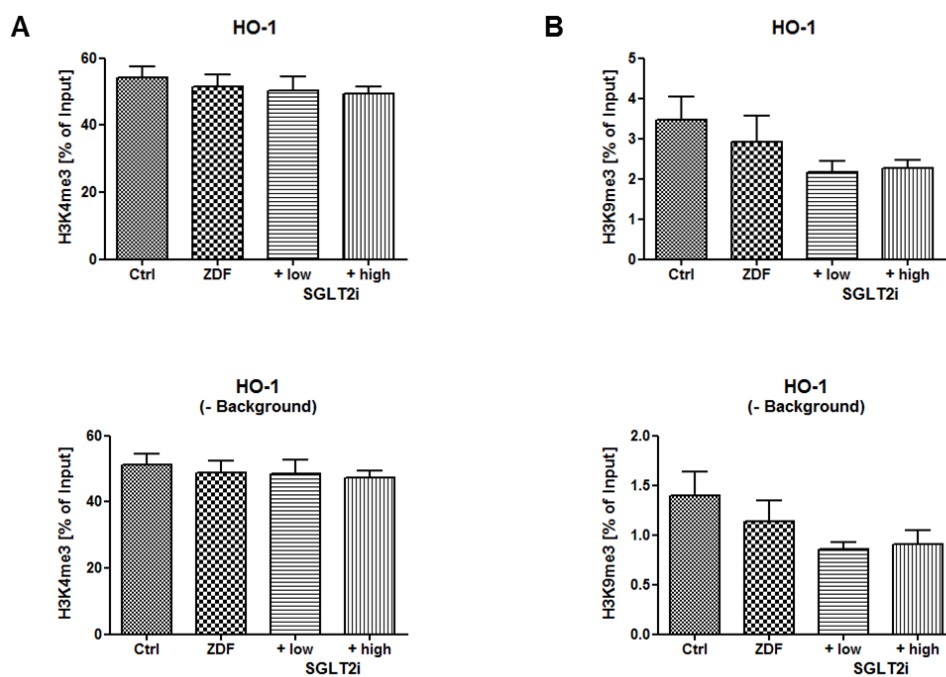
Figure 51 - Effects of empagliflozin (SGLT2i) treatment on epigenetic regulation of HO-1. Levels of histone marks **H3K4me3 (A)** and **H3K9me3 (B)** were measured by ChIP analysis in regulatory regions of the gene HO-1. The data are expressed as % of input and are the means ± SEM from 10 (A) or 4 (B) animals/group. No significant differences were observed.
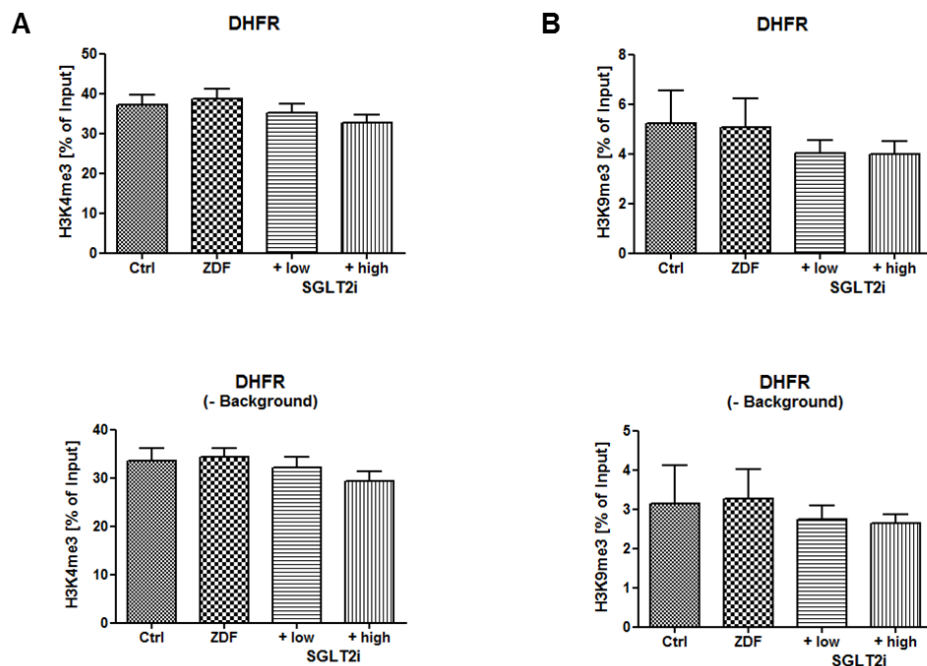
Figure 52 - Effects of empagliflozin (SGLT2i) treatment on epigenetic regulation of DHFR. Levels of histone marks **H3K4me3 (A)** and **H3K9me3 (B)** were measured by ChIP analysis in regulatory regions of the gene DHFR. The data are expressed as % of input and are the means ± SEM from 10 (A) or 4 (B) animals/group. No significant differences were observed.

In the promoter region of eNOS the gene activating epigenetic mark H3K4me3 was found to be significantly decreased in all ZDF groups including the ones treated with SGLT2i (Figure 53 A). Since there was no effect on eNOS expression (also seen in mRNA qPCR), this indicates that the rescue of endothelial function that was observed in empagliflozin-treated rats is not due to eNOS upregulation but probably due to an improvement in the $^{\bullet}$NO/cGMP signaling pathway.

The glucotoxicity marker RAGE exhibited slightly (but insignificantly) increased activating H3K4me3 promoter marking in ZDF rats, whereas under empagliflozin therapy this trend was reversed (Figure 53 B). H3K9 trimethylation of eNOS and RAGE could not be determined, as signals were not considerably deviating from background signals (not shown).

ChIP analysis of the promoter region of the inflammatory marker interferon-γ (IFN-γ) indicated slightly (but insignificantly) increased H3K4me3 levels in diabetic rats, which were reduced by trend in SGLT2i-treated animals (Figure 54 A). Transcription-repressing H3K9me3 levels at the IFN-γ gene were not changed between control and diabetic animals, but were also lowered upon empagliflozin therapy (Figure 54 B). However, it has to be taken into account that, in this case, both H3K4me3 and H3K9me3 marks were measured at a very low percentage, so any significance for IFN-γ expression regulation remains to be determined.
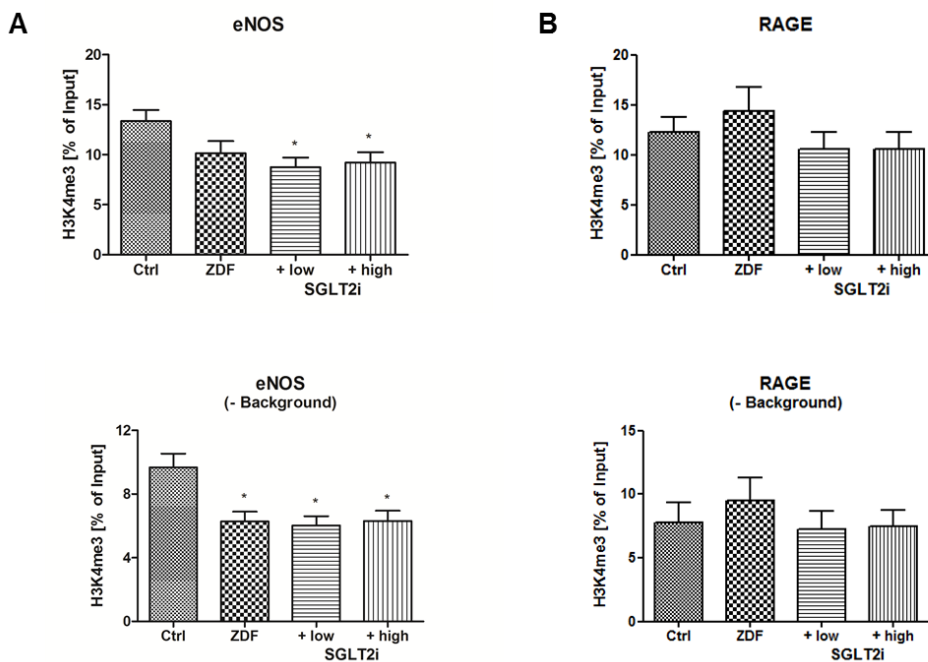
Figure 53 - Effects of empagliflozin (SGLT2i) treatment on epigenetic regulation of eNOS (A) and RAGE (B). Levels of the histone mark **H3K4me3** were measured by ChIP analysis in regulatory regions of the genes eNOS and RAGE. The data are expressed as % of input and are the means ± SEM from 10 animals/group. *, $p<0.05$ vs. control group.
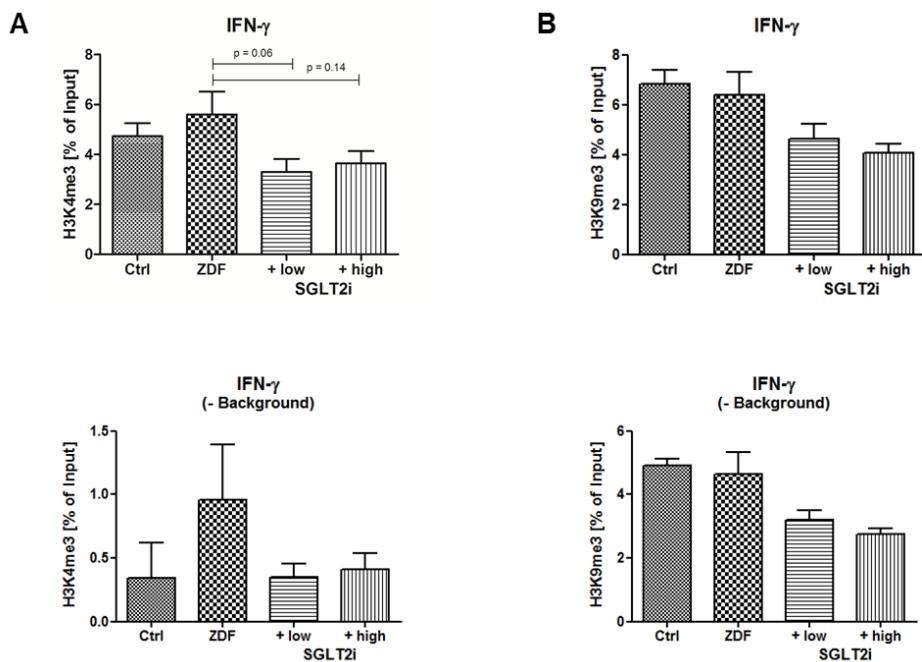
Figure 54 - Effects of empagliflozin (SGLT2i) treatment on epigenetic regulation of the inflammatory marker IFN-γ. Levels of histone marks **H3K4me3 (A)** and **H3K9me3 (B)** were measured by ChIP analysis in the promoter region of the gene IFN-γ. The data are expressed as % of input and are the means ± SEM from 10 (A) or 4 (B) animals/group. No significant differences.

Furthermore, histone modifications on the gene for the cytokine-inducible nitric oxide synthase (iNOS/NOS2) were analyzed at the promoter site and at two different regulatory intron regions. In all three genomic regions, there was no significant difference in H3K4me3 modification between control and ZDF rats, but the empagliflozin-treated rats showed considerably decreased epigenetic regulation by H3K4 trimethylation in the promoter region of NOS2 (Figure 55 A), which may explain part of the normalized NOS2 mRNA signal in the high dose SGLT2i group. In the regulatory intron regions a stable trend for reduced H3K4me3 was observed in medicated rats compared to untreated rats (Figure 55 B, C). The overall yield (% of input) of H3K4me3-modified NOS2 was substantially higher than the background when targeting the intron regions instead of the promoter region. Repressive H3K9me3-modification was only detected above baseline in intron2.2 of NOS2, where ZDF and low-dose treated ZDF rats showed similarly decreased H3K9me3 signal compared to control rats (Figure 55 D). Yet, high-dose SGLT2i-treated ZDF rats displayed even ~30% less H3K9me3 NOS2 modification than untreated ZDF rats.

These results indicate that treatment with empagliflozin is likely to confer epigenetic effects. Whether these effects are a consequence of glucose lowering or represent a specific property of empagliflozin (e.g. by off-target pleiotropic effects) remains to be investigated.
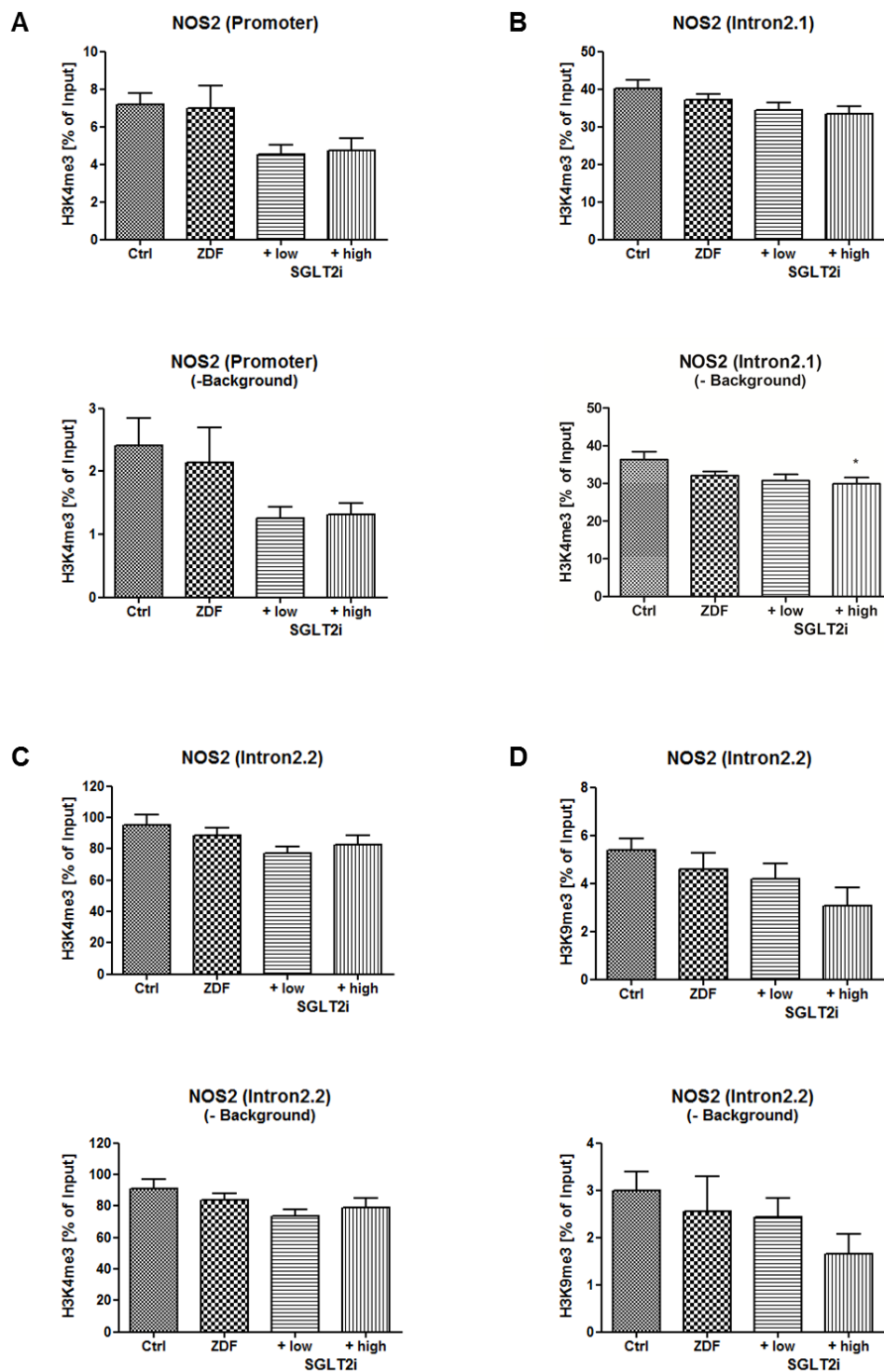
Figure 55 - Effects of empagliflozin (SGLT2i) treatment on epigenetic regulation of the immune defense enzyme NOS2. Levels of histone marks **H3K4me3 (A-C)** and **H3K9me3 (D)** were measured by ChIP analysis in the promoter region (A) and two different intron regulatory regions (B-C) of the gene NOS2. The data are expressed as % of input and are the means ± SEM from 10 (A-C) or 4 (D) animals/group. *, $p < 0.05$ vs. control group.

In order to analyze the protective and potentially pleiotropic effects of empagliflozin with regards to glucotoxicity, human umbilical vein endothelial cells (HUVECs) were cultured under hyperglycemic conditions (30 mM glucose) for up to 6 days (collaboration with A. Karpi). Empagliflozin (EMPA) was administered at concentrations of 1 µM or 10 µM on day 3 of hyperglycemia for another 2 or 3 days. In addition, the cells were also treated with the dipeptidyl peptidase-4 (DPP-4) inhibitor sitagliptin (SITA) or the RAGE inhibitor FPS-ZM1 at the same concentrations and times to allow a head-to-head comparison of these antidiabetic drugs.

Viability of hyperglycemic HUVECs was then assessed by qualitative and quantitative evaluation of living cells. It was observed that cell density decreased time-dependently, while cell shape changed to an elongated, activated state in the hyperglycemic groups (Figure 56 C) (see all images in Appendix p.197). In addition, increased detachment and accumulation of apoptotic cell bodies was detected upon hyperglycemia. On day 6, living cells were manually counted using the Cell B software (Olympus) and cell numbers were compared between normoglycemic and hyperglycemic groups, as well as hyperglycemic groups that had been treated with the compounds as indicated (Figure 56 A). Especially the higher (supra-pharmacological) concentrations of empagliflozin and the dipeptidyl peptidase-4 inhibitor sitagliptin conferred visible protection against glucotoxicity and normalized the cell density and shape almost completely, indicating potent (pleiotropic) protective effects on hyperglycemic endothelial cells (a glucose decrease in the medium can be excluded). The RAGE inhibitor FPS-ZM1 showed an intermediate effect on glucotoxicity, at least demonstrating the therapeutic potential of interruption of the AGE/RAGE signaling pathway.

As a read-out of eNOS activity and to indicate the state of endothelial function upon hyperglycemia, nitrite formation in response to stimulation with acetylcholine was determined in HUVECs. For this purpose, the supernatant medium containing the produced nitrite was mixed with 2,3-diaminonaphthalene under acidic conditions leading to the formation of a highly fluorescent triazol product, which was quantitatively measured by HPLC analysis. In accordance with the data on cell shape and density, the nitrite formation was substantially decreased in hyperglycemic HUVECs but was restored by all drugs in a concentration-dependent fashion (Figure 56 B). Although only minor differences between the effectiveness of the drugs were observed, empagliflozin (EMPA) was slightly more beneficial than SITA and the RAGE inhibitor FPS-ZM1.

All in all, the cell experiments show that the protective effects of empagliflozin are not only due to urinary glucose removal from the kidney but also appear in cultured endothelial cells. Thus, the SGLT2

inhibitor empagliflozin may have pleiotropic effects that contribute to its ability to improve hyperglycemia-induced vascular complications.
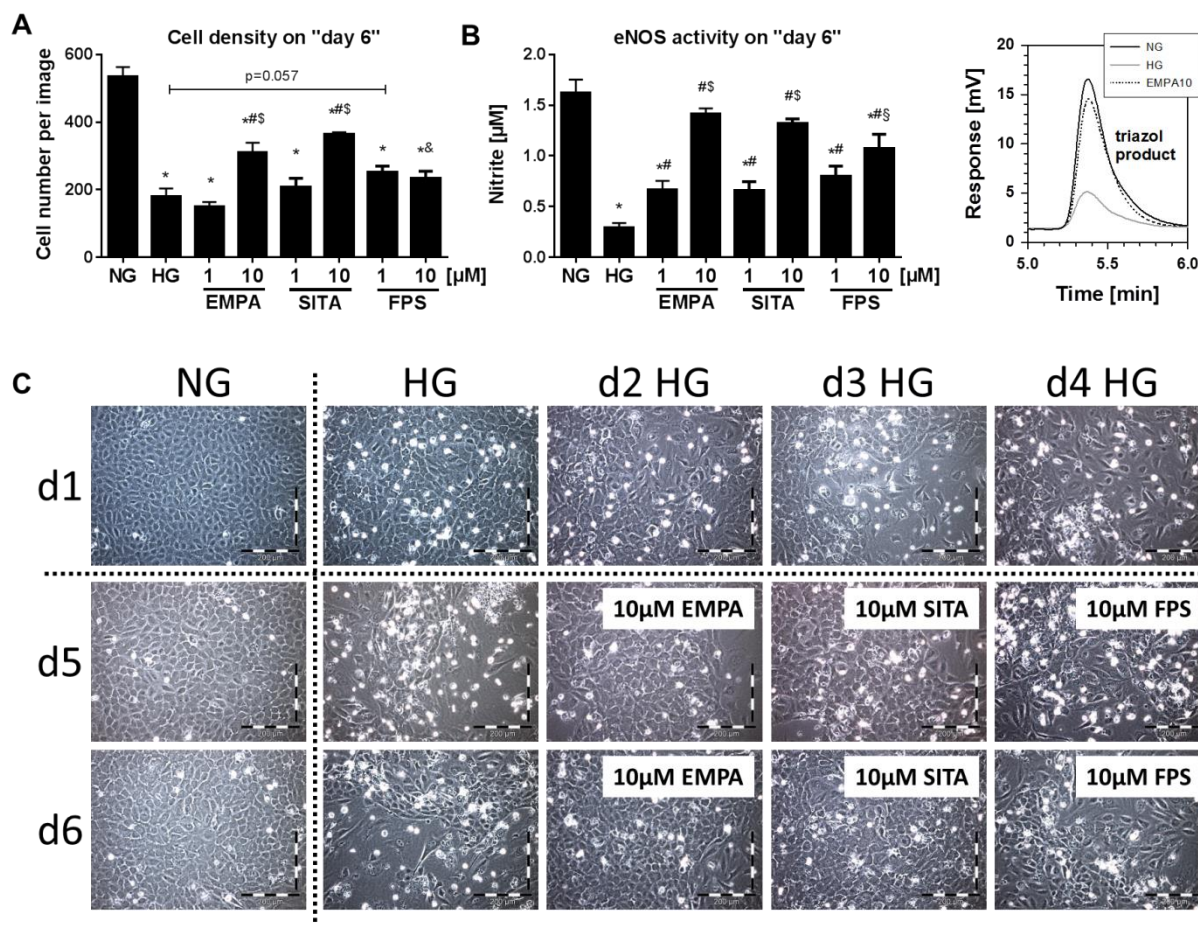
Figure 56 - Protective effects of empagliflozin (EMPA), the DPP-4 inhibitor sitagliptin (SITA) and the RAGE inhibitor FPS-ZM1 on cultured hyperglycemic human umbilical vein endothelial cells (HUVECs). Viability of hyperglycemic HUVECs was assessed after 2 or 3 days (on d5 or d6) incubation with the respective compound by qualitative and quantitative evaluation of living cells (density and shape) (A, C). Nitrite formation in response to acetylcholine (1 µM) in the supernatant of cells was determined by HPLC-based quantification of the fluorescent triazol product resulting from acidic conversion of 2,3-diaminonaphthaleneby nitrosating species (B). Representative chromatograms are shown besides the quantitative data. The data are the means ± SEM from at least 5 independent experiments. *, $p<0.05$ vs. NG; #, $p<0.05$ vs. HG; $, $p<0.05$ vs. same 1 µM group; §, $p<0.05$ vs. EMPA10; &, $p<0.05$ vs. SITA10. *Graphs were taken from our publication Steven et al. 2017 [412].*

In summary, these data provide insight into the mode of action of empagliflozin, demonstrating that empagliflozin normalizes vascular function and oxidative stress in diabetic ZDF rats. Also, empagliflozin reduces glucotoxicity and inflammation and confers glycemic control, as well as epigenetic and pleiotropic effects.

5.5   Oxidative stress and epigenetic investigation in H9c2 cardiomyocytes

Since cell models are easier to manipulate and effects more reproducible, the cell line H9c2 was acquired in order to investigate ROS-induced epigenetic changes. These cells are rat cardiomyoblasts derived from embryonic BD1X rat heart tissue by B. Kimes and B. Brandt that exhibit many of the properties of skeletal muscle [439]. Upon confluency H9c2 cells start to differentiate into cardiomyocytes and further fuse to form multinucleated myotubes, getting an elongated shape and positioning in a parallel fashion. There are numerous publications about pathological implications induced by oxidative stress in these cells with relevance for the development of cardiovascular diseases [440-449]. Based on these premises, the interplay of redox signaling and epigenetic regulation and its resulting effects on gene expression, as well as pathology and viability of H9c2 cells was investigated.

In a preliminary assessment, H9c2 myoblasts were grown for 3 days and then treated with exogenous oxidative stimuli, i.e. increasing concentrations of hydrogen peroxide for 4 h or 24 h. Subsequent analysis of expression of epigenetic regulators and histone modifications failed due to technical problems. As seen in Figure 57, H_2O_2 treatment resulted in high loss of cell material at concentrations of 100 µM H_2O_2 and higher. As a consequence, measurement of protein content by Bradford assay yielded no reliable quantification, resulting in unequal loading of samples in Western and dot blot, mirrored by disparities in loading controls or Ponceau stainings. This circumstance made analyses very intricate and problematic because normalization is difficult and could falsify results due to extrapolation. In response to treatment with 10 µM and 50 µM H_2O_2 no major changes in expression of epigenetic regulators were observed.

4h incubation with H₂O₂

Ctrl   10 µM H₂O₂   50 µM H₂O₂

100 µM H₂O₂   250 µM H₂O₂   500 µM H₂O₂

24h incubation with H₂O₂

Ctrl   10 µM H₂O₂   50 µM H₂O₂
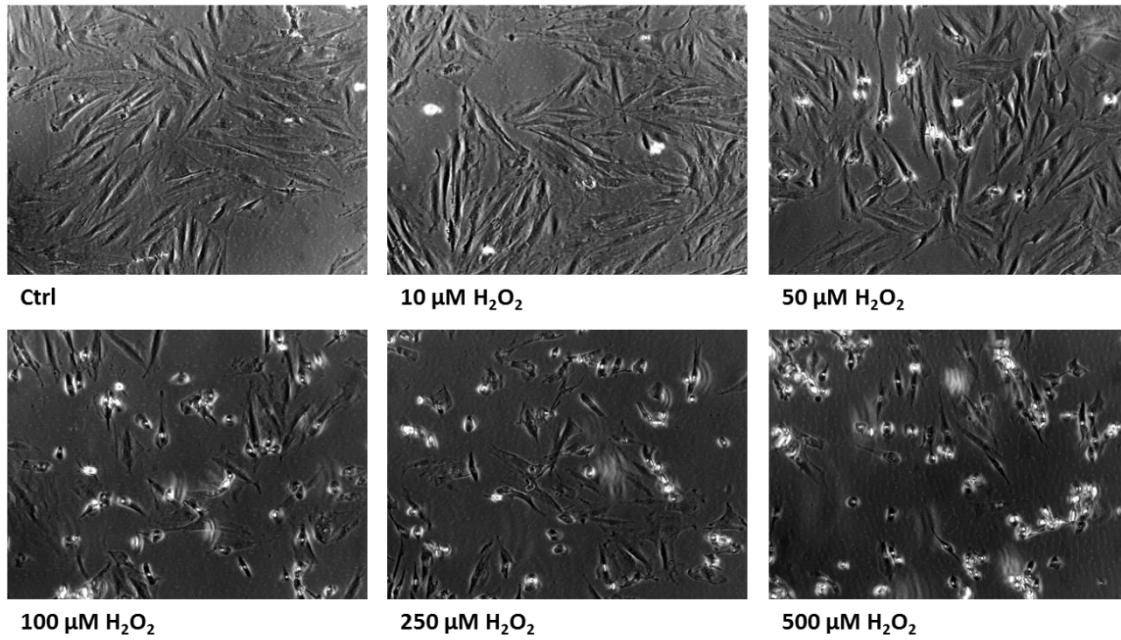
100 µM H₂O₂   250 µM H₂O₂   500 µM H₂O₂
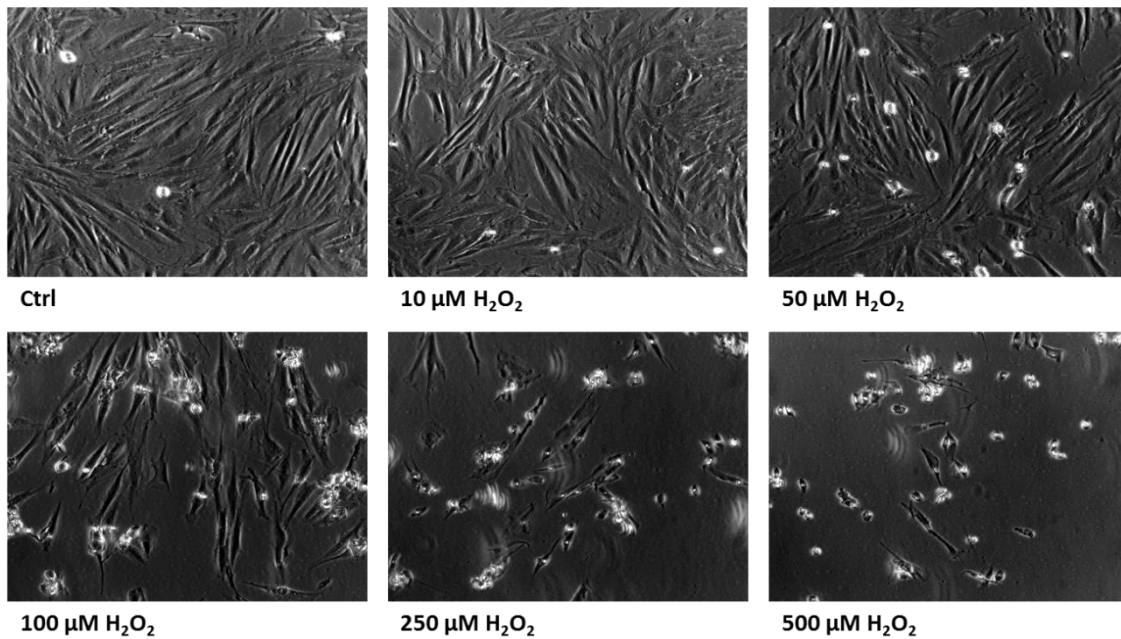
Figure 57 - H9c2 rat cardiomyoblasts were treated with increasing concentrations of hydrogen peroxide for 4 hours or 24 hours. Increased cell loss can clearly be observed upon treatment with H_2O_2 at concentrations of 100 µM and higher. Of note, the differentiation process can nicely be perceived when comparing cells at 4 h and 24 h post-treatment, as cells start to elongate and align in a parallel position. Images are representative for n=5 independent experiments.

5.5.1 Doxorubicin-induced cardiomyopathy in H9c2 cardiomyocytes

In response to these problems, it was decided to establish a less harsh and more indirect approach for inducing ROS formation (also with higher clinical relevance), which would provide a sustainable effect on the cell nature without immediately causing too extensive cell loss.

The anthracycline doxorubicin (Dox) is a potent chemotherapeutic agent used for the treatment of several adult and pediatric cancers, whose therapeutic efficacy is limited as it is known to induce severe cardiotoxicity [375, 376, 450]. Doxorubicin-induced cardiomyopathy is strongly linked to increased cardiac oxidative stress and mitochondrial dysfunction. Thus, H9c2 cardiomyocytes were exposed to doxorubicin in order to establish a model of doxorubicin-induced cardiotoxicity allowing the analysis of global histone mark changes, as well as changes in expression of histone modifiers and the association to doxorubicin-induced ROS generation. Since it was reported by Branco *et al.* that doxorubicin toxicity is higher in differentiated H9c2 cells, i.e. cardiomyotubes [451], the H9c2 myoblastic cells were grown for 7 days until a multinucleated, elongated phenotype was reached. Cells were then incubated with 1 µM or 5 µM doxorubicin for 24 h or 48 h. As can be visually observed in Figure 58, doxorubicin treatment led to a time- and concentration-dependent increase of cell death. Afterwards, cells were lysed and subjected to further investigation. Of note, also detached apoptotic cells from the medium supernatant (SN) were included in the analysis. Due to its red color, the amount of doxorubicin-uptake in the cells can be clearly seen in the collected cell pellets. As shown in Figure 23 in the Methods part (4.1.4, p.53), the amount of adherent cells decreases, whereas the amount of detached cells gathered from the medium increases upon increasing doxorubicin concentrations compared to untreated cells. This effect was even more pronounced at 48 h of doxorubicin incubation. In the medium supernatant of untreated control cells no substantial amount of dead cells could be harvested and was therefore not included in further analysis.

Before treatment

24h incubation with doxorubicin   **48h incubation with doxorubicin**

Ctrl

1 µM Dox

5 µM Dox
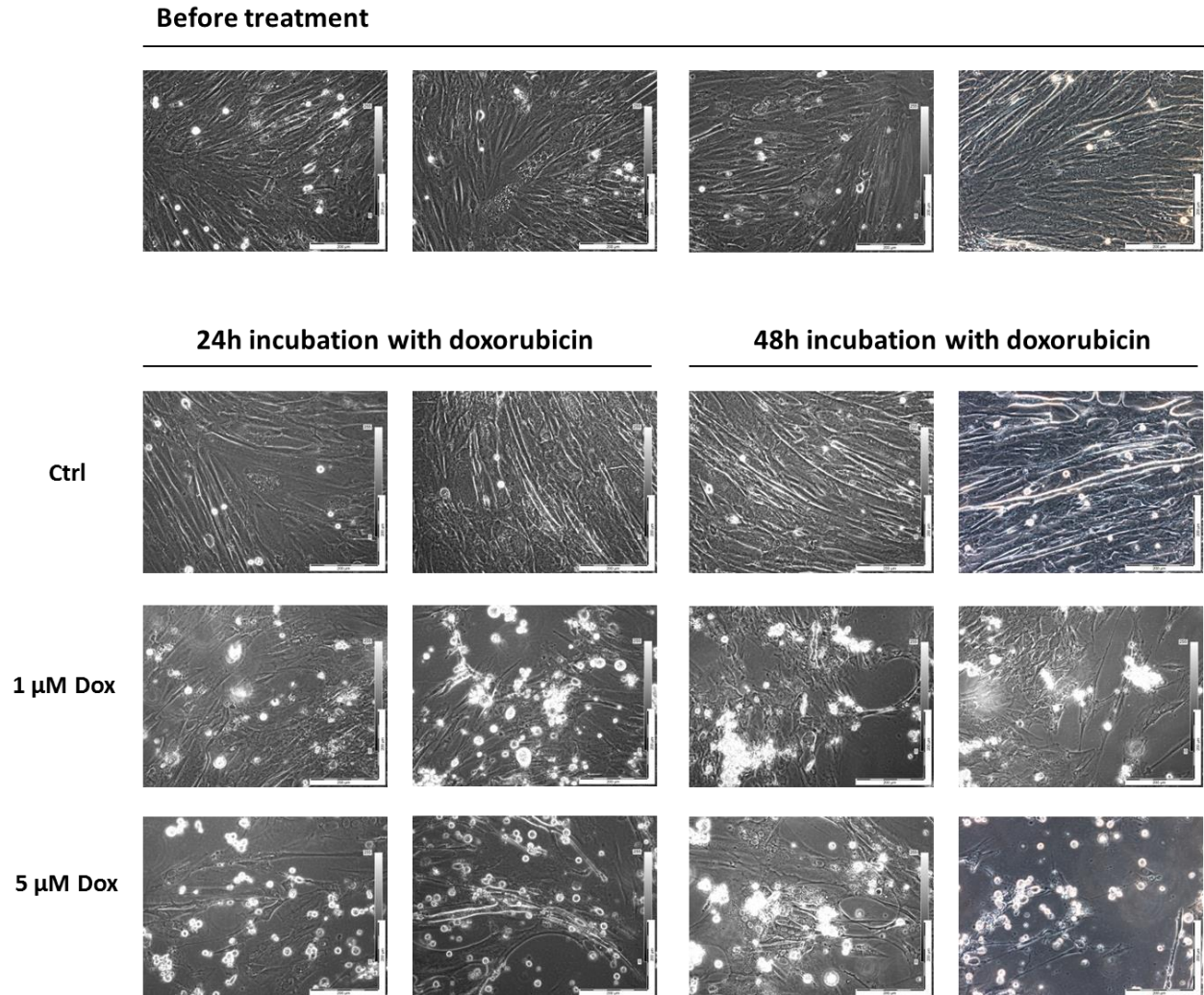
Figure 58 - Effects of doxorubicin (Dox) treatment on differentiated H9c2 cardiomyocytes. H9c2 were grown for 7 days to instigate cell differentiation. On the day of treatment, H9c2 cells were aligned in parallel and had reached a multinucleated, elongated phenotype (top). After 24 h (left) and 48 h (right) after doxorubicin (Dox) addition, increasing amounts of apoptotic cell bodies are visible. Images are representative for n=4 independent experiments**.**

Cell lysates were then analyzed via Western blot to check for apoptotic markers. Caspase-3 cleavage and fractin formation as indicators for apoptotic cell death were highly enriched in the fractions of detached cells in the supernatant (SN), but were also elevated in surviving adherent doxorubicin-treated cells, indicating that these cells are in a "pre-apoptotic" state (Figure 59, Figure 60). It is noteworthy, though, that depending on the housekeeping protein that was used for normalization (actin or GAPDH), quantification differed in some cases. This occurrence was seen repeatedly in Western blot experiments, which is why both evaluation results are always shown.

Effects of doxorubicin treatment on oxidative stress in H9c2 cells were determined by dot blot analysis of the ROS-induced protein modifications 3-nitrotyrosine (3-NT) and malondialdehyde (MDA) (Figure 61). Increased levels of 3-NT and MDA were detected in all groups compared to control. In surviving pre-apoptotic cells, treatment with 5 µM of doxorubicin (5 µM Dox) resulted in higher ROS formation than 1 µM doxorubicin (1 µM Dox) (Figure 61 A-D). Interestingly, higher levels of MDA were detected in apoptotic cells that had been treated with 1 µM doxorubicin (1 µM Dox-SN) than in 5 µM doxorubicin-treated apoptotic (5 µM Dox-SN) cells at 24 h and at 48 h (Figure 61 C, D). The same was true for 3-NT levels at 48 h (Figure 61 B).

As another indicator for oxidative stress, the expression of the antioxidant superoxide dismutase was assessed by Western blot (Figure 62). At 24 h of doxorubicin incubation, pre-apoptotic cells displayed a concentration-dependent increase of SOD2 expression, whereas in apoptotic cells expression was not significantly changed compared to control cells. Therefore, at least the pre-apoptotic cells showed a correlation between 3-NT or MDA formation and SOD2 expression at 24 h (Figure 62 A). After 48 h incubation with doxorubicin, pre-apoptotic cells that had been incubated with 5 µM doxorubicin showed a 2-3 fold increase in SOD2 expression, whereas there was no change at 1 µM doxorubicin (Figure 62 B). But interestingly, in the apoptotic fraction of 1 µM Dox-treated cells (1 µM Dox-SN) SOD2 expression was dramatically increased. In contrast, apoptotic 5 µM Dox-treated cells (5 µM Dox-SN) displayed only minor increase in SOD2 levels. This expression pattern resembled the pattern of MDA levels observed at 48 h and to a somewhat lesser extent also the levels of 3-NT at 48 h (Figure 61 B, D).
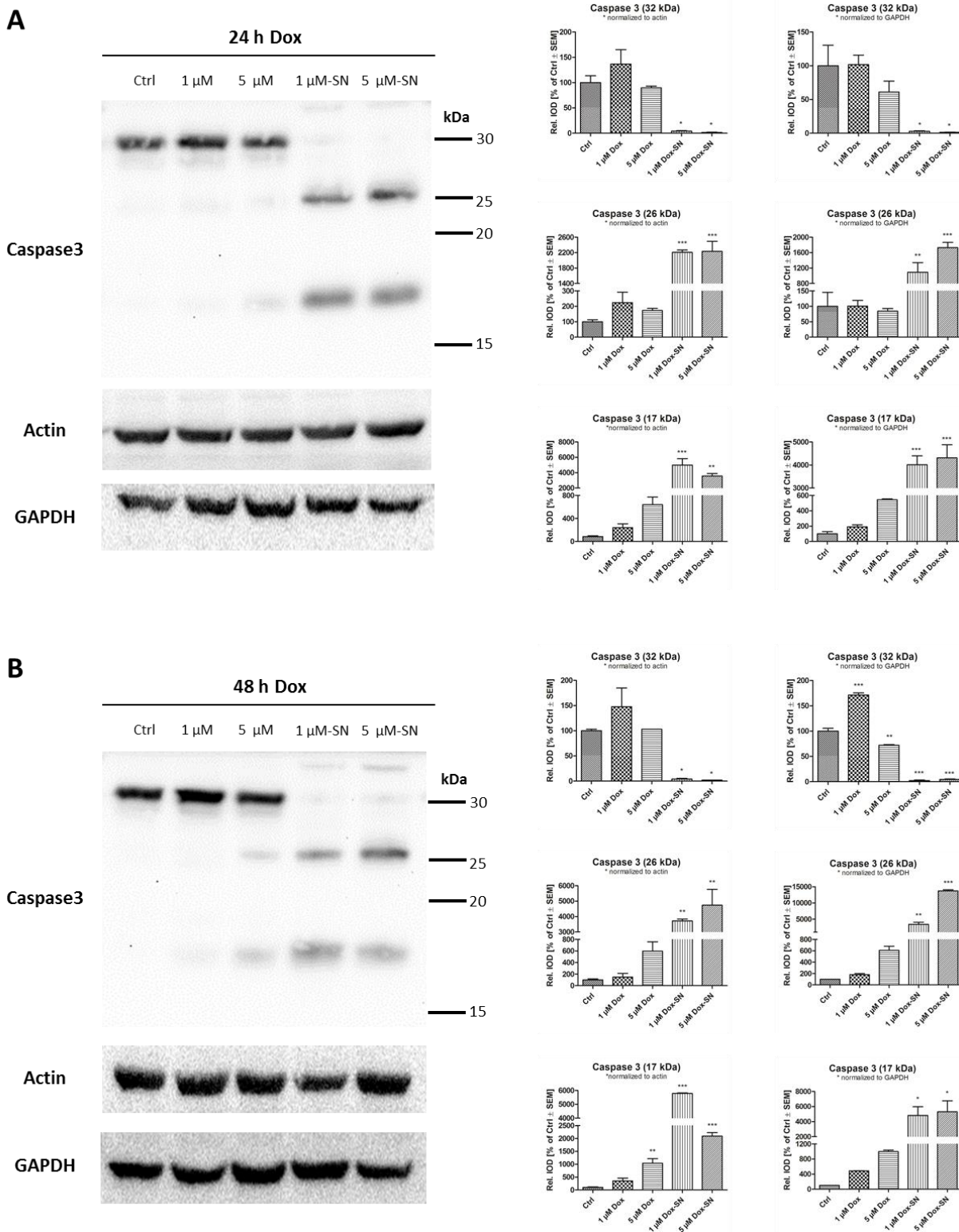
Figure 59 - Proteolytic cleavage of caspase 3, as marker of apoptosis, is increased in doxorubicin (Dox)-treated H9c2 cells.
Levels of inactivated pro-caspase 3 at 32 kDa and the active cleaved caspase 3 at 17 kDa, as well as an additional caspase 3 active subunit at 26 kDa, were assessed by Western blot analysis in attached control and doxorubicin (Dox)-treated cells, as well as detached cells collected from the supernatant (SN). Representative blots are shown along with the densitometric quantification, either normalized to actin (left) or GAPDH (right). Data are the means ± SEM from 2 experiments. *, p<0.05 vs. control; **, p<0.01 vs. control; ***, p<0.005 vs. control.
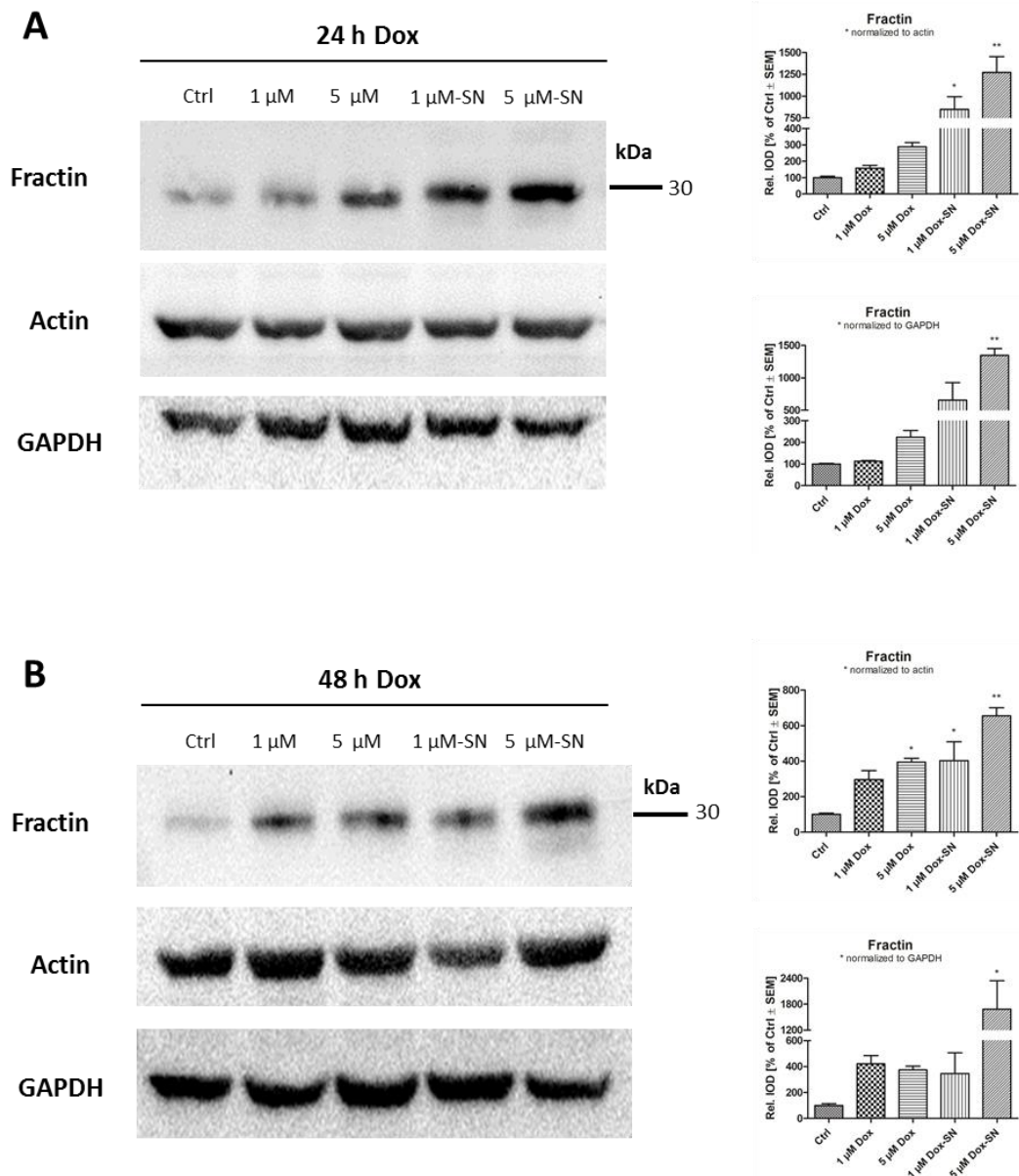
Figure 60 - Fractin, as marker of apoptosis, is enriched in doxorubicin (Dox)-treated H9c2 cells. Levels of the apoptosis-specific fragment fractin were assessed by Western blot analysis in attached control and doxorubicin (Dox)-treated cells, as well as detached cells collected from the supernatant (SN). Representative blots are shown along with the densitometric quantification, either normalized to actin (top) or GAPDH (bottom). Data are the means ± SEM from 2 experiments. *, p<0.05 vs. control; **, p<0.01 vs. control; ***, p<0.005 vs. control.
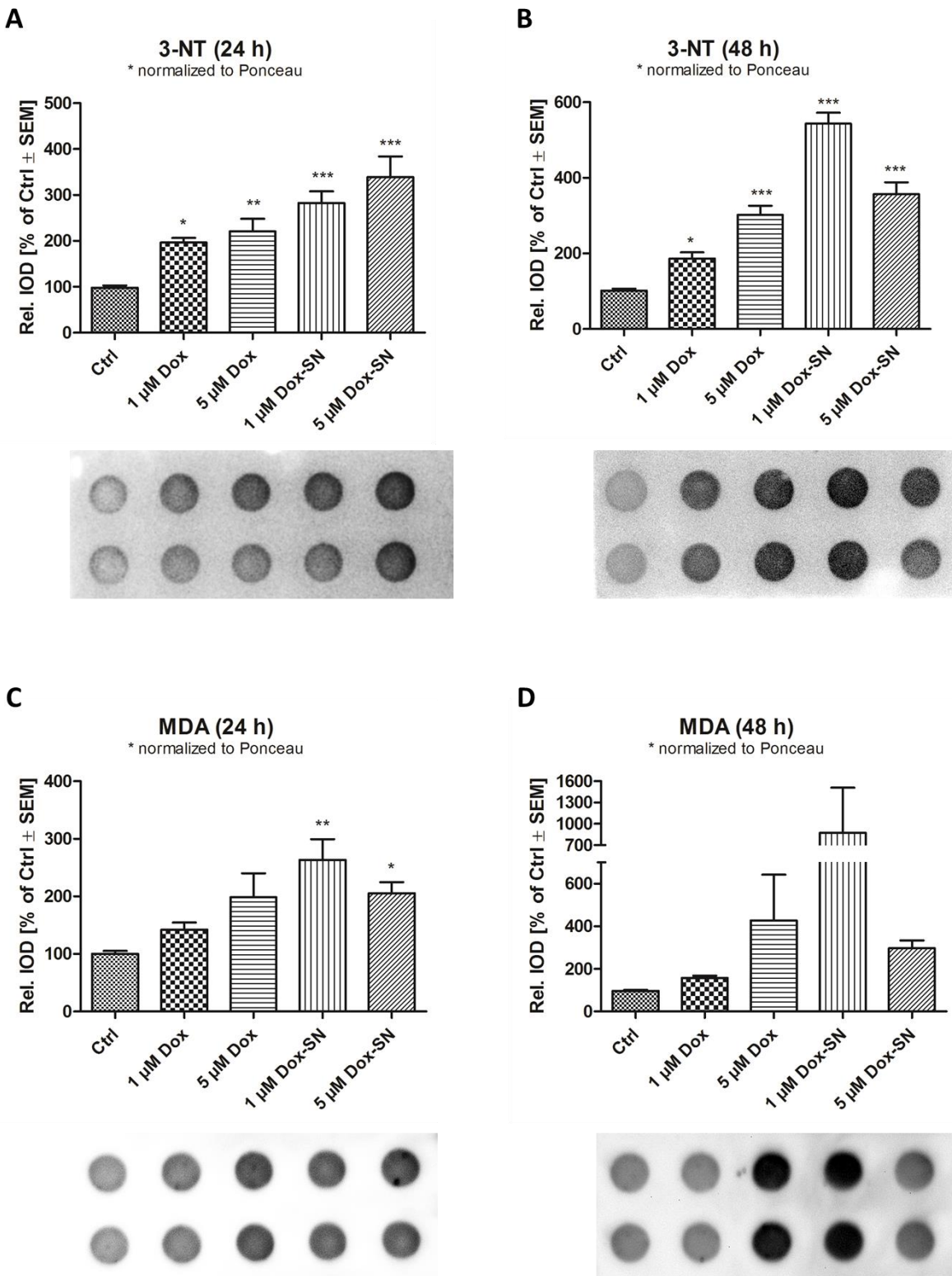
Figure 61 - Effects of doxorubicin (Dox) treatment on ROS-induced protein modifications in H9c2 cardiomyocytes. Levels of 3-nitrotyrosine (3-NT)- and malondialdehyde (MDA)-modified proteins were measured by dot blot analysis in lysates of H9c2 cells after 24 h or 48 h of doxorubicin (Dox) treatment. IOD was evaluated and normalized to Ponceau S staining. Representative blots are shown below the densitometric quantification. Data are the means ± SEM from 4 experiments. *, p<0.05 vs. control; **, p<0.01 vs. control; ***, p<0.005 vs. control.

Figure 62 – Effect of doxorubicin (Dox) treatment on SOD2 expression in H9c2 cells. Levels of SOD2 expression were assessed by Western blot analysis in attached control and doxorubicin (Dox)-treated cells, as well as detached cells collected from the supernatant (SN). Representative blots are shown along with the densitometric quantification, either normalized to actin (top) or GAPDH (bottom). Data are the means ± SEM from 2 experiments. *, $p < 0.05$ vs. control; **, $p < 0.01$ vs. control; ***, $p < 0.005$ vs. control.

In order to investigate effects of doxorubicin treatment and accompanying oxidative stress on epigenetic mechanisms in H9c2 cardiomyocytes, the expression of several epigenetic modulators, i.e. histone deacetylases or histone demethylases, was analyzed via Western blot.

The NAD$^+$-dependent protein deacetylase sirtuin1 (Sirt1) belongs to class III histone deacetylases and plays a vital role in the regulation of metabolism and stress responses. Its activity has been shown to be affected by redox regulation [452]. In a previous study doxorubicin induced a dose-dependent (0.1 µM - 10 µM) decrease in the expression of Sirt1 and another sirtuin homolog, Sirt3, in H9c2 cardiomyocytes [440]. Here, Western blot analysis of Sirt1 expression in 1 µM and 5 µM Dox-exposed pre-apoptotic and apoptotic H9c2 cells resulted in the detection of three bands at ~110 kDa, at ~95 kDa and at ~85 kDa (Figure 63). The predicted molecular weight of Sirt1 is 82 kDa (correlating with the 85 kDa band), but it is often detected at 110 kDa due to post-translational glycosylation leading to differences in gel migration [453]. This glycosylated form of Sirt1 slightly increased in 1 µM Dox-treated pre-apoptotic cells and almost completely disappeared in the apoptotic cells. Levels of unglycosylated Sirt1 at 85 kDa concentration-dependently decreased upon Dox-treatment and were nearly vanished in the apoptotic fraction. While Sirt1 levels in 1 µM Dox-treated pre-apoptotic cells varied between 60-80% of control both at 24 h and 48 h, Sirt1 levels in 5 µM Dox-treated cells decreased from ~30% of control at 24 h to 5-11% of control at 48 h. The 95 kDa band probably represents the SIRT1-ΔExon8 isoform resulting from alternative splicing, which has been shown to exhibit distinct stress sensitivity [454]. Levels of this isoform were substantially increased in the apoptotic cells, and a 1.5-2.5 fold increase compared to control was also observed in 5 µM Dox-treated pre-apoptotic cells both at 24 h and 48 h post-treatment.

Next, another prominent histone deacetylase, HDAC2, was subjected to Western blot analysis with regards to changes in expression levels upon doxorubicin exposure. HDAC2 is a member of the class I mammalian histone deacetylases involved in regulating chromatin structure during transcription. Chronic doxorubicin treatment was shown to down-regulate HDAC2 expression in a murine model of doxorubicin-induced cardiomyopathy [455]. Furthermore, a link between oxidative stress and reduced HDAC2 levels/activity has repeatedly been reported in studies about COPD [456-458]. As can be seen in Figure 64, two bands were detected at ~60 kDa and ~50 kDa. HDAC2 is 55 kDa in size, but is known to migrate at 60 kDa in SDS-PAGE. At both time points apoptotic cells expressed significantly less HDAC2 compared to control cells. Additionally, HDAC2 levels in pre-apoptotic 1 µM Dox-treated cells were also significantly decreased. Interestingly, there was no obvious effect on 5 µM Dox-treated cells at 48 h and even a slight increase in HDAC2 levels at 24 h. In general, HDAC2 expression was lower in both fractions of 1 µM-Dox treated cells than in the respective 5 µM Dox-treated groups. The identity of the 50 kDa

band is unknown, but could be assigned to an HDAC2 isoform. According to UniProt at least in humans an HDAC2 isoform 2 of ~52 kDa has been reported (UniProtKB Q92769-3), which is likely to also be present in rats. On the other hand, the 50 kDa band could be associated with the undesired antibody-recognition of HDAC3 at 49 kDa due to sequence homology between HDAC2 and HDAC3. However, 50 kDa HDAC2 levels were significantly increased in the apoptotic fractions at 24 h and 48 h. A trend of increased expression was also observed in 5 µM Dox-treated pre-apoptotic cells, which was more apparent at 48 h.
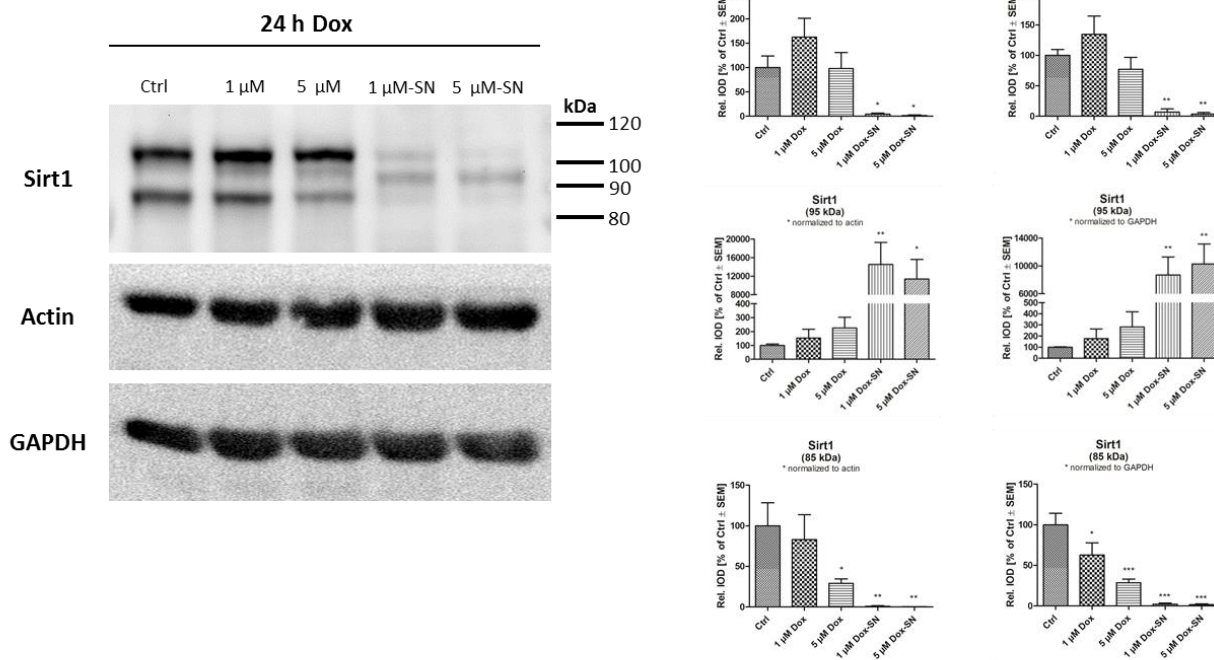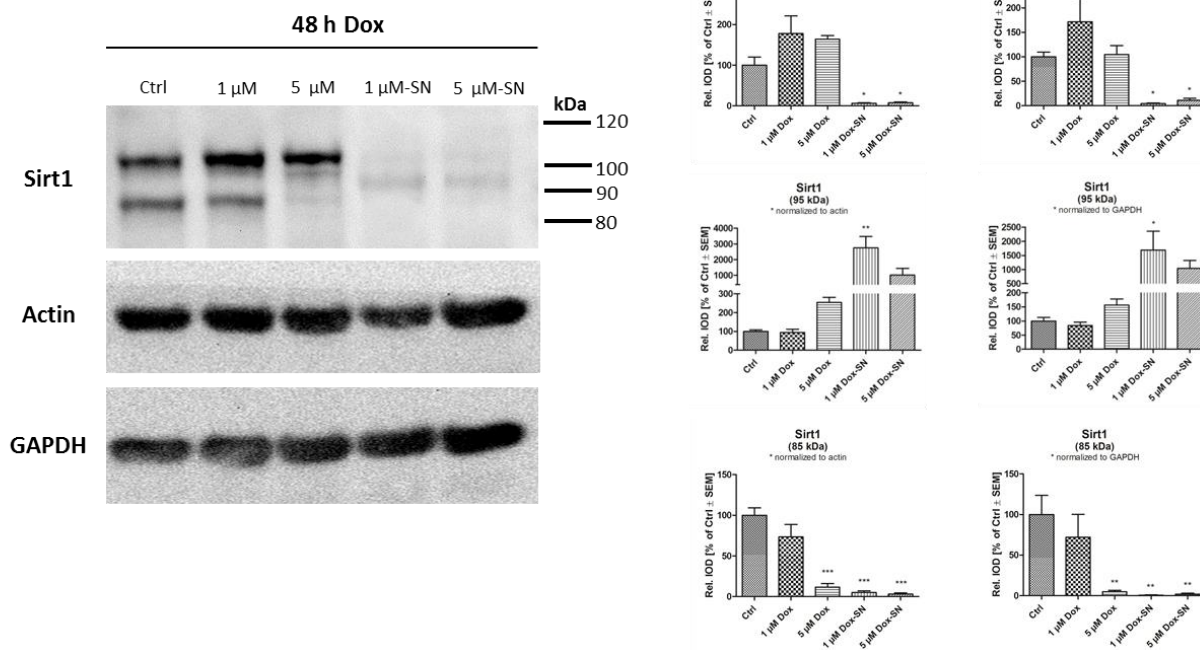
Figure 63 - Effect of doxorubicin (Dox) treatment on Sirt1 expression in H9c2 cells. Levels of Sirt1 expression were assessed by Western blot analysis. Bands were observed at ~110 kDa, at ~95 kDa and ~85 kDa. Representative blots are shown along with the densitometric quantification, either normalized to actin (left) or GAPDH (right). Data are the means ± SEM from 4 experiments. *, $p < 0.05$ vs. control; **, $p < 0.01$ vs. control; ***, $p < 0.005$ vs. control.
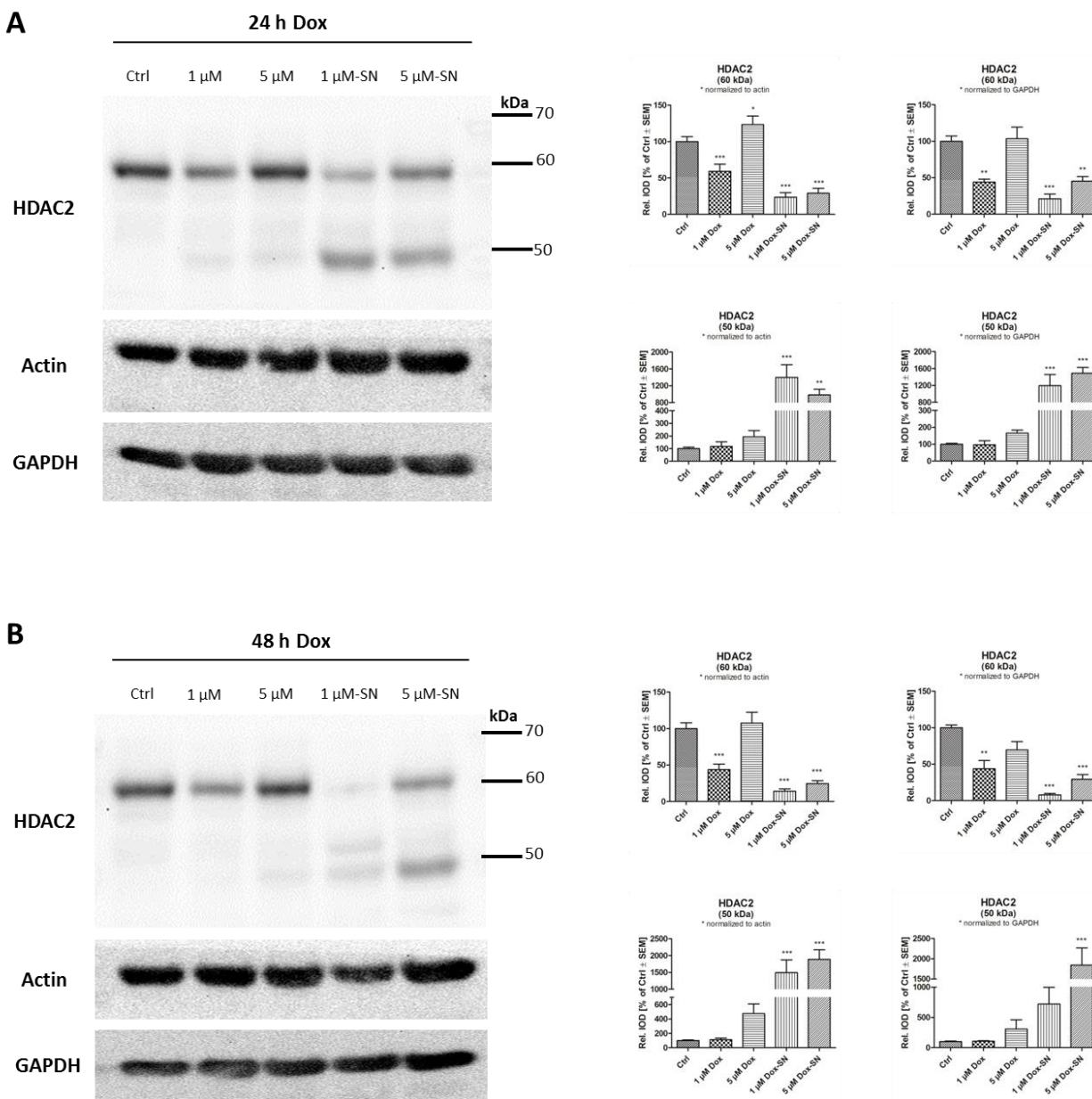
Figure 64 - Effect of doxorubicin (Dox) treatment on HDAC2 expression in H9c2 cells. Levels of HDAC2 expression were assessed by Western blot analysis. Bands were observed at ~50 kDa and ~60 kDa. Representative blots are shown along with the densitometric quantification, either normalized to actin (left) or GAPDH (right). Data are the means ± SEM from 4 experiments. *, $p < 0.05$ vs. control; **, $p < 0.01$ vs. control; ***, $p < 0.005$ vs. control.

The Jumonji C domain-containing histone lysine demethylase KDM3A belongs to the family of mononuclear Fe(II)-dependent dioxygenases that use 2-oxoglutarate (2-OG) and oxygen as cosubstrates for oxidative demethylation. Enhanced levels of KDM4A, KDM4B and KDM3A expression have been found in patients with heart failure [459]. In line with that, KDM3A expression in Dox-treated cardiomyocytes concentration-dependently increased compared to control at both 24 h and 48 h of exposure (the band detected at ~140 kDa represents the enzyme) (Figure 65). In both apoptotic fractions KDM3A levels were considerably higher than in their respective pre-apoptotic counterpart. Of note, at 24 h KDM3A levels of 1 µM Dox-treated apoptotic cells exceeded levels in 5 µM Dox-treated pre-apoptotic cells, whereas at 48 h a similar amount of KDM3A was detected in these groups. Another band was observed migrating above the highest marker band at 220 kDa, which may possibly represent a KDM3A dimer. It has previously been reported that KDM3A forms a homodimer through its catalytic domain to enable the effective execution of two-step demethylation of dimethylated H3K9 into the null methylation state [460]. The amount of the alleged KDM3A dimer was reduced in 5 µM Dox-treated cells and completely abolished in apoptotic cells at both time points (Figure 65).

Another histone lysine demethylase, LSD1, is associated with the regulation of cellular energy metabolism through coupling with cellular FAD biosynthesis [216]. LSD1 has been found to be implicated in cardiovascular diseases such as hypertension or diabetes [125, 461]. Therefore, effects on LSD1 expression were also examined in H9c2 cardiomyocytes in response to doxorubicin-induced cardiotoxicity. No significant changes compared to the control group could be observed at 24 h of exposure due to deviations between the individual experiments (Figure 66). At 48 h LSD1 levels were reduced to 27-30% of control in 1 µM Dox-treated pre-apoptotic cells and to 11-23% in the respective apoptotic counterpart (1 µM Dox-SN). In 5 µM Dox-treated pre-apoptotic and apoptotic cells LSD1 expression was also decreased compared to control, but the effect was less pronounced (38-61% of Ctrl for 5 µM Dox and 51-60% of Ctrl for 5 µM Dox-SN).
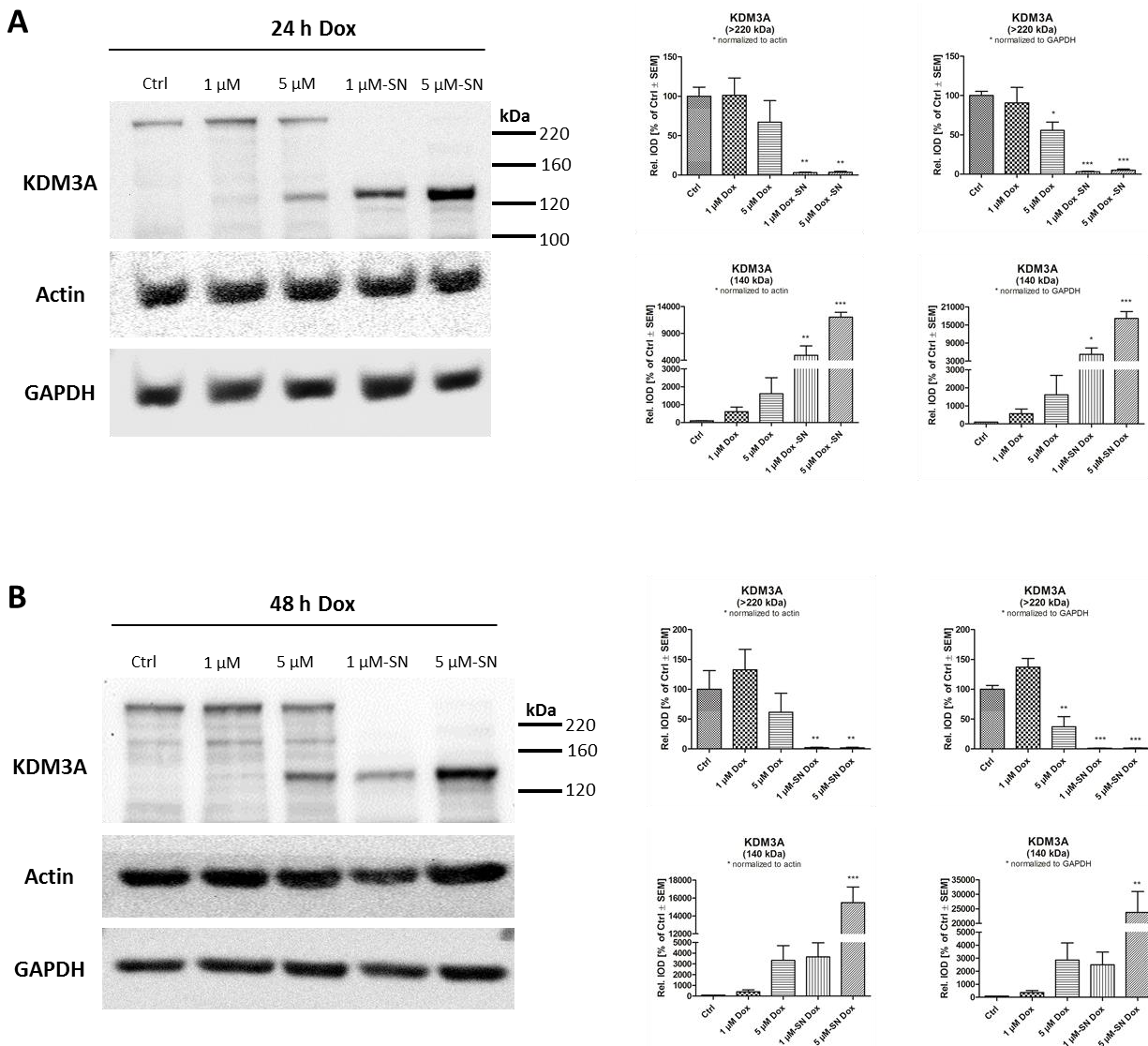
Figure 65 - Effect of doxorubicin (Dox) treatment on KDM3A expression in H9c2 cells. Levels of KDM3A expression were assessed by Western blot analysis. Bands were observed at >220 kDa and ~140 kDa. Representative blots are shown along with the densitometric quantification, either normalized to actin (left) or GAPDH (right). Data are the means ± SEM from 4 experiments. *, p<0.05 vs. control; **, p<0.01 vs. control; ***, p<0.005 vs. control.
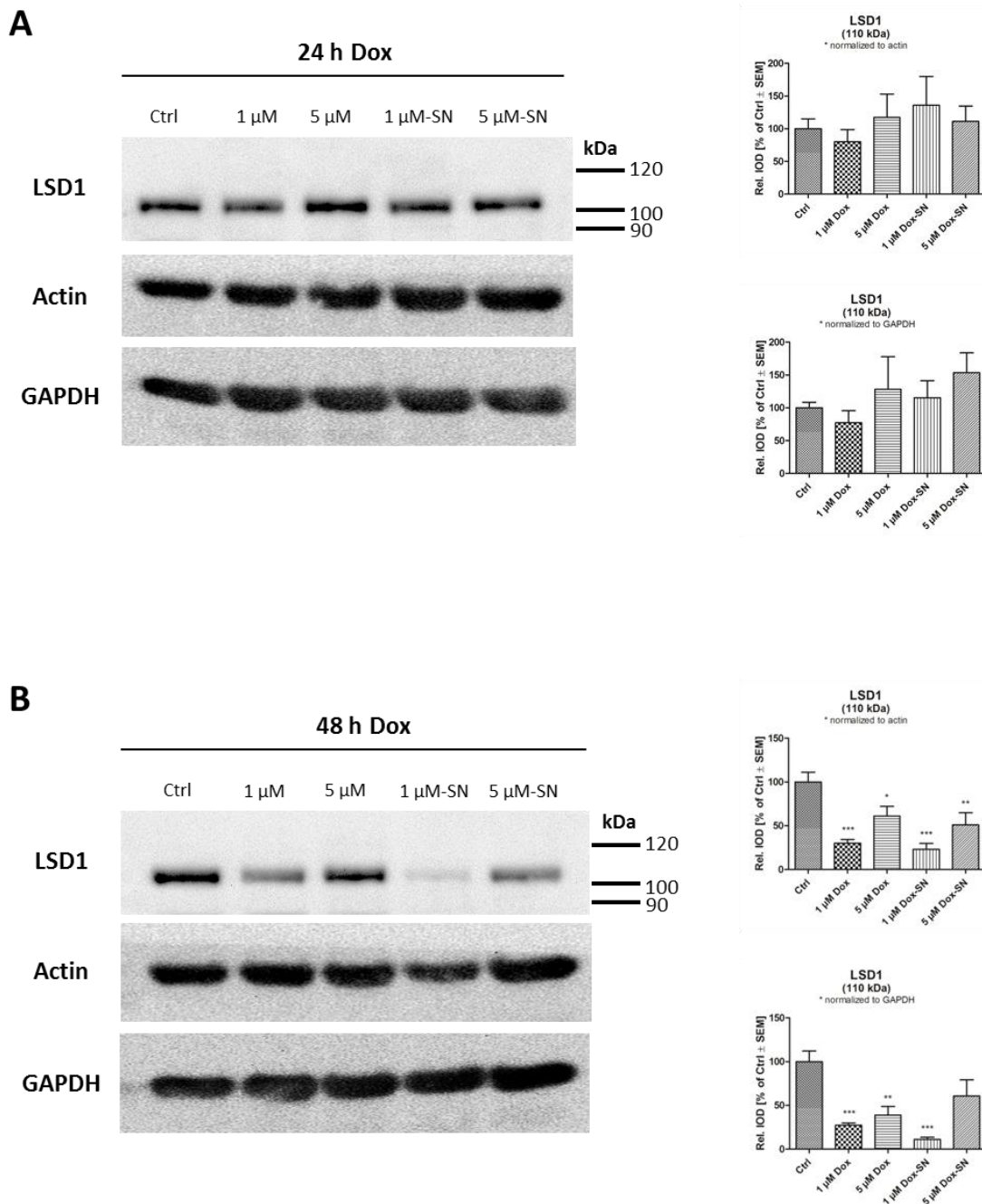
Figure 66- Effect of doxorubicin (Dox) treatment on LSD1 expression in H9c2 cells. Levels of LSD1 expression were assessed by Western blot analysis. A band was observed at ~110 kDa. Representative blots are shown along with the densitometric quantification, either normalized to actin (top) or GAPDH (bottom). Data are the means ± SEM from 4 experiments. *, $p < 0.05$ vs. control; **, $p < 0.01$ vs. control; ***, $p < 0.005$ vs. control.

In different models of diabetes, hyperglycemia and ROS have been shown to induce and/or activate the H3K4 methyltransferase Set7 [462, 463]. Furthermore, Set7 plays a role in the regulation of genes associated with inflammation or vascular (dys)function [194, 354]. Here, no significant differences were observed between control cells and 1 µM Dox-treated pre-apoptotic cells at both time points (Figure 67). Upon treatment with 5 µM Dox, however, Set7 levels in pre-apoptotic cells were increased by 75-90% at 24 h and significantly increased by around 2.5-5 fold at 48 h. In the respective 5 µM Dox-treated apoptotic fraction (5 µM Dox-SN) no major expression changes occurred. Interestingly, in two of four experiments Set7 expression in 1 µM Dox-treated apoptotic cells (1 µM Dox-SN) was highly increased at 24 h, whereas in the other two experiments the expression pattern was similar to 48 h exposure, where the expression levels in these cells were not essentially different compared to control cells. These findings are mirrored in the high standard error in the overall expression evaluation of those cells at 24 h.

SMYD1, a muscle-specific histone methyltransferase, plays an essential role in cardiac differentiation and morphogenesis [198, 464]. It has been demonstrated previously that cardiac-specific deletion of SMYD1 in adult mice leads to hypertrophy and heart failure, whereas it is upregulated during disease to prevent pathological cell growth [465]. It has been proposed that SMYD1 plays an essential role in the regulation of mitochondrial metabolism in the adult heart [466]. At 24 h of 1 µM Dox-exposure SMYD1 levels were slightly decreased to 60-70% of control in pre-apoptotic cells (Figure 68). Expression in the correspondent apoptotic fraction (1 µM Dox-SN) seemed to be slightly increased compared to control, but this effect can be refuted due to deviations between experiments similar to the results seen for Set7 expression. 5 µM Dox-exposure for 24 h did not alter SMYD1 levels in pre-apoptotic cells, but considerably decreased expression in apoptotic cells. 48 h treatment with 1 µM Dox decreased SMYD1 amounts in pre-apoptotic cells substantially to ~20% of control, while there was no distinct effect seen in the apoptotic cells, as normalization to actin or GAPDH indicated a slight increase or decrease, respectively. Exposure to 5 µM Dox for 48 h caused SMYD1 expression to increase to 140-300% of control in pre-apoptotic cells, but was decreased to ~60% in apoptotic cells.

A

B
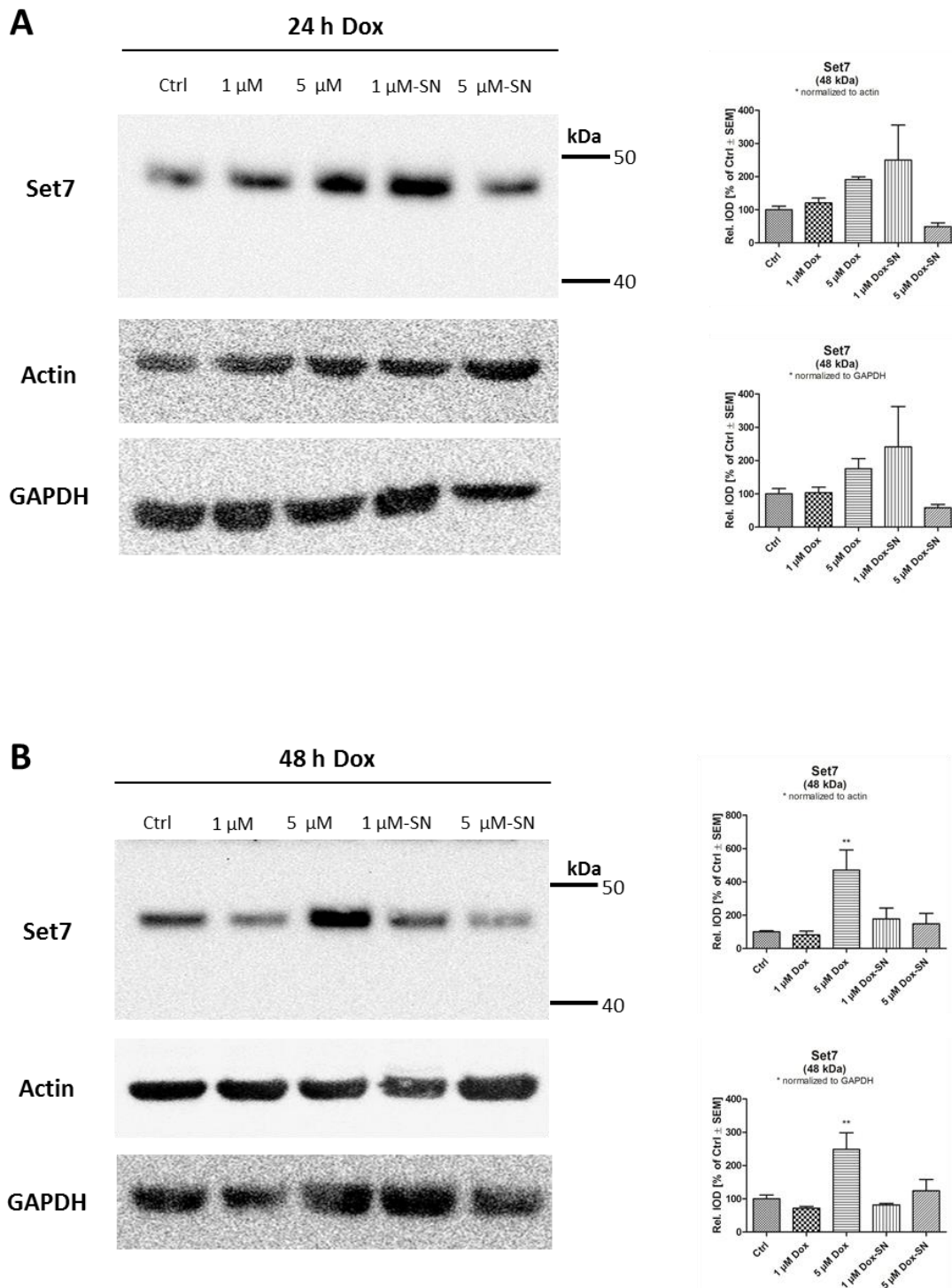
Figure 67 - Effect of doxorubicin (Dox) treatment on Set7 expression in H9c2 cells. Levels of Set7 expression were assessed by Western blot analysis. A band was observed at ~48 kDa. Representative blots are shown along with the densitometric quantification, either normalized to actin (left) or GAPDH (right). Data are the means ± SEM from 4 experiments. *, p<0.05 vs. control; **, p<0.01 vs. control; ***, p<0.005 vs. control.
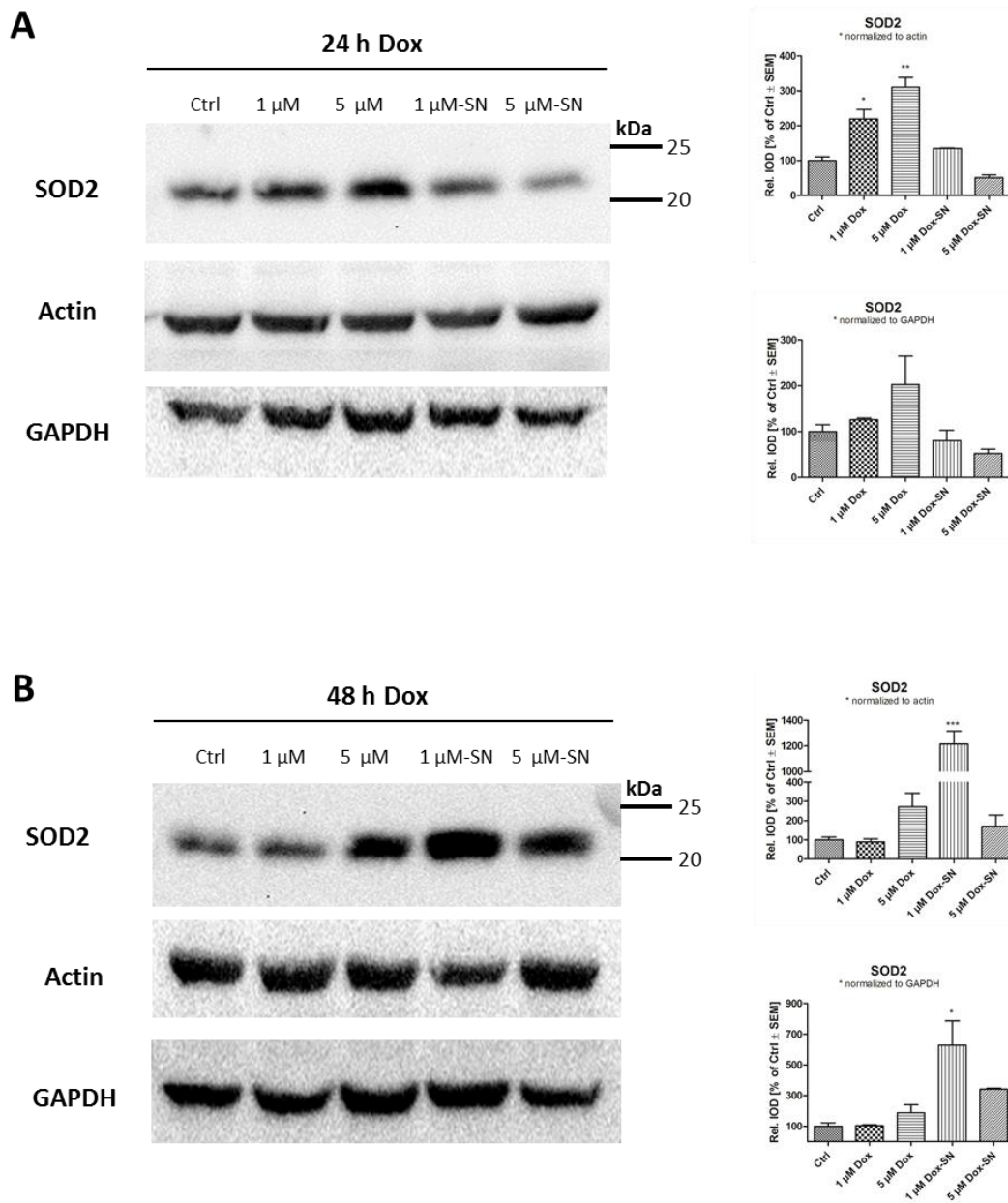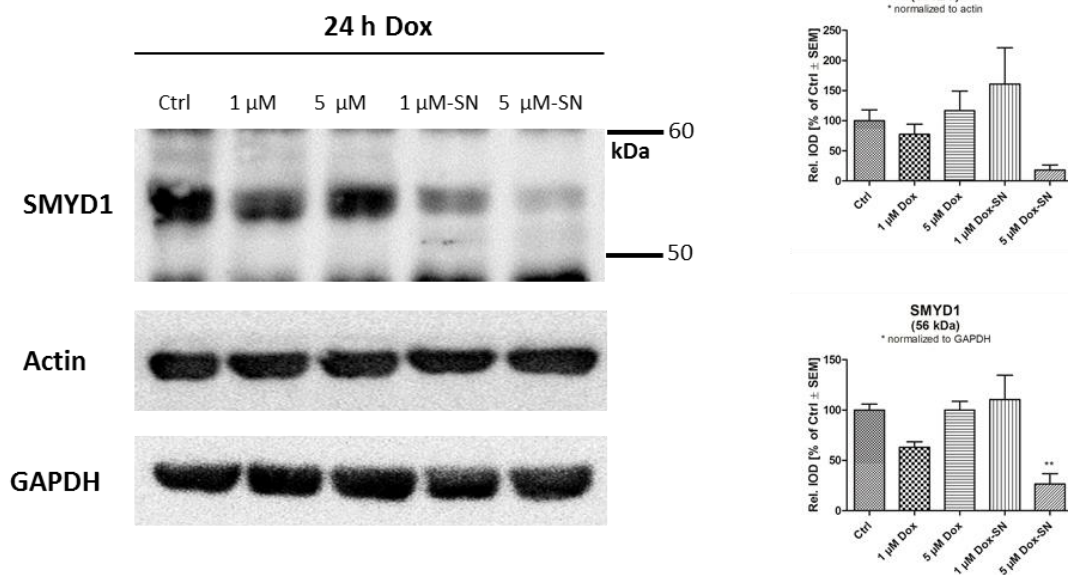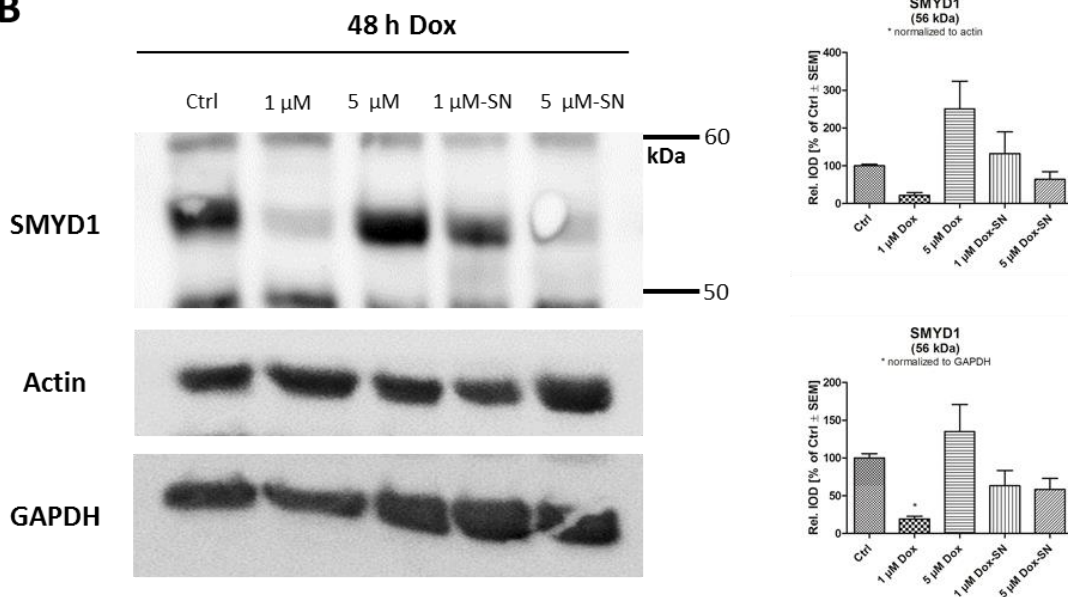
Figure 68 - Effect of doxorubicin (Dox) treatment on SMYD1 expression in H9c2 cells. Levels of SMYD1 expression were assessed by Western blot analysis. A band was observed at ~56 kDa. Representative blots are shown along with the densitometric quantification, either normalized to actin (left) or GAPDH (right). Data are the means ± SEM from 4 experiments. *, $p<0.05$ vs. control; **, $p<0.01$ vs. control; ***, $p<0.005$ vs. control.

In light of all the differential effects on the expression of epigenetic modulators that were observed in response to doxorubicin-induced cardiotoxicity in H9c2 cells, differences in global histone modification patterns were investigated. Histones were isolated by acidic extraction from the DNA-containing pellets remaining from the corresponding H9c2 cell lysates. Histone fractions were subjected to Western blot analysis and individual histone modifications were visualized by applying the respective antibodies. Global changes in levels of different histone 3 methylation marks, i.e. H3K4me3, H3K9me1/2/3, could not reliably be determined in cardiomyocytes upon doxorubicin treatment, but more research may be necessary to confidently rule out any alterations of these modifications (data not shown). However, histone 3 acetylation concentration-dependently decreased in pre-apoptotic cells both at 24 h and 48 h of doxorubicin exposure at a comparable rate (39-46% of Ctrl at 1 µM Dox, 12-15% of Ctrl at 5 µM Dox) (Figure 69). H3Ac levels in the apoptotic cells were also significantly reduced compared to control cells (to ~10-20% of Ctrl), but it is noteworthy that in some cases the levels of overall histone 3, to which H3Ac is normalized, were also less in these cells than in control cells; therefore this data might be somewhat extrapolated.

All in all, doxorubicin exposure did have evident effects on ROS formation, as well as on certain epigenetic modulators and histone acetylation in H9c2 cardiomyocytes. However, it remains to be analyzed if and how redox signaling and epigenetic modulation are interrelated in this model.

A

B
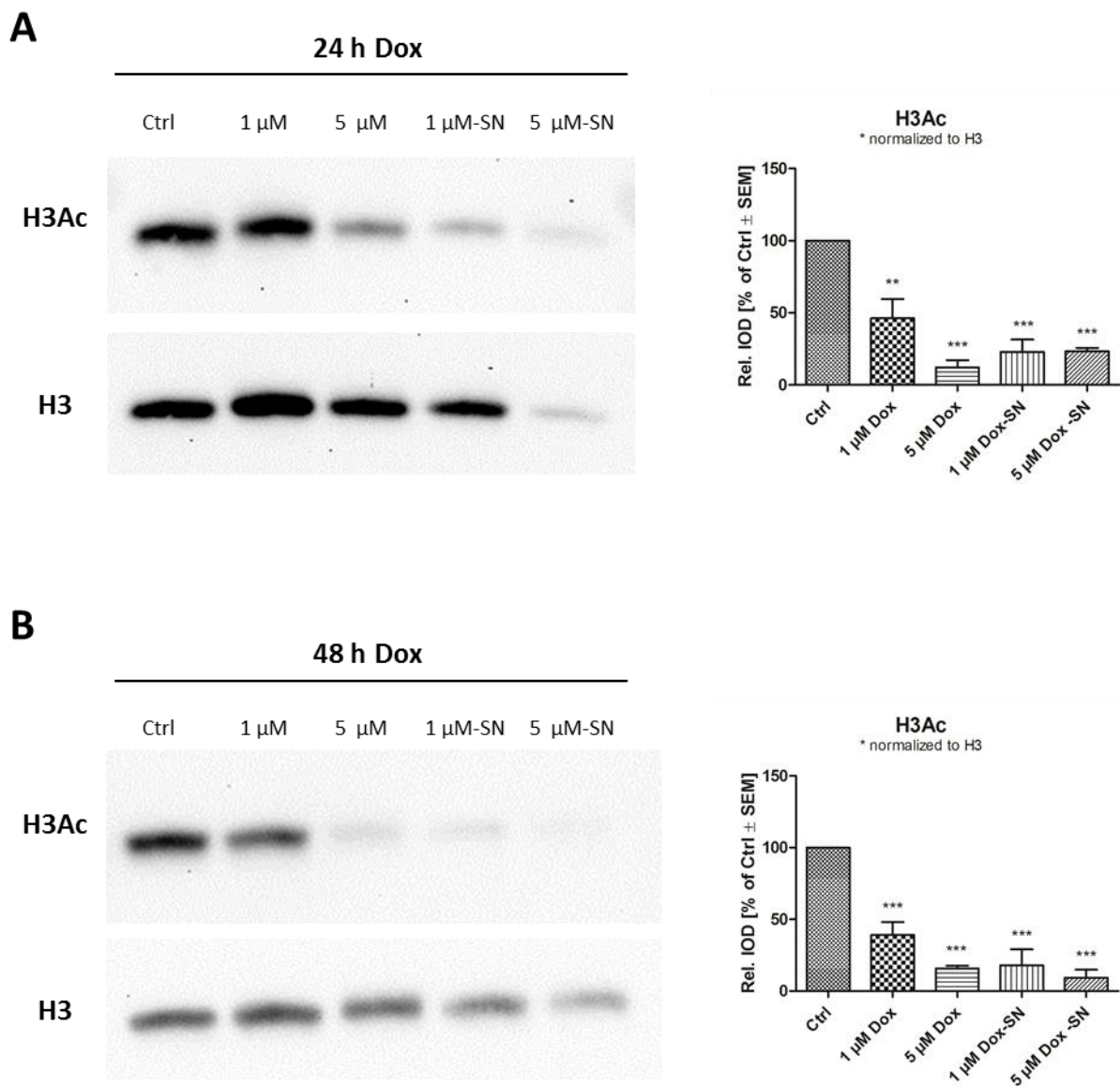
Figure 69 - Effect of doxorubicin (Dox) treatment on global histone 3 acetylation in H9c2 cells. Levels of acetylated histone 3 (H3Ac) were assessed by Western blot analysis of histone extracts. Representative blots are shown along with the densitometric quantification. H3Ac modification was normalized to total histone 3 (H3) levels. Data are the means ± SEM from 4 experiments. *, $p < 0.05$ vs. control; **, $p < 0.01$ vs. control; ***, $p < 0.005$ vs. control.

6   Discussion

6.1   Detection of protein S-nitros(yl)ation by immuno-spin trapping

Nitric oxide ($^{\bullet}$NO), a reactive free radical generated from arginine by nitric oxide synthases (NOS), is an important signaling molecule for both intracellular and extracellular messaging in diverse physiological processes. $^{\bullet}$NO was shown to affect cGMP signaling, neuronal transmission, and has anti-microbial, anti-inflammatory, and anti-cytotoxic effects [45, 46]. Under oxidative stress conditions $^{\bullet}$NO can interact with superoxide to produce reactive nitrogen species (RNS) that can cause alterations in macromolecules and cause severe cell damage. However, under normal circumstances nitric oxide is indispensable for cell physiology and signaling. Covalent attachment of a nitroso ("NO") group to the thiol in protein cysteine residues forms S-nitrosothiols (SNOs) via redox-mediated reactions. This reversible process is termed S-nitros(yl)ation and is used by cells to modulate protein function and stability, regulate gene expression, and provide NO donors for transnitrosation reactions with thiol-containing amino acids, peptides, and proteins [104]. Generally, isolated thiols form relatively stable S-nitrosothiols, while the nitros(yl)ation of adjacent thiols leads to intramolecular disulfide ring closure [467]. Practically all enzymes contain cysteine residues that can be subjected to S-nitros(yl)ation, whereby this process often acts as an activity switch. For instance, the functional regulation of the NMDA receptor, HIF1α, or NFkB have all been reported to involve S-nitros(yl)ation [468-470]. Nitros(yl)ation of biological thiols is mostly mediated by nitric oxide derivatives N_2O_3, metal-nitrosyl complexes, and peroxynitrite [471, 472]. The most prevalent method to detect protein S-nitrosothiols is the biotin switch assay (BTSA), which consists of three principal steps. First, the free cysteine thiol (-SH) groups are blocked; secondly nitros(yl)ated thiols (-SNO) are reduced by ascorbate. Finally, the newly formed thiol (-SH) groups are S-biotinylated. The degree of biotinylation and thus S-nitros(yl)ation is then determined by either anti-biotin immunoblotting or streptavidin pulldown followed by immunoblotting for the protein of interest [473, 474]. However, increasing data questions the reliability of this assay and even reports that application of the BTSA may give false positive results [475-477]. Hence, other approaches are necessary to determine protein-SNO content. It is established that protein S-nitrosothiols undergo photolytic homolysis to $^{\bullet}$NO and protein thiyl radicals upon irradiation with visible light [478]. This effect has been used as the foundation of DMPO-mediated spin trapping as a measure of S-nitros(yl)ation. DMPO spin trapping is an established method for the detection of free radicals that is usually analyzed by EPR. In the case of SNO detection the initial step is creating thiyl radicals from nitros(yl)ated thiols by irradiation and subsequent reaction with DMPO to a nitrone free radical product. This can be analyzed by EPR or upon redox-based

stabilization to a non-radical nitrone-protein-adduct by immunological techniques. During the past decade, Mason and colleagues have developed antibodies that react with DMPO-protein adducts and have shown that they work well for Western blot analysis, immunostaining, and immunofluorescence [112, 479]. This method of DMPO immuno-spin trapping greatly expands the utility of EPR analysis and bears great potential for the precise detection of S-nitros(yl)ated proteins, but also other protein- and DNA-centered free radicals (e.g. in amino acid side chains or DNA bases).

In the present study, DMPO immuno-spin trapping was established and validated in order to have a solid readout assay to measure the extent of S-nitros(yl)ation in proteins in response to oxidative stress. As initial reactant for S-nitros(yl)ation isolated NAD(P)$^+$-dependent aldehyde dehydrogenase and isocitrate dehydrogenase (Figure 70) were employed, since they contain reactive cysteine residues and constitute biologically relevant targets of metabolic cycle and aldehyde detoxification, as both have been shown to be inhibited by S-nitros(yl)ation [480, 481].
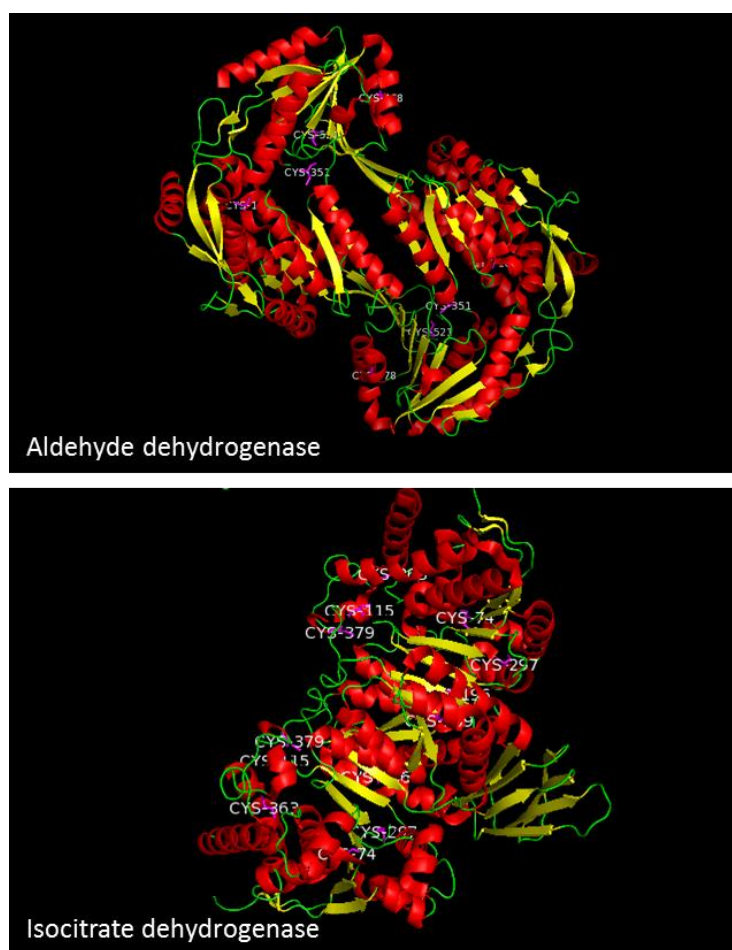
Figure 70 – Crystal structure of aldehyde dehydrogenase and isocitrate dehydrogenase with all cysteine residues labeled in purple. Structures were generated from protein database files and rendered using the program PyMol (Schrödinger, Version EduPyMOL-v1.7.4.4).

It has previously been shown by Daiber *et al.* that at physiologically low levels of $^\bullet$NO in the nanomolar range the optimal approach to induce nitros(yl)ation favors a mechanism via peroxynitrite interaction with $^\bullet$NO instead of the autoxidation of $^\bullet$NO [103]. The latter would comprise the formation of N_2O_3, which is a well-known nitros(yl)ating agent, but this reaction is very slow at low $^\bullet$NO concentrations and therefore not a suitable model for biological S-nitros(yl)ation [103, 482]. Instead, they showed that the optimal ratio for nitros(yl)ation while mimicking low physiological fluxes is the stoichiometric release of $^\bullet$NO and $^\bullet$O$_2^-$ in a ratio of 3:1. This was achieved by treatment with equimolar concentrations of the NO-donor SPENO, which releases two molecules of $^\bullet$NO, and the peroxynitrite generating compound Sin-1, whose aerobic thermal decomposition releases $^\bullet$NO and $^\bullet$O$_2^-$ at equal rates. It was calculated that ~1-10 µM Sin-1 form steady-state levels of $^\bullet$NO in the low nanomolar range, thereby closely mimicking physiological conditions in the cell. Accordingly, assay parameters in the present study were adapted to those suggested by Daiber *et al.* High fluxes of $^\bullet$NO provided by 1 mM SPENO or 20 mM acidic KNO_2 were applied as positive controls, however, those high concentrations do not represent physiological conditions. Application of high Sin-1 concentrations is not reliable as positive control since this may result in overoxidation of thiols to sulfoxides or Sin-1 autoxidation may be prevented by shortage of oxygen.

Here, rising fluxes of $^\bullet$NO resulted in increased S-nitros(yl)ation of ALDH and ICDH as indicated by stronger DMPO signals, thereby confirming the usefulness and validity of the DMPO immuno-spin trapping assay. Nevertheless, purified proteins only represent a simplified part of the complex biological situation. When performing this assay in cells that had been exposed to ROS or nitros(yl)ating agents, it failed to indicate any significant changes in S-nitros(yl)ation levels (DMPO intensity). However, complications may have been due to high background of free radicals (due to cell lysis or heating upon irradiation), which can form protein-DMPO-adducts, that may be detected as false positives. Further optimization may surely allow the use of DMPO immuno-spin trapping for the detection of S-nitros(yl)ation also in cell systems. The use of this assay for the detection of biological free radicals in general and not specific for PSNOs has already been demonstrated *in vivo* in organelles, cells, and tissue [483].

Despite the encountered difficulties, DMPO immuno-spin trapping is a promising method for the detection and quantification of protein S-nitros(yl)ation. In addition, tagging S-nitros(yl)ated proteins with DMPO also provides a foundation for the analysis of substrate identification and selectivity (e.g. via DMPO-mediated immunoprecipitation).

6.2 Hyperglycemia and oxidative stress in the endothelial cell line EA.hy926

Hyperglycemia in diabetes is a major risk factor for the development of cardiovascular diseases, as it is associated with inflammation and increased oxidative stress, leading to vascular dysfunction [284, 307, 308, 310, 313, 484-486]. Endothelial cell models are often used to study the underlying mechanisms of diabetic vascular complications and to investigate the adverse effects of high glucose levels on vascular function. It is well established that generation of ROS is highly increased in diabetes and this effect has also repeatedly been demonstrated in various endothelial cell lines, such as HAECs, BAECs, HCAEC, HMVEC, HGEC, EA.hy926 or HUVECs upon hyperglycemic conditions mimicking the diabetic milieu [409, 425-428, 487-498]. Glucotoxicity-induced oxidative stress is associated with compromised eNOS function, impaired •NO/cGMP signaling and endothelial dysfunction [499-501]. As described in the introduction (1.6.1, p.38), hyperglycemia can induce oxidative stress via several mechanisms including glucose autoxidation, increased formation of advanced glycation end-products (AGEs), and activation of the polyol pathway. Increased ROS formation induces the activation of several transcription factors and signaling pathways involved in the pathogenesis of chronic complications, including protein kinase C (PKC), c-Jun N-terminal kinase (JNK), p38 mitogen-activated protein kinase (MAPK), and nuclear factor kappa-B (NFkB) [6, 324]. Activation of PKCs has frequently been reported in cultured vascular cells exposed to high glucose and vascular tissues isolated from animal models of diabetes mellitus [311, 426-428, 497, 502-505]. PKCs are phospholipid-dependent serine/threonine kinases that are involved in a variety of pathways that regulate cell growth, death, and stress responsiveness. Excess superoxide in hyperglycemia can activate PKCs in two ways: the superoxide anion inhibits the key glycolytic enzyme glyceraldehyde-3-phosphate dehydrogenase (GAPDH), thereby disrupting the glycolysis pathway, resulting in an increased flux of dihydroxyacetone phosphate (DHAP) to diacylglycerol (DAG), which is a known physiological PKC activator [505-508]. ROS can also directly activate PKCs by modifying critical cysteine residues within their N-terminal zinc-finger regulatory (phorbol ester/DAG-binding) domain. Upon oxidation, the autoinhibitory function of the regulatory domain is compromised, resulting in stimulation of cellular PKC catalytic activity [508-512]. PKC isoforms are known to activate NADPH oxidases (mainly NOX2), as their kinase activity is required for the phosphorylation-dependent assembly of several cytosolic NOX subunits to become catalytically active [508, 513]. Therefore, glucotoxicity-associated ROS formation induces PKC activation, which in turn activates NOX, thereby increasing ROS generation in a positive feedback loop (Figure 71). ROS overproduction via a PKC-dependent NOX activation has been implicated in a variety of pathophysiological conditions, including neurodegenerative disorders [514], cardiovascular diseases, such as atherosclerosis [502, 515-517], hypertension [518, 519],

diabetes [520-523], and cancer [524]. On another note, high glucose was shown to increase the expression of endothelin-converting enzyme (ECE-1) and, consequently, levels of the vasoconstrictor endothelin-1 (ET-1), dependent on PKC activation [427, 428, 525]. In addition, PKC contributes to endothelial dysfunction by impairing eNOS function and promoting eNOS uncoupling. There are many reports that PKC mediates eNOS phosphorylation at Thr495 in the calmodulin-binding domain, resulting in eNOS inactivation and decreased $^\bullet$NO production [526-532]. Along with PKC-dependent NOX-induced superoxide generation, eNOS eventually becomes uncoupled, preferentially forming superoxide at the expense of $^\bullet$NO synthesis [533]. In summary, hyperglycemia enhances free radical production, inducing signaling pathways such as PKC-dependent NOX-activation, ultimately resulting in endothelial dysfunction and oxidative damage. Therefore, clinical studies are investigating PKC inhibitors for treatment and prevention of diabetic vascular complications [534].
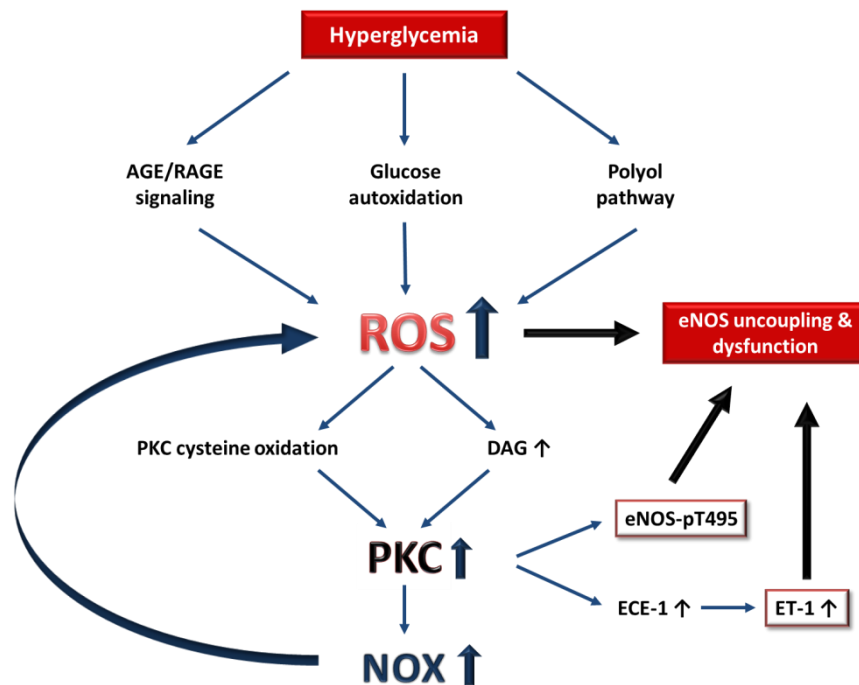
Figure 71 - Molecular pathways of hyperglycemia-induced ROS formation and effects on PKC activity and eNOS dysfunction. *AGE, advanced glycation end products; DAG, diacylglycerol; ECE-1, endothelin converting enzyme-1; eNOS, endothelial nitric oxide synthase; eNOS-pT495, eNOS phosphorylated at threonine 495; ET-1, endothelin-1; NOX, NADPH oxidase; PKC, protein kinase C; RAGE, receptor for AGE; ROS, reactive oxygen species.*

All the described mechanisms that induce enhanced ROS formation and endothelial dysfunction in hyperglycemic conditions have been reported to occur in the endothelial EA.hy926 cell model treated with high glucose [425-428, 498]. Even our own group demonstrated in 2012 that high glucose concentrations significantly increased ROS generation in EA.hy926 as well as in HUVEC cells [409]. For

these reasons, the same experimental setup as previously described by Karbach *et al.* was used in order to have a reliable model of oxidative stress with physiological relevance. However, the reported major increase in ROS formation under hyperglycemic conditions could not be reproduced and only minor effects were observed. Even several assay adjustments, such as application of different batches of D-glucose or FCS, starving cells prior to or during the treatment, changing incubation times, and co-incubation with pro-inflammatory IL-1β did not result in considerable differences in ROS formation between low and high glucose groups. Possibly, there was a systematic error that could not be identified. One hypothesis is that low glucose control cells already exhibited oxidative stress, which led to measurement on a high background, which could explain the low, but consistent increases in ROS formation.

Consequently, this cell model was excluded as non-reliable oxidative stress model and was not used for further investigation of ROS-associated epigenetic changes. In the future, an alternative approach for inducing oxidative stress in endothelial cells could be used by incubating cells with synthetic AGEs, which are commercially available (e.g. BSA-AGE).

6.3 ROS formation and epigenetic investigation in the setting of glutathione peroxidase-1 deficiency and aging

In response to the difficulties encountered in searching for a suitable oxidative stress model, it was decided to investigate tissue samples from an animal model with already defined oxidative stress-related complications. Oelze *et al.* have shown previously that ablation of the antioxidant protein glutathione peroxidase-1 (GPx-1) potentiates age-dependent vascular dysfunction and ROS/RNS formation in mice [416]. The authors demonstrated that aging itself caused eNOS dysfunction and uncoupling via adverse eNOS phosphorylation and S-glutathionylation, along with inflammation and oxidative stress. These effects were further increased in aged GPx-1 deficient (GPx-1$^{-/-}$) mice. Glutathione peroxidase is an intracellular antioxidant enzyme that enzymatically reduces hydrogen peroxide as the major substrate to water and therefore plays an important role in regulating the cellular redox state [44]. Aging is generally associated with increased free radical production along with reduced antioxidant defense, resulting in the accumulation of cellular damage over the course of a lifetime [535-537]. This makes aging a major risk factor for the onset and development of cardiovascular diseases [538].

On the basis of guaranteed presence of high ROS levels in the aged groups, this model was applied to analyze molecular effects of ROS on epigenetic processes. Of note, the intention was not to investigate

any changes associated with endothelial dysfunction or aging, but rather general epigenetic alterations and modifications in response to elevated ROS levels. The astonishing correlation in 3-nitrotyrosine (3-NT) and H3K9me2 patterns observed in dot blots led to the assumption that the increased oxidative stress in the aged groups affected global H3K9 dimethylation, even more so in the old GPx$^{-/-}$ mice. Increased H3K9me2 levels in response to hypoxia- or metal-induced oxidative stress have been reported previously [124, 293, 539-541]. Inhibition of oxygen-dependent Jumonji histone demethylases or increased enzymatic activity of G9a, a histone 3 lysine 9 methyltransferase, were found to be responsible for elevated global levels of this histone mark [293, 541]. However, here, histone 3 monomer bands from acidic histone extracts that were subsequently analyzed by Western blot did not show any changes in dimethylation. But higher molecular weight bands were observed that were positive for H3K9me2, H3 and H4 and were highly increased in the aged animals, especially in aged GPx$^{-/-}$ mice. Since the detected weights matched the masses calculated for H3-H4 dimers and (H3-H4)$_2$ tetramers, it was hypothesized that the additional bands may represent these nucleosomal building blocks. In the nucleosome, histones are assembled as an octamer consisting of two H2A-H2B heterodimers and a (H3-H4)$_2$ tetramer that forms from dimerization of H3-H4 heterodimers [142]. Histone interaction occurs via their histone fold domain, which is a highly conserved structural motif constructed from three α-helices connected by two unstructured loops [542]. The two H3-H4 pairs form the tetramer through the interaction of the α2-helix and α3-helix of H3 and H3', respectively, resulting in a 4-helix bundle. To produce the octamer each α3-helix in the two H2A-H2B dimers interacts with the respective α3-helix of H4 in the tetramer forming two H2B-H4 associations. The H3-H3' and H2B-H4 α-helix bundles exhibit several additional hydrophobic interactions and hydrogen bonds [142]. In general, the H3-H4 tetramer and H2A-H2B dimers are more stable than the fully assembled octamer in solutions at low salt concentrations, whereas in presence of DNA or high salt concentration the octamer is more stable [543]. However, in the present study, detection of histone oligomers was not expected due to sample denaturation and reduction prior to Western blotting. Thus, it was assumed that a covalent bond may have formed stabilizing H3-H4 dimers and tetramers. Of note, it is known that in oxidizing conditions a covalent disulfide bond is formed linking H3-cysteine110 to a histone 3 dimer, which is, however, easily reversible under fully reducing conditions [430]. Histone 4 does not contain any cysteine residues. Like cysteine, tyrosine is one of the amino acids that are most susceptible to oxidation. Various tyrosine derivatives such as nitrotyrosine, dityrosine and halogenated tyrosine can be formed upon exposure to free radicals. Dityrosine (DT) is a tyrosine dimer derived from tyrosyl radicals that can be induced by ROS, metal-catalyzed oxidation, ultraviolet irradiation, and peroxidases [434, 435]. ROS-induced dityrosine formation is generally mediated by

peroxynitrite, which is present in its protonated form peroxynitrous acid (ONOOH) under physiological pH conditions. Peroxynitrous acid readily dissociates into the highly reactive hydroxyl radical ($^\bullet$OH) and the nitrogen dioxide radical ($^\bullet$NO$_2$). This induces the formation of an unstable tyrosyl radical, which is either nitrated by $^\bullet$NO$_2$, generating 3-nitrotyrosine, or at higher substrate levels forms a covalent bond with another tyrosyl radical, generating o,o'-dityrosine (Figure 72) [544, 545].
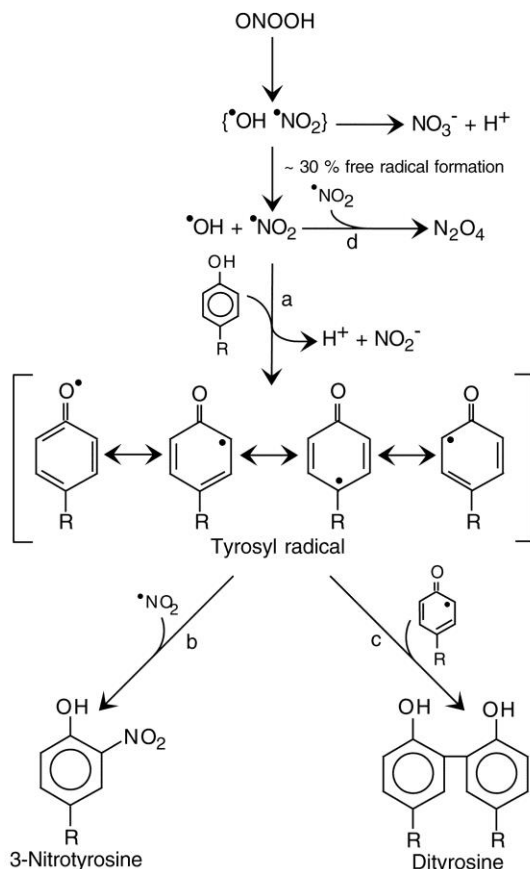
Figure 72 - Mechanism of tyrosine nitration and dityrosine formation. Tyrosyl radicals can be generated by ROS, metal-catalyzed oxidation, ultraviolet irradiation, and peroxidases. Here, the tyrosyl radical is formed in response to peroxynitrous acid homolysis into $^\bullet$OH and $^\bullet$NO$_2$ (a). In the presence of the $^\bullet$NO$_2$ radical nitration via a radical based mechanism takes place, yielding 3-nitrotyrosine (b). Alternatively, two tyrosyl radicals can dimerize by forming a covalent bond, yielding dityrosine (c). *Taken from Pfeiffer et al. 2000 [545].*

Inter- and intramolecular cross-linking between protein tyrosine residues can induce oligomerization and aggregation [96]. For instance, in Parkinson's disease, which is accompanied by highly elevated oxidative and nitrative stress, formation of nitrated α-synuclein and dityrosine cross-linking is observed. This leads to the generation of an α-synuclein homodimer that serves as seed for further α-synuclein aggregation assembling into β-sheet rich fibrils, making up Lewy bodies, the hallmark of Parkinson's disease [546-548]. Furthermore, dityrosine cross-links have been found in atherosclerotic lesions, lipofuscin of pyramidal neurons of aged human brains or amyloid plaques from Alzheimer's disease patients [549-

551]. Khan *et al.* have reported that exposure to peroxynitrite induces dityrosine formation in histone H2A, H2B and H3 leading to intramolecular (but not intermolecular) cross-linking [431-433]. In addition, it was shown by Deeg *et al.* that tyrosyl radicals in H2B, generated by irradiation, not only formed intramolecular cross-links between tyrosines in close proximity, but also intermolecular bonds between isolated tyrosines [552]. As H3 contains three and H4 four tyrosine residues, oligomerization via intermolecular dityrosine cross-linking may also be possible. Although there is no data available about dityrosine bonds between H3 and H4, tyrosine nitration of these histones has been previously demonstrated *in vitro* and *in vivo* [433, 544, 553]. In the study by Haqqani *et al.*, nitration was restricted to Tyr72 and Tyr98 in histone H4, and Tyr41 in histone H3. It was suggested that the reason why the other tyrosine residues were not nitrated is their proximity to a cysteine or methionine residue, which alternatively become oxidized under the oxidative/nitrative stress conditions [553]. On the basis of these findings, H3-H4 dityrosine cross-linking did not seem unlikely. Indeed, the alleged histone H3-H4 oligomers were found to correlate with increased dityrosine formation in the aged groups detected via a respective DT-specific antibody. Yet, the existence of an intermolecular H3-H4 dityrosine cross-link in H3-precipitates and histone extracts from kidney lysates of old GPx$^{-/-}$mice was not confirmed by mass spectrometry. Even though in the MS analysis of histone extracts traces of histones were found in higher molecular weight bands than their monomer correspondents, their presence was probably not due to a covalent cross-link but possibly due to insufficient denaturation (despite application of denaturing and reducing conditions) and therefore remaining histone assembly in dimers and tetramers as is present in the nucleosome. Furthermore, MS analysis detected a big amount of immunoglobulins, which were first attributed to the mouse antibodies used for H3-immunoprecipitation, but were later found to be intrinsic mouse immunoglobulins, as they were detected by an anti-mouse antibody in the lysate itself. Therefore, the observed bands that were presumed to be histone oligomers actually originated from endogenous mouse immunoglobulin heavy and light chains, which were increased in the aged groups due to increased inflammation and infiltration of immune cells in the examined mouse heart and kidney tissues. A pro-inflammatory phenotype is a general feature in aging, and the analyzed samples have in fact been shown by Oelze *et al.* to exhibit increased inflammatory markers and infiltration of leukocytes in aged tissue, especially upon GPx ablation [416]. Also, GPx deficiency itself has previously been shown to promote a cytokine-induced proinflammatory state [554].

In conclusion, all aforementioned discoveries on cross-linked histone oligomers containing dityrosine bridges were interpreted falsely due to the recognition of tissue-intrinsic mouse immunoglobulins by the anti-mouse secondary antibody used in conjunction with the primary mouse monoclonal H3-, H4-,

H3K9me2- and dityrosine antibodies. Of note, the same effect of detecting intrinsic immunoglobulins had also been observed in diabetic rats using the same mouse antibodies, which can be attributed to high homology between rat and mouse immunoglobulin constant regions and concurrent cross-reaction of antibodies [555].

In addition, oxidation experiments with purified recombinant histones also did not result in dityrosine cross-links between histones 3 and 4, although presumable H3 dimerization was observed, which can occur via formation of cysteine-disulfide bridges, as described previously. However, lack of protein presence on the blot under some oxidation conditions was observed by Ponceau staining and may suggest histone aggregation or modification that prevented them from entering the gel. Nevertheless, there was no solid confirmation found that histone 3 and 4 oligomerize by forming dityrosine cross-links under oxidative conditions.

6.4 Epigenetic investigation of diabetic complications in ZDF rats and effect of the SGLT2 inhibitor empagliflozin

Type 2 diabetes mellitus is a growing health problem and a major risk factor for cardiovascular diseases. Hyperglycemia and glucotoxicity in diabetes are considered to substantially contribute to the adverse effects on vascular function, such as oxidative stress and inflammation. Therefore, glucose-lowering drugs are a promising strategy to prevent hyperglycemia-induced cardiovascular complications. The SGLT2 inhibitor empagliflozin has been shown to lower blood glucose by selectively blocking the sodium-glucose co-transporter 2 in the kidney, thereby inhibiting glucose reabsorption and promoting increased urinary glucose excretion (see Introduction 1.6.1.1, Figure 21, p.41) In the EMPA-REG OUTCOME® trial of 2015, empagliflozin has been demonstrated to reduce overall cardiovascular mortality of T2DM patients at high cardiovascular risk [371, 372]. The study by Steven *et al.*, which involves part of this thesis, provided insight into the mode of action of empagliflozin, especially its effects on glucotoxicity, beta-cell function, inflammation, oxidative stress and endothelial dysfunction in Zucker diabetic fatty (ZDF) rats that were used as a model of T2DM [412]. It was demonstrated that chronic treatment of ZDF rats with empagliflozin prevented glucotoxicity, as well as associated AGE/RAGE signaling and inflammation. In addition, empagliflozin reduced oxidative stress and normalized vascular function. These beneficial effects are likely due to the prevention of hyperglycemia, suggesting that hyperglycemia and glucotoxicity are upstream of all other complications seen in diabetes (summarized in the proposed mechanistic scheme in Figure 76). Glucotoxicity comprises increased levels of glucose oxidation products, such as methylglyoxal, and formation of AGEs, as well as the subsequent increase in AGE/RAGE

interaction, which induces a broad proinflammatory response and production of ROS via NOXs [314-316]. All these effects were shown to be improved by empagliflozin treatment. Implication of AGE/RAGE signaling in vascular complications has already been shown previously in diabetic rats, where it not only increased oxidative stress but also impaired $^{\bullet}$NO/cGMP signaling [556, 557]. Our data support these results, as it was found that several factors involved in the regulation of the integrity of the $^{\bullet}$NO/cGMP pathway, such as eNOS- and VASP-phosphorylation or DHFR expression, were dysregulated in diabetic animals, but were rescued upon glucose lowering by empagliflozin. The detailed mechanism of the $^{\bullet}$NO/cGMP pathway is depicted in Figure 73. Disruption of $^{\bullet}$NO/cGMP signaling by oxidative stressors has repeatedly been reported to cause vascular dysfunction [295, 558]. Consequently, endothelial dysfunction as measured by endothelium-dependent relaxation by the vasodilator acetylcholine (ACh) in aortic rings was observed in ZDF rats. Interestingly, Huang *et al.* demonstrated that in diabetic nephropathy AGE/RAGE signaling significantly suppressed $^{\bullet}$NO/cGMP signaling, which could be restored by application of NO-donors along with antioxidants [559]. Implication of AGE/RAGE interaction in diabetic vascular diseases was also corroborated by studies that demonstrated that inhibition of RAGE improved late-stage diabetic complications including hind limb ischemia and retinopathy in T1DM mice [560, 561], nephropathy in ZDF and T1DM rats [562, 563] and microvascular damage in T1DM rats and T2DM mice [564, 565].
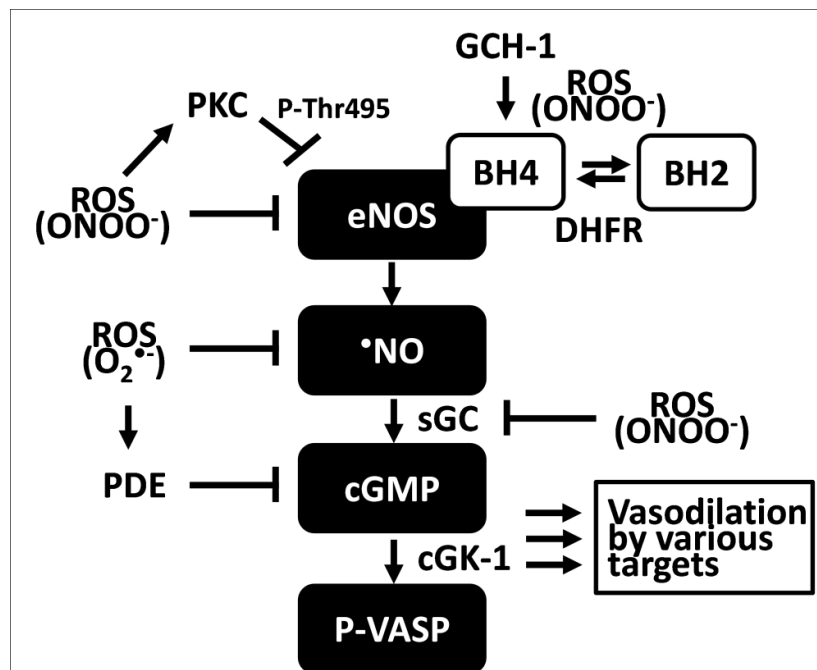
Figure 73 - Scheme illustrating the $^{\bullet}$NO/cGMP signaling pathway leading to vasodilation with the major sites for its oxidative inactivation. BH4, tetrahydrobiopterin; cGK-1, cGMP-dependent protein kinase 1; DHFR, dihydrofolate reductase; GCH-1, GTP-cyclohydrolase-1; PDE, phosphodiesterase; PKC, protein kinase C; P-VASP, phosphorylated (Ser239) vasodilator stimulated phosphoprotein; ROS, reactive oxygen species. sGC, soluble guanylate cyclase. *Taken from Steven et al. 2017 [412].*

The improvement of $^•$NO/cGMP signaling by empagliflozin observed in our study is most likely attributed to prevention of oxidative damage of this pathway. It can be ruled out that upregulation of eNOS is accountable for the rescue, as neither an increase in mRNA nor in the activating histone mark H3K4me3 in the eNOS promoter were observed in SGLT2i-treated rats. AGE/RAGE-associated inflammation and ROS formation in ZDF rats was confirmed in several tissues and blood by several assays including the detection of oxidative stress markers (3-NT, 4-HNE, MDA) and protein and mRNA expression data (NOX2, HO-1, IFN-γ, COX2, NOS2). Implication of hyperglycemia as causal effector of endothelial dysfunction, oxidative stress and inflammation was illustrated by linear regression analysis for correlations between fasting blood glucose or glycosylated hemoglobin (HbA1c) and endothelial function (ACh efficacy), zymosan A-induced whole blood oxidative burst and serum levels of the inflammation marker C-reactive protein (CRP) (Figure 74). Increasing blood glucose levels or HbA1c values were inversely correlated with endothelial function of aortic ring segments, whereas positive correlation was observed for oxidative stress and inflammation, highlighting the importance of glycemic control to prevent glucotoxicity. All of these adverse effects in diabetic animals were normalized by empagliflozin treatment in accordance with previously reported data in a T1DM model and a model of atherosclerosis [566, 567].
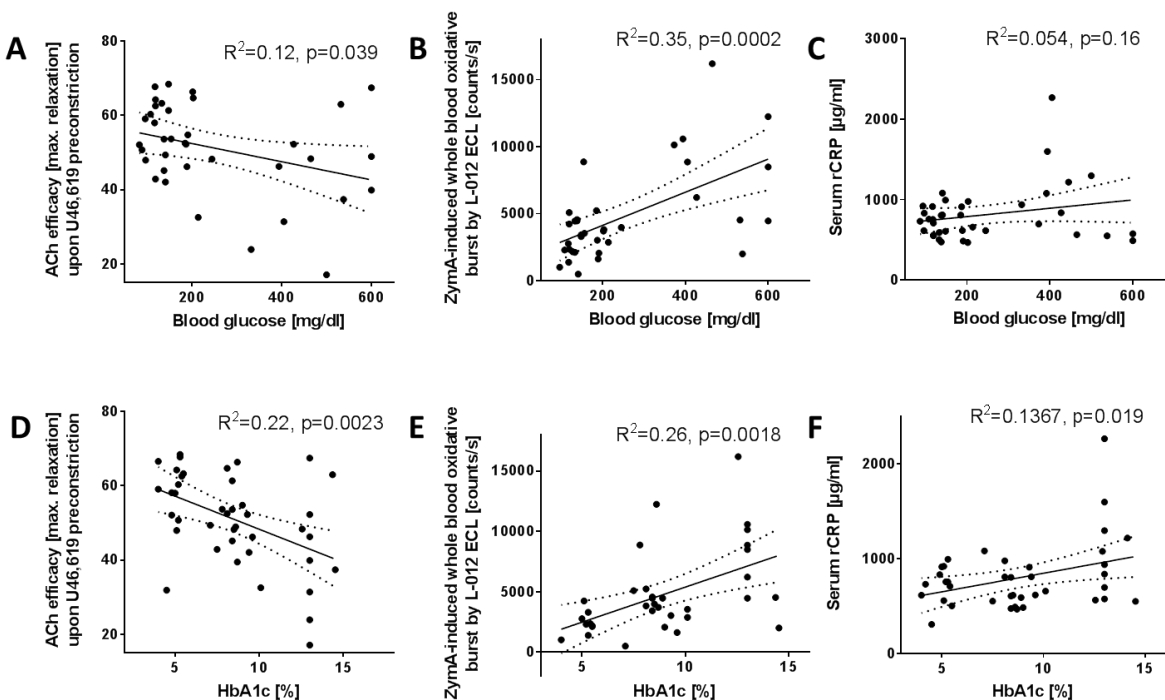
Figure 74 - Linear regression analysis for correlations between fasting blood glucose (A-C) or HbA1c (D-F) and endothelial function (ACh efficacy, A and D), zymosan A-induced whole blood oxidative burst (B, E), serum CRP levels (C, F). p-values and correlation coefficients (R^2) are provided in the graphs. *Data was collected by co-authors. Graphs were taken from our publication Steven et al. 2017 [412].*

Interestingly, empagliflozin seemed to also confer pleiotropic effects, since it was demonstrated that it improved viability and $^\bullet$NO formation in HUVECs under hyperglycemic conditions. As it can be ruled out that these positive effects were due to glucosuria, and since the presence and function of SGLT2 in endothelial cells is not clear, beneficial outcomes may have resulted from other mechanisms induced by empagliflozin, possibly including epigenetic pathways. Considering the presented cell studies, it should be noted, that the employed empagliflozin concentrations were supra-pharmacological (1 and 10 µM) as compared to the circulating levels expected in the empagliflozin treated rats (approximately 100-250 nM). This may represent a potential limitation of the *in vitro* experiments in cultured HUVECs. Remarkably, empagliflozin (at 500 nM) has also been shown to exert protective effects on cultured endothelial cells and even cardiomyocytes by increasing cell viability and ATP content in a diabetic milieu mimicked by co-incubation with AGEs [568].

Here, the DPP-4 inhibitor sitagliptin and the RAGE inhibitor FPS-ZM1, two other glucose-induced stress-lowering drugs, were investigated in hyperglycemic HUVECs alongside. Sitagliptin showed very similar protective effects compared to empagliflozin in these *in vitro* settings. However, a recent multi-cohort meta-analysis review reported that the use of SGLT2 inhibitors was associated with better mortality outcomes than DPP-4 inhibitors in type 2 diabetic patients [569]. The also significant effect on glucotoxicity by the RAGE inhibitor FPS-ZM1 demonstrated the great therapeutic potential of interruption of the AGE/RAGE signaling pathway. RAGE inhibitors are increasingly being studied, not only as a promising treatment option for diabetic vascular complications but also for Alzheimer's disease [563, 565, 570-575].

Increasing evidence demonstrates major roles of epigenetic pathways in diabetes, some of them appearing in a vital crosstalk with oxidative stress [6, 304] (see Introduction 1.6.1, p.38). In the current study we intended to determine if expression changes in genes that are involved in oxidative stress, glycemic control or inflammation, as observed in diabetic ZDF rats, were caused by epigenetic regulation through histone modifications and if SGLT2i treatment could antagonize these effects. While there is an adequate amount of data concerning histone mark patterns in diabetes, no data has been reported about epigenetic effects of empagliflozin so far. It has been shown previously that global differences in H3K4 trimethylation are associated with overweight and type 2 diabetes [438]. Moreover, the repressive histone mark H3K9me3 has been found to be involved in metabolic memory and decreased at promoters of inflammatory genes, promoting their expression in diabetic models [331, 346]. Therefore it was decided to determine the presence of these histone marks on the presented genes via ChIP assay. Other histone marks, such as H3K27me3 or global histone acetylation, were supposed to be investigated as

well, but this could not be accomplished due to time limitation. In general, ChIP with H3K4me3 antibodies was more successful than with H3K9me3 antibodies, meaning the genes of interest were found to be associated with H3K4me3 at a higher percentage as with H3K9me3. This may have several reasons. Downregulation of a gene does not necessarily mean that H3K9me3 is upregulated, many more mechanisms can be involved, including histone deacetylation or (de)methylation. Generally, active marks such as H3K4me2/3 and H3K36me2/3 display a higher turnover rate, whereas known repressive marks, such as H3K9me2/3 or H3K27me2/3, turn over more slowly [423]. The low signal achieved by H3K9me3 ChIP may also be due to weak primer specificity, as there was no data available for primer design indicating which specific regions to target for enriched H3K9me3 marks. However, it is suggested that H3K9me3 marks are distributed relatively homogeneously within the promoter region and the gene body of suppressed genes (Figure 75 b) [151, 423].
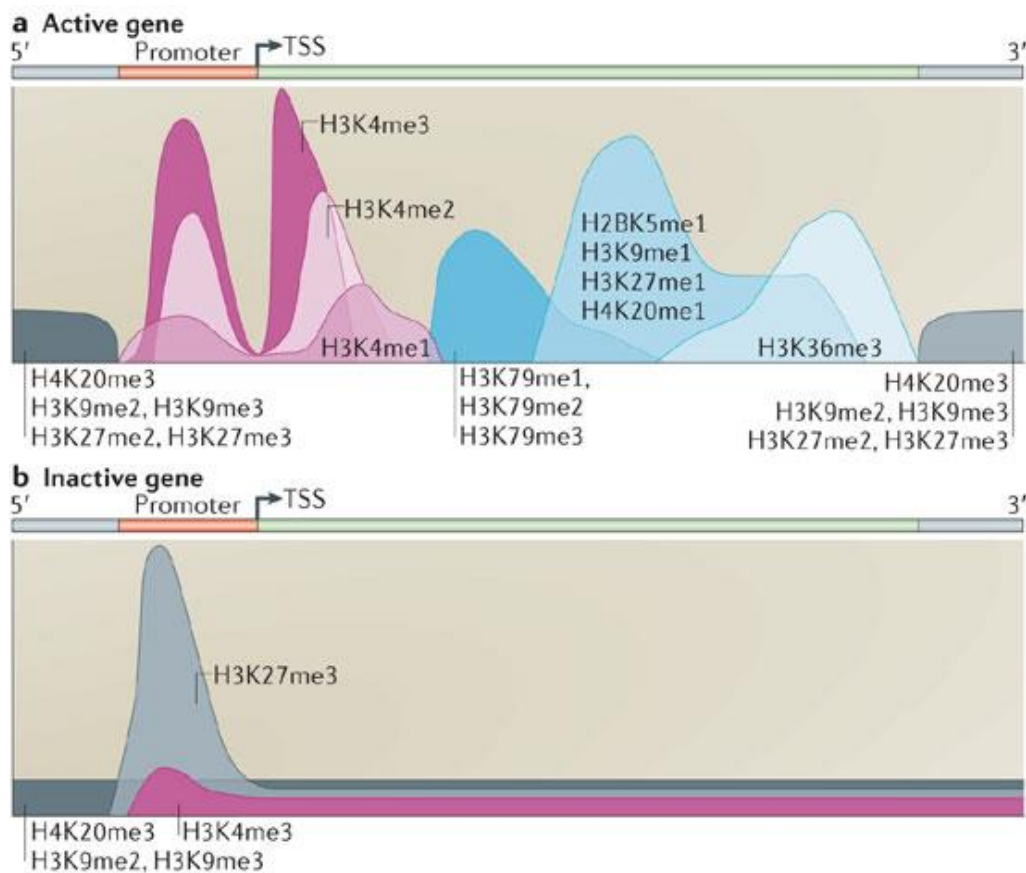
Nature Reviews | Molecular Cell Biology

Figure 75 - Distribution of histone modifications on active and silenced genes. Active genes (a) are highly enriched in the modifications H3K4me1/2/3 (and also histone acetylation; not shown here) in the promoter region. At the transcriptional start site (TSS) there is a nucleosomedepleted region (NDR) within the promoter. Active modifications such as methylation of H3K79 or H3K36 are present in the body of these genes, mainly at enhancer sites. In inactive genes (b) H3K27me3 is enriched at the promoter. The repressive marks H3K9me2/3 and H4K20me3 are broadly distributed on inactive regions. *Taken from Kooistra and Helin 2012 [424].*

Since most primers that were designed targeted the promoter region, it would have been very interesting to also perform ChIP with H3K27me3 antibodies, since this mark is supposedly enriched at the promoter region in silenced genes and may have resulted in a better signal (Figure 75 b) [151, 423].

Additionally, for ChIP experiments, the quality of the antibody is an essential factor. Low yield of H3K9me3-associated genes may have also been due to low specificity of the H3K9me3 antibody. Only ~10 % of the gene desert regions were found to be associated with H3K9me3, which could be due to insufficient recognition of the histone mark by the antibody; however, it is also possible that there was no 100% H3K9me3 signal in gene desert because its repression can also be due to presence of other repressive histone marks like H3K9me2 or H3K27me3. On the other hand, low levels of H3K9me3 were found at the active control gene GAPDH, therefore this was considered as background signals. Most genes analyzed here did not have H3K9me3 modifications above baseline and the ones that exceeded the baseline displayed such low signal that physiological relevance of any changes in H3K9me3 levels may be limited.

The histone mark H3K4me3 is typically enriched in promoter regions, but can also be found in regulatory regions promoting transcription enhancement [66, 67]. The region around the transcription start site (TSS) is usually nucleosome-depleted, thus free from any histone modifications (Figure 75 a). Also, H3K4me3 marks often appear in proximity to CpG islands. Therefore, the primers designed for this study were targeted to either promoter or CpG-rich intron regions. Even though there were no differences in H3K4me3 levels observed in the DHFR gene in the current study, the overall high yield of H3K4me3 associated to the DHFR gene implies that the designed primers target a site of rich H3K4 accumulation in the DHFR gene. Therefore, these primers can be recommended for future use for H3K4me3 analysis in DHFR via ChIP. The same was found true for the primers for HO-1 and both primers targeting the intron 2 of NOS2. This is also an important result, as success in obtaining high-quality ChIP data critically depends on good primer design. Designing the DNA oligonucleotide primers needed for ChIP-qPCR is considerably more challenging and time-intensive than for other qPCR methods. First of all, ChIP primers must target very specific regions, such as certain binding sites or, like in this case, a genomic region that is enriched in a respective histone mark. Therefore, the options for primer design are limited. Furthermore, the quality of the DNA may be impaired due to sample processing during the ChIP assay. In addition, the quantity of available DNA gained from ChIP is often low. The ability to base a ChIP analysis on a primer that reliably targets a region that is rich in the investigated mark is of big advantage.

In the present study, a trend for H3K4me3-mediated gene activation was found for RAGE in diabetic ZDF rats, which was reversed upon SGLT2i treatment. Increased AGE formation and a consequential upregulation of RAGE are established occurrences in diabetes mellitus [312, 316, 318, 484, 576-578]. Epigenetic regulation of RAGE expression by histone modifications has previously been demonstrated in a mouse model of T2DM (db/db mice) [579]. It was shown that the transcriptional activation marks H3K9Ac, H3K14Ac, H3K4me36 and H3K4me1 were increased in the RAGE promoter of diabetic animals, while the repressive marks H3K9me2, H3K9me3, and H3K27me3 marks were decreased, promoting RAGE transcription in these diabetic animals. However, they did not observe any significant differences in the permissive marks H3K4me2 and H3K4me3 in this model.

Here, H3K4me3 modification of eNOS was found to be decreased in all ZDF groups compared to control; however, this decrease was not mirrored in mRNA levels, which showed no differences in any of the groups. Interestingly, it has been reported that the expression of eNOS is controlled by a specific histone code described as H3K9ac and H3K12ac along with H3K4me2 and H3K4me3 [580]. So it is possible that the eNOS promoters of control rats were associated with more H3K4me3 modifications, but not in that specific pattern, leading to a higher yield in H3K4me3 ChIP, but not increased mRNA expression compared to ZDF rats. Of note, this histone code pattern was reported to be influenced by HDACs and H3K4 methylation inhibitors, resulting in decreased eNOS expression [462, 580, 581]. Therefore, modulation of epigenetic marks at the eNOS promoter could become a potential target for treating endothelial dysfunction.

Diabetes is usually accompanied by a proinflammatory phenotype. Accordingly, ZDF rats exhibited significantly higher expression of the cytokine IFN-γ, which was prevented by empagliflozin treatment. Also, increased levels of H3K4me3 were observed at the IFN-γ promoter of ZDF rats, which were decreased in the SGLT2i groups, nicely correlating with the observed mRNA expression pattern. However, the measured levels were only slightly above background levels, questioning the biological relevance. Interestingly, the repressive mark H3K9me3 was also lowered in empagliflozin treated rats, but seemed to have no effect on mRNA expression. This may have to do with the technical difficulties observed for H3K9me3 ChIP discussed above. Of note, IFN-γ has repeatedly been shown to influence epigenetic pathways by regulating the expression or function of histone modifiers, such as Sirt1 or KDM6B [582-584].

It is known that hyperglycemia and cytokines strongly induce NOS2 expression. During hyperglycemia, NFkB becomes activated by H3K4 methylation and, together with activated RAGE, mediates the

expression of the inflammatory mediators IL-6, TNF and NOS2 in macrophages [585, 586]. In agreement with this, it has been shown that the NFkB binding site on the IL1b, TNF-α, and NOS2 promoters exhibited increased H3K4me3 levels in macrophages of diet induced obesity (DIO) mice compared with controls [587]. In the ZDF diabetic animals no H3K4me3-mediated epigenetic upregulation of NOS2 could be determined, in contrast to the significant increase in mRNA levels compared to control. However, the activating H3K4me3 mark was clearly down-regulated at the NOS2 promoter in empagliflozin-treated rats.

Interestingly, it was observed throughout all experiments that empagliflozin-treated diabetic rats generally exhibited decreased H3K4me3 and H3K9me3 levels (even if ZDF was not increased) compared to Ctrl and ZDF. This suggests that empagliflozin may possibly confer epigenetic effects by itself, for instance by affecting the functions of histone methyltransferases or demethylases. This could have an effect on other genes implicated in the pathology of T2DM, leading to an improvement of the pathological effect of T2DM in addition to glucose lowering. Nevertheless, this hypothesis is quite bold and will require a lot of further research.

Another interesting observation was that the beneficial effects of empagliflozin were quite similar independently of the administered dose. Possibly, the therapeutic potential of empagliflozin is already exploited at the low dose.

In summary, the presented study demonstrated that administration of the SGLT2 inhibitor empagliflozin antagonized the development of oxidative stress, AGE/RAGE signaling and inflammation in type 2 diabetic ZDF rats, with beneficial effects on their vascular function (Figure 76). These results are in agreement with the EMPA-REG OUTCOME® trial that reported that empagliflozin reduces the cardiovascular and overall mortality in T2DM patients at high cardiovascular risk [371, 372]. Empagliflozin-mediated improvements are mainly being attributed to its glucose lowering capability, preventing glucotoxicity and all downstream consequences. However, other pleiotropic properties of the drug may play a role in its therapeutic outcomes as supported by the beneficial effects of empagliflozin in hyperglycemic endothelial cell cultures. Therefore, inhibition of SGLT2 presents an attractive anti-diabetic therapy and warrants further exploration in combinational therapeutic approaches.
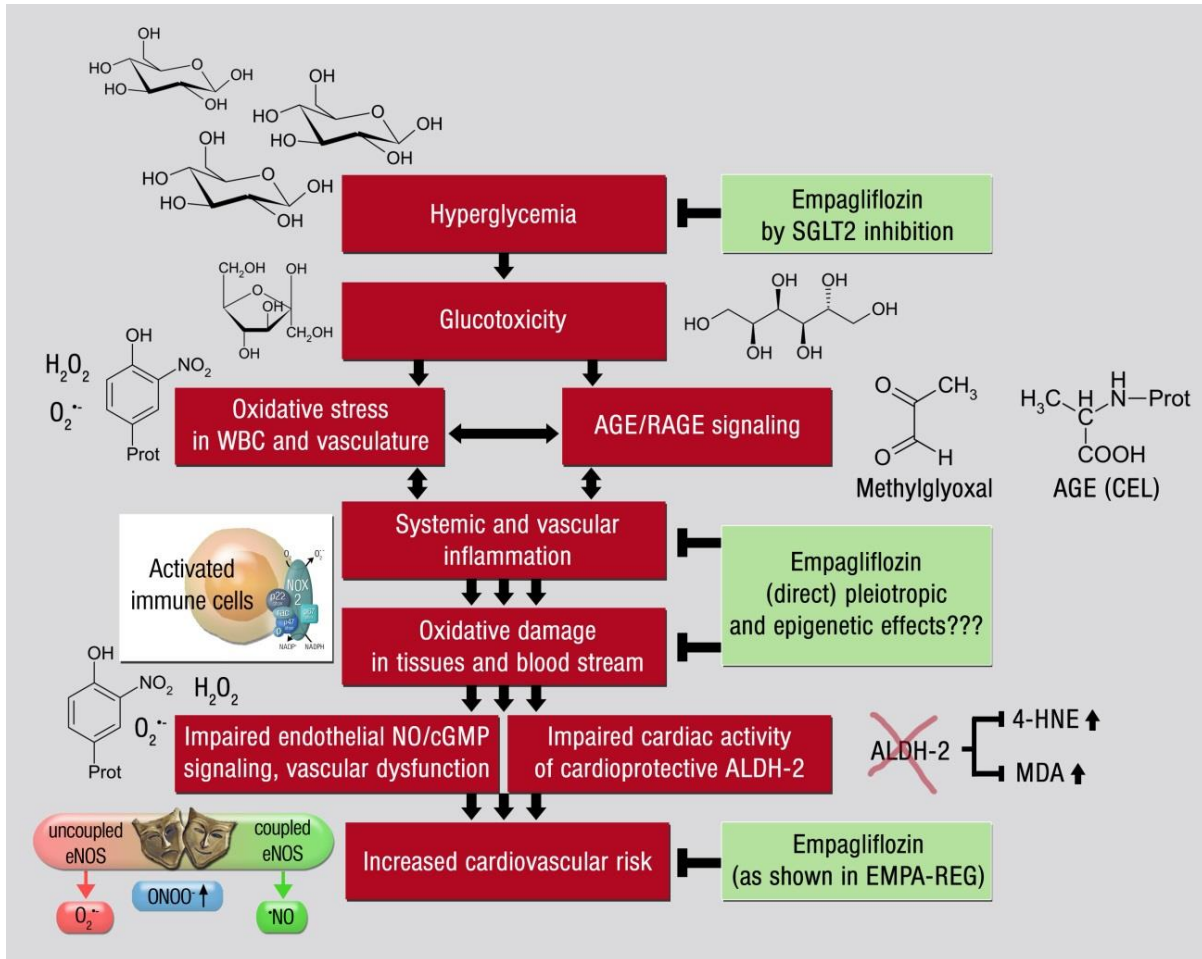
Figure 76 - Hypothetical scheme on empagliflozin-conferred protection in T2DM. The normalization of the glycemic condition and prevention of glucotoxicity are the major beneficial properties of empagliflozin and other SGLT2i but (direct) epigenetic and pleiotropic effects may also contribute. The secondary pathologies oxidative stress, AGE/RAGE signaling, inflammation with subsequent vascular dysfunction and increased cardiovascular risk are accordingly improved by the primary action of empagliflozin (the latter shown by the EMPA-REG OUTCOME® trial). *Scheme taken from our publication Steven et al. 2017 [412].*

6.4.1 Investigation of epigenetic drugs for diabetes and obesity

Drugs with epigenetic properties are sparking increasing interest as potential therapeutic agents in the treatment of diabetes and obesity and there are several major classes of epigenetic modifiers in various stages of study [588]. HDAC inhibitors (HDACis) have been suggested as potent therapeutic agents in the treatment of T1DM and T2DM due to the role of HDACs in beta-cell function and proliferation, as well as improvement of insulin resistance and inhibition of adipogenesis [589-591]. Promising HDACis include valproic acid (VPA), sodium phenylbutyrate, Vorinostat and Givinostat. Clinical trials for the use of VPA and sodium phenylbutyrate in the treatment of diabetes and obesity are ongoing (Table 3) [588]. Furthermore, the HAT inhibitor curcumin was suggested to be effective as an intervention drug to prevent the development of diabetes [592]. DNMT regulation was shown to have an important role in

the development of diabetes, therefore inhibition of DNMT by hydralazine, procainamide, MG98 or RG108 might have a beneficial effect on its treatment [588]. Also, HDM inhibitors are being investigated as drugs targeting T2DM. The HDM inhibitor tranylcypromine, for instance, was shown to inhibit lysine-specific demethylases (LSD1 and LSD2), which are involved in gluconeogenesis and metabolic expenditure [593]. Of extremely prominent interest is the research on sirtuin-activating compounds, especially the natural polyphenolic compound resveratrol. In a meta-analysis of 11 clinical trials resveratrol was found to improve glycemic control and insulin sensitivity in T2DM patients [594]. Table 3 lists current clinical trials of epigenetic drugs in the treatment of diabetes and obesity [588]. In summary, epigenetic processes have emerged as an area of interest for novel drug discovery, which could revolutionize the treatment of diabetes and obesity.

Clinical trials of epigenetic drugs in the treatment of diabetes and obesity[a].

Drug	Conditions	Status	NCT number	Phase
HDACi				
VPA	Obesity	Terminated	NCT00298857	Phase IV
	Diabetes	Completed	NCT00287352	Phase I
Sodium phenylbutyrate	Insulin resistance, diabetes, obesity	Completed	NCT00771901	N/A
	Diabetes and insulin resistance	Completed	NCT00533559	Phase IV
STAC				
Resveratrol	T2DM	Completed	NCT01038089	N/A
	T2DM	Completed	NCT01677611	Phase I
	Impaired glucose tolerance	Completed	NCT01593605	N/A
	Obesity and diabetes	Completed	NCT02247596	Phase II
	Obesity, metabolic syndrome, diabetes, aging	Completed	NCT00823381	N/A
	Obesity, insulin sensitivity, T2DM	Completed	NCT01302639	N/A
	Metabolic syndrome, obesity	Completed	NCT01150955	N/A
	T2DM	Completed	NCT00937222	N/A
	Obesity, NAFLD	Completed	NCT01446276	N/A
	Obesity, inflammation, insulin sensitivity, osteoporosis	Completed	NCT01412645	N/A
	Obesity	Completed	NCT00998504	N/A
	Obesity	Completed	NCT01717820	N/A
	Metabolic syndrome X	Completed	NCT02114892	Phase II
	Fatty liver	Completed	NCT01464801	N/A
	Obesity	Completed	NCT01518764	N/A
HATi				
Curcumin	Diabetes	Completed	NCT01646047	N/A
	Diabetes	Completed	NCT01029327	N/A
DNMTi				
Hydralazine	Atherosclerosis, CVD, hypercholesterolemia, hypertension, T2DM, coronary disease	Completed	NCT00000620	Phase III

[a] The list is compiled from ClinicalTrials.gov using the key words 'drugs and diabetes'; and 'drugs and obesity' where the 'drugs' are substituted with different epigenetic drugs. Only completed clinical trials are shown in the table. *Abbreviations*: NCT, ClinicalTrials.gov Identifier number; N/A, not available.

Table 3 - Clinical trials of epigenetic drugs in the treatment of diabetes and obesity. *Taken from Arguelles et al. 2016 [588].*

6.5 Oxidative stress and epigenetic investigation in H9c2 cardiomyocytes

ROS generation in response to environmental changes is associated with increased cardiovascular risk. There are numerous publications about pathological implications induced by oxidative stress with relevance for the development of cardiovascular diseases [5, 283, 284, 449, 595-598]. Recent investigations using cardiac myocyte systems in culture show that ROS and oxidative stress can cause multiple changes in cell structure and function that are associated with the failing heart, and which appear to be related to the quantity and type of ROS [598-600]. For example, it has been reported that direct addition of ROS led to apoptosis in different kinds of cardiomyocyte cultures, while surviving cells underwent hypertrophy [600-603]. Here, the rat cardiomyoblastic cell line H9c2 was applied as a model system to analyze the development of cardiomyopathy in response to oxidative stress. H9c2 cardiomyoblasts were derived from embryonic BD1X rat heart tissue by B. Kimes and B. Brandt and have the potential to differentiate into cardiomyocytes and further fuse to form multinucleated myotubes, ultimately exhibiting many of the properties of skeletal muscle [439]. The interplay of redox signaling and epigenetic regulation and its resulting effects on gene expression, as well as pathology and viability of H9c2 cells was investigated. At first, hydrogen peroxide was employed to induce oxidative stress. It has been demonstrated before that H_2O_2 induced hypertrophy and apoptosis in H9c2 cells via activation of stress-activated protein kinases and NFkB upregulation [598, 602, 604]. Here, considerable cell loss by cell detachment indicating apoptosis was observed at concentrations higher than 100 µM H_2O_2. Morphological changes of cells, like swelling or enlargement, were not clearly apparent; however, it is not necessarily expectable to already see hypertrophic characteristics in the surviving cells after only 4 or 24 h treatment. The extensive cell loss raised technical difficulties for further analysis, since subsequent protein quantification was problematic as lysate content fell below detection limit in Bradford assay. This made comparisons between treatments complicated as they depended on normalization, a factor that may falsify results due to extrapolation.

6.5.1 Doxorubicin-induced cardiotoxicity in H9c2 cardiomyocytes

In light of these challenges, another model depicting the pathophysiology of myocardial failure with involvement of ROS formation was established, i.e. doxorubicin-induced cardiomyopathy in differentiated H9c2 cardiomyocytes. The anthracycline doxorubicin (Dox) is a potent chemotherapeutic agent used for the treatment of a broad range of cancers [373, 375, 376]. However, the clinical use of doxorubicin is limited by the risk of development of severe cardiotoxicity. Dependent on the dosage,

~5-50% of patients treated with doxorubicin or its derivatives develop chronic cardiac complications up to 10-15 years after the cessation of doxorubicin chemotherapy [375, 381].

In order to combat cancer cells, doxorubicin acts via different mechanisms to produce a range of cytotoxic effects. It is known that doxorubicin binds to DNA-associated enzymes and intercalates between DNA base pairs, thereby interfering with topoisomerase-II (Top2α)-mediated DNA uncoiling and thus disrupting DNA repair or transcription [374, 605]. Other doxorubicin actions include free radical generation via several mechanisms, such as disruption of the mitochondrial transport chain, activation of ROS-generating enzymes, or decreased expression of cellular antioxidant defenses, as described in the Introduction (1.6.2, p.41) [375, 380, 389]. Furthermore, doxorubicin has an influence on the regulation of the Bcl-2/Bax apoptosis pathway. Doxorubicin was shown to downregulate mRNA levels of the anti-apoptotic factor Bcl-2, whilst the pro-apoptotic factor Bax was upregulated, thereby shifting the balance toward pro-apoptotic signaling [374, 375]. All these actions of doxorubicin ultimately induce programmed cell death. While these mechanisms are very effective in restricting cancer growth, doxorubicin also induces apoptosis and necrosis in healthy tissue causing toxicity in the brain, liver, kidney and heart [374]. Yet, the actions by which doxorubicin affects cancer cells are not entirely the same as those that affect cardiac cells. The reason for this is that cardiomyocytes are generally not replicative, and Top2α, the key target of doxorubicin, is not expressed in quiescent cells and undetectable in heart tissues [606]. Increased oxidative stress has been established as the primary cause of doxorubicin cardiotoxicity, as is evident from increased levels of ROS and lipid peroxidation, as well as decreased levels of antioxidants and sulfhydryl groups in respective cell and animal models [375, 384-388]. Cardiomyocytes are particularly susceptible to free radical damage because of their high oxidative metabolism and relatively poor antioxidant defenses [607]. Additional to causing mitochondrial dysfunction through ROS formation, other proposed mechanisms of doxorubicin cardiotoxicity include inhibition of nucleic acid and protein synthesis [608], release of vasoactive amines [609], altered adrenergic function [610] and downregulation of cardiac-specific genes, leading to decreased expression of contractile proteins, such as α-actinin, myosin and troponin [380]. Furthermore, doxorubicin treatment has also been associated with iNOS and eNOS upregulation, as well as eNOS uncoupling, thereby enhancing superoxide (and ultimately peroxynitrite) formation and promoting vascular endothelial cell injury [380, 611-614]. Evidence suggests that doxorubicin causes apoptotic cell death not only in cardiomyocytes but also endothelial cells, therefore rendering the cardiovascular system particularly susceptible to doxorubicin toxicity [380].

In the present study, apoptotic cell death was observed in H9c2 cardiomyocytes at 1 µM and 5 µM doxorubicin exposure for 24 h and 48 h, as was depicted by caspase-3 cleavage and fractin formation. Visual observation revealed that the amount of apoptotic cells was time- and dose-dependently increased. In line with doxorubicin's ability to induce peroxynitrite formation, 3-nitrotyrosine (3-NT) levels were found elevated upon doxorubicin exposure in apoptotic as well as in surviving cells. Another direct effect of doxorubicin-mediated ROS formation is lipid peroxidation, the end products of which are reactive aldehydes, such as malondialdehyde (MDA). Elevated MDA levels in response to doxorubicin treatment have repeatedly been reported in various cell and tissue models [615-617]. Here, MDA modification of proteins was also increased in all doxorubicin-treated H9c2 cells. As another marker of oxidative stress the expression of the mitochondrial antioxidant enzyme SOD2 was analyzed. It has been demonstrated before that induction of SOD2 up-regulation can counteract cardiotoxic effects induced by doxorubicin exposure [404-406], suggesting that in the present study H9c2 cells may initiate a coping-mechanism by overexpressing SOD2 in response to doxorubicin treatment. In general, when combining SOD2 levels in surviving and apoptotic cells of each treatment, the expression was increased upon doxorubicin exposure. However, after 24 h treatment the SOD2 levels in the apoptotic cells were not elevated compared to control cells. Possibly, insufficient protection by SOD2 actually became the reason that cells underwent apoptosis, whereas cells with increased SOD2 protection survived. At 48 h, also apoptotic cells exhibited increased SOD2 levels, but concluding from the oxidative marks seen in dot blot, ROS formation exceeded SOD2-mediated ROS scavenging and even high SOD2-levels could not protect doxorubicin-exposed cells from oxidative stress and apoptosis. Additional to oxidative stress possibly other doxorubicin mechanisms may have played a role in inducing apoptosis.

No effective treatment specific for established doxorubicin-induced cardiomyopathy is presently available. Typically, conventional therapies for congestive heart failure are utilized, including ACE inhibitors, beta-blockers and loop diuretics for volume management [618, 619]. However, extensive research is being done to discover preventative treatments. Most of the pharmacologic agents that have been tested to reduce or prevent doxorubicin cardiotoxicity have the potential to reduce oxidative stress. Accordingly, compounds with documented antioxidant properties, such as probucol, superoxide dismutase, vitamin C, resveratrol, and dexrazoxane have been reported to decrease doxorubicin cardiotoxicity [619-623]. The iron-chelating agent dexrazoxane has been approved by the FDA and is available for clinical use as combination therapy with anthracyclines; however, in practice it is used infrequently because it can induce myelosuppression [376]. While antioxidant therapy revealed favorable effects *in vitro* and in animal models, results of clinical studies have been inconsistent and

require further investigation [624]. Also, the focus on potential antioxidant cardioprotection is currently moving away to targeting the cellular mechanisms that cause apoptosis instead [375]. Anyway, it is important to fully unravel the molecular signaling pathway mediating doxorubicin-induced cardiotoxicity, including redox regulation and epigenetic processes, in order to develop novel approaches for the treatment or prevention of cardiomyopathy without affecting the antitumor activity.

6.5.1.1 *Effect of doxorubicin-induced cardiotoxicity on Sirt1 expression in H9c2 cells*

It is well-known that oxidative stress plays a vital role in the development of cardiovascular diseases. At the same time, epigenetic changes are implicated in the pathogenesis of CVDs and epigenetic regulators have been shown to be affected by increased ROS levels. The interplay between these factors was investigated in the doxorubicin-induced cardiomyopathy model in H9c2 cardiomyocytes by analyzing expression levels of certain epigenetic modulators.

Sirtuins are a class of enzymes characterized by sequence similarity to the yeast progenitor sirtuin "silent information regulator 2" (Sir2). Seven sirtuins have been found in mammalian cells, which play key roles in the regulation of metabolism, stress responses, genome stability, and ageing [625]. Sirtuins possess protein deacetylase activity and were classified as class III histone deacetylases (HDAC); therefore they are implicated in gene silencing. Since their activity is dependent on the cofactor NAD^+, these enzymes are quite sensitive to metabolic and redox changes. Sirt1 is the most evolutionarily conserved mammalian sirtuin and has been the most intensively investigated in the cardiovascular system [249]. Cardiac deficiency of Sirt1 was described to result in dilated cardiomyopathy and mitochondrial dysfunction [626, 627]. It has been shown that increased ROS formation exerts differential effects on Sirt1 activity and expression. For instance, oxidative stress is associated with intracellular NAD^+ depletion and therefore impaired Sirt1 function [247, 628, 629]. Furthermore, oxidative stress decreased Sirt1 levels or activity in models of doxorubicin-induced cardiotoxicity, oxidant stress-induced diabetic retinopathy, myocardial infarction, stroke or in a setting of metabolic syndrome [125, 630]. In contrast, Sirt1 expression was found to be increased in response to ROS, dependent on ROS-induced HIF1α up-regulation, in models of cardiac hypertrophy, heart failure and in aged hearts, probably as a compensatory reaction [249]. It seems that there is an essential crosstalk between oxidative stress and Sirt1 expression dependent on the levels of ROS, the cell type and the stimulatory context. In a context-dependent manner, these factors can control reciprocally each other's functional activities, directly or via an integrated signaling network [248]. Hence, disturbing the optimal signaling balance between the level of ROS production and Sirt1 activity ultimately leads to disease.

Here, Sirt1 expression was down-regulated in doxorubicin induced cardiomyocyte injury, accompanied by elevated oxidative stress and cell apoptosis. These results coincide with data by Ruan *et al.*, who also reported reduced Sirt1 levels upon doxorubicin exposure in cultured primary neonatal rat ventricular myocytes [630]. Moreover, they showed that induction of Sirt1 overexpression protected cardiomyocytes from oxidative stress and apoptosis by disrupting the p38 MAPK apoptotic pathway, thus ameliorating doxorubicin-induced cardiotoxicity.

A ~110 kDa band was observed additionally in the present study, which was proposed by several antibody providers to appear due to Sirt1 glycosylation. Han *et al.* demonstrated in 2017 that O-GlcNAcylation of Sirt1 enhances its deacetylase activity and promotes cytoprotection under stress, thereby preventing stress-induced apoptosis [453]. This could explain why only extremely low levels of glycosylated Sirt1 were observed in the apoptotic fraction of doxorubicin-treated H9c2 cells. In the surviving cells and control cells, glycosylation was clearly existent and was increased in the surviving 1 µM doxorubicin-treated cells, most likely as protection from apoptosis. Nonetheless, it is unclear why it was not elevated in the cells treated with 5 µM doxorubicin as well. Furthermore, high levels of a 95 kDa Sirt1 band were detected in apoptotic cells, which probably represents a SIRT1-ΔExon8 isoform that has been reported by Lynch *et al*. [454]. They found that this isoform retains minimal deacetylase activity and exhibits distinct stress sensitivity, attributed to the stress sensor p53's ability to influence Sirt1 splice variation. In turn, SIRT1-ΔExon8 can regulate p53 through acetylation creating an auto-regulatory loop. The existence of alternative Sirt1 isoforms with distinct characteristics provides insight into the complex role of Sirt1 and may provide an explanation for previously observed conflicting results. In fact, reported functions attributed to Sirt1 may be distributed between Sirt1 isoforms [454, 631].

Resveratrol, a natural polyphenolic compound mainly found in grapes, has been shown to significantly increase Sirt1 activity through an allosteric interaction, resulting in the increase of Sirt1 affinity for both NAD$^+$ and the acetylated substrate [632]. It is known that resveratrol exhibits numerous protective features; amongst other effects it can reduce the risk of metabolic and cardiovascular diseases and protect cardiomyocytes from apoptosis [627, 633, 634]. In fact, it has specifically been reported that resveratrol protects cardiomyocytes against doxorubicin-induced apoptosis and therefore cardiac toxicity *in vitro* and *in vivo* [630, 634-638]. In accordance with the observation that Sirt1 expression was decreased following doxorubicin treatment accompanied by increased cardiomyocyte apoptosis, Sirt1 activation by resveratrol prevented these adverse events and thereby protected cardiac cells against doxorubicin-induced injuries. A reason for this is that Sirt1 up-regulation results in increased p53 deacetylation and therefore reduced p53-mediated cardiomyocyte apoptosis by transcription-dependent

and -independent mechanisms [638]. Moreover, Sirt1-mediated ER homeostasis was rescued by resveratrol, counteracting the doxorubicin-induced ER stress response [636]. Additionally, resveratrol's beneficial effects are associated with mitochondrial stabilization through increased antioxidant defense and activation of PGC-1α, a regulator of mitochondrial biogenesis [627, 633, 635].

Collectively, the histone deacetylase Sirt1 may serve as a potential therapeutic target for doxorubicin-induced cardiomyopathy, while the Sirt1 agonist resveratrol emerges as a promising candidate for early treatment to prevent cardiac injury by doxorubicin therapy.

6.5.1.2 *Effect of doxorubicin-induced cardiotoxicity on HDAC2 expression in H9c2 cells*

Another prominent histone deacetylase that was analyzed in the context of doxorubicin-induced cardiomyopathy was HDAC2, which belongs to class I of the mammalian HDAC family. Studies in mice and cultured cardiomyocytes have identified both class I and class II HDACs as key regulators of cardiac growth and disease [639]. While class II HDACs have been described to repress hypertrophy, class I HDAC2 was found to be a pro-hypertrophic mediator [174, 640, 641]. Kee *et al.* demonstrated that HDAC2 enzyme activity increased in response to hypertrophic stimuli [640]. Moreover, it was shown by Trivedi *et al.* that genetic disruption of HDAC2 resulted in resistance against hypertrophic stimuli, whereas gain-of-function of HDAC2 induced cardiac hypertrophy significantly [174]. In a murine model of doxorubicin-induced cardiomyopathy, chronic treatment with low-dose doxorubicin caused specific changes in the transcriptional profile of several histone deacetylases [455]. Specifically, doxorubicin treatment induced significant down-regulation of HDAC2 mRNA and protein levels, while HDAC4 and HDAC5, anti-hypertrophic class II HDACs, were up-regulated, probably as a coping mechanism counteracting cardiomyopathy. Concerning the relation between oxidative stress and HDAC2, it has been shown that ROS decrease HDAC2 activity and expression through generating post-translational modifications (PTMs), which impair enzymatic function and can result in proteasomal degradation [128, 243]. While inhibition of HDAC2 enzyme activity through PTMs was reported to result in amplified inflammation [242, 243], other studies have demonstrated that class I-selective HDAC inhibitors can efficiently reduce cardiac hypertrophy under pathological conditions [641, 642]. Therefore, the role of HDAC2 function/inhibition in cardiomyopathy with regards to oxidative stress may be regarded as controversial.

In the present study, HDAC2 expression was found to be decreased in cardiomyocytes upon low-dose (1 μM) doxorubicin treatment, in consistence with the previously mentioned observations in a murine model of doxorubicin-induced cardiomyopathy. Apoptotic cells also exhibited significantly reduced

HDAC2 levels. Surprisingly, a higher dose (5 μM) of doxorubicin did not show an effect on the expression of HDAC2 in surviving cells; however, the impact on HDAC2 activity, which could contribute to changes in expression levels, was not determined. An additional band observed at 50 kDa could be attributed to a potential ~52 kDa HDAC2 isoform (UniProt [29]), or to undesired antibody-recognition of HDAC3 at 49 kDa due to sequence homology between HDAC2 and HDAC3 (both are class I HDACs) [158]. Nonetheless, the reason for the substantial increase of the 50 kDa band levels in apoptotic cells remains unclear, since the role of the HDAC2 isoform has not been described in detail yet, and HDAC3 is supposed to exert similar effects as HDAC2 upon cardiomyopathy or oxidative stress. The additional band could also represent a degradation product of HDAC2 due to increased proteolysis in apoptosis, though it is questionable if this would result in the detection of such a precisely sized band and not a degradation ladder.

HDAC2 presents itself as an interesting therapeutic target in the prevention of cardiac disorders and heart failure, since studies in small animal models have shown that inhibitors of class I HDACs can blunt cardiac hypertrophy and preserve cardiac function [643]. Nevertheless, further research including larger animal studies and the use of more realistic models will be necessary before the efficacy of these compounds can be assessed in clinical trials.

6.5.1.3 Effect of doxorubicin-induced cardiotoxicity on KDM3A expression in H9c2 cells

In human and rodent failing hearts, differential histone methylation patterns have been observed in various gene clusters [270, 274, 280]. Maintaining histone methylation balance was shown to play a key role in heart development and the pathogenesis of congenital heart defects and adult cardiovascular diseases [644]. During the process of pathological hypertrophy, adult differentiated cardiomyocytes undergo epigenetic cardiac remodeling, where the expression of fetal genes, such as atrial natriuretic peptide (ANP) and brain natriuretic peptide (BNP), is reactivated [645]. This reprogramming of fetal genes has been proposed as a cardioprotective response, aimed at increasing cardiac efficiency under conditions of stress, and was found to be closely associated with increased H3K9 demethylation. Specifically, it has been demonstrated that H3K9me2/3 levels were decreased in promoter regions of disease-specific genes, including ANP and BNP, in human failing myocardium and in mouse cardiomyocytes in response to hypertrophic stresses. Elevated H3K9 demethylation correlated inversely with up-regulated global levels of Jumonji demethylases KDM3A, KDM4A and KDM4B [459, 646]. In agreement with the described findings, the data in the present study also show a clear increase of KDM3A expression in H9c2 cardiomyocytes upon doxorubicin-induced cardiomyopathy. Levels of KDM3A increased dependent on doxorubicin concentration and were considerably higher in their respective

apoptotic fraction. This may be caused by more elevated ROS levels in the apoptotic cells. The JmjC histone lysine demethylases are Fe(II)-dependent dioxygenases and use 2-oxoglutarate and oxygen as cosubstrates for oxidative demethylation. Therefore KDMs are fairly sensitive to redox metabolism. In fact, H_2O_2 or $^\bullet$NO have been shown to disrupt KDM activity [124, 217]. Moreover, ROS, $^\bullet$NO and hypoxia were shown to upregulate the expression of several KDMs [217, 251, 647]. Hence, quenched KDM activity in response to hypoxia or ROS might lead to a compensatory increase in KDM expression as a counteracting mechanism.

In addition, possible KDM3A dimer formation was observed. It has previously been reported that KDM3A forms a homodimer through its catalytic domain to enable the effective execution of two-step demethylation of dimethylated H3K9 into the null methylation state [460]. Decrease of dimer detection and complete abolishment in apoptotic cells may be due to oxidative modifications at the catalytic site, which might hinder dimerization. Nevertheless, it should be mentioned that it is odd to detect these dimers under denaturing, reducing conditions, which were applied here, and therefore the bands may stem from a different source.

To summarize, upregulation of JmjC KDMs may sustain H3K9 demethylation in the course of heart failure and further investigation of the underlying pathways may help to identify novel targets to improve the treatment of cardiovascular diseases, since impaired methylation balance has been described as an important factor inducing cardiac defects.

6.5.1.4 *Effect of doxorubicin-induced cardiotoxicity on LSD1 expression in H9c2 cells*

Adding to this subject, it has also been shown that appropriate H3K4me3 level is critical to maintain cellular homeostasis in differentiated cardiac cells [648]. While KDM3A specifically demethylates Lys-9 of histone H3, the FAD-dependent histone lysine demethylase LSD1 can remove both H3K4 and H3K9 lysine methyl residues, dependent on the biological context. LSD1 has been found to be implicated in cardiovascular diseases such as hypertension or diabetes [125, 346, 461]. For instance, it has been reported that in mice during high-salt diet, LSD1 deficiency led to enhanced vascular contraction, reduced expression of cardiac and vascular eNOS and guanylate cyclase, thereby disturbing the $^\bullet$NO/cGMP relaxation pathway, causing hypertension [649]. Furthermore, LSD1 is associated with the regulation of cellular energy metabolism through coupling with cellular FAD biosynthesis [43]. As aberrant cellular energy metabolism is associated with a wide range of metabolic diseases, including diabetes, cardiovascular diseases and cancer, the crosstalk between epigenetic regulators and metabolic state provides an interesting field for investigation. Here, global LSD1 levels were investigated upon

cardiotoxic incentive. However, no substantial changes in LSD1 expression were observed at 24 h of doxorubicin exposure. Interestingly, controversial results were obtained at 48 h post doxorubicin treatment, since LSD1 levels were significantly decreased compared to control in all groups, but were visibly more reduced in cells treated with the lower dose of doxorubicin. Possibly, the stark decrease of LSD1 expression may have caused a conversion to a compensatory increase in expression levels at a certain point in cells treated with the higher dose. Nevertheless, the exact role of LSD1 in cardiomyopathy remains to be investigated in order to elucidate which underlying pathways are affected and how histone methylation balance is disrupted due to altered LSD1 function and expression.

6.5.1.5   Effect of doxorubicin-induced cardiotoxicity on Set7 expression in H9c2 cells

The histone methylation status can also be modified through the action of histone methyltransferases, such as Set7 or SMYD1. Set7, which specifically monomethylates lysine 4 of histone H3, has been shown to play a key role in diabetic vascular complications [463, 650]. Specifically, Set7 has been proposed as a critical mediator of hyperglycemic memory, a phenomenon where epigenetic changes in vascular gene expression in response to hyperglycemia are sustained even after return to normoglycemia, which may ultimately cause vascular dysfunction [462, 651]. Furthermore, Set7 induces pro-inflammatory responses through NFκB transcription activation and subsequent upregulation of cytokine production, and regulates mitochondrial function and ROS signaling partly via repression of antioxidant genes, indicating that Set7 itself contributes to ROS formation [194, 354, 652]. In a recent study from 2018, Dang *et al.* showed that Set7 expression was significantly up-regulated in rat cardiomyocytes in response to hypoxia/reoxygenation (H/R) injury [653]. Moreover, they demonstrated that forced overexpression of Set7 markedly enhanced H/R-induced apoptosis and ROS production, whereas Set7 knockdown or inhibition decreased ROS generation via promotion of the Nrf2-mediated antioxidant response and protected cells from apoptosis. In contrast, knockdown of Set7 has been associated with increased sensitivity to DNA damage and genotoxic stress elicited by doxorubicin in cancer cells, thus rendering these cells more susceptible to apoptosis [654]. Set7 deficient cells displayed altered expression of a number of genes involved in DNA damage signaling and repair, cell cycle checkpoints, and apoptosis. Set7 may also be directly implicated in apoptosis regulation through methylation of the apoptosis inducing factor p53 [655]. Here, Set7 expression was clearly upregulated in response to 5 µM doxorubicin-induced cardiomyopathy, which constitutes an expectable result given Set7's role in inflammation and ROS signaling. However, the Set7 expression patterns in the Dox-treated apoptotic cells are more difficult to comprehend. The diverse outcome of expression levels may be attributed to a highly dynamic response to pathological stimuli or the uncertain implication of Set7 in the complex

processes of apoptotic cell death. In addition, evidence points to Set7 being an effector of ROS formation itself; in turn however, under conditions of oxidative stress the cofactor for HMTs, S-adenosylmethionine (SAM), is reduced, restricting Set7 methylation activity as described in the Introduction (1.5, p.34). Thus, the role of Set7 in cardiac disease and associated oxidative stress and apoptosis will have to be further investigated.

6.5.1.6 *Effect of doxorubicin-induced cardiotoxicity on SMYD1 expression in H9c2 cells*

The muscle-specific histone methyltransferase SMYD1 plays an essential role in cardiac differentiation and morphogenesis [198, 464]. Defects or deletions in the gene encoding SMYD1 lead to retarded maturation of ventricular cardiomyocytes during cardiac development, causing fetal mortality [198]. In adult mice inducible cardiac-specific deletion of SMYD1 was shown to cause hypertrophy, organ remodeling and heart failure; thus it was proposed that SMYD1 expression or activation is responsible for restricting pathological cell growth in the adult heart and that constitutive SMYD1 activity is essential for normal heart function [465]. Correspondingly, upregulation of SMYD1 has been observed during disease in order to antagonize cardiac complications in a mouse model of pressure overload-induced hypertrophy and in diseased human heart [465, 466, 656]. It was suggested that an essential role of SMYD1 in the adult heart is to regulate mitochondrial metabolism. Loss of SMYD1 has been demonstrated to result in significant reduction in mitochondrial respiration capacity, in concordance with the down-regulation of OXPHOS proteins and PGC-1α [466]. In line with this, it was shown that the redox regulator and antioxidant protein Trx1 significantly promoted the expression of SMYD1, 2, 3 and 5 [657]. In the present study, expression patterns of SMYD1 are quite inconsistent, also because of deviations between single experiments. The expected up-regulation of SMYD1 was only observed at 48 h in 5 µM doxorubicin-treated pre-apoptotic cells and, in some cases, in apoptotic cells treated with 1 µM doxorubicin at 24h. The reduction in SMYD1 levels in apoptotic 5 µM doxorubicin-treated cells is probably the cause for cell death due to adverse effects in response to SMYD1 loss. There seems to be a dynamic interplay between compensatory upregulation of SMYD1 granting cardiomyocyte protection, and cell death due to insufficient SMYD1 expression and disrupted mitochondrial regulation.

SMYD1 can act as a transcriptional activator by performing mono-, di-, and trimethylation on lysine 4 of histone 3. In contrast, SMYD1 can recruit and interact with the histone deacetylases HDAC1, HDAC2 and HDAC3 and, through this interaction, functions as a histone deacetylase-dependent transcriptional repressor [198]. Interestingly, the pre-apoptotic doxorubicin-treated cells present a similar expression pattern of SMYD1 and HDAC2, where both enzymes are reduced at 1 µM doxorubicin, but unchanged or

even slightly increased at 5 µM doxorubicin. However, the relevance of this observation will have to be further elucidated.

In general, it is also noteworthy that histone methyltransferases (HMTs) require S-adenosyl methionine (SAM) as a cofactor, the availability of which is affected by ROS production. Increased oxidative stress reduces SAM levels, thereby leading to decreased activity of HMTs [125]. Impaired function of HMTs may also be responsible for compensatory increases in HMT expression levels. Interestingly, it has been shown previously that co-administration of SAM decreased doxorubicin-induced cardiotoxicity in rats [658].

All in all, histone modifying enzymes have been shown to play all kinds of roles in cardiac pathologies and therefore provide interesting therapeutic targets opening new avenues to the treatment of cardiac diseases.

6.5.1.7   ROS-induced modifications on histone modulators

In addition to changes in expression patterns of epigenetic modulators in response to various signaling pathways, the concomitant increase in ROS formation during doxorubicin-induced cardiomyopathy may also have a crucial effect on expression and activity of epigenetic regulators due to the introduction of physical redox modifications by free radicals on these enzymes. For instance, sirtuins possess a highly conserved zinc tetra-thiolate motif within their catalytic pocket, which is required for their deacetylase activity along with the cofactor NAD^+. There is broad evidence that ROS/RNS can inhibit Sirt1 deacetylase function through inducing cysteine S-nitros(yl)ation, S-glutathionylation or carbonylation at the active site [240, 246, 452, 659-661]. Similarly, Sirt3 has been shown to be carbonylated and inactivated by 4-HNE [662]. Class I HDACs, on the other hand, use a different deacetylation mechanism requiring Zn^{2+} ions as cofactors, but have also been shown to be highly prone to ROS-induced post-translational modifications, with the prime target being their conserved, surface-exposed cysteine residues [243]. S-glutathionylation, S-nitros(yl)ation, tyrosine nitration, acetylation and phosphorylation of class I HDACs have all been reported in oxidative stress related diseases [128, 242-244, 641, 660, 663]. Generally, these modifications are associated with decreased HDAC activity or impaired target binding. In addition, it has been demonstrated that class I HDACs are alkylated and inhibited by several reactive aldehydes, as repeatedly observed in models of COPD [239, 243, 664]. In this respect, it was also suggested that inhibition of HDACs by ROS might be a physiological response in order to protect cells from oxidative stress-mediated dysregulation [36].

Furthermore, JmjC demethylases can be inhibited by nitrosative stress. It has been shown that KDM3A activity is disrupted by NO through directly binding to Fe(II) forming a nitrosyl-iron complex in the catalytic pocket, ultimately leading to an increase of H3K9me2 [217].

Direct oxidative modification in response to ROS exposure was not yet reported for the histone demethylase LSD1 or the histone methyltransferases Set7 or SMYD1. However, it was shown very recently that SMYD2 is susceptible to S-glutathionylation in response to ROS, resulting in decreased myofibril integrity [665].

In the present study, the addressed epigenetic modulators were investigated for the presence of redox modifications via immunoprecipitation with 3-NT, 4-HNE and MDA antibodies. Unfortunately, analyses failed due to technical difficulties and lack of time.

6.5.1.8   Effects of doxorubicin-induced cardiotoxicity on histones/ histone marks

Naturally, effects of doxorubicin-induced cardiomyopathy on expression or activity of chromatin modifiers affect histone modulation. Animal models of heart failure have revealed that cardiomyocytes of failing hearts showed changes in epigenetic profiles of H3K4 and H3K9 methylation marks that may be attributable to ROS-induced changes in histone demethylase activity [134, 270, 274, 646, 648]. This has also been observed in humans with heart failure [270, 274, 280, 666]. Of note, however, those differential methylation markings referred to global alterations of H3K4me3 and H3K9me3 levels at specific promoters of genes involved in cardiac function, but there were no global changes in the overall extent of histone methylation levels.

Decreased overall global levels of H3Ac have been repeatedly reported in several types of cancers, highlighting the importance of further exploring HDAC inhibitors as potential therapeutic application [667-670]. There has, so far, been no report of overall genome-wide changes in H3Ac levels in cardiomyopathy; however there is lots of data concerning altered histone acetylation levels at certain gene promoters implicated in cardiac function and inflammation due to dysregulation of HATs and HDACs [671]. For instance, suppression of anti-hypertrophic regulator genes through decreased histone acetylation due to upregulation of class I HDACs may induce cardiac hypertrophy [640]. Here, a gradual decline in global H3Ac levels was observed depending on doxorubicin concentration and cell viability status. It is questionable, if the decrease in H3Ac levels can be attributed to the presently analyzed HDACs, Sirt1 and HDAC2, since there was no obvious increase in expression and there was no investigation of activity. The results may be based on the activity of other histone deacetylases or an unbalanced interplay of HATs and HDACs. It remains to be investigated if such effects on histone

acetylation may also be observed *in vivo* in models of doxorubicin-induced cardiomyopathy and to unravel the implications of these results for cardiac pathogenesis.

Interestingly, it has also been reported that histones are increasingly evicted from chromatin in response to doxorubicin treatment, deregulating the DNA damage response, the epigenome and transcriptome [672]. It may be possible that oxidative stress implied in doxorubicin toxicity may exert direct effects on histones (without involvement of histone modifying enzymes), resulting in histone glutathionylation, carbonylation, nitration or even dityrosine cross-linking (as discussed in 6.3).

Further studies will be necessary to provide a reliable basis for the evaluation of histone modification patterns in patients with cardiovascular related diseases in order to prove clinical benefits of the use of epigenetic drugs. Targeting specific chromatin remodeling factors and histone modifiers may represent a promising strategy for the prevention or treatment of some cardiac complications. Aside from that, it seems obvious to develop antioxidant drugs to counteract the consequences of high ROS levels in disease; however, antioxidants have already been widely tested as a treatment for neurodegenerative diseases, CVDs and cancer, yielding contradictory results, ranging from improvement of the disease to accelerated progression [673-677]. In the case of anti-cancer therapy antioxidants may also have the undesired side-effect to suppress the anti-tumorigenic properties of drugs such as doxorubicin. Furthermore, one has to take into consideration that ROS have both protective and damaging effects on cells, hence it may be essential to only target distinct parts of the ROS-dependent response. A comprehensive understanding of the interplay of ROS and epigenetic mechanisms in cardiovascular related diseases may lead to the development of novel and targeted treatment options, generating the potential to improve the quality of life of millions of CVD patients worldwide.

6.6 Confidence and accuracy of Western blot analyses

Western blotting (WB) is one of the most commonly used laboratory techniques for identifying and characterizing proteins even in a crude mixture. The ability of immunoblots to detect a "needle in a haystack" has been considered a critical tool in many areas of biological research, being applied in protein expression studies, antibody screening or clinical immunodiagnostics. Initially, the Western blot technique was only regarded as a tool for qualitative, not quantitative, analyses of proteins due to the high possibility of disparities in execution between investigators; nonetheless, with increasingly refined WB methodology and equipment at hand, WB is nowadays widely used to quantitate protein abundance [678]. Still, the confidence and accuracy of quantitative Western blot analyses are more and more being questioned. The key strategies to ensure precise and reproducible WB results include proper sample

integrity and preparation, confirming antibody specificity, validating the linear range of the detection system, preventing signal saturation, and selecting the best normalization method implementing acceptable loading controls [679, 680]. Normalization to the total quantity of loaded protein is a crucial element in accurately quantifying protein expression. Currently, housekeeping proteins (HKPs) like actin, tubulin or GAPDH are commonly used to check for equal loading or to compensate potential loading differences. However, these proteins are usually of high abundance creating the problem that they are rarely in the same linear detection range as the target protein of interest [681, 682]. Furthermore, it has been demonstrated that HKP levels can actually vary under certain experimental conditions [683, 684]. Moreover, HKPs may often be post-translationally modified, which can also potentially affect quantification [679].

Taking these findings into account, protein expression measured by WB analyses was normalized to two different HKPs where possible in this study. Similarly, dot blot results were always normalized to total protein loading as displayed via Ponceau staining of the blot. In this context, it is being argued lately that also in Western blot total protein staining generally represents a superior loading control due to minor technical and biological variation compared to HKP expression [685, 686]. There are now increasing numbers of kits marketed for the purpose of staining gels or blots to check loading [680].

To be completely safe, it may be of advantage to always expand WB analyses by additionally performing quantitative PCR assays in order to get clearer results. These methods nicely complement each other. Whereas qPCR measurement of mRNA levels is highly specific, it cannot assess alternate appearance of proteins, such as in response to alternative splicing, degradation or post-translational modifications. WB analysis, in turn, may be able to display such changes depending on the antibody epitope.

Unfortunately, in the present study it was not possible to perform PCR analyses for the detection of expression levels in the model of doxorubicin-induced cardiotoxicity in H9c2 cells due to lack of time and financial reasons.

7 Summary

Oxidative stress is caused by an imbalance between the production of reactive oxygen species (ROS) and the neutralization of these species by antioxidant systems, leading to a disruption of redox signaling, oxidative damage and potential pathological consequences, including cardiovascular complications. There is a growing body of evidence that ROS influence epigenetic pathways by affecting the function or levels of epigenetic modulators, such as histone modifying enzymes. Since epigenetic modifications are increasingly recognized as major players in cardiovascular disease development and progression, investigation of the interplay between redox signaling and epigenetic regulation is of particular interest in this context.

A readout assay for the detection of protein S-nitros(yl)ation, a redox modification, was established using an approach consisting of light-induced homolysis of nitros(yl)ated proteins and subsequent immuno-spin trapping of generated protein radicals via 5,5-dimethyl-1-pyrroline N-oxide (DMPO) and a respective antibody.

In order to investigate ROS-induced epigenetic changes, a suitable model system with elevated ROS formation had to be established. Culturing endothelial cells under hyperglycemic conditions is known to generate increased oxidative stress. However, no substantial effects on ROS formation and histone methylation and acetylation patterns could be observed in the endothelial cell line EA.hy926 upon hyperglycemia, possibly due to a systematical technical error that, however, could not be identified despite multiple methodological variations.

In mice deficient in the antioxidant protein glutathione peroxidase-1 (GPx-1) endothelial dysfunction and enhanced ROS levels have been reported previously, an effect that was further potentiated by aging. Epigenetic analysis of this model led to the hypothesis of potential dityrosine cross-linking between histone 3 and histone 4 accompanied by enhanced histone 3 lysine 9 dimethylation upon increased oxidative stress. However, upon further investigation by mass spectrometry and exclusion of antibody cross-reactivity to IgGs in the animal samples this assumption was revealed to be false.

In a published study by our group it was demonstrated that empagliflozin, a selective sodium-glucose co-transporter 2 inhibitor (SGLT2i), reduced glucotoxicity and thereby prevented the development of endothelial dysfunction, reduced oxidative stress and exhibited anti-inflammatory effects in ZDF rats, an animal model for type 2 diabetes mellitus (T2DM). Investigation of involved epigenetic mechanisms by chromatin immunoprecipitation (ChIP) analysis revealed an effect of empagliflozin treatment on

expression of glucotoxicity- and inflammation-markers in diabetic animals via altered histone methylation patterns.

Finally, the interplay of increased ROS formation and epigenetic alterations was studied in H9c2 cardiomyocytes with a doxorubicin-induced cardiotoxic phenotype. It was discovered that doxorubicin treatment affected the expression of certain epigenetic modulators in correlation with increased oxidative stress markers. Given that epigenetic changes are reversible, they represent potential intervention targets as well as biomarkers that can be addressed for drug discovery. Thus, establishing a comprehensive understanding of the interplay of ROS and epigenetic mechanisms in cardiovascular related diseases may lead to the development of novel and precisely targeted treatment options.

8 Zusammenfassung

Der Ausdruck „oxidativer Stress" bezeichnet ein Ungleichgewicht zwischen der Entstehung freier reaktiver Sauerstoffradikale (ROS) und deren Neutralisierung durch anti-oxidative Mechanismen. Oxidativer Stress führt zur Beeinträchtigung der zellulären Redox-Regulation, Entstehung oxidativer Schädigungen und letztendlich zu möglichen pathologischen Konsequenzen, wie z.B. kardiovaskulären Erkrankungen. Immer mehr Forschungsresultate deuten darauf hin, dass ROS epigenetische Prozesse beeinflussen, indem sie die Funktion oder Konzentration epigenetischer Modulatoren, wie z.B. Histon-Modifikatoren, verändern. Da epigenetische Modifikationen zunehmend mit der Entwicklung und dem Fortschreiten kardiovaskulärer Erkrankungen in Verbindung gebracht werden, ist es von großem Interesse das Zusammenspiel von Redox-Signalwegen und epigenetischer Regulierung vor diesem Hintergrund zu untersuchen.

In dieser Arbeit wurde zunächst ein Testverfahren zur Detektion von Protein S-Nitros(yl)ierung, einer Redox-Modifikation, erstellt. Dieses beinhaltete die Licht-induzierte Homolyse der nitros(yl)ierten Proteine, Immuno-Spin Trapping der entstehenden Radikale mithilfe von 5,5-Dimethyl-1-pyrroline N-oxid (DMPO) und Detektion durch einen entsprechenden Antikörper.

Um ROS-induzierte epigenetische Veränderungen zu untersuchen, musste ein geeignetes Modellsystem etabliert werden, welches erhöhten oxidativen Stress aufweist. Es ist bekannt, dass Endothelzellen bei Kultivierung mit erhöhter Glukose-Konzentration vermehrt ROS bilden. Dennoch konnten gegenwärtig in diesem Modell keine erheblichen Effekte auf die ROS-Bildung und Histon-Modifikationen festgestellt werden, was möglicherweise auf ein systematisches methodologisches Problem zurückzuführen ist, das trotz intensiver Variation der Versuchsbedingungen nicht identifiziert werden konnte.

In einer vorherigen Studie wurde in Mäusen mit Knock-out des anti-oxidativen Enzyms Glutathionperoxidase-1 (GPx-1) eine endotheliale Dysfunktion und erhöhter oxidativer Stress verzeichnet, wobei dieser Effekt bei höherem Alter verstärkt war. Epigenetische Analysen dieses Modells führten zu der Hypothese, dass bei hohem oxidativen Stress Dityrosin-Brücken (=kovalente Bindungen) zwischen Histon 3 und Histon 4 gebildet werden, zusammen mit verstärkter Dimethylierung von Lysin 9 an Histon 3 (H3K9me2). Allerdings stellte sich bei weiteren Untersuchungen mittels Massenspektrometrie und Verwendung von Sekundärantikörpern mit garantierter Abwesenheit von Kreuzreaktivitäten gegenüber den IgGs der Tierproben heraus, dass diese Annahme falsch war.

In einer von uns publizierten Studie wurde gezeigt, dass Empagliflozin, ein selektiver Inhibitor des Natrium-Glukose Cotransporters 2, die Glukotoxizität in ZDF Ratten, einem Modell für Typ 2 Diabetes Mellitus, verminderte und dadurch sowohl die Entwicklung einer endothelialen Dysfunktion verhinderte, als auch oxidativen Stress verringerte und anti-entzündlich wirkte. Die Charakterisierung involvierter epigenetischer Mechanismen mittels Chromatin-Immunopräzipitation (ChIP)-basierter Analyse zeigte einen Effekt von Empagliflozin auf die Expression bestimmter Glukotoxizitäts- und Entzündungsmarker in diabetischen Tieren durch veränderte Histon-Methylierungsmuster.

Abschließend wurde das Zusammenspiel von ROS-Entstehung und epigenetischen Veränderungen in H9c2 Kardiomyozyten unter Bedingungen von Doxorubicin-induziertem Kardiotoxizitätsphänotyp analysiert. Dabei wurde festgestellt, dass die Doxorubicin-Behandlung in Korrelation mit erhöhtem oxidativen Stress die Expression bestimmter epigenetischer Modulatoren beeinflusste. Da epigenetische Veränderungen reversibel sind, stellen sie potenzielle Angriffspunkte zur therapeutischen Intervention dar und könnten auch als Biomarker pathologischer Prozesse fungieren. Daher ist ein umfassendes Verständnis des Zusammenwirkens von ROS und epigenetischer Mechanismen in kardiovaskulären Erkrankungen von großem Wert für die Entwicklung neuer und gezielter Behandlungsmöglichkeiten.

9   Literature

1.   Phaniendra, A., D.B. Jestadi, and L. Periyasamy, *Free radicals: properties, sources, targets, and their implication in various diseases.* Indian journal of clinical biochemistry : IJCB, 2015. **30**(1): p. 11-26.
2.   Egea, J., et al., *European contribution to the study of ROS: A summary of the findings and prospects for the future from the COST action BM1203 (EU-ROS).* Redox Biol, 2017. **13**: p. 94-162.
3.   Betteridge, D.J., *What is oxidative stress?* Metabolism, 2000. **49**(2 Suppl 1): p. 3-8.
4.   Luo, M., et al., *Redox regulation of DNA repair: implications for human health and cancer therapeutic development.* Antioxid Redox Signal, 2010. **12**(11): p. 1247-69.
5.   Singh, N., et al., *Oxidative stress and heart failure.* Mol Cell Biochem, 1995. **147**(1-2): p. 77-81.
6.   Feng, B., M.A. Ruiz, and S. Chakrabarti, *Oxidative-stress-induced epigenetic changes in chronic diabetic complications.* Can J Physiol Pharmacol, 2013. **91**(3): p. 213-20.
7.   Valko, M., et al., *Free radicals and antioxidants in normal physiological functions and human disease.* Int J Biochem Cell Biol, 2007. **39**(1): p. 44-84.
8.   Cadenas, E. and K.J. Davies, *Mitochondrial free radical generation, oxidative stress, and aging.* Free Radic Biol Med, 2000. **29**(3-4): p. 222-30.
9.   Griendling, K.K., D. Sorescu, and M. Ushio-Fukai, *NAD(P)H oxidase: role in cardiovascular biology and disease.* Circ Res, 2000. **86**(5): p. 494-501.
10.   Geiszt, M., *NADPH oxidases: new kids on the block.* Cardiovasc Res, 2006. **71**(2): p. 289-99.
11.   Hayes, P. and U.G. Knaus, *Balancing reactive oxygen species in the epigenome: NADPH oxidases as target and perpetrator.* Antioxid Redox Signal, 2013. **18**(15): p. 1937-45.
12.   Nisimoto, Y., et al., *Nox4: a hydrogen peroxide-generating oxygen sensor.* Biochemistry, 2014. **53**(31): p. 5111-20.
13.   Drummond, G.R. and C.G. Sobey, *Endothelial NADPH oxidases: which NOX to target in vascular disease?* Trends Endocrinol Metab, 2014. **25**(9): p. 452-63.
14.   Schroder, K., et al., *Nox4 is a protective reactive oxygen species generating vascular NADPH oxidase.* Circ Res, 2012. **110**(9): p. 1217-25.
15.   Kuppusamy, P. and J.L. Zweier, *Characterization of free radical generation by xanthine oxidase. Evidence for hydroxyl radical generation.* J Biol Chem, 1989. **264**(17): p. 9880-4.
16.   Roy, P., M.P. Sajan, and A.P. Kulkarni, *Lipoxygenase-mediated glutathione oxidation and superoxide generation.* J Biochem Toxicol, 1995. **10**(2): p. 111-20.
17.   Kunkel, S.L., et al., *Production of cyclooxygenase products and superoxide anion by macrophages in response to chemotactic factors.* Prostaglandins, 1982. **24**(6): p. 789-99.
18.   Wu, Y., et al., *Molecular mechanisms underlying chronic inflammation-associated cancers.* Cancer Lett, 2014. **345**(2): p. 164-73.
19.   Berry, C., et al., *Investigation into the sources of superoxide in human blood vessels: angiotensin II increases superoxide production in human internal mammary arteries.* Circulation, 2000. **101**(18): p. 2206-12.
20.   Landmesser, U., et al., *Angiotensin II induces endothelial xanthine oxidase activation: role for endothelial dysfunction in patients with coronary disease.* Arterioscler Thromb Vasc Biol, 2007. **27**(4): p. 943-8.
21.   Kowaltowski, A.J., et al., *Mitochondria and reactive oxygen species.* Free Radic Biol Med, 2009. **47**(4): p. 333-43.
22.   Zelko, I.N., T.J. Mariani, and R.J. Folz, *Superoxide dismutase multigene family: a comparison of the CuZn-SOD (SOD1), Mn-SOD (SOD2), and EC-SOD (SOD3) gene structures, evolution, and expression.* Free Radic Biol Med, 2002. **33**(3): p. 337-49.
23.   Crapo, J.D., et al., *Copper,zinc superoxide dismutase is primarily a cytosolic protein in human cells.* Proc Natl Acad Sci U S A, 1992. **89**(21): p. 10405-9.
24.   Tsang, C.K., et al., *Superoxide dismutase 1 acts as a nuclear transcription factor to regulate oxidative stress resistance.* Nature Communications, 2014. **5**: p. 3446.
25.   Keller, G.A., et al., *Cu,Zn superoxide dismutase is a peroxisomal enzyme in human fibroblasts and hepatoma cells.* Proc Natl Acad Sci U S A, 1991. **88**(16): p. 7381-5.

26. Barra, D., et al., *The primary structure of human liver manganese superoxide dismutase.* J Biol Chem, 1984. **259**(20): p. 12595-601.

27. Weisiger, R.A. and I. Fridovich, *Mitochondrial superoxide simutase. Site of synthesis and intramitochondrial localization.* J Biol Chem, 1973. **248**(13): p. 4793-6.

28. Karnati, S., et al., *Mammalian SOD2 is exclusively located in mitochondria and not present in peroxisomes.* Histochem Cell Biol, 2013. **140**(2): p. 105-17.

29. UniProt Consortium, T., *UniProt: the universal protein knowledgebase.* Nucleic Acids Research, 2018. **46**(5): p. 2699-2699.

30. Fukai, T. and M. Ushio-Fukai, *Superoxide dismutases: role in redox signaling, vascular function, and diseases.* Antioxid Redox Signal, 2011. **15**(6): p. 1583-606.

31. Folz, R.J. and J.D. Crapo, *Extracellular superoxide dismutase (SOD3): tissue-specific expression, genomic characterization, and computer-assisted sequence analysis of the human EC SOD gene.* Genomics, 1994. **22**(1): p. 162-71.

32. Gómez Alvarez, E., et al., *Unexpectedly high indoor hydroxyl radical concentrations associated with nitrous acid.* Proceedings of the National Academy of Sciences of the United States of America, 2013. **110**(33): p. 13294-13299.

33. Fenton, H.J.H., *LXXIII.—Oxidation of tartaric acid in presence of iron.* Journal of the Chemical Society, Transactions, 1894. **65**(0): p. 899-910.

34. Liochev, S.I. and I. Fridovich, *Superoxide and iron: partners in crime.* IUBMB Life, 1999. **48**(2): p. 157-61.

35. Haber, F., J. Weiss, and J. Pope William, *The catalytic decomposition of hydrogen peroxide by iron salts.* Proceedings of the Royal Society of London. Series A - Mathematical and Physical Sciences, 1934. **147**(861): p. 332-351.

36. Kreuz, S. and W. Fischle, *Oxidative stress signaling to chromatin in health and disease.* Epigenomics, 2016. **8**(6): p. 843-62.

37. Poosch, M.S. and R.K. Yamazaki, *Determination of peroxisomal fatty acyl-CoA oxidase activity using a lauroyl-CoA-based fluorometric assay.* Biochim Biophys Acta, 1986. **884**(3): p. 585-93.

38. Nordgren, M. and M. Fransen, *Peroxisomal metabolism and oxidative stress.* Biochimie, 2014. **98**: p. 56-62.

39. Malhotra, J.D. and R.J. Kaufman, *Endoplasmic reticulum stress and oxidative stress: a vicious cycle or a double-edged sword?* Antioxid Redox Signal, 2007. **9**(12): p. 2277-93.

40. Mates, J.M., C. Perez-Gomez, and I. Nunez de Castro, *Antioxidant enzymes and human diseases.* Clin Biochem, 1999. **32**(8): p. 595-603.

41. Rhee, S.G., et al., *Peroxiredoxin, a novel family of peroxidases.* IUBMB Life, 2001. **52**(1-2): p. 35-41.

42. Birben, E., et al., *Oxidative stress and antioxidant defense.* World Allergy Organ J, 2012. **5**(1): p. 9-19.

43. Bonekamp, N.A., et al., *Reactive oxygen species and peroxisomes: struggling for balance.* Biofactors, 2009. **35**(4): p. 346-55.

44. Lubos, E., J. Loscalzo, and D.E. Handy, *Glutathione peroxidase-1 in health and disease: from molecular mechanisms to therapeutic opportunities.* Antioxid Redox Signal, 2011. **15**(7): p. 1957-97.

45. Tuteja, N., et al., *Nitric Oxide as a Unique Bioactive Signaling Messenger in Physiology and Pathophysiology.* Journal of biomedicine & biotechnology, 2004. **2004**(4): p. 227-237.

46. Förstermann, U. and W.C. Sessa, *Nitric oxide synthases: regulation and function.* European heart journal, 2012. **33**(7): p. 829-837d.

47. Denninger, J.W. and M.A. Marletta, *Guanylate cyclase and the .NO/cGMP signaling pathway.* Biochim Biophys Acta, 1999. **1411**(2-3): p. 334-50.

48. Ignarro, L.J., et al., *Endothelium-derived relaxing factor produced and released from artery and vein is nitric oxide.* Proceedings of the National Academy of Sciences, 1987. **84**(24): p. 9265-9269.

49. Warner, T.D., et al., *Effects of cyclic GMP on smooth muscle relaxation.* Adv Pharmacol, 1994. **26**: p. 171-94.

50. Buechler, W.A., et al., *Soluble guanylyl cyclase and platelet function.* Ann N Y Acad Sci, 1994. **714**: p. 151-7.

51. Jaffrey, S.R. and S.H. Snyder, *Nitric oxide: a neural messenger.* Annu Rev Cell Dev Biol, 1995. **11**: p. 417-40.

52. Alderton, W.K., C.E. Cooper, and R.G. Knowles, *Nitric oxide synthases: structure, function and inhibition.* Biochem J, 2001. **357**(Pt 3): p. 593-615.

53. Andrew, P.J. and B. Mayer, *Enzymatic function of nitric oxide synthases.* Cardiovasc Res, 1999. **43**(3): p. 521-31.

54.   Luiking, Y.C., M.P. Engelen, and N.E. Deutz, *Regulation of nitric oxide production in health and disease.* Curr Opin Clin Nutr Metab Care, 2010. **13**(1): p. 97-104.

55.   Mas, M., *A Close Look at the Endothelium: Its Role in the Regulation of Vasomotor Tone.* European Urology Supplements, 2009. **8**(2): p. 48-57.

56.   Dudzinski, D.M., et al., *The regulation and pharmacology of endothelial nitric oxide synthase.* Annu Rev Pharmacol Toxicol, 2006. **46**: p. 235-76.

57.   Kleinert, H., et al., *Regulation of the expression of inducible nitric oxide synthase.* Eur J Pharmacol, 2004. **500**(1-3): p. 255-66.

58.   Kleinert, H., P.M. Schwarz, and U. Forstermann, *Regulation of the expression of inducible nitric oxide synthase.* Biol Chem, 2003. **384**(10-11): p. 1343-64.

59.   Landmesser, U., et al., *Oxidation of tetrahydrobiopterin leads to uncoupling of endothelial cell nitric oxide synthase in hypertension.* J Clin Invest, 2003. **111**(8): p. 1201-9.

60.   Luo, S., et al., *Molecular mechanisms of endothelial NO synthase uncoupling.* Curr Pharm Des, 2014. **20**(22): p. 3548-53.

61.   Alp, N.J. and K.M. Channon, *Regulation of endothelial nitric oxide synthase by tetrahydrobiopterin in vascular disease.* Arterioscler Thromb Vasc Biol, 2004. **24**(3): p. 413-20.

62.   Xia, Y., et al., *Nitric oxide synthase generates superoxide and nitric oxide in arginine-depleted cells leading to peroxynitrite-mediated cellular injury.* Proc Natl Acad Sci U S A, 1996. **93**(13): p. 6770-4.

63.   Zweier, J.L., et al., *Enzyme-independent formation of nitric oxide in biological tissues.* Nat Med, 1995. **1**(8): p. 804-9.

64.   Li, H., et al., *Nitric oxide production from nitrite occurs primarily in tissues not in the blood: critical role of xanthine oxidase and aldehyde oxidase.* J Biol Chem, 2008. **283**(26): p. 17855-63.

65.   Raubach, K.H., et al., *Double-blind randomized multicenter study on the efficacy of trapidil versus isosorbide dinitrate in stable angina pectoris.* Clin Cardiol, 1997. **20**(5): p. 483-8.

66.   Miller, M.R. and R.M. Wadsworth, *Understanding organic nitrates--a vein hope?* British journal of pharmacology, 2009. **157**(4): p. 565-567.

67.   Münzel, T., S. Steven, and A. Daiber, *Organic nitrates: Update on mechanisms underlying vasodilation, tolerance and endothelial dysfunction.* Vascular Pharmacology, 2014. **63**(3): p. 105-113.

68.   Miller, M.R. and I.L. Megson, *Recent developments in nitric oxide donor drugs.* Br J Pharmacol, 2007. **151**(3): p. 305-21.

69.   Katsumi, H., M. Nishikawa, and M. Hashida, *Development of nitric oxide donors for the treatment of cardiovascular diseases.* Cardiovasc Hematol Agents Med Chem, 2007. **5**(3): p. 204-8.

70.   Beckman, J.S. and W.H. Koppenol, *Nitric oxide, superoxide, and peroxynitrite: the good, the bad, and ugly.* Am J Physiol, 1996. **271**(5 Pt 1): p. C1424-37.

71.   Radi, R., et al., *Peroxynitrite-induced membrane lipid peroxidation: the cytotoxic potential of superoxide and nitric oxide.* Arch Biochem Biophys, 1991. **288**(2): p. 481-7.

72.   Ischiropoulos, H. and A.B. al-Mehdi, *Peroxynitrite-mediated oxidative protein modifications.* FEBS Lett, 1995. **364**(3): p. 279-82.

73.   Douki, T. and J. Cadet, *Peroxynitrite mediated oxidation of purine bases of nucleosides and isolated DNA.* Free Radic Res, 1996. **24**(5): p. 369-80.

74.   Pall, M.L., *Nitric oxide synthase partial uncoupling as a key switching mechanism for the NO/ONOO- cycle.* Med Hypotheses, 2007. **69**(4): p. 821-5.

75.   Munzel, T., et al., *Pathophysiological role of oxidative stress in systolic and diastolic heart failure and its therapeutic implications.* Eur Heart J, 2015. **36**(38): p. 2555-64.

76.   Lu, J. and A. Holmgren, *The thioredoxin antioxidant system.* Free Radic Biol Med, 2014. **66**: p. 75-87.

77.   Gromer, S., S. Urig, and K. Becker, *The thioredoxin system--from science to clinic.* Med Res Rev, 2004. **24**(1): p. 40-89.

78.   Holmgren, A., *Antioxidant function of thioredoxin and glutaredoxin systems.* Antioxid Redox Signal, 2000. **2**(4): p. 811-20.

79.   Espinosa-Diez, C., et al., *Antioxidant responses and cellular adjustments to oxidative stress.* Redox Biol, 2015. **6**: p. 183-97.

80.   Gozzelino, R., V. Jeney, and M.P. Soares, *Mechanisms of Cell Protection by Heme Oxygenase-1.* Annual Review of Pharmacology and Toxicology, 2010. **50**(1): p. 323-354.

81. Waza, A.A., et al., *A review on heme oxygenase-1 induction: is it a necessary evil.* Inflamm Res, 2018. **67**(7): p. 579-588.

82. Ferreira, A., et al., *A central role for free heme in the pathogenesis of severe malaria: the missing link?* J Mol Med (Berl), 2008. **86**(10): p. 1097-111.

83. Hsu, F.F., et al., *Signal peptide peptidase-mediated nuclear localization of heme oxygenase-1 promotes cancer cell proliferation and invasion independent of its enzymatic activity.* Oncogene, 2015. **34**(18): p. 2410-1.

84. Lin, Q., et al., *Heme oxygenase-1 protein localizes to the nucleus and activates transcription factors important in oxidative stress.* J Biol Chem, 2007. **282**(28): p. 20621-33.

85. Biswas, C., et al., *Nuclear heme oxygenase-1 (HO-1) modulates subcellular distribution and activation of Nrf2, impacting metabolic and anti-oxidant defenses.* The Journal of biological chemistry, 2014. **289**(39): p. 26882-26894.

86. Nimse, S.B. and D. Pal, *Free radicals, natural antioxidants, and their reaction mechanisms.* RSC Advances, 2015. **5**(35): p. 27986-28006.

87. Lu, J.M., et al., *Chemical and molecular mechanisms of antioxidants: experimental approaches and model systems.* J Cell Mol Med, 2010. **14**(4): p. 840-60.

88. Santos, C.X., E.I. Anjos, and O. Augusto, *Uric acid oxidation by peroxynitrite: multiple reactions, free radical formation, and amplification of lipid oxidation.* Arch Biochem Biophys, 1999. **372**(2): p. 285-94.

89. Squadrito, G.L., et al., *Reaction of uric acid with peroxynitrite and implications for the mechanism of neuroprotection by uric acid.* Arch Biochem Biophys, 2000. **376**(2): p. 333-7.

90. Augustyniak, A., et al., *Natural and synthetic antioxidants: an updated overview.* Free Radic Res, 2010. **44**(10): p. 1216-62.

91. Santos, A.L. and A.B. Lindner, *Protein Posttranslational Modifications: Roles in Aging and Age-Related Disease.* Oxidative medicine and cellular longevity, 2017. **2017**: p. 5716409-5716409.

92. Stadtman, E.R. and R.L. Levine, *Free radical-mediated oxidation of free amino acids and amino acid residues in proteins.* Amino Acids, 2003. **25**(3-4): p. 207-18.

93. Ryan, B.J., A. Nissim, and P.G. Winyard, *Oxidative post-translational modifications and their involvement in the pathogenesis of autoimmune diseases.* Redox Biol, 2014. **2**: p. 715-24.

94. Bierhaus, A., et al., *AGEs and their interaction with AGE-receptors in vascular disease and diabetes mellitus. I. The AGE concept.* Cardiovasc Res, 1998. **37**(3): p. 586-600.

95. Simat, T.J. and H. Steinhart, *Oxidation of Free Tryptophan and Tryptophan Residues in Peptides and Proteins.* J Agric Food Chem, 1998. **46**(2): p. 490-498.

96. Heinecke, J.W., et al., *Tyrosyl radical generated by myeloperoxidase catalyzes the oxidative cross-linking of proteins.* J Clin Invest, 1993. **91**(6): p. 2866-72.

97. Alvarez, B., et al., *Peroxynitrite-dependent tryptophan nitration.* Chem Res Toxicol, 1996. **9**(2): p. 390-6.

98. Nuriel, T., A. Hansler, and S.S. Gross, *Protein nitrotryptophan: Formation, significance and identification.* Journal of Proteomics, 2011. **74**(11): p. 2300-2312.

99. Stadtman, E.R., J. Moskovitz, and R.L. Levine, *Oxidation of methionine residues of proteins: biological consequences.* Antioxid Redox Signal, 2003. **5**(5): p. 577-82.

100. Nagy, P. and C.C. Winterbourn, *Chapter 6 - Redox Chemistry of Biological Thiols*, in *Advances in Molecular Toxicology*, J.C. Fishbein, Editor. 2010, Elsevier. p. 183-222.

101. Cadenas, E. and L. Packer, *Thiol Redox Transitions in Cell Signaling*. 2010: Elsevier Science.

102. Jacob, C., et al., *Control of oxidative posttranslational cysteine modifications: from intricate chemistry to widespread biological and medical applications.* Chem Res Toxicol, 2012. **25**(3): p. 588-604.

103. Daiber, A., et al., *Chemical model systems for cellular nitros(yl)ation reactions.* Free Radic Biol Med, 2009. **47**(4): p. 458-67.

104. Stamler, J.S., et al., *S-nitrosylation of proteins with nitric oxide: synthesis and characterization of biologically active compounds.* Proc Natl Acad Sci U S A, 1992. **89**(1): p. 444-8.

105. Bechtold, E. and S.B. King, *Chemical methods for the direct detection and labeling of S-nitrosothiols.* Antioxid Redox Signal, 2012. **17**(7): p. 981-91.

106. Wang, Y., et al., *S-nitrosylation: an emerging redox-based post-translational modification in plants.* J Exp Bot, 2006. **57**(8): p. 1777-84.

107. Foster, M.W., D.T. Hess, and J.S. Stamler, *Protein S-nitrosylation in health and disease: a current perspective.* Trends Mol Med, 2009. **15**(9): p. 391-404.

108. Hess, D.T., et al., *Protein S-nitrosylation: purview and parameters.* Nat Rev Mol Cell Biol, 2005. **6**(2): p. 150-66.

109. Finkelstein, E., G.M. Rosen, and E.J. Rauckman, *Spin trapping of superoxide and hydroxyl radical: practical aspects.* Arch Biochem Biophys, 1980. **200**(1): p. 1-16.

110. Dikalov, S.I. and D.G. Harrison, *Methods for detection of mitochondrial and cellular reactive oxygen species.* Antioxidants & redox signaling, 2014. **20**(2): p. 372-382.

111. Griendling, K.K., et al., *Measurement of Reactive Oxygen Species, Reactive Nitrogen Species, and Redox-Dependent Signaling in the Cardiovascular System: A Scientific Statement From the American Heart Association.* Circulation research, 2016. **119**(5): p. e39-e75.

112. Mason, R.P., *Using anti-5,5-dimethyl-1-pyrroline N-oxide (anti-DMPO) to detect protein radicals in time and space with immuno-spin trapping.* Free Radic Biol Med, 2004. **36**(10): p. 1214-23.

113. Daiber, A., et al., *Measurement of NAD(P)H oxidase-derived superoxide with the luminol analogue L-012.* Free Radic Biol Med, 2004. **36**(1): p. 101-11.

114. Zielonka, J., J. Vasquez-Vivar, and B. Kalyanaraman, *Detection of 2-hydroxyethidium in cellular systems: a unique marker product of superoxide and hydroethidine.* Nat Protoc, 2008. **3**(1): p. 8-21.

115. Robinson, K.M., M.S. Janes, and J.S. Beckman, *The selective detection of mitochondrial superoxide by live cell imaging.* Nat Protoc, 2008. **3**(6): p. 941-7.

116. Zhou, M., et al., *A stable nonfluorescent derivative of resorufin for the fluorometric determination of trace hydrogen peroxide: applications in detecting the activity of phagocyte NADPH oxidase and other oxidases.* Anal Biochem, 1997. **253**(2): p. 162-8.

117. Zhao, B., F.A. Summers, and R.P. Mason, *Photooxidation of Amplex Red to resorufin: implications of exposing the Amplex Red assay to light.* Free radical biology & medicine, 2012. **53**(5): p. 1080-1087.

118. Wojtala, A., et al., *Chapter Thirteen - Methods to Monitor ROS Production by Fluorescence Microscopy and Fluorometry*, in *Methods in Enzymology*, L. Galluzzi and G. Kroemer, Editors. 2014, Academic Press. p. 243-262.

119. Belousov, V.V., et al., *Genetically encoded fluorescent indicator for intracellular hydrogen peroxide.* Nature Methods, 2006. **3**: p. 281.

120. Weller, J., et al., *Response properties of the genetically encoded optical H2O2 sensor HyPer.* Free Radic Biol Med, 2014. **76**: p. 227-41.

121. Yan, L.J. and M.J. Forster, *Chemical probes for analysis of carbonylated proteins: a review.* J Chromatogr B Analyt Technol Biomed Life Sci, 2011. **879**(17-18): p. 1308-15.

122. Halliwell, B. and M. Whiteman, *Measuring reactive species and oxidative damage in vivo and in cell culture: how should you do it and what do the results mean?* Br J Pharmacol, 2004. **142**(2): p. 231-55.

123. Baird, A.-M., K. O'Byrne, and S. Gray, *Reactive Oxygen Species and Reactive Nitrogen Species in Epigenetic Modifications*, in *Systems Biology of Free Radicals and Antioxidants*, I. Laher, Editor. 2014, Springer Berlin Heidelberg. p. 437-455.

124. Niu, Y., et al., *Oxidative stress alters global histone modification and DNA methylation.* Free Radic Biol Med, 2015. **82**: p. 22-8.

125. Kietzmann, T., et al., *The epigenetic landscape related to reactive oxygen species formation in the cardiovascular system.* Br J Pharmacol, 2017. **174**(12): p. 1533-1554.

126. Lin, Y., et al., *Involvement of MicroRNAs in hydrogen peroxide-mediated gene regulation and cellular injury response in vascular smooth muscle cells.* J Biol Chem, 2009. **284**(12): p. 7903-13.

127. Jajoo, S., et al., *Essential role of NADPH oxidase-dependent reactive oxygen species generation in regulating microRNA-21 expression and function in prostate cancer.* Antioxid Redox Signal, 2013. **19**(16): p. 1863-76.

128. Cyr, A.R. and F.E. Domann, *The redox basis of epigenetic modifications: from mechanisms to functional consequences.* Antioxid Redox Signal, 2011. **15**(2): p. 551-89.

129. Dupont, C., D.R. Armant, and C.A. Brenner, *Epigenetics: definition, mechanisms and clinical perspective.* Seminars in reproductive medicine, 2009. **27**(5): p. 351-357.

130. Feinberg, A.P., *Phenotypic plasticity and the epigenetics of human disease.* Nature, 2007. **447**(7143): p. 433-40.

131.   Jabbari, K. and G. Bernardi, *Cytosine methylation and CpG, TpG (CpA) and TpA frequencies.* Gene, 2004. **333**: p. 143-149.
132.   Jones, P.A. and D. Takai, *The role of DNA methylation in mammalian epigenetics.* Science, 2001. **293**(5532): p. 1068-70.
133.   Miranda, T.B. and P.A. Jones, *DNA methylation: the nuts and bolts of repression.* J Cell Physiol, 2007. **213**(2): p. 384-90.
134.   Kim, G.H., J.J. Ryan, and S.L. Archer, *The role of redox signaling in epigenetics and cardiovascular disease.* Antioxid Redox Signal, 2013. **18**(15): p. 1920-36.
135.   Ahmed, H., *Promoter Methylation in Prostate Cancer and its Application for the Early Detection of Prostate Cancer Using Serum and Urine Samples.* Biomark Cancer, 2010. **2010**(2): p. 17-33.
136.   Svedruzic, Z.M., *Dnmt1 structure and function.* Prog Mol Biol Transl Sci, 2011. **101**: p. 221-54.
137.   Okano, M., et al., *DNA methyltransferases Dnmt3a and Dnmt3b are essential for de novo methylation and mammalian development.* Cell, 1999. **99**(3): p. 247-57.
138.   Ito, S., et al., *Tet proteins can convert 5-methylcytosine to 5-formylcytosine and 5-carboxylcytosine.* Science (New York, N.Y.), 2011. **333**(6047): p. 1300-1303.
139.   Branco, M.R., G. Ficz, and W. Reik, *Uncovering the role of 5-hydroxymethylcytosine in the epigenome.* Nat Rev Genet, 2011. **13**(1): p. 7-13.
140.   Rasmussen, K.D. and K. Helin, *Role of TET enzymes in DNA methylation, development, and cancer.* Genes Dev, 2016. **30**(7): p. 733-50.
141.   Turk, P.W., et al., *DNA adduct 8-hydroxyl-2'-deoxyguanosine (8-hydroxyguanine) affects function of human DNA methyltransferase.* Carcinogenesis, 1995. **16**(5): p. 1253-5.
142.   Luger, K., et al., *Crystal structure of the nucleosome core particle at 2.8 A resolution.* Nature, 1997. **389**(6648): p. 251-60.
143.   Kornberg, R.D., *Chromatin structure: a repeating unit of histones and DNA.* Science, 1974. **184**(4139): p. 868-71.
144.   Szerlong, H.J. and J.C. Hansen, *Nucleosome distribution and linker DNA: connecting nuclear function to dynamic chromatin structure.* Biochemistry and cell biology = Biochimie et biologie cellulaire, 2011. **89**(1): p. 24-34.
145.   Alberts, B., et al., *Molecular Biology of the Cell 4th Edition: International Student Edition*. 2002: Routledge.
146.   Kouzarides, T., *Chromatin modifications and their function.* Cell, 2007. **128**(4): p. 693-705.
147.   Peterson, C.L. and M.A. Laniel, *Histones and histone modifications.* Curr Biol, 2004. **14**(14): p. R546-51.
148.   Strahl, B.D. and C.D. Allis, *The language of covalent histone modifications.* Nature, 2000. **403**(6765): p. 41-5.
149.   Jenuwein, T. and C.D. Allis, *Translating the histone code.* Science, 2001. **293**(5532): p. 1074-80.
150.   Haberland, M., R.L. Montgomery, and E.N. Olson, *The many roles of histone deacetylases in development and physiology: implications for disease and therapy.* Nat Rev Genet, 2009. **10**(1): p. 32-42.
151.   Kimura, H., *Histone modifications for human epigenome analysis.* J Hum Genet, 2013. **58**(7): p. 439-45.
152.   Handy, D.E., R. Castro, and J. Loscalzo, *Epigenetic modifications: basic mechanisms and role in cardiovascular disease.* Circulation, 2011. **123**(19): p. 2145-56.
153.   Eslaminejad, M.B., N. Fani, and M. Shahhoseini, *Epigenetic regulation of osteogenic and chondrogenic differentiation of mesenchymal stem cells in culture.* Cell J, 2013. **15**(1): p. 1-10.
154.   Pruitt, K., *Chapter One - Molecular and Cellular Changes During Cancer Progression Resulting From Genetic and Epigenetic Alterations*, in *Progress in Molecular Biology and Translational Science*, K. Pruitt, Editor. 2016, Academic Press. p. 3-47.
155.   Bannister, A.J. and T. Kouzarides, *Regulation of chromatin by histone modifications.* Cell Res, 2011. **21**(3): p. 381-95.
156.   Galdieri, L., et al., *Protein acetylation and acetyl coenzyme a metabolism in budding yeast.* Eukaryotic cell, 2014. **13**(12): p. 1472-1483.
157.   Rye, P.T., et al., *Advances in label-free screening approaches for studying histone acetyltransferases.* J Biomol Screen, 2011. **16**(10): p. 1186-95.
158.   Seto, E. and M. Yoshida, *Erasers of histone acetylation: the histone deacetylase enzymes.* Cold Spring Harb Perspect Biol, 2014. **6**(4): p. a018713.

159. Chen, H.P., Y.T. Zhao, and T.C. Zhao, *Histone deacetylases and mechanisms of regulation of gene expression.* Crit Rev Oncog, 2015. **20**(1-2): p. 35-47.

160. Li, Y., et al., *A mini-review on Sirtuin activity assays.* Biochemical and Biophysical Research Communications, 2015. **467**(3): p. 459-466.

161. Shore, D., M. Squire, and K.A. Nasmyth, *Characterization of two genes required for the position-effect control of yeast mating-type genes.* EMBO J, 1984. **3**(12): p. 2817-23.

162. Houtkooper, R.H., E. Pirinen, and J. Auwerx, *Sirtuins as regulators of metabolism and healthspan.* Nat Rev Mol Cell Biol, 2012. **13**(4): p. 225-238.

163. Barneda-Zahonero, B. and M. Parra, *Histone deacetylases and cancer.* Molecular oncology, 2012. **6**(6): p. 579-589.

164. Bosch-Presegue, L. and A. Vaquero, *The dual role of sirtuins in cancer.* Genes Cancer, 2011. **2**(6): p. 648-62.

165. Chang, H.C. and L. Guarente, *SIRT1 and other sirtuins in metabolism.* Trends Endocrinol Metab, 2014. **25**(3): p. 138-45.

166. Choi, J.E. and R. Mostoslavsky, *Sirtuins, metabolism, and DNA repair.* Curr Opin Genet Dev, 2014. **26**: p. 24-32.

167. Oberdoerffer, P., et al., *SIRT1 redistribution on chromatin promotes genomic stability but alters gene expression during aging.* Cell, 2008. **135**(5): p. 907-18.

168. Boutant, M. and C. Canto, *SIRT1 metabolic actions: Integrating recent advances from mouse models.* Mol Metab, 2014. **3**(1): p. 5-18.

169. Bao, J. and M.N. Sack, *Protein deacetylation by sirtuins: delineating a post-translational regulatory program responsive to nutrient and redox stressors.* Cellular and Molecular Life Sciences, 2010. **67**(18): p. 3073-3087.

170. Segre, C.V. and S. Chiocca, *Regulating the regulators: the post-translational code of class I HDAC1 and HDAC2.* J Biomed Biotechnol, 2011. **2011**: p. 690848.

171. Yang, X.J. and E. Seto, *The Rpd3/Hda1 family of lysine deacetylases: from bacteria and yeast to mice and men.* Nat Rev Mol Cell Biol, 2008. **9**(3): p. 206-18.

172. RUIJTER, A.J.M.d., et al., *Histone deacetylases (HDACs): characterization of the classical HDAC family.* Biochemical Journal, 2003. **370**(3): p. 737-749.

173. Reichert, N., M.A. Choukrallah, and P. Matthias, *Multiple roles of class I HDACs in proliferation, differentiation, and development.* Cell Mol Life Sci, 2012. **69**(13): p. 2173-87.

174. Trivedi, C.M., et al., *Hdac2 regulates the cardiac hypertrophic response by modulating Gsk3 beta activity.* Nat Med, 2007. **13**(3): p. 324-31.

175. Xie, M. and J.A. Hill, *HDAC-dependent ventricular remodeling.* Trends Cardiovasc Med, 2013. **23**(6): p. 229-35.

176. Brunmeir, R., S. Lagger, and C. Seiser, *Histone deacetylase HDAC1/HDAC2-controlled embryonic development and cell differentiation.* Int J Dev Biol, 2009. **53**(2-3): p. 275-89.

177. Guan, J.S., et al., *HDAC2 negatively regulates memory formation and synaptic plasticity.* Nature, 2009. **459**(7243): p. 55-60.

178. Zeng, W., A.R. Ball, Jr., and K. Yokomori, *HP1: heterochromatin binding proteins working the genome.* Epigenetics, 2010. **5**(4): p. 287-292.

179. Vermeulen, M., et al., *Selective anchoring of TFIID to nucleosomes by trimethylation of histone H3 lysine 4.* Cell, 2007. **131**(1): p. 58-69.

180. Greer, E.L. and Y. Shi, *Histone methylation: a dynamic mark in health, disease and inheritance.* Nature reviews. Genetics, 2012. **13**(5): p. 343-357.

181. Heintzman, N.D., et al., *Distinct and predictive chromatin signatures of transcriptional promoters and enhancers in the human genome.* Nat Genet, 2007. **39**(3): p. 311-8.

182. Di Lorenzo, A. and M.T. Bedford, *Histone arginine methylation.* FEBS Lett, 2011. **585**(13): p. 2024-31.

183. Hancock, R.L., et al., *Epigenetic regulation by histone demethylases in hypoxia.* Epigenomics, 2015. **7**(5): p. 791-811.

184. Walport, L.J., et al., *Arginine demethylation is catalysed by a subset of JmjC histone lysine demethylases.* Nature Communications, 2016. **7**: p. 11974.

185. Feng, Q., et al., *Methylation of H3-lysine 79 is mediated by a new family of HMTases without a SET domain.* Curr Biol, 2002. **12**(12): p. 1052-8.

186. Huang, J. and S.L. Berger, *The emerging field of dynamic lysine methylation of non-histone proteins.* Curr Opin Genet Dev, 2008. **18**(2): p. 152-8.

187. Dillon, S.C., et al., *The SET-domain protein superfamily: protein lysine methyltransferases.* Genome Biol, 2005. **6**(8): p. 227.

188. Morera, L., M. Lübbert, and M. Jung, *Targeting histone methyltransferases and demethylases in clinical trials for cancer therapy.* Clinical epigenetics, 2016. **8**: p. 57-57.

189. Keating, S.T. and A. El-Osta, *Transcriptional regulation by the Set7 lysine methyltransferase.* Epigenetics, 2013. **8**(4): p. 361-72.

190. Martens, J.H., et al., *Cascade of distinct histone modifications during collagenase gene activation.* Mol Cell Biol, 2003. **23**(5): p. 1808-16.

191. Francis, J., et al., *Pdx-1 links histone H3-Lys-4 methylation to RNA polymerase II elongation during activation of insulin transcription.* J Biol Chem, 2005. **280**(43): p. 36244-53.

192. Kwon, T., et al., *Mechanism of histone lysine methyl transfer revealed by the structure of SET7/9-AdoMet.* EMBO J, 2003. **22**(2): p. 292-303.

193. Dhayalan, A., et al., *Specificity analysis-based identification of new methylation targets of the SET7/9 protein lysine methyltransferase.* Chem Biol, 2011. **18**(1): p. 111-20.

194. He, S., et al., *Lysine Methyltransferase SETD7 (SET7/9) Regulates ROS Signaling through mitochondria and NFE2L2/ARE pathway.* Sci Rep, 2015. **5**: p. 14368.

195. Tao, Y., et al., *The histone methyltransferase Set7/9 promotes myoblast differentiation and myofibril assembly.* J Cell Biol, 2011. **194**(4): p. 551-65.

196. Spellmon, N., et al., *Structure and function of SET and MYND domain-containing proteins.* Int J Mol Sci, 2015. **16**(1): p. 1406-28.

197. Leinhart, K. and M. Brown, *SET/MYND Lysine Methyltransferases Regulate Gene Transcription and Protein Activity.* Genes (Basel), 2011. **2**(1): p. 210-8.

198. Gottlieb, P.D., et al., *Bop encodes a muscle-restricted protein containing MYND and SET domains and is essential for cardiac differentiation and morphogenesis.* Nat Genet, 2002. **31**(1): p. 25-32.

199. Tan, X., et al., *SmyD1, a histone methyltransferase, is required for myofibril organization and muscle contraction in zebrafish embryos.* Proc Natl Acad Sci U S A, 2006. **103**(8): p. 2713-8.

200. Rasmussen, T.L., et al., *Smyd1 facilitates heart development by antagonizing oxidative and ER stress responses.* PLoS One, 2015. **10**(3): p. e0121765.

201. Park, C.Y., et al., *skNAC, a Smyd1-interacting transcription factor, is involved in cardiac development and skeletal muscle growth and regeneration.* Proc Natl Acad Sci U S A, 2010. **107**(48): p. 20750-5.

202. Tracy, C., et al., *The Smyd Family of Methyltransferases: Role in Cardiac and Skeletal Muscle Physiology and Pathology.* Curr Opin Physiol, 2018. **1**: p. 140-152.

203. Bannister, A.J., R. Schneider, and T. Kouzarides, *Histone methylation: dynamic or static?* Cell, 2002. **109**(7): p. 801-6.

204. Shi, Y., et al., *Histone demethylation mediated by the nuclear amine oxidase homolog LSD1.* Cell, 2004. **119**(7): p. 941-53.

205. Tsukada, Y., et al., *Histone demethylation by a family of JmjC domain-containing proteins.* Nature, 2006. **439**(7078): p. 811-6.

206. Pedersen, M.T. and K. Helin, *Histone demethylases in development and disease.* Trends Cell Biol, 2010. **20**(11): p. 662-71.

207. Rotili, D. and A. Mai, *Targeting Histone Demethylases: A New Avenue for the Fight against Cancer.* Genes Cancer, 2011. **2**(6): p. 663-79.

208. Metzger, E., et al., *LSD1 demethylates repressive histone marks to promote androgen-receptor-dependent transcription.* Nature, 2005. **437**(7057): p. 436-9.

209. Perillo, B., et al., *DNA oxidation as triggered by H3K9me2 demethylation drives estrogen-induced gene expression.* Science, 2008. **319**(5860): p. 202-6.

210. Li, J., A. Braganza, and R.W. Sobol, *Base excision repair facilitates a functional relationship between Guanine oxidation and histone demethylation.* Antioxid Redox Signal, 2013. **18**(18): p. 2429-43.

211. Mikhed, Y., et al., *Redox regulation of genome stability by effects on gene expression, epigenetic pathways and DNA damage/repair.* Redox Biol, 2015. **5**: p. 275-89.

212. Luka, Z., et al., *Histone demethylase LSD1 is a folate-binding protein.* Biochemistry, 2011. **50**(21): p. 4750-6.

213. Luka, Z., et al., *Crystal structure of the histone lysine specific demethylase LSD1 complexed with tetrahydrofolate.* Protein Sci, 2014. **23**(7): p. 993-8.

214. Garcia, B.A., et al., *Folate deficiency affects histone methylation.* Medical hypotheses, 2016. **88**: p. 63-67.

215. Maiques-Diaz, A. and T.C. Somervaille, *LSD1: biologic roles and therapeutic targeting.* Epigenomics, 2016. **8**(8): p. 1103-16.

216. Hino, S., et al., *FAD-dependent lysine-specific demethylase-1 regulates cellular energy expenditure.* Nat Commun, 2012. **3**: p. 758.

217. Hickok, J.R., et al., *Nitric oxide modifies global histone methylation by inhibiting Jumonji C domain-containing demethylases.* J Biol Chem, 2013. **288**(22): p. 16004-15.

218. Tian, X. and J. Fang, *Current perspectives on histone demethylases.* Acta Biochim Biophys Sin (Shanghai), 2007. **39**(2): p. 81-8.

219. Okada, Y., K. Tateishi, and Y. Zhang, *Histone demethylase JHDM2A is involved in male infertility and obesity.* J Androl, 2010. **31**(1): p. 75-8.

220. Tateishi, K., et al., *Role of Jhdm2a in regulating metabolic gene expression and obesity resistance.* Nature, 2009. **458**(7239): p. 757-61.

221. Inagaki, T., et al., *Obesity and metabolic syndrome in histone demethylase JHDM2a-deficient mice.* Genes Cells, 2009. **14**(8): p. 991-1001.

222. Saha, A., J. Wittmeyer, and B.R. Cairns, *Chromatin remodelling: the industrial revolution of DNA around histones.* Nat Rev Mol Cell Biol, 2006. **7**(6): p. 437-47.

223. Wang, G.G., C.D. Allis, and P. Chi, *Chromatin remodeling and cancer, Part II: ATP-dependent chromatin remodeling.* Trends Mol Med, 2007. **13**(9): p. 373-80.

224. Bao, Y. and X. Shen, *SnapShot: Chromatin remodeling: INO80 and SWR1.* Cell, 2011. **144**(1): p. 158-158.e2.

225. Chen, W., et al., *Chapter Nine - Chromatin Remodeling and Plant Immunity*, in *Advances in Protein Chemistry and Structural Biology*, R. Donev, Editor. 2017, Academic Press. p. 243-260.

226. Djebali, S., et al., *Landscape of transcription in human cells.* Nature, 2012. **489**(7414): p. 101-8.

227. van der Harst, P., L.J. de Windt, and J.C. Chambers, *Translational Perspective on Epigenetics in Cardiovascular Disease.* Journal of the American College of Cardiology, 2017. **70**(5): p. 590-606.

228. Peschansky, V.J. and C. Wahlestedt, *Non-coding RNAs as direct and indirect modulators of epigenetic regulation.* Epigenetics, 2014. **9**(1): p. 3-12.

229. Santosh, B., A. Varshney, and P.K. Yadava, *Non-coding RNAs: biological functions and applications.* Cell Biochemistry and Function, 2015. **33**(1): p. 14-22.

230. Mercer, T.R. and J.S. Mattick, *Structure and function of long noncoding RNAs in epigenetic regulation.* Nat Struct Mol Biol, 2013. **20**(3): p. 300-7.

231. Rinn, J.L., et al., *Functional demarcation of active and silent chromatin domains in human HOX loci by noncoding RNAs.* Cell, 2007. **129**(7): p. 1311-23.

232. Krol, J., I. Loedige, and W. Filipowicz, *The widespread regulation of microRNA biogenesis, function and decay.* Nat Rev Genet, 2010. **11**(9): p. 597-610.

233. Yamakuchi, M., M. Ferlito, and C.J. Lowenstein, *miR-34a repression of SIRT1 regulates apoptosis.* Proc Natl Acad Sci U S A, 2008. **105**(36): p. 13421-6.

234. Dana, H., et al., *Molecular Mechanisms and Biological Functions of siRNA.* International journal of biomedical science : IJBS, 2017. **13**(2): p. 48-57.

235. Lam, J.K.W., et al., *siRNA Versus miRNA as Therapeutics for Gene Silencing.* Molecular Therapy - Nucleic Acids, 2015. **4**: p. e252.

236. Kaikkonen, M.U., M.T. Lam, and C.K. Glass, *Non-coding RNAs as regulators of gene expression and epigenetics.* Cardiovasc Res, 2011. **90**(3): p. 430-40.

237. Madugundu, G.S., J. Cadet, and J.R. Wagner, *Hydroxyl-radical-induced oxidation of 5-methylcytosine in isolated and cellular DNA.* Nucleic acids research, 2014. **42**(11): p. 7450-7460.

238. Hitchler, M.J. and F.E. Domann, *Redox regulation of the epigenetic landscape in cancer: a role for metabolic reprogramming in remodeling the epigenome.* Free Radic Biol Med, 2012. **53**(11): p. 2178-87.

239. Rajendrasozhan, S., H. Yao, and I. Rahman, *Current perspectives on role of chromatin modifications and deacetylases in lung inflammation in COPD.* COPD, 2009. **6**(4): p. 291-7.

240. Santos, L., C. Escande, and A. Denicola, *Potential Modulation of Sirtuins by Oxidative Stress.* Oxid Med Cell Longev, 2016. **2016**: p. 9831825.

241. Afanas'ev, I., *New nucleophilic mechanisms of ros-dependent epigenetic modifications: comparison of aging and cancer.* Aging Dis, 2014. **5**(1): p. 52-62.

242. Osoata, G.O., et al., *Nitration of distinct tyrosine residues causes inactivation of histone deacetylase 2.* Biochem Biophys Res Commun, 2009. **384**(3): p. 366-71.

243. Doyle, K. and F.A. Fitzpatrick, *Redox signaling, alkylation (carbonylation) of conserved cysteines inactivates class I histone deacetylases 1, 2, and 3 and antagonizes their transcriptional repressor function.* J Biol Chem, 2010. **285**(23): p. 17417-24.

244. Nott, A., et al., *S-Nitrosylation of histone deacetylase 2 induces chromatin remodelling in neurons.* Nature, 2008. **455**(7211): p. 411-5.

245. Ago, T., et al., *A redox-dependent pathway for regulating class II HDACs and cardiac hypertrophy.* Cell, 2008. **133**(6): p. 978-93.

246. Hwang, J.W., et al., *Redox regulation of SIRT1 in inflammation and cellular senescence.* Free Radic Biol Med, 2013. **61**: p. 95-110.

247. Braidy, N., et al., *Age related changes in NAD+ metabolism oxidative stress and Sirt1 activity in wistar rats.* PLoS One, 2011. **6**(4): p. e19194.

248. Salminen, A., K. Kaarniranta, and A. Kauppinen, *Crosstalk between Oxidative Stress and SIRT1: Impact on the Aging Process.* Int J Mol Sci, 2013. **14**(2): p. 3834-59.

249. Matsushima, S. and J. Sadoshima, *The role of sirtuins in cardiac disease.* Am J Physiol Heart Circ Physiol, 2015. **309**(9): p. H1375-89.

250. Rajendran, R., et al., *Sirtuins: molecular traffic lights in the crossroad of oxidative stress, chromatin remodeling, and transcription.* J Biomed Biotechnol, 2011. **2011**: p. 368276.

251. Salminen, A., K. Kaarniranta, and A. Kauppinen, *Hypoxia-Inducible Histone Lysine Demethylases: Impact on the Aging Process and Age-Related Diseases.* Aging Dis, 2016. **7**(2): p. 180-200.

252. Han, P., et al., *Chromatin remodeling in cardiovascular development and physiology.* Circ Res, 2011. **108**(3): p. 378-96.

253. Luxen, S., S.A. Belinsky, and U.G. Knaus, *Silencing of DUOX NADPH oxidases by promoter hypermethylation in lung cancer.* Cancer Res, 2008. **68**(4): p. 1037-45.

254. Shames, D.S., et al., *A genome-wide screen for promoter methylation in lung cancer identifies novel methylation markers for multiple malignancies.* PLoS Med, 2006. **3**(12): p. e486.

255. Ling, Q., et al., *Epigenetic silencing of dual oxidase 1 by promoter hypermethylation in human hepatocellular carcinoma.* Am J Cancer Res, 2014. **4**(5): p. 508-17.

256. Siuda, D., et al., *Transcriptional regulation of Nox4 by histone deacetylases in human endothelial cells.* Basic Res Cardiol, 2012. **107**(5): p. 283.

257. Zelko, I.N. and R.J. Folz, *Regulation of Oxidative Stress in Pulmonary Artery Endothelium. Modulation of Extracellular Superoxide Dismutase and NOX4 Expression Using Histone Deacetylase Class I Inhibitors.* Am J Respir Cell Mol Biol, 2015. **53**(4): p. 513-24.

258. Manea, S.A., et al., *Regulation of Nox enzymes expression in vascular pathophysiology: Focusing on transcription factors and epigenetic mechanisms.* Redox Biol, 2015. **5**: p. 358-66.

259. Manea, S.A., et al., *Epigenetic regulation of vascular NADPH oxidase expression and reactive oxygen species production by histone deacetylase-dependent mechanisms in experimental diabetes.* Redox Biol, 2018. **16**: p. 332-343.

260. Cyr, A.R., M.J. Hitchler, and F.E. Domann, *Regulation of SOD2 in cancer by histone modifications and CpG methylation: closing the loop between redox biology and epigenetics.* Antioxid Redox Signal, 2013. **18**(15): p. 1946-55.

261. Hitchler, M.J., L.W. Oberley, and F.E. Domann, *Epigenetic silencing of SOD2 by histone modifications in human breast cancer cells.* Free radical biology & medicine, 2008. **45**(11): p. 1573-1580.

262. Zhong, Q. and R.A. Kowluru, *Epigenetic modification of Sod2 in the development of diabetic retinopathy and in the metabolic memory: role of histone methylation.* Invest Ophthalmol Vis Sci, 2013. **54**(1): p. 244-50.

263. Archer, S.L., et al., *Epigenetic attenuation of mitochondrial superoxide dismutase 2 in pulmonary arterial hypertension: a basis for excessive cell proliferation and a new therapeutic target.* Circulation, 2010. **121**(24): p. 2661-71.

264. Mendis, S., et al., *Global Atlas on Cardiovascular Disease Prevention and Control*. 2011: World Health Organization in collaboration with the World Heart Federation and the World Stroke Organization.

265. Giedrimiene, D. and R. King, *Abstract 207: Burden of Cardiovascular Disease (CVD) on Economic Cost. Comparison of Outcomes in US and Europe.* Circulation: Cardiovascular Quality and Outcomes, 2017. **10**(suppl_3): p. A207-A207.

266. Dunbar, S.B., et al., *Projected Costs of Informal Caregiving for Cardiovascular Disease: 2015 to 2035: A Policy Statement From the American Heart Association.* Circulation, 2018. **137**(19): p. e558-e577.

267. Yusuf, S., et al., *Effect of potentially modifiable risk factors associated with myocardial infarction in 52 countries (the INTERHEART study): case-control study.* Lancet, 2004. **364**(9438): p. 937-52.

268. Fryar, C.D., T.C. Chen, and X. Li, *Prevalence of uncontrolled risk factors for cardiovascular disease: United States, 1999-2010.* NCHS Data Brief, 2012(103): p. 1-8.

269. Abi Khalil, C., *The emerging role of epigenetics in cardiovascular disease.* Ther Adv Chronic Dis, 2014. **5**(4): p. 178-87.

270. Mahmoud, S.A. and C. Poizat, *Epigenetics and chromatin remodeling in adult cardiomyopathy.* J Pathol, 2013. **231**(2): p. 147-57.

271. Ordovas, J.M. and C.E. Smith, *Epigenetics and cardiovascular disease.* Nat Rev Cardiol, 2010. **7**(9): p. 510-9.

272. Tingare, A., B. Thienpont, and H.L. Roderick, *Epigenetics in the heart: the role of histone modifications in cardiac remodelling.* Biochem Soc Trans, 2013. **41**(3): p. 789-96.

273. Backs, J. and T. McKinsey, *Epigenetics in Cardiac Disease*. 2016: Springer International Publishing.

274. Lorenzen, J.M., F. Martino, and T. Thum, *Epigenetic modifications in cardiovascular disease.* Basic Res Cardiol, 2012. **107**(2): p. 245.

275. Webster, A.L., M.S. Yan, and P.A. Marsden, *Epigenetics and cardiovascular disease.* Can J Cardiol, 2013. **29**(1): p. 46-57.

276. O'Hagan, H.M., et al., *Oxidative damage targets complexes containing DNA methyltransferases, SIRT1, and polycomb members to promoter CpG Islands.* Cancer Cell, 2011. **20**(5): p. 606-19.

277. Turunen, M.P., E. Aavik, and S. Yla-Herttuala, *Epigenetics and atherosclerosis.* Biochim Biophys Acta, 2009. **1790**(9): p. 886-91.

278. Post, W.S., et al., *Methylation of the estrogen receptor gene is associated with aging and atherosclerosis in the cardiovascular system.* Cardiovasc Res, 1999. **43**(4): p. 985-91.

279. Movassagh, M., et al., *Distinct epigenomic features in end-stage failing human hearts.* Circulation, 2011. **124**(22): p. 2411-22.

280. Kaneda, R., et al., *Genome-wide histone methylation profile for heart failure.* Genes Cells, 2009. **14**(1): p. 69-77.

281. Zhang, M. and A.M. Shah, *ROS signalling between endothelial cells and cardiac cells.* Cardiovasc Res, 2014. **102**(2): p. 249-57.

282. Brown, D.I. and K.K. Griendling, *Regulation of signal transduction by reactive oxygen species in the cardiovascular system.* Circ Res, 2015. **116**(3): p. 531-49.

283. Hare, J.M., *Oxidative stress and apoptosis in heart failure progression.* Circ Res, 2001. **89**(3): p. 198-200.

284. Jay, D., H. Hitomi, and K.K. Griendling, *Oxidative stress and diabetic cardiovascular complications.* Free Radic Biol Med, 2006. **40**(2): p. 183-92.

285. Son, S.M., *Reactive oxygen and nitrogen species in pathogenesis of vascular complications of diabetes.* Diabetes Metab J, 2012. **36**(3): p. 190-8.

286. Laukkanen, M.O., et al., *Local hypomethylation in atherosclerosis found in rabbit ec-sod gene.* Arterioscler Thromb Vasc Biol, 1999. **19**(9): p. 2171-8.

287. Hai, Z. and W. Zuo, *Aberrant DNA methylation in the pathogenesis of atherosclerosis.* Clin Chim Acta, 2016. **456**: p. 69-74.

288. Dong, C., W. Yoon, and P.J. Goldschmidt-Clermont, *DNA methylation and atherosclerosis.* J Nutr, 2002. **132**(8 Suppl): p. 2406s-2409s.

289. Bonnet, S., et al., *An abnormal mitochondrial-hypoxia inducible factor-1alpha-Kv channel pathway disrupts oxygen sensing and triggers pulmonary arterial hypertension in fawn hooded rats: similarities to human pulmonary arterial hypertension.* Circulation, 2006. **113**(22): p. 2630-41.

290. Bowers, R., et al., *Oxidative stress in severe pulmonary hypertension.* Am J Respir Crit Care Med, 2004. **169**(6): p. 764-9.

291. Matsushima, S., et al., *Increased oxidative stress in the nucleus caused by Nox4 mediates oxidation of HDAC4 and cardiac hypertrophy.* Circ Res, 2013. **112**(4): p. 651-63.

292. Johnson, A.B., N. Denko, and M.C. Barton, *Hypoxia induces a novel signature of chromatin modifications and global repression of transcription.* Mutat Res, 2008. **640**(1-2): p. 174-9.

293. Chen, H., et al., *Hypoxic stress induces dimethylated histone H3 lysine 9 through histone methyltransferase G9a in mammalian cells.* Cancer Res, 2006. **66**(18): p. 9009-16.

294. Feletou, M. and P.M. Vanhoutte, *Endothelial dysfunction: a multifaceted disorder (The Wiggers Award Lecture).* Am J Physiol Heart Circ Physiol, 2006. **291**(3): p. H985-1002.

295. Daiber, A., et al., *Crosstalk of mitochondria with NADPH oxidase via reactive oxygen and nitrogen species signalling and its role for vascular function.* British Journal of Pharmacology, 2017. **174**(12): p. 1670-1689.

296. Matouk, C.C. and P.A. Marsden, *Epigenetic regulation of vascular endothelial gene expression.* Circ Res, 2008. **102**(8): p. 873-87.

297. Fish, J.E., et al., *Hypoxic repression of endothelial nitric-oxide synthase transcription is coupled with eviction of promoter histones.* J Biol Chem, 2010. **285**(2): p. 810-26.

298. Hyndman, K.A., et al., *Histone deacetylase 1 reduces NO production in endothelial cells via lysine deacetylation of NO synthase 3.* Am J Physiol Heart Circ Physiol, 2014. **307**(5): p. H803-9.

299. Lambert, P. and P.J. Bingley, *What is Type 1 Diabetes?* Medicine, 2002. **30**(1): p. 1-5.

300. Chatterjee, S., K. Khunti, and M.J. Davies, *Type 2 diabetes.* Lancet, 2017. **389**(10085): p. 2239-2251.

301. Arden, G.B. and S. Sivaprasad, *Hypoxia and oxidative stress in the causation of diabetic retinopathy.* Curr Diabetes Rev, 2011. **7**(5): p. 291-304.

302. Cai, L. and Y.J. Kang, *Cell death and diabetic cardiomyopathy.* Cardiovasc Toxicol, 2003. **3**(3): p. 219-28.

303. Duraisamy, A.J., et al., *Epigenetics and Regulation of Oxidative Stress in Diabetic Retinopathy.* Investigative ophthalmology & visual science, 2018. **59**(12): p. 4831-4840.

304. Kowluru, R.A., et al., *Oxidative stress and epigenetic modifications in the pathogenesis of diabetic retinopathy.* Progress in Retinal and Eye Research, 2015. **48**: p. 40-61.

305. Rösen, P., et al., *The role of oxidative stress in the onset and progression of diabetes and its complications: asummary of a Congress Series sponsored byUNESCO-MCBN, the American Diabetes Association and the German Diabetes Society.* Diabetes/Metabolism Research and Reviews, 2001. **17**(3): p. 189-212.

306. Haskins, K., et al., *Oxidative stress in type 1 diabetes.* Ann N Y Acad Sci, 2003. **1005**: p. 43-54.

307. Folli, F., et al., *The role of oxidative stress in the pathogenesis of type 2 diabetes mellitus micro- and macrovascular complications: avenues for a mechanistic-based therapeutic approach.* Curr Diabetes Rev, 2011. **7**(5): p. 313-24.

308. Rolo, A.P. and C.M. Palmeira, *Diabetes and mitochondrial function: role of hyperglycemia and oxidative stress.* Toxicol Appl Pharmacol, 2006. **212**(2): p. 167-78.

309. Bonnefont-Rousselot, D., *Glucose and reactive oxygen species.* Curr Opin Clin Nutr Metab Care, 2002. **5**(5): p. 561-8.

310. Ceriello, A. and E. Motz, *Is oxidative stress the pathogenic mechanism underlying insulin resistance, diabetes, and cardiovascular disease? The common soil hypothesis revisited.* Arterioscler Thromb Vasc Biol, 2004. **24**(5): p. 816-23.

311. Nishikawa, T., et al., *Normalizing mitochondrial superoxide production blocks three pathways of hyperglycaemic damage.* Nature, 2000. **404**(6779): p. 787-90.

312. Nowotny, K., et al., *Advanced Glycation End Products and Oxidative Stress in Type 2 Diabetes Mellitus.* Biomolecules, 2015. **5**(1): p. 194-222.

313. Basta, G., A.M. Schmidt, and R. De Caterina, *Advanced glycation end products and vascular inflammation: implications for accelerated atherosclerosis in diabetes.* Cardiovasc Res, 2004. **63**(4): p. 582-92.

314. Yan, S.D., et al., *Enhanced cellular oxidant stress by the interaction of advanced glycation end products with their receptors/binding proteins.* J Biol Chem, 1994. **269**(13): p. 9889-97.

315. Wautier, M.P., et al., *Activation of NADPH oxidase by AGE links oxidant stress to altered gene expression via RAGE.* Am J Physiol Endocrinol Metab, 2001. **280**(5): p. E685-94.

316. Schmidt, A.M., et al., *Advanced glycation endproducts interacting with their endothelial receptor induce expression of vascular cell adhesion molecule-1 (VCAM-1) in cultured human endothelial cells and in mice. A potential mechanism for the accelerated vasculopathy of diabetes.* J Clin Invest, 1995. **96**(3): p. 1395-403.

317. Yamagishi, S., et al., *Role of advanced glycation end products (AGEs) and oxidative stress in vascular complications in diabetes.* Biochim Biophys Acta, 2012. **1820**(5): p. 663-71.

318. Goldin, A., et al., *Advanced glycation end products: sparking the development of diabetic vascular injury.* Circulation, 2006. **114**(6): p. 597-605.

319. Brownlee, M., *Biochemistry and molecular cell biology of diabetic complications.* Nature, 2001. **414**: p. 813.

320. Steinberg, H.O. and A.D. Baron, *Vascular function, insulin resistance and fatty acids.* Diabetologia, 2002. **45**(5): p. 623-34.

321. Stojiljkovic, M.P., et al., *Increasing plasma fatty acids elevates F2-isoprostanes in humans: implications for the cardiovascular risk factor cluster.* J Hypertens, 2002. **20**(6): p. 1215-21.

322. Bouloumie, A., et al., *Leptin induces oxidative stress in human endothelial cells.* FASEB J, 1999. **13**(10): p. 1231-8.

323. Yamagishi, S.I., et al., *Leptin induces mitochondrial superoxide production and monocyte chemoattractant protein-1 expression in aortic endothelial cells by increasing fatty acid oxidation via protein kinase A.* J Biol Chem, 2001. **276**(27): p. 25096-100.

324. Evans, J.L., et al., *Are Oxidative Stress–Activated Signaling Pathways Mediators of Insulin Resistance and β-Cell Dysfunction?* Diabetes, 2003. **52**(1): p. 1-8.

325. Ling, C. and L. Groop, *Epigenetics: a molecular link between environmental factors and type 2 diabetes.* Diabetes, 2009. **58**(12): p. 2718-25.

326. Villeneuve, L.M. and R. Natarajan, *Epigenetics of diabetic complications.* Expert review of endocrinology & metabolism, 2010. **5**(1): p. 137-148.

327. Villeneuve, L.M. and R. Natarajan, *The role of epigenetics in the pathology of diabetic complications.* Am J Physiol Renal Physiol, 2010. **299**(1): p. F14-25.

328. Pirola, L., et al., *Epigenetic phenomena linked to diabetic complications.* Nat Rev Endocrinol, 2010. **6**(12): p. 665-75.

329. Reddy, M.A. and R. Natarajan, *Epigenetics in diabetic kidney disease.* J Am Soc Nephrol, 2011. **22**(12): p. 2182-5.

330. El-Osta, A., et al., *Transient high glucose causes persistent epigenetic changes and altered gene expression during subsequent normoglycemia.* Journal of Experimental Medicine, 2008. **205**(10): p. 2409-2417.

331. Villeneuve, L.M., et al., *Epigenetic histone H3 lysine 9 methylation in metabolic memory and inflammatory phenotype of vascular smooth muscle cells in diabetes.* Proceedings of the National Academy of Sciences of the United States of America, 2008. **105**(26): p. 9047-9052.

332. Zhong, Q. and R.A. Kowluru, *Epigenetic Changes in Mitochondrial Superoxide Dismutase in the Retina and the Development of Diabetic Retinopathy.* Diabetes, 2011. **60**(4): p. 1304-1313.

333. Miao, F., et al., *Evaluating the Role of Epigenetic Histone Modifications in the Metabolic Memory of Type 1 Diabetes.* Diabetes, 2014. **63**(5): p. 1748-1762.

334. Reddy, M.A., E. Zhang, and R. Natarajan, *Epigenetic mechanisms in diabetic complications and metabolic memory.* Diabetologia, 2015. **58**(3): p. 443-55.

335. Chen, S., et al., *Transcriptional coactivator p300 regulates glucose-induced gene expression in endothelial cells.* Am J Physiol Endocrinol Metab, 2010. **298**(1): p. E127-37.

336. Kaur, H., et al., *Diabetes-induced extracellular matrix protein expression is mediated by transcription coactivator p300.* Diabetes, 2006. **55**(11): p. 3104-11.

337. Calabrese, V., et al., *Oxidative stress, glutathione status, sirtuin and cellular stress response in type 2 diabetes.* Biochim Biophys Acta, 2012. **1822**(5): p. 729-36.

338. Mortuza, R., B. Feng, and S. Chakrabarti, *SIRT1 reduction causes renal and retinal injury in diabetes through endothelin 1 and transforming growth factor β1.* Journal of cellular and molecular medicine, 2015. **19**(8): p. 1857-1867.

339. Chiu, J., et al., *Oxidative stress-induced, poly(ADP-ribose) polymerase-dependent upregulation of ET-1 expression in chronic diabetic complications.* Can J Physiol Pharmacol, 2008. **86**(6): p. 365-72.

340. Xu, B., et al., *PARP activation and the alteration of vasoactive factors and extracellular matrix protein in retina and kidney in diabetes.* Diabetes Metab Res Rev, 2008. **24**(5): p. 404-12.

341. Ziyadeh, F.N., *Different roles for TGF-beta and VEGF in the pathogenesis of the cardinal features of diabetic nephropathy.* Diabetes Res Clin Pract, 2008. **82 Suppl 1**: p. S38-41.

342. Majumdar, P., et al., *Leptin and endothelin-1 mediated increased extracellular matrix protein production and cardiomyocyte hypertrophy in diabetic heart disease.* Diabetes Metab Res Rev, 2009. **25**(5): p. 452-63.

343. Miao, F., et al., *In vivo chromatin remodeling events leading to inflammatory gene transcription under diabetic conditions.* J Biol Chem, 2004. **279**(17): p. 18091-7.

344. Shanmugam, N., I.T. Gaw Gonzalo, and R. Natarajan, *Molecular mechanisms of high glucose-induced cyclooxygenase-2 expression in monocytes.* Diabetes, 2004. **53**(3): p. 795-802.

345. Hofmann, M.A., et al., *Insufficient glycemic control increases nuclear factor-kappa B binding activity in peripheral blood mononuclear cells isolated from patients with type 1 diabetes.* Diabetes Care, 1998. **21**(8): p. 1310-6.

346. Reddy, M.A., et al., *Role of the lysine-specific demethylase 1 in the proinflammatory phenotype of vascular smooth muscle cells of diabetic mice.* Circ Res, 2008. **103**(6): p. 615-23.

347. Feng, B., et al., *miR-146a-Mediated extracellular matrix protein production in chronic diabetes complications.* Diabetes, 2011. **60**(11): p. 2975-84.

348. Fu, Y., et al., *Regulation of NADPH Oxidase Activity Is Associated with miRNA-25-Mediated NOX4 Expression in Experimental Diabetic Nephropathy.* American Journal of Nephrology, 2010. **32**(6): p. 581-589.

349. Wang, Q., et al., *MicroRNA-377 is up-regulated and can lead to increased fibronectin production in diabetic nephropathy.* Faseb j, 2008. **22**(12): p. 4126-35.

350. Chen, Z., et al., *Regulation of SIRT1 by Oxidative Stress-Responsive miRNAs and a Systematic Approach to Identify Its Role in the Endothelium.* Antioxidants & Redox Signaling, 2013. **19**(13): p. 1522-1538.

351. Raciti, G.A., et al., *Personalized medicine and Type 2 diabetes: lesson from epigenetics.* Epigenomics, 2014. **6**(2): p. 229-238.

352. Bell, C.G., et al., *Genome-wide DNA methylation analysis for diabetic nephropathy in type 1 diabetes mellitus.* BMC Med Genomics, 2010. **3**: p. 33.

353. Maghbooli, Z., et al., *Global DNA methylation as a possible biomarker for diabetic retinopathy.* Diabetes/Metabolism Research and Reviews, 2015. **31**(2): p. 183-189.

354. Keating, S.T., J. Plutzky, and A. El-Osta, *Epigenetic Changes in Diabetes and Cardiovascular Risk.* Circ Res, 2016. **118**(11): p. 1706-22.

355. Keating, S.T. and A. El-Osta, *Epigenetic changes in diabetes.* Clin Genet, 2013. **84**(1): p. 1-10.

356. Reddy, M.A. and R. Natarajan, *Epigenetic mechanisms in diabetic vascular complications.* Cardiovasc Res, 2011. **90**(3): p. 421-9.

357. Karachanak-Yankova, S., et al., *Epigenetic alterations in patients with type 2 diabetes mellitus.* 2015. **18**(2): p. 15.

358. Dunn, C.J. and D.H. Peters, *Metformin. A review of its pharmacological properties and therapeutic use in non-insulin-dependent diabetes mellitus.* Drugs, 1995. **49**(5): p. 721-49.

359. Pfeiffer, A.F.H. and H.H. Klein, *The treatment of type 2 diabetes.* Deutsches Arzteblatt international, 2014. **111**(5): p. 69-82.

360. Stark Casagrande, S., et al., *The Prevalence of Meeting A1C, Blood Pressure, and LDL Goals Among People With Diabetes, 1988–2010.* Diabetes Care, 2013. **36**(8): p. 2271-2279.

361. Elkinson, S. and L.J. Scott, *Canagliflozin: first global approval.* Drugs, 2013. **73**(9): p. 979-88.

362. Vivian, E.M., *Dapagliflozin: a new sodium-glucose cotransporter 2 inhibitor for treatment of type 2 diabetes.* Am J Health Syst Pharm, 2015. **72**(5): p. 361-72.

363. Fala, L., *Jardiance (Empagliflozin), an SGLT2 Inhibitor, Receives FDA Approval for the Treatment of Patients with Type 2 Diabetes.* Am Health Drug Benefits, 2015. **8**(Spec Feature): p. 92-5.

364. Neumiller, J.J., J.R. White, and R.K. Campbell, *Sodium-Glucose Co-Transport Inhibitors.* Drugs, 2010. **70**(4): p. 377-385.

365. Gerich, J.E., *Role of the kidney in normal glucose homeostasis and in the hyperglycaemia of diabetes mellitus: therapeutic implications.* Diabetic Medicine, 2010. **27**(2): p. 136-142.

366. Wright, E.M., D.D. Loo, and B.A. Hirayama, *Biology of human sodium glucose transporters.* Physiol Rev, 2011. **91**(2): p. 733-94.

367. Whalen, K., S. Miller, and E.S. Onge, *The Role of Sodium-Glucose Co-Transporter 2 Inhibitors in the Treatment of Type 2 Diabetes.* Clin Ther, 2015. **37**(6): p. 1150-66.

368. Scheen, A.J. and N. Paquot, *Metabolic effects of SGLT-2 inhibitors beyond increased glucosuria: A review of the clinical evidence.* Diabetes & Metabolism, 2014. **40**(6, Supplement 1): p. S4-S11.

369. Grempler, R., et al., *Empagliflozin, a novel selective sodium glucose cotransporter-2 (SGLT-2) inhibitor: characterisation and comparison with other SGLT-2 inhibitors.* Diabetes Obes Metab, 2012. **14**(1): p. 83-90.

370. Scheen, A.J., *Pharmacokinetic and pharmacodynamic profile of empagliflozin, a sodium glucose co-transporter 2 inhibitor.* Clinical pharmacokinetics, 2014. **53**(3): p. 213-225.

371. Zinman, B., et al., *Empagliflozin, Cardiovascular Outcomes, and Mortality in Type 2 Diabetes.* New England Journal of Medicine, 2015. **373**(22): p. 2117-2128.

372. investigators, t.E.-R.O.t., et al., *Heart failure outcomes with empagliflozin in patients with type 2 diabetes at high cardiovascular risk: results of the EMPA-REG OUTCOME® trial.* European Heart Journal, 2016. **37**(19): p. 1526-1534.

373. McGowan, J.V., et al., *Anthracycline Chemotherapy and Cardiotoxicity.* Cardiovascular drugs and therapy, 2017. **31**(1): p. 63-75.

374. Tacar, O., P. Sriamornsak, and C.R. Dass, *Doxorubicin: an update on anticancer molecular action, toxicity and novel drug delivery systems.* J Pharm Pharmacol, 2013. **65**(2): p. 157-70.

375. Octavia, Y., et al., *Doxorubicin-induced cardiomyopathy: from molecular mechanisms to therapeutic strategies.* J Mol Cell Cardiol, 2012. **52**(6): p. 1213-25.

376. Chatterjee, K., et al., *Doxorubicin cardiomyopathy.* Cardiology, 2010. **115**(2): p. 155-62.

377. Kremer, L.C., et al., *Anthracycline-induced clinical heart failure in a cohort of 607 children: long-term follow-up study.* J Clin Oncol, 2001. **19**(1): p. 191-6.

378. Jain, D., *Cardiotoxicity of doxorubicin and other anthracycline derivatives.* J Nucl Cardiol, 2000. **7**(1): p. 53-62.

379. Lefrak, E.A., et al., *A clinicopathologic analysis of adriamycin cardiotoxicity.* Cancer, 1973. **32**(2): p. 302-14.

380. Takemura, G. and H. Fujiwara, *Doxorubicin-induced cardiomyopathy from the cardiotoxic mechanisms to management.* Prog Cardiovasc Dis, 2007. **49**(5): p. 330-52.

381. Swain, S.M., F.S. Whaley, and M.S. Ewer, *Congestive heart failure in patients treated with doxorubicin: a retrospective analysis of three trials.* Cancer, 2003. **97**(11): p. 2869-79.

382. Von Hoff, D.D., et al., *Risk factors for doxorubicin-induced congestive heart failure.* Ann Intern Med, 1979. **91**(5): p. 710-7.

383. Felker, G.M., et al., *Underlying causes and long-term survival in patients with initially unexplained cardiomyopathy.* N Engl J Med, 2000. **342**(15): p. 1077-84.

384. Xu, M.F., et al., *Effects by doxorubicin on the myocardium are mediated by oxygen free radicals.* Life Sci, 2001. **68**(8): p. 889-901.

385. Simunek, T., et al., *Anthracycline-induced cardiotoxicity: overview of studies examining the roles of oxidative stress and free cellular iron.* Pharmacol Rep, 2009. **61**(1): p. 154-71.

386. Kalyanaraman, B., E. Perez-Reyes, and R.P. Mason, *Spin-trapping and direct electron spin resonance investigations of the redox metabolism of quinone anticancer drugs.* Biochim Biophys Acta, 1980. **630**(1): p. 119-30.

387. Olson, R.D., et al., *Regulatory role of glutathione and soluble sulfhydryl groups in the toxicity of adriamycin.* J Pharmacol Exp Ther, 1980. **215**(2): p. 450-4.

388. Doroshow, J.H., et al., *The effect of doxorubicin on hepatic and cardiac glutathione.* Res Commun Chem Pathol Pharmacol, 1979. **26**(2): p. 285-95.

389. Zhu, H., et al., *Doxorubicin Redox Biology: Redox Cycling, Topoisomerase Inhibition, and Oxidative Stress.* React Oxyg Species (Apex), 2016. **1**(3): p. 189-198.

390. Berthiaume, J.M. and K.B. Wallace, *Adriamycin-induced oxidative mitochondrial cardiotoxicity.* Cell Biol Toxicol, 2007. **23**(1): p. 15-25.

391. Davies, K.J. and J.H. Doroshow, *Redox cycling of anthracyclines by cardiac mitochondria. I. Anthracycline radical formation by NADH dehydrogenase.* J Biol Chem, 1986. **261**(7): p. 3060-7.

392. Suliman, H.B., et al., *The CO/HO system reverses inhibition of mitochondrial biogenesis and prevents murine doxorubicin cardiomyopathy.* J Clin Invest, 2007. **117**(12): p. 3730-41.

393. Piantadosi, C.A., et al., *Heme oxygenase-1 regulates cardiac mitochondrial biogenesis via Nrf2-mediated transcriptional control of nuclear respiratory factor-1.* Circ Res, 2008. **103**(11): p. 1232-40.

394. Aryal, B. and V.A. Rao, *Deficiency in Cardiolipin Reduces Doxorubicin-Induced Oxidative Stress and Mitochondrial Damage in Human B-Lymphocytes.* PLoS One, 2016. **11**(7): p. e0158376.

395. Wojnowski, L., et al., *NAD(P)H oxidase and multidrug resistance protein genetic polymorphisms are associated with doxorubicin-induced cardiotoxicity.* Circulation, 2005. **112**(24): p. 3754-62.

396. Deng, S., et al., *Gp91phox-containing NAD(P)H oxidase increases superoxide formation by doxorubicin and NADPH.* Free Radic Biol Med, 2007. **42**(4): p. 466-73.

397. Zhao, Y., et al., *Nox2 NADPH oxidase promotes pathologic cardiac remodeling associated with Doxorubicin chemotherapy.* Cancer Res, 2010. **70**(22): p. 9287-97.

398. Gilleron, M., et al., *NADPH oxidases participate to doxorubicin-induced cardiac myocyte apoptosis.* Biochem Biophys Res Commun, 2009. **388**(4): p. 727-31.

399. Ma, J., et al., *Rac1 signalling mediates doxorubicin-induced cardiotoxicity through both reactive oxygen species-dependent and -independent pathways.* Cardiovasc Res, 2013. **97**(1): p. 77-87.

400. Siveski-Iliskovic, N., et al., *Probucol protects against adriamycin cardiomyopathy without interfering with its antitumor effect.* Circulation, 1995. **91**(1): p. 10-5.

401. Doroshow, J.H., G.Y. Locker, and C.E. Myers, *Enzymatic defenses of the mouse heart against reactive oxygen metabolites: alterations produced by doxorubicin.* J Clin Invest, 1980. **65**(1): p. 128-35.

402. Gao, J., et al., *Glutathione peroxidase 1-deficient mice are more susceptible to doxorubicin-induced cardiotoxicity.* Biochim Biophys Acta, 2008. **1783**(10): p. 2020-9.

403. Xiong, Y., et al., *Attenuation of doxorubicin-induced contractile and mitochondrial dysfunction in mouse heart by cellular glutathione peroxidase.* Free Radic Biol Med, 2006. **41**(1): p. 46-55.

404. Chaiswing, L., et al., *Manganese superoxide dismutase and inducible nitric oxide synthase modify early oxidative events in acute adriamycin-induced mitochondrial toxicity.* Mol Cancer Ther, 2005. **4**(7): p. 1056-64.

405. Pani, G., et al., *Deregulated manganese superoxide dismutase expression and resistance to oxidative injury in p53-deficient cells.* Cancer Res, 2000. **60**(16): p. 4654-60.

406. Kim, D.S., et al., *Protective effect of calceolarioside on adriamycin-induced cardiomyocyte toxicity.* Eur J Pharmacol, 2006. **541**(1-2): p. 24-32.

407. Wenzel, P., et al., *ALDH-2 deficiency increases cardiovascular oxidative stress--evidence for indirect antioxidative properties.* Biochem Biophys Res Commun, 2008. **367**(1): p. 137-43.

408. Ferreira, A., et al., *Altered mitochondrial epigenetics associated with subchronic doxorubicin cardiotoxicity.* Toxicology, 2017. **390**: p. 63-73.

409. Karbach, S., et al., *Hyperglycemia and oxidative stress in cultured endothelial cells--a comparison of primary endothelial cells with an immortalized endothelial cell line.* J Diabetes Complications, 2012. **26**(3): p. 155-62.

410. Deshwal, S., et al., *Monoamine oxidase-dependent endoplasmic reticulum-mitochondria dysfunction and mast cell degranulation lead to adverse cardiac remodeling in diabetes.* Cell Death Differ, 2018.

411. Baudin, B., et al., *A protocol for isolation and culture of human umbilical vein endothelial cells.* Nat Protoc, 2007. **2**(3): p. 481-5.

412. Steven, S., et al., *The SGLT2 inhibitor empagliflozin improves the primary diabetic complications in ZDF rats.* Redox Biol, 2017. **13**: p. 370-385.

413. Bradford, M.M., *A rapid and sensitive method for the quantitation of microgram quantities of protein utilizing the principle of protein-dye binding.* Anal Biochem, 1976. **72**: p. 248-54.

414. Oelze, M., et al., *Vascular dysfunction in streptozotocin-induced experimental diabetes strictly depends on insulin deficiency.* J Vasc Res, 2011. **48**(4): p. 275-84.

415. Oelze, M., et al., *Nebivolol inhibits superoxide formation by NADPH oxidase and endothelial dysfunction in angiotensin II-treated rats.* Hypertension, 2006. **48**(4): p. 677-84.

416. Oelze, M., et al., *Glutathione peroxidase-1 deficiency potentiates dysregulatory modifications of endothelial nitric oxide synthase and vascular dysfunction in aging.* Hypertension, 2014. **63**(2): p. 390-6.

417. Roy, S. and V. Kumar, *A Practical Approach on SDS PAGE for Separation of Protein*. 2014.

418. Sengupta, R., T.R. Billiar, and D.A. Stoyanovsky, *Studies toward the analysis of S-nitrosoproteins.* Org Biomol Chem, 2009. **7**(2): p. 232-4.

419. Wenzel, P., et al., *First evidence for a crosstalk between mitochondrial and NADPH oxidase-derived reactive oxygen species in nitroglycerin-triggered vascular dysfunction.* Antioxid Redox Signal, 2008. **10**(8): p. 1435-47.

420. Kröller-Schön, S., et al., *Molecular mechanisms of the crosstalk between mitochondria and NADPH oxidase through reactive oxygen species-studies in white blood cells and in animal models.* Antioxidants & redox signaling, 2014. **20**(2): p. 247-266.

421. Daiber, A., et al., *Oxidative stress and mitochondrial aldehyde dehydrogenase activity: a comparison of pentaerythritol tetranitrate with other organic nitrates.* Mol Pharmacol, 2004. **66**(6): p. 1372-82.

422. Collas, P. and J.A. Dahl, *Chop it, ChIP it, check it: the current status of chromatin immunoprecipitation.* Front Biosci, 2008. **13**: p. 929-43.

423. Barth, T.K. and A. Imhof, *Fast signals and slow marks: the dynamics of histone modifications.* Trends Biochem Sci, 2010. **35**(11): p. 618-26.

424. Kooistra, S.M. and K. Helin, *Molecular mechanisms and potential functions of histone demethylases.* Nature Reviews Molecular Cell Biology, 2012. **13**: p. 297.

425. Manduteanu, I., et al., *Effect of enoxaparin on high glucose-induced activation of endothelial cells.* Eur J Pharmacol, 2003. **477**(3): p. 269-76.

426. Rosenkranz, A.C., et al., *Endothelial antioxidant actions of dihydropyridines and angiotensin converting enzyme inhibitors.* Eur J Pharmacol, 2006. **529**(1-3): p. 55-62.

427. Keynan, S., et al., *Increased expression of endothelin-converting enzyme-1c isoform in response to high glucose levels in endothelial cells.* J Vasc Res, 2004. **41**(2): p. 131-40.

428. Khamaisi, M., et al., *Role of protein kinase C in the expression of endothelin converting enzyme-1.* Endocrinology, 2009. **150**(3): p. 1440-9.

429. Cocheme, H.M. and M.P. Murphy, *Complex I is the major site of mitochondrial superoxide production by paraquat.* J Biol Chem, 2008. **283**(4): p. 1786-98.

430. Camerini-Otero, R.D. and G. Felsenfeld, *Histone H3 disulfide dimers and nucleosome structure.* Proc Natl Acad Sci U S A, 1977. **74**(12): p. 5519-23.

431. Khan, M.A., et al., *Role of peroxynitrite induced structural changes on H2B histone by physicochemical method.* Int J Biol Macromol, 2016. **82**: p. 31-8.

432. Khan, M.A., et al., *Impact of peroxynitrite modification on structure and immunogenicity of H2A histone.* Scand J Immunol, 2009. **69**(2): p. 99-109.

433. Dixit, K., et al., *Physicochemical studies on peroxynitrite-modified H3 histone.* Int J Biol Macromol, 2010. **46**(1): p. 20-6.

434. Huggins, T.G., et al., *Formation of o-tyrosine and dityrosine in proteins during radiolytic and metal-catalyzed oxidation.* J Biol Chem, 1993. **268**(17): p. 12341-7.

435. Malencik, D.A. and S.R. Anderson, *Dityrosine as a product of oxidative stress and fluorescent probe.* Amino Acids, 2003. **25**(3-4): p. 233-47.

436. Correia, M., et al., *UV-light exposure of insulin: pharmaceutical implications upon covalent insulin dityrosine dimerization and disulphide bond photolysis.* PLoS One, 2012. **7**(12): p. e50733.

437. Rieg, T., et al., *Increase in SGLT1-mediated transport explains renal glucose reabsorption during genetic and pharmacological SGLT2 inhibition in euglycemia.* Am J Physiol Renal Physiol, 2014. **306**(2): p. F188-93.

438. Jufvas, A., et al., *Global differences in specific histone H3 methylation are associated with overweight and type 2 diabetes.* Clin Epigenetics, 2013. **5**(1): p. 15.

439. Kimes, B.W. and B.L. Brandt, *Properties of a clonal muscle cell line from rat heart.* Exp Cell Res, 1976. **98**(2): p. 367-81.

440. Cheung, K.G., et al., *Sirtuin-3 (SIRT3) Protein Attenuates Doxorubicin-induced Oxidative Stress and Improves Mitochondrial Respiration in H9c2 Cardiomyocytes.* J Biol Chem, 2015. **290**(17): p. 10981-93.

441. Bagul, P.K., et al., *Resveratrol ameliorates cardiac oxidative stress in diabetes through deacetylation of NFkB-p65 and histone 3.* J Nutr Biochem, 2015. **26**(11): p. 1298-307.

442. Han, S.S., et al., *Investigating the Mechanism of Hyperglycemia-Induced Fetal Cardiac Hypertrophy.* PLoS One, 2015. **10**(9): p. e0139141.

443. Cai, L., et al., *Hyperglycemia-induced apoptosis in mouse myocardium: mitochondrial cytochrome C-mediated caspase-3 activation pathway.* Diabetes, 2002. **51**(6): p. 1938-48.

444. Li, H., et al., *Adiponectin ameliorates hyperglycemia-induced cardiac hypertrophy and dysfunction by concomitantly activating Nrf2 and Brg1.* Free Radic Biol Med, 2015. **84**: p. 311-21.

445. Atale, N., et al., *Cardioprotective role of Syzygium cumini against glucose-induced oxidative stress in H9C2 cardiac myocytes.* Cardiovasc Toxicol, 2013. **13**(3): p. 278-89.

446. Kumar, S. and S.L. Sitasawad, *N-acetylcysteine prevents glucose/glucose oxidase-induced oxidative stress, mitochondrial damage and apoptosis in H9c2 cells.* Life Sci, 2009. **84**(11-12): p. 328-36.

447. Kumar, S., V. Kain, and S.L. Sitasawad, *High glucose-induced Ca2+ overload and oxidative stress contribute to apoptosis of cardiac cells through mitochondrial dependent and independent pathways.* Biochim Biophys Acta, 2012. **1820**(7): p. 907-20.

448. Li, K., et al., *Glutamine Reduces the Apoptosis of H9C2 Cells Treated with High-Glucose and Reperfusion through an Oxidation-Related Mechanism.* PLoS One, 2015. **10**(7): p. e0132402.

449. Oyama, K., K. Takahashi, and K. Sakurai, *Hydrogen peroxide induces cell cycle arrest in cardiomyoblast H9c2 cells, which is related to hypertrophy.* Biol Pharm Bull, 2011. **34**(4): p. 501-6.

450. Corna, G., et al., *Doxorubicin paradoxically protects cardiomyocytes against iron-mediated toxicity: role of reactive oxygen species and ferritin.* J Biol Chem, 2004. **279**(14): p. 13738-45.

451. Branco, A.F., et al., *Differentiation-dependent doxorubicin toxicity on H9c2 cardiomyoblasts.* Cardiovasc Toxicol, 2012. **12**(4): p. 326-40.

452. Zee, R.S., et al., *Redox regulation of sirtuin-1 by S-glutathiolation.* Antioxid Redox Signal, 2010. **13**(7): p. 1023-32.

453. Han, C., et al., *O-GlcNAcylation of SIRT1 enhances its deacetylase activity and promotes cytoprotection under stress.* Nat Commun, 2017. **8**(1): p. 1491.

454. Lynch, C.J., et al., *SIRT1 undergoes alternative splicing in a novel auto-regulatory loop with p53.* PLoS One, 2010. **5**(10): p. e13502.

455. Piotrowska, I., M. Isalan, and M. Mielcarek, *Early transcriptional alteration of histone deacetylases in a murine model of doxorubicin-induced cardiomyopathy.* PLoS One, 2017. **12**(6): p. e0180571.

456. To, M., et al., *Reduced HDAC2 in skeletal muscle of COPD patients.* Respir Res, 2017. **18**(1): p. 99.

457. Ito, K., et al., *Decreased histone deacetylase activity in chronic obstructive pulmonary disease.* N Engl J Med, 2005. **352**(19): p. 1967-76.

458. Sundar, I.K., H. Yao, and I. Rahman, *Oxidative stress and chromatin remodeling in chronic obstructive pulmonary disease and smoking-related diseases.* Antioxid Redox Signal, 2013. **18**(15): p. 1956-71.

459. Hohl, M., et al., *HDAC4 controls histone methylation in response to elevated cardiac load.* J Clin Invest, 2013. **123**(3): p. 1359-70.

460. Goda, S., et al., *Control of histone H3 lysine 9 (H3K9) methylation state via cooperative two-step demethylation by Jumonji domain containing 1A (JMJD1A) homodimer.* J Biol Chem, 2013. **288**(52): p. 36948-56.

461. Friso, S., et al., *Epigenetics and arterial hypertension: the challenge of emerging evidence.* Transl Res, 2015. **165**(1): p. 154-65.

462. Rajasekar, P., et al., *Epigenetic Changes in Endothelial Progenitors as a Possible Cellular Basis for Glycemic Memory in Diabetic Vascular Complications.* J Diabetes Res, 2015. **2015**: p. 436879.

463. Yuan, H., et al., *Epigenetic Histone Modifications Involved in Profibrotic Gene Regulation by 12/15-Lipoxygenase and Its Oxidized Lipid Products in Diabetic Nephropathy.* Antioxid Redox Signal, 2016. **24**(7): p. 361-75.

464. Wu, J., et al., *Biochemical characterization of human SET and MYND domain-containing protein 2 methyltransferase.* Biochemistry, 2011. **50**(29): p. 6488-97.

465. Franklin, S., et al., *The chromatin-binding protein Smyd1 restricts adult mammalian heart growth.* Am J Physiol Heart Circ Physiol, 2016. **311**(5): p. H1234-H1247.

466. Warren, J.S., et al., *Histone methyltransferase Smyd1 regulates mitochondrial energetics in the heart.* Proc Natl Acad Sci U S A, 2018. **115**(33): p. E7871-E7880.

467. Arnelle, D.R. and J.S. Stamler, *NO+, NO, and NO- donation by S-nitrosothiols: implications for regulation of physiological functions by S-nitrosylation and acceleration of disulfide formation.* Arch Biochem Biophys, 1995. **318**(2): p. 279-85.

468. Lipton, S.A., et al., *A redox-based mechanism for the neuroprotective and neurodestructive effects of nitric oxide and related nitroso-compounds.* Nature, 1993. **364**(6438): p. 626-32.

469. Sumbayev, V.V., et al., *HIF-1 alpha protein as a target for S-nitrosation.* FEBS Lett, 2003. **535**(1-3): p. 106-12.

470. Kelleher, Z.T., et al., *NOS2 regulation of NF-kappaB by S-nitrosylation of p65.* J Biol Chem, 2007. **282**(42): p. 30667-72.

471. Nash, K.M., A. Rockenbauer, and F.A. Villamena, *Reactive nitrogen species reactivities with nitrones: theoretical and experimental studies.* Chem Res Toxicol, 2012. **25**(8): p. 1581-97.

472. Martinez-Ruiz, A. and S. Lamas, *S-nitrosylation: a potential new paradigm in signal transduction.* Cardiovasc Res, 2004. **62**(1): p. 43-52.

473. Jaffrey, S.R. and S.H. Snyder, *The biotin switch method for the detection of S-nitrosylated proteins.* Sci STKE, 2001. **2001**(86): p. pl1.

474. Forrester, M.T., et al., *Detection of protein S-nitrosylation with the biotin-switch technique.* Free Radic Biol Med, 2009. **46**(2): p. 119-26.

475. Giustarini, D., et al., *Is ascorbate able to reduce disulfide bridges? A cautionary note.* Nitric Oxide, 2008. **19**(3): p. 252-8.

476. Landino, L.M., et al., *Ascorbic acid reduction of microtubule protein disulfides and its relevance to protein S-nitrosylation assays.* Biochem Biophys Res Commun, 2006. **340**(2): p. 347-52.

477. Huang, B. and C. Chen, *An ascorbate-dependent artifact that interferes with the interpretation of the biotin switch assay.* Free Radic Biol Med, 2006. **41**(4): p. 562-7.

478. Barrett, J., D.F. Debenham, and J. Glauser, *The electronic spectrum and photolysis of S-nitrosotoluene-α-thiol.* Chemical Communications (London), 1965(12): p. 248-249.

479. Detweiler, C.D., et al., *Immunological identification of the heart myoglobin radical formed by hydrogen peroxide.* Free Radic Biol Med, 2002. **33**(3): p. 364-9.

480. Moon, K.-H., B.-J. Kim, and B.J. Song, *Inhibition of mitochondrial aldehyde dehydrogenase by nitric oxide-mediated S-nitrosylation.* FEBS letters, 2005. **579**(27): p. 6115-6120.

481. Yang, E.S., et al., *Inactivation of NADP(+)-dependent isocitrate dehydrogenase by nitric oxide.* Free Radic Biol Med, 2002. **33**(7): p. 927-37.

482. Ford, P.C., D.A. Wink, and D.M. Stanbury, *Autoxidation kinetics of aqueous nitric oxide.* FEBS Lett, 1993. **326**(1-3): p. 1-3.

483. Mason, R.P., *Imaging free radicals in organelles, cells, tissue, and in vivo with immuno-spin trapping.* Redox Biol, 2016. **8**: p. 422-9.

484. Yao, D. and M. Brownlee, *Hyperglycemia-induced reactive oxygen species increase expression of the receptor for advanced glycation end products (RAGE) and RAGE ligands.* Diabetes, 2010. **59**(1): p. 249-55.

485. Kassab, A. and A. Piwowar, *Cell oxidant stress delivery and cell dysfunction onset in type 2 diabetes.* Biochimie, 2012. **94**(9): p. 1837-48.

486. Di Mario, U. and G. Pugliese, *15th Golgi lecture: from hyperglycaemia to the dysregulation of vascular remodelling in diabetes.* Diabetologia, 2001. **44**(6): p. 674-92.

487. Patel, H., et al., *Hyperglycemia induces differential change in oxidative stress at gene expression and functional levels in HUVEC and HMVEC.* Cardiovasc Diabetol, 2013. **12**: p. 142.

488. Xue, M., et al., *Activation of NF-E2-related factor-2 reverses biochemical dysfunction of endothelial cells induced by hyperglycemia linked to vascular disease.* Diabetes, 2008. **57**(10): p. 2809-17.

489. Cifarelli, V., et al., *C-peptide reduces high-glucose-induced apoptosis of endothelial cells and decreases NAD(P)H-oxidase reactive oxygen species generation in human aortic endothelial cells.* Diabetologia, 2011. **54**(10): p. 2702-12.

490. Castilho, A., et al., *Heme oxygenase-1 protects retinal endothelial cells against high glucose- and oxidative/nitrosative stress-induced toxicity.* PLoS One, 2012. **7**(8): p. e42428.

491. Hoshiyama, M., et al., *Effect of high glucose on nitric oxide production and endothelial nitric oxide synthase protein expression in human glomerular endothelial cells.* Nephron Exp Nephrol, 2003. **95**(2): p. e62-8.

492. Pala, L., et al., *Different modulation of dipeptidyl peptidase-4 activity between microvascular and macrovascular human endothelial cells.* Acta Diabetol, 2012. **49 Suppl 1**: p. S59-63.

493. Du, X., K. Stocklauser-Farber, and P. Rosen, *Generation of reactive oxygen intermediates, activation of NF-kappaB, and induction of apoptosis in human endothelial cells by glucose: role of nitric oxide synthase?* Free Radic Biol Med, 1999. **27**(7-8): p. 752-63.

494. Jansen, F., et al., *High glucose condition increases NADPH oxidase activity in endothelial microparticles that promote vascular inflammation.* Cardiovasc Res, 2013. **98**(1): p. 94-106.

495. Piconi, L., et al., *Constant and intermittent high glucose enhances endothelial cell apoptosis through mitochondrial superoxide overproduction.* Diabetes Metab Res Rev, 2006. **22**(3): p. 198-203.

496. Quijano, C., et al., *Enhanced mitochondrial superoxide in hyperglycemic endothelial cells: direct measurements and formation of hydrogen peroxide and peroxynitrite.* Am J Physiol Heart Circ Physiol, 2007. **293**(6): p. H3404-14.

497. Quagliaro, L., et al., *Intermittent high glucose enhances apoptosis related to oxidative stress in human umbilical vein endothelial cells: the role of protein kinase C and NAD(P)H-oxidase activation.* Diabetes, 2003. **52**(11): p. 2795-804.

498. Koziel, A., et al., *The influence of high glucose on the aerobic metabolism of endothelial EA.hy926 cells.* Pflügers Archiv - European Journal of Physiology, 2012. **464**(6): p. 657-669.

499. Guzik, T.J., et al., *Mechanisms of increased vascular superoxide production in human diabetes mellitus: role of NAD(P)H oxidase and endothelial nitric oxide synthase.* Circulation, 2002. **105**(14): p. 1656-62.

500. Hink, U., et al., *Mechanisms underlying endothelial dysfunction in diabetes mellitus.* Circ Res, 2001. **88**(2): p. E14-22.

501. Triggle, C.R. and H. Ding, *A review of endothelial dysfunction in diabetes: a focus on the contribution of a dysfunctional eNOS.* J Am Soc Hypertens, 2010. **4**(3): p. 102-15.

502. Inoguchi, T., et al., *High glucose level and free fatty acid stimulate reactive oxygen species production through protein kinase C--dependent activation of NAD(P)H oxidase in cultured vascular cells.* Diabetes, 2000. **49**(11): p. 1939-45.

503. Inoguchi, T., et al., *Protein kinase C-dependent increase in reactive oxygen species (ROS) production in vascular tissues of diabetes: role of vascular NAD(P)H oxidase.* J Am Soc Nephrol, 2003. **14**(8 Suppl 3): p. S227-32.

504. Koya, D. and G.L. King, *Protein kinase C activation and the development of diabetic complications.* Diabetes, 1998. **47**(6): p. 859-66.

505. Ishii, H., D. Koya, and G.L. King, *Protein kinase C activation and its role in the development of vascular complications in diabetes mellitus.* J Mol Med (Berl), 1998. **76**(1): p. 21-31.

506. Lee, T.S., et al., *Activation of protein kinase C by elevation of glucose concentration: proposal for a mechanism in the development of diabetic vascular complications.* Proc Natl Acad Sci U S A, 1989. **86**(13): p. 5141-5.

507. Park, J.Y., S.W. Ha, and G.L. King, *The role of protein kinase C activation in the pathogenesis of diabetic vascular complications.* Perit Dial Int, 1999. **19 Suppl 2**: p. S222-7.

508. Cosentino-Gomes, D., N. Rocco-Machado, and J.R. Meyer-Fernandes, *Cell signaling through protein kinase C oxidation and activation.* International journal of molecular sciences, 2012. **13**(9): p. 10697-10721.

509. Gopalakrishna, R. and S. Jaken, *Protein kinase C signaling and oxidative stress.* Free Radic Biol Med, 2000. **28**(9): p. 1349-61.

510. Rhee, S.G., et al., *Hydrogen peroxide: a key messenger that modulates protein phosphorylation through cysteine oxidation.* Sci STKE, 2000. **2000**(53): p. pe1.

511. Giorgi, C., et al., *Redox control of protein kinase C: cell- and disease-specific aspects.* Antioxid Redox Signal, 2010. **13**(7): p. 1051-85.

512. Waldron, R.T., et al., *Oxidative stress induces protein kinase C-mediated activation loop phosphorylation and nuclear redistribution of protein kinase D.* J Biol Chem, 2004. **279**(26): p. 27482-93.

513. Brandes, R.P., N. Weissmann, and K. Schroder, *Nox family NADPH oxidases: Molecular mechanisms of activation.* Free Radic Biol Med, 2014. **76**: p. 208-26.

514. Joglar, B., et al., *The inflammatory response in the MPTP model of Parkinson's disease is mediated by brain angiotensin: relevance to progression of the disease.* J Neurochem, 2009. **109**(2): p. 656-69.

515. El Benna, J., et al., *Phosphorylation of the respiratory burst oxidase subunit p47phox as determined by two-dimensional phosphopeptide mapping. Phosphorylation by protein kinase C, protein kinase A, and a mitogen-activated protein kinase.* J Biol Chem, 1996. **271**(11): p. 6374-8.

516. Devaraj, S., et al., *C-reactive protein stimulates superoxide anion release and tissue factor activity in vivo.* Atherosclerosis, 2009. **203**(1): p. 67-74.

517. Romero, M., et al., *Quercetin inhibits vascular superoxide production induced by endothelin-1: Role of NADPH oxidase, uncoupled eNOS and PKC.* Atherosclerosis, 2009. **202**(1): p. 58-67.

518. Dikalov, S.I., et al., *Mitochondrial reactive oxygen species and calcium uptake regulate activation of phagocytic NADPH oxidase.* Am J Physiol Regul Integr Comp Physiol, 2012. **302**(10): p. R1134-42.

519. Yang, J., et al., *Protein kinase C-dependent NAD(P)H oxidase activation induced by type 1 diabetes in renal medullary thick ascending limb.* Hypertension, 2010. **55**(2): p. 468-73.

520. Plumb, R.D., et al., *NAD(P)H-dependent superoxide production in platelets: the role of angiotensin II and protein kinase C.* Clin Biochem, 2005. **38**(7): p. 607-13.

521. Soetikno, V., et al., *Curcumin attenuates diabetic nephropathy by inhibiting PKC-alpha and PKC-beta1 activity in streptozotocin-induced type I diabetic rats.* Mol Nutr Food Res, 2011. **55**(11): p. 1655-65.

522. Ha, H. and H.B. Lee, *Reactive oxygen species amplify glucose signalling in renal cells cultured under high glucose and in diabetic kidney.* Nephrology (Carlton), 2005. **10 Suppl**: p. S7-10.

523. Wei, X.F., et al., *Advanced oxidation protein products induce mesangial cell perturbation through PKC-dependent activation of NADPH oxidase.* Am J Physiol Renal Physiol, 2009. **296**(2): p. F427-37.

524. Lin, R.Z., et al., *Tumor-induced endothelial cell apoptosis: roles of NAD(P)H oxidase-derived reactive oxygen species.* J Cell Physiol, 2011. **226**(7): p. 1750-62.

525. Park, J.Y., et al., *Induction of endothelin-1 expression by glucose: an effect of protein kinase C activation.* Diabetes, 2000. **49**(7): p. 1239-48.

526. Chen, F., et al., *PKC-dependent phosphorylation of eNOS at T495 regulates eNOS coupling and endothelial barrier function in response to G+ -toxins.* PLoS One, 2014. **9**(7): p. e99823.

527. Matsubara, M., et al., *Regulation of endothelial nitric oxide synthase by protein kinase C.* J Biochem, 2003. **133**(6): p. 773-81.

528. Michell, B.J., et al., *Coordinated control of endothelial nitric-oxide synthase phosphorylation by protein kinase C and the cAMP-dependent protein kinase.* J Biol Chem, 2001. **276**(21): p. 17625-8.

529. Chu, S. and H.G. Bohlen, *High concentration of glucose inhibits glomerular endothelial eNOS through a PKC mechanism.* American Journal of Physiology-Renal Physiology, 2004. **287**(3): p. F384-F392.

530. Lin, M.I., et al., *Phosphorylation of threonine 497 in endothelial nitric-oxide synthase coordinates the coupling of L-arginine metabolism to efficient nitric oxide production.* J Biol Chem, 2003. **278**(45): p. 44719-26.

531. Fleming, I., et al., *Phosphorylation of Thr(495) regulates Ca(2+)/calmodulin-dependent endothelial nitric oxide synthase activity.* Circ Res, 2001. **88**(11): p. E68-75.

532. Harris, M.B., et al., *Reciprocal phosphorylation and regulation of endothelial nitric-oxide synthase in response to bradykinin stimulation.* J Biol Chem, 2001. **276**(19): p. 16587-91.

533. Roberts, A.C. and K.E. Porter, *Cellular and molecular mechanisms of endothelial dysfunction in diabetes.* Diab Vasc Dis Res, 2013. **10**(6): p. 472-82.

534. Das Evcimen, N. and G.L. King, *The role of protein kinase C activation and the vascular complications of diabetes.* Pharmacol Res, 2007. **55**(6): p. 498-510.

535. Harman, D., *Aging: a theory based on free radical and radiation chemistry.* J Gerontol, 1956. **11**(3): p. 298-300.

536. Cencioni, C., et al., *Oxidative stress and epigenetic regulation in ageing and age-related diseases.* Int J Mol Sci, 2013. **14**(9): p. 17643-63.

537. Davalli, P., et al., *ROS, Cell Senescence, and Novel Molecular Mechanisms in Aging and Age-Related Diseases.* Oxidative medicine and cellular longevity, 2016. **2016**: p. 3565127-3565127.

538. Lakatta, E.G., *Arterial and cardiac aging: major shareholders in cardiovascular disease enterprises: Part III: cellular and molecular clues to heart and arterial aging.* Circulation, 2003. **107**(3): p. 490-7.

539. Chervona, Y. and M. Costa, *The control of histone methylation and gene expression by oxidative stress, hypoxia, and metals.* Free Radic Biol Med, 2012. **53**(5): p. 1041-7.

540. Chen, H., et al., *Nickel Ions Increase Histone H3 Lysine 9 Dimethylation and Induce Transgene Silencing.* Molecular and Cellular Biology, 2006. **26**(10): p. 3728-3737.

541. Tausendschon, M., N. Dehne, and B. Brune, *Hypoxia causes epigenetic gene regulation in macrophages by attenuating Jumonji histone demethylase activity.* Cytokine, 2011. **53**(2): p. 256-62.

542. Arents, G. and E.N. Moudrianakis, *The histone fold: a ubiquitous architectural motif utilized in DNA compaction and protein dimerization.* Proc Natl Acad Sci U S A, 1995. **92**(24): p. 11170-4.

543.   Ruiz-Carrillo, A. and J.L. Jorcano, *An octamer of core histones in solution: central role of the H3-H4 tetramer in the self-assembly.* Biochemistry, 1979. **18**(5): p. 760-8.

544.   Prutz, W.A., et al., *Reactions of nitrogen dioxide in aqueous model systems: oxidation of tyrosine units in peptides and proteins.* Arch Biochem Biophys, 1985. **243**(1): p. 125-34.

545.   Pfeiffer, S., K. Schmidt, and B. Mayer, *Dityrosine formation outcompetes tyrosine nitration at low steady-state concentrations of peroxynitrite. Implications for tyrosine modification by nitric oxide/superoxide in vivo.* J Biol Chem, 2000. **275**(9): p. 6346-52.

546.   Al-Hilaly, Y.K., et al., *The involvement of dityrosine crosslinking in α-synuclein assembly and deposition in Lewy Bodies in Parkinson's disease.* Scientific Reports, 2016. **6**: p. 39171.

547.   Souza, J.M., et al., *Dityrosine cross-linking promotes formation of stable alpha -synuclein polymers. Implication of nitrative and oxidative stress in the pathogenesis of neurodegenerative synucleinopathies.* J Biol Chem, 2000. **275**(24): p. 18344-9.

548.   Schildknecht, S., et al., *Oxidative and nitrative alpha-synuclein modifications and proteostatic stress: implications for disease mechanisms and interventions in synucleinopathies.* J Neurochem, 2013. **125**(4): p. 491-511.

549.   Kato, Y., et al., *Immunohistochemical detection of dityrosine in lipofuscin pigments in the aged human brain.* FEBS Lett, 1998. **439**(3): p. 231-4.

550.   Kato, Y., et al., *Immunochemical detection of protein dityrosine in atherosclerotic lesion of apo-E-deficient mice using a novel monoclonal antibody.* Biochem Biophys Res Commun, 2000. **275**(1): p. 11-5.

551.   Al-Hilaly, Y.K., et al., *A central role for dityrosine crosslinking of Amyloid-β in Alzheimer's disease.* Acta Neuropathol Commun, 2013. **1**: p. 83.

552.   Deeg, K.J., L. Katsikas, and W. Schnabel, *High energy radiation effects in single histones. I. Preparation of histones and irradiation of histone H2B.* Int J Radiat Biol Relat Stud Phys Chem Med, 1987. **51**(3): p. 527-40.

553.   Haqqani, A.S., J.F. Kelly, and H.C. Birnboim, *Selective nitration of histone tyrosine residues in vivo in mutatect tumors.* J Biol Chem, 2002. **277**(5): p. 3614-21.

554.   Lubos, E., et al., *Glutathione peroxidase-1 deficiency augments proinflammatory cytokine-induced redox signaling and human endothelial cell activation.* J Biol Chem, 2011. **286**(41): p. 35407-17.

555.   Bruggemann, M., et al., *Immunoglobulin heavy chain locus of the rat: striking homology to mouse antibody genes.* Proc Natl Acad Sci U S A, 1986. **83**(16): p. 6075-9.

556.   Sun, M., et al., *Deposition of advanced glycation end products (AGE) and expression of the receptor for AGE in cardiovascular tissue of the diabetic rat.* Int J Exp Pathol, 1998. **79**(4): p. 207-22.

557.   Wautier, J.L., et al., *Advanced glycation end products (AGEs) on the surface of diabetic erythrocytes bind to the vessel wall via a specific receptor inducing oxidant stress in the vasculature: a link between surface-associated AGEs and diabetic complications.* Proceedings of the National Academy of Sciences, 1994. **91**(16): p. 7742-7746.

558.   Daiber, A., et al., *Targeting vascular (endothelial) dysfunction.* Br J Pharmacol, 2016.

559.   Huang, J.S., et al., *Effects of nitric oxide and antioxidants on advanced glycation end products-induced hypertrophic growth in human renal tubular cells.* Toxicol Sci, 2009. **111**(1): p. 109-19.

560.   Tekabe, Y., et al., *Treatment effect with anti-RAGE F(ab')2 antibody improves hind limb angiogenesis and blood flow in Type 1 diabetic mice with left femoral artery ligation.* Vascular Medicine, 2015. **20**(3): p. 212-218.

561.   Li, G., et al., *Beneficial effects of a novel RAGE inhibitor on early diabetic retinopathy and tactile allodynia.* Mol Vis, 2011. **17**: p. 3156-65.

562.   Grauballe, M.B., et al., *Blockade of RAGE in Zucker obese rats with experimental periodontitis.* Journal of Periodontal Research, 2017. **52**(1): p. 97-106.

563.   Sanajou, D., et al., *Reduction of renal tubular injury with a RAGE inhibitor FPS-ZM1, valsartan and their combination in streptozotocin-induced diabetes in the rat.* Eur J Pharmacol, 2019. **842**: p. 40-48.

564.   Bassirat, M. and Z. Khalil, *Short- and long-term modulation of microvascular responses in streptozotocin-induced diabetic rats by glycosylated products.* Journal of Diabetes and its Complications, 2010. **24**(1): p. 64-72.

565.   Labazi, H., et al., *Novel RAGE Antagonist, FPS-ZM1, Reverses Mesenteric Arteriolar Remodeling in Type 2 Diabetic db/db Mice.* The FASEB Journal, 2017. **31**(1_supplement): p. 673.8-673.8.

566.   Oelze, M., et al., *The sodium-glucose co-transporter 2 inhibitor empagliflozin improves diabetes-induced vascular dysfunction in the streptozotocin diabetes rat model by interfering with oxidative stress and glucotoxicity.* PLoS One, 2014. **9**(11): p. e112394.

567.   Han, J.H., et al., *The beneficial effects of empagliflozin, an SGLT2 inhibitor, on atherosclerosis in ApoE−/− mice fed a western diet.* Diabetologia, 2017. **60**(2): p. 364-376.

568.   Andreadou, I., et al., *Empagliflozin Limits Myocardial Infarction in Vivo and Cell Death in Vitro: Role of STAT3, Mitochondria, and Redox Aspects.* Frontiers in Physiology, 2017. **8**.

569.   Zheng, S.L., et al., *Association Between Use of Sodium-Glucose Cotransporter 2 Inhibitors, Glucagon-like Peptide 1 Agonists, and Dipeptidyl Peptidase 4 Inhibitors With All-Cause Mortality in Patients With Type 2 Diabetes: A Systematic Review and Meta-analysis.* Jama, 2018. **319**(15): p. 1580-1591.

570.   Brodeur, M.R., et al., *Reduction of advanced-glycation end products levels and inhibition of RAGE signaling decreases rat vascular calcification induced by diabetes.* PLoS One, 2014. **9**(1): p. e85922.

571.   Jud, P. and H. Sourij, *Therapeutic options to reduce advanced glycation end products in patients with diabetes mellitus: A review.* Diabetes Res Clin Pract, 2018. **148**: p. 54-63.

572.   Wang, H., et al., *Targeted inhibition of RAGE reduces amyloid-beta influx across the blood-brain barrier and improves cognitive deficits in db/db mice.* Neuropharmacology, 2018. **131**: p. 143-153.

573.   Hong, Y., et al., *Effects of RAGE-Specific Inhibitor FPS-ZM1 on Amyloid-beta Metabolism and AGEs-Induced Inflammation and Oxidative Stress in Rat Hippocampus.* Neurochem Res, 2016. **41**(5): p. 1192-9.

574.   Deane, R., et al., *A multimodal RAGE-specific inhibitor reduces amyloid β-mediated brain disorder in a mouse model of Alzheimer disease.* The Journal of clinical investigation, 2012. **122**(4): p. 1377-1392.

575.   Bongarzone, S., et al., *Targeting the Receptor for Advanced Glycation Endproducts (RAGE): A Medicinal Chemistry Perspective.* Journal of Medicinal Chemistry, 2017. **60**(17): p. 7213-7232.

576.   Li, J. and A.M. Schmidt, *Characterization and functional analysis of the promoter of RAGE, the receptor for advanced glycation end products.* J Biol Chem, 1997. **272**(26): p. 16498-506.

577.   Yamagishi, S., et al., *Receptor for advanced glycation end products (RAGE): a novel therapeutic target for diabetic vascular complication.* Curr Pharm Des, 2008. **14**(5): p. 487-95.

578.   Chawla, D., et al., *Role of advanced glycation end product (AGE)-induced receptor (RAGE) expression in diabetic vascular complications.* Microvasc Res, 2014. **95**: p. 1-6.

579.   Reddy, M.A., et al., *Losartan reverses permissive epigenetic changes in renal glomeruli of diabetic db/db mice.* Kidney international, 2014. **85**(2): p. 362-373.

580.   Fish, J.E., et al., *The expression of endothelial nitric-oxide synthase is controlled by a cell-specific histone code.* J Biol Chem, 2005. **280**(26): p. 24824-38.

581.   Ohtani, K., et al., *Epigenetic regulation of endothelial lineage committed genes in pro-angiogenic hematopoietic and endothelial progenitor cells.* Circ Res, 2011. **109**(11): p. 1219-29.

582.   Sha, J., et al., *Interferon gamma (IFN-γ) disrupts energy expenditure and metabolic homeostasis by suppressing SIRT1 transcription.* Nucleic Acids Research, 2011. **40**(4): p. 1609-1620.

583.   Yıldırım-Buharalıoğlu, G., et al., *Regulation of Epigenetic Modifiers, Including KDM6B, by Interferon-γ and Interleukin-4 in Human Macrophages.* Frontiers in immunology, 2017. **8**: p. 92-92.

584.   Qiao, Y., et al., *IFN-γ Induces Histone 3 Lysine 27 Trimethylation in a Small Subset of Promoters to Stably Silence Gene Expression in Human Macrophages.* Cell reports, 2016. **16**(12): p. 3121-3129.

585.   Jin, X., et al., *Advanced Glycation End Products Enhance Macrophages Polarization into M1 Phenotype through Activating RAGE/NF-κB Pathway.* BioMed Research International, 2015. **2015**: p. 12.

586.   Ahmed, M., M.P.J. de Winther, and J. Van den Bossche, *Epigenetic mechanisms of macrophage activation in type 2 diabetes.* Immunobiology, 2017. **222**(10): p. 937-943.

587.   Kimball, A.S., et al., *The Histone Methyltransferase MLL1 Directs Macrophage-Mediated Inflammation in Wound Healing and Is Altered in a Murine Model of Obesity and Type 2 Diabetes.* Diabetes, 2017. **66**(9): p. 2459-2471.

588.   Arguelles, A.O., et al., *Are epigenetic drugs for diabetes and obesity at our door step?* Drug Discov Today, 2016. **21**(3): p. 499-509.

589.   Khan, S. and G.B. Jena, *Protective role of sodium butyrate, a HDAC inhibitor on beta-cell proliferation, function and glucose homeostasis through modulation of p38/ERK MAPK and apoptotic pathways: Study in juvenile diabetic rat.* Chemico-Biological Interactions, 2014. **213**: p. 1-12.

590. Christensen, D.P., et al., *Histone deacetylase (HDAC) inhibition as a novel treatment for diabetes mellitus.* Molecular Medicine, 2011. **17**(5-6): p. 378-390.

591. Ye, J., *Improving Insulin Sensitivity With HDAC Inhibitor.* Diabetes, 2013. **62**(3): p. 685-687.

592. Chuengsamarn, S., et al., *Curcumin Extract for Prevention of Type 2 Diabetes.* Diabetes Care, 2012. **35**(11): p. 2121-2127.

593. Binda, C., et al., *Biochemical, Structural, and Biological Evaluation of Tranylcypromine Derivatives as Inhibitors of Histone Demethylases LSD1 and LSD2.* Journal of the American Chemical Society, 2010. **132**(19): p. 6827-6833.

594. Liu, K., et al., *Effect of resveratrol on glucose control and insulin sensitivity: a meta-analysis of 11 randomized controlled trials.* The American Journal of Clinical Nutrition, 2014. **99**(6): p. 1510-1519.

595. Cesselli, D., et al., *Oxidative stress-mediated cardiac cell death is a major determinant of ventricular dysfunction and failure in dog dilated cardiomyopathy.* Circ Res, 2001. **89**(3): p. 279-86.

596. Dhalla, A.K., M.F. Hill, and P.K. Singal, *Role of oxidative stress in transition of hypertrophy to heart failure.* J Am Coll Cardiol, 1996. **28**(2): p. 506-14.

597. Kwon, S.H., et al., *H(2)O(2) regulates cardiac myocyte phenotype via concentration-dependent activation of distinct kinase pathways.* J Mol Cell Cardiol, 2003. **35**(6): p. 615-21.

598. Sawyer, D.B., et al., *Role of oxidative stress in myocardial hypertrophy and failure.* J Mol Cell Cardiol, 2002. **34**(4): p. 379-88.

599. Antunes, F. and E. Cadenas, *Cellular titration of apoptosis with steady state concentrations of H(2)O(2): submicromolar levels of H(2)O(2) induce apoptosis through Fenton chemistry independent of the cellular thiol state.* Free Radic Biol Med, 2001. **30**(9): p. 1008-18.

600. Chen, Q.M., et al., *Hydrogen peroxide dose dependent induction of cell death or hypertrophy in cardiomyocytes.* Arch Biochem Biophys, 2000. **373**(1): p. 242-8.

601. Aikawa, R., et al., *Oxidative stress activates extracellular signal-regulated kinases through Src and Ras in cultured cardiac myocytes of neonatal rats.* J Clin Invest, 1997. **100**(7): p. 1813-21.

602. Turner, N.A., et al., *Oxidative stress induces DNA fragmentation and caspase activation via the c-Jun NH2-terminal kinase pathway in H9c2 cardiac muscle cells.* J Mol Cell Cardiol, 1998. **30**(9): p. 1789-801.

603. Aoki, H., et al., *Direct activation of mitochondrial apoptosis machinery by c-Jun N-terminal kinase in adult cardiac myocytes.* J Biol Chem, 2002. **277**(12): p. 10244-50.

604. Li, Y., et al., *Propofol protects against hydrogen peroxide-induced apoptosis in cardiac H9c2 cells is associated with the NF-kappaB activation and PUMA expression.* Eur Rev Med Pharmacol Sci, 2014. **18**(10): p. 1517-24.

605. Thorn, C.F., et al., *Doxorubicin pathways: pharmacodynamics and adverse effects.* Pharmacogenet Genomics, 2011. **21**(7): p. 440-6.

606. Zhao, L. and B. Zhang, *Doxorubicin induces cardiotoxicity through upregulation of death receptors mediated apoptosis in cardiomyocytes.* Sci Rep, 2017. **7**: p. 44735.

607. Greaves, P., *7 - Cardiovascular System*, in *Histopathology of Preclinical Toxicity Studies (Third edition)*, P. Greaves, Editor. 2007, Academic Press: New York. p. 270-333.

608. Arena, E., et al., *Repair kinetics of DNA, RNA and proteins in the tissues of mice treated with doxorubicin.* Arzneimittelforschung, 1979. **29**(6): p. 901-2.

609. Bristow, M.R., et al., *Acute and chronic cardiovascular effects of doxorubicin in the dog: the cardiovascular pharmacology of drug-induced histamine release.* J Cardiovasc Pharmacol, 1980. **2**(5): p. 487-515.

610. Tong, J., P.K. Ganguly, and P.K. Singal, *Myocardial adrenergic changes at two stages of heart failure due to adriamycin treatment in rats.* Am J Physiol, 1991. **260**(3 Pt 2): p. H909-16.

611. Vasquez-Vivar, J., et al., *Endothelial nitric oxide synthase-dependent superoxide generation from adriamycin.* Biochemistry, 1997. **36**(38): p. 11293-7.

612. Kalivendi, S.V., et al., *Doxorubicin-induced apoptosis is associated with increased transcription of endothelial nitric-oxide synthase. Effect of antiapoptotic antioxidants and calcium.* J Biol Chem, 2001. **276**(50): p. 47266-76.

613. Mukhopadhyay, P., et al., *Role of superoxide, nitric oxide, and peroxynitrite in doxorubicin-induced cell death in vivo and in vitro.* Am J Physiol Heart Circ Physiol, 2009. **296**(5): p. H1466-83.

614. Aldieri, E., et al., *Doxorubicin induces an increase of nitric oxide synthesis in rat cardiac cells that is inhibited by iron supplementation.* Toxicol Appl Pharmacol, 2002. **185**(2): p. 85-90.

615.	Singal, P.K. and G.N. Pierce, *Adriamycin stimulates low-affinity Ca2+ binding and lipid peroxidation but depresses myocardial function.* Am J Physiol, 1986. **250**(3 Pt 2): p. H419-25.

616.	Julicher, R.H., et al., *The role of lipid peroxidation in acute doxorubicin-induced cardiotoxicity as studied in rat isolated heart.* J Pharm Pharmacol, 1986. **38**(4): p. 277-82.

617.	Benchekroun, M.N. and J. Robert, *Measurement of doxorubicin-induced lipid peroxidation under the conditions that determine cytotoxicity in cultured tumor cells.* Anal Biochem, 1992. **201**(2): p. 326-30.

618.	Singal, P.K. and N. Iliskovic, *Doxorubicin-induced cardiomyopathy.* N Engl J Med, 1998. **339**(13): p. 900-5.

619.	Volkova, M. and R. Russell, 3rd, *Anthracycline cardiotoxicity: prevalence, pathogenesis and treatment.* Curr Cardiol Rev, 2011. **7**(4): p. 214-20.

620.	Akolkar, G., et al., *Vitamin C mitigates oxidative/nitrosative stress and inflammation in doxorubicin-induced cardiomyopathy.* Am J Physiol Heart Circ Physiol, 2017. **313**(4): p. H795-H809.

621.	Lipshultz, S.E., et al., *The effect of dexrazoxane on myocardial injury in doxorubicin-treated children with acute lymphoblastic leukemia.* N Engl J Med, 2004. **351**(2): p. 145-53.

622.	Rezk, Y.A., et al., *Use of resveratrol to improve the effectiveness of cisplatin and doxorubicin: study in human gynecologic cancer cell lines and in rodent heart.* Am J Obstet Gynecol, 2006. **194**(5): p. e23-6.

623.	Singal, P.K., et al., *Combination therapy with probucol prevents adriamycin-induced cardiomyopathy.* J Mol Cell Cardiol, 1995. **27**(4): p. 1055-63.

624.	Ladas, E.J., et al., *Antioxidants and cancer therapy: a systematic review.* J Clin Oncol, 2004. **22**(3): p. 517-28.

625.	Preyat, N. and O. Leo, *Sirtuin deacylases: a molecular link between metabolism and immunity.* J Leukoc Biol, 2013. **93**(5): p. 669-80.

626.	Planavila, A., et al., *Dilated cardiomyopathy and mitochondrial dysfunction in Sirt1-deficient mice: a role for Sirt1-Mef2 in adult heart.* J Mol Cell Cardiol, 2012. **53**(4): p. 521-31.

627.	Ma, S., et al., *SIRT1 Activation by Resveratrol Alleviates Cardiac Dysfunction via Mitochondrial Regulation in Diabetic Cardiomyopathy Mice.* Oxid Med Cell Longev, 2017. **2017**: p. 4602715.

628.	Canto, C., A.A. Sauve, and P. Bai, *Crosstalk between poly(ADP-ribose) polymerase and sirtuin enzymes.* Mol Aspects Med, 2013. **34**(6): p. 1168-201.

629.	Furukawa, A., et al., *H2O2 accelerates cellular senescence by accumulation of acetylated p53 via decrease in the function of SIRT1 by NAD+ depletion.* Cell Physiol Biochem, 2007. **20**(1-4): p. 45-54.

630.	Ruan, Y., et al., *SIRT1 suppresses doxorubicin-induced cardiotoxicity by regulating the oxidative stress and p38MAPK pathways.* Cell Physiol Biochem, 2015. **35**(3): p. 1116-24.

631.	Deota, S., et al., *Identification of a Tissue-Restricted Isoform of SIRT1 Defines a Regulatory Domain that Encodes Specificity.* Cell Rep, 2017. **18**(13): p. 3069-3077.

632.	Howitz, K.T., et al., *Small molecule activators of sirtuins extend Saccharomyces cerevisiae lifespan.* Nature, 2003. **425**(6954): p. 191-6.

633.	Lagouge, M., et al., *Resveratrol improves mitochondrial function and protects against metabolic disease by activating SIRT1 and PGC-1alpha.* Cell, 2006. **127**(6): p. 1109-22.

634.	Liu, M.H., et al., *Resveratrol inhibits doxorubicin-induced cardiotoxicity via sirtuin 1 activation in H9c2 cardiomyocytes.* Exp Ther Med, 2016. **12**(2): p. 1113-1118.

635.	Danz, E.D., et al., *Resveratrol prevents doxorubicin cardiotoxicity through mitochondrial stabilization and the Sirt1 pathway.* Free Radic Biol Med, 2009. **46**(12): p. 1589-97.

636.	Lou, Y., et al., *Resveratrol prevents doxorubicin-induced cardiotoxicity in H9c2 cells through the inhibition of endoplasmic reticulum stress and the activation of the Sirt1 pathway.* Int J Mol Med, 2015. **36**(3): p. 873-80.

637.	Oktem, G., et al., *Resveratrol attenuates doxorubicin-induced cellular damage by modulating nitric oxide and apoptosis.* Exp Toxicol Pathol, 2012. **64**(5): p. 471-9.

638.	Zhang, C., et al., *Resveratrol attenuates doxorubicin-induced cardiomyocyte apoptosis in mice through SIRT1-mediated deacetylation of p53.* Cardiovasc Res, 2011. **90**(3): p. 538-45.

639.	McKinsey, T.A. and E.N. Olson, *Cardiac histone acetylation--therapeutic opportunities abound.* Trends Genet, 2004. **20**(4): p. 206-13.

640.	Kee, H.J., et al., *Activation of histone deacetylase 2 by inducible heat shock protein 70 in cardiac hypertrophy.* Circ Res, 2008. **103**(11): p. 1259-69.

641. Eom, G.H. and H. Kook, *Role of histone deacetylase 2 and its posttranslational modifications in cardiac hypertrophy.* BMB Rep, 2015. **48**(3): p. 131-8.

642. Kook, H., et al., *Cardiac hypertrophy and histone deacetylase-dependent transcriptional repression mediated by the atypical homeodomain protein Hop.* J Clin Invest, 2003. **112**(6): p. 863-71.

643. Abend, A. and I. Kehat, *Histone deacetylases as therapeutic targets--from cancer to cardiac disease.* Pharmacol Ther, 2015. **147**: p. 55-62.

644. Zhang, Q.J. and Z.P. Liu, *Histone methylations in heart development, congenital and adult heart diseases.* Epigenomics, 2015. **7**(2): p. 321-30.

645. Dirkx, E., P.A. da Costa Martins, and L.J. De Windt, *Regulation of fetal gene expression in heart failure.* Biochim Biophys Acta, 2013. **1832**(12): p. 2414-24.

646. Zhang, Q.J., et al., *The histone trimethyllysine demethylase JMJD2A promotes cardiac hypertrophy in response to hypertrophic stimuli in mice.* J Clin Invest, 2011. **121**(6): p. 2447-56.

647. He, C., et al., *Cu,Zn-Superoxide Dismutase-Mediated Redox Regulation of Jumonji Domain Containing 3 Modulates Macrophage Polarization and Pulmonary Fibrosis.* Am J Respir Cell Mol Biol, 2016. **55**(1): p. 58-71.

648. Stein, A.B., et al., *Loss of H3K4 methylation destabilizes gene expression patterns and physiological functions in adult murine cardiomyocytes.* J Clin Invest, 2011. **121**(7): p. 2641-50.

649. Pojoga, L.H., et al., *Histone demethylase LSD1 deficiency during high-salt diet is associated with enhanced vascular contraction, altered NO-cGMP relaxation pathway, and hypertension.* Am J Physiol Heart Circ Physiol, 2011. **301**(5): p. H1862-71.

650. Paneni, F., et al., *Adverse epigenetic signatures by histone methyltransferase Set7 contribute to vascular dysfunction in patients with type 2 diabetes mellitus.* Circ Cardiovasc Genet, 2015. **8**(1): p. 150-8.

651. Okabe, J., et al., *Distinguishing hyperglycemic changes by Set7 in vascular endothelial cells.* Circ Res, 2012. **110**(8): p. 1067-76.

652. Li, Y., et al., *Role of the histone H3 lysine 4 methyltransferase, SET7/9, in the regulation of NF-kappaB-dependent inflammatory genes. Relevance to diabetes and inflammation.* J Biol Chem, 2008. **283**(39): p. 26771-81.

653. Dang, Y., et al., *Inhibition of SETD7 protects cardiomyocytes against hypoxia/reoxygenation-induced injury through regulating Keap1/Nrf2 signaling.* Biomedicine & Pharmacotherapy, 2018. **106**: p. 842-849.

654. Lezina, L., et al., *KMT Set7/9 affects genotoxic stress response via the Mdm2 axis.* Oncotarget, 2015. **6**(28): p. 25843-55.

655. Kurash, J.K., et al., *Methylation of p53 by Set7/9 mediates p53 acetylation and activity in vivo.* Mol Cell, 2008. **29**(3): p. 392-400.

656. Borlak, J. and T. Thum, *Hallmarks of ion channel gene expression in end-stage heart failure.* FASEB J, 2003. **17**(12): p. 1592-608.

657. Liu, T., et al., *Master redox regulator Trx1 upregulates SMYD1 & modulates lysine methylation.* Biochim Biophys Acta, 2015. **1854**(12): p. 1816-22.

658. Russo, S., et al., *Effects of S-adenosylmethionine (SAMe) on doxorubicin-induced cardiotoxicity in the rat.* J Med, 1994. **25**(1-2): p. 65-89.

659. Caito, S., et al., *SIRT1 is a redox-sensitive deacetylase that is post-translationally modified by oxidants and carbonyl stress.* FASEB J, 2010. **24**(9): p. 3145-59.

660. Kornberg, M.D., et al., *GAPDH mediates nitrosylation of nuclear proteins.* Nat Cell Biol, 2010. **12**(11): p. 1094-100.

661. Gu, C., et al., *Impaired cardiac SIRT1 activity by carbonyl stress contributes to aging-related ischemic intolerance.* PLoS One, 2013. **8**(9): p. e74050.

662. Fritz, K.S., et al., *4-Hydroxynonenal inhibits SIRT3 via thiol-specific modification.* Chem Res Toxicol, 2011. **24**(5): p. 651-62.

663. Ito, K., et al., *Oxidative stress reduces histone deacetylase 2 activity and enhances IL-8 gene expression: role of tyrosine nitration.* Biochem Biophys Res Commun, 2004. **315**(1): p. 240-5.

664. Galligan, J.J. and L.J. Marnett, *Histone Adduction and Its Functional Impact on Epigenetics.* Chem Res Toxicol, 2017. **30**(1): p. 376-387.

665. Munkanatta Godage, D.N.P., et al., *SMYD2 glutathionylation contributes to degradation of sarcomeric proteins.* Nat Commun, 2018. **9**(1): p. 4341.

666. Nguyen, A.T., et al., *DOT1L regulates dystrophin expression and is critical for cardiac function.* Genes Dev, 2011. **25**(3): p. 263-74.

667. Kanao, K., et al., *Decreased acetylation of histone H3 in renal cell carcinoma: a potential target of histone deacetylase inhibitors.* J Urol, 2008. **180**(3): p. 1131-6.

668. Barlesi, F., et al., *Global histone modifications predict prognosis of resected non small-cell lung cancer.* J Clin Oncol, 2007. **25**(28): p. 4358-64.

669. Elsheikh, S.E., et al., *Global histone modifications in breast cancer correlate with tumor phenotypes, prognostic factors, and patient outcome.* Cancer Res, 2009. **69**(9): p. 3802-9.

670. Mosashvilli, D., et al., *Global histone acetylation levels: prognostic relevance in patients with renal cell carcinoma.* Cancer Sci, 2010. **101**(12): p. 2664-9.

671. Wang, Y., et al., *Dysregulation of histone acetyltransferases and deacetylases in cardiovascular diseases.* Oxid Med Cell Longev, 2014. **2014**: p. 641979.

672. Pang, B., et al., *Drug-induced histone eviction from open chromatin contributes to the chemotherapeutic effects of doxorubicin.* Nat Commun, 2013. **4**: p. 1908.

673. Montero, D., et al., *Effect of antioxidant vitamin supplementation on endothelial function in type 2 diabetes mellitus: a systematic review and meta-analysis of randomized controlled trials.* Obes Rev, 2014. **15**(2): p. 107-16.

674. Rafieian-Kopaie, M. and H. Nasri, *On the Occasion of World Cancer Day 2015; the Possibility of Cancer Prevention or Treatment with Antioxidants: The Ongoing Cancer Prevention Researches.* Int J Prev Med, 2015. **6**: p. 108.

675. Galasko, D.R., et al., *Antioxidants for Alzheimer disease: a randomized clinical trial with cerebrospinal fluid biomarker measures.* Arch Neurol, 2012. **69**(7): p. 836-41.

676. Jin, H., et al., *Mitochondria-targeted antioxidants for treatment of Parkinson's disease: preclinical and clinical outcomes.* Biochim Biophys Acta, 2014. **1842**(8): p. 1282-94.

677. Lee, I.M., et al., *Vitamin E in the primary prevention of cardiovascular disease and cancer: the Women's Health Study: a randomized controlled trial.* JAMA, 2005. **294**(1): p. 56-65.

678. Burnette, W.N., *Western blotting : remembrance of past things.* Methods Mol Biol, 2009. **536**: p. 5-8.

679. Ghosh, R., J.E. Gilda, and A.V. Gomes, *The necessity of and strategies for improving confidence in the accuracy of western blots.* Expert Rev Proteomics, 2014. **11**(5): p. 549-60.

680. McDonough, A.A., et al., *Considerations when quantitating protein abundance by immunoblot.* Am J Physiol Cell Physiol, 2015. **308**(6): p. C426-33.

681. Dittmer, A. and J. Dittmer, *Beta-actin is not a reliable loading control in Western blot analysis.* Electrophoresis, 2006. **27**(14): p. 2844-5.

682. Bell, G., *Quantifying western blots: none more black.* BMC Biol, 2016. **14**(1): p. 116.

683. Schmittgen, T.D. and B.A. Zakrajsek, *Effect of experimental treatment on housekeeping gene expression: validation by real-time, quantitative RT-PCR.* J Biochem Biophys Methods, 2000. **46**(1-2): p. 69-81.

684. Nie, X., et al., *An appropriate loading control for western blot analysis in animal models of myocardial ischemic infarction.* Biochem Biophys Rep, 2017. **12**: p. 108-113.

685. P., M.C., *Tubulin or Not Tubulin: Heading Toward Total Protein Staining as Loading Control in Western Blots.* PROTEOMICS, 2017. **17**(20): p. 1600189.

686. Gilda, J.E. and A.V. Gomes, *Stain-Free total protein staining is a superior loading control to beta-actin for Western blots.* Anal Biochem, 2013. **440**(2): p. 186-8.

10 Appendix

Abbreviations

$^\bullet$NO	Nitric oxide
$^\bullet$O$_2^-$	Superoxide anion radical
2-HE	2-hydroxyethidium
2-OG	2-oxoglutarate (α-ketoglutarate)
3-NT	3-nitrotyrosine
4-HNE	4-hydroxynonenal
5'-UTR	5'-untranslated region
5caC	5-carboxylcytosine
5fC	5-formylcytosine
5hmC	5-hydroxymethylcytosine
5mC	5-methylcytosine
8-oxodG	8-oxo-2'-deoxyguanosine
ACE	Angiotensin-converting enzyme
Acetyl-CoA	Acetyl-Coenzyme A
ADMA	Asymmetric dimethylarginine
AGE	Advanced glycation end products
ALDH	Aldehyde dehydrogenase
ANP	Atrial natriuretic peptide
APS	Ammonium persulfate
ATP	Adenosine triphosphate
Bcl-2	B-cell lymphoma 2
BER	Base excision repair
BH$_4$	(6R-)5,6,7,8-tetrahydrobiopterin
BNP	Brain natriuretic peptide
bp	Base pair
BSA	Bovine serum albumin
CaM	Calmodulin
CAT	Catalase
cGMP	Cyclic guanosine monophosphate
CHF	Congestive heart failure
ChIP	Chromatin immunoprecipitation
COX	Cyclooxygenase
CpG	Cytosine-guanosine dinucleotide (5'-C-phosphate-G-3')
CRP	C-reactive protein
Ct	Cycle threshold
Ctrl	Control
Cu	Copper
CuSO$_4$	Copper sulfate
CVD	Cardiovascular disease
CYP450	Cytochrome P450
DAG	Diacylglycerol
DEANO	Diethylamine NONOate
DETANO	Diethylenetriamine NONOate

DHAP	Dihydroxyacetone phosphate
DHE	Dihydroethidium
DHFR	Dihydrofolate reductase
DM	Diabetes mellitus
DMEM	Dulbecco's modified Eagle's medium
DMP	Dimethyl pimelimidate
DMPO	5,5-Dimethyl-1-Pyrroline N-Oxide
DNA	Deoxyribonucleic acid
DNMT	DNA methyltransferase
DOPA	3,4-dihydroxyphenylalanine
DOT1-L	Disruptor of telomeric silencing 1-like
Dox	Doxorubicin
DPP-4	Dipeptidyl peptidase-4
DSB	DNA double-strand break
dsDNA	Double strand DNA
DT	Dityrosine
DTT	Dithiothreitol
Duox	Dual oxidase
E^+	Ethidium
EC	Extracellular
ECE-1	Endothelin-converting enzyme
ECL	Enhanced chemiluminescence
ECM	Extracellular matrix
EDRF	Endothelium-derived relaxing factor
EDTA	Ethylene diamine tetraacetic acid
EGTA	Ethylene glycol tetraacetic acid
EMPA	Empagliflozin
eNOS	Endothelial nitric oxide synthase (type 3)
EPR	Electron paramagnetic resonance
ER	Endoplasmatic reticulum
ESR	Electron-spin resonance
ET-1	Endothelin-1
Ex./Em.	Excitation/Emission
FAD	Flavin adenine dinucleotide
FBS	Fetal bovine serum
FCS	Fetal calf serum
FDA	US Food and Drug Administration
$FeSO_4$	Iron sulfate
FMN	Flavin mononucleotide
FOXO	Forkhead box O
GAPDH	Glyceraldehyde 3-phosphate dehydrogenase
GCH-1	GTP-cyclohydrolase-1
GLP-1	Glucagon-like peptide-1
GPx	Glutathione peroxidase
GR	Glutathione reductase
GSH	Glutathione
GSNO	S-nitroso-glutathione
GSSG	Glutathione disulfide

GST	Glutathione S-transferase
GTP	Guanosine triphosphate
h	Hour
H/R	Hypoxia/reoxygenation
H_2O_2	Hydrogen peroxide
H3/ H4	Histone 3/ Histone 4
$H3K_xme_y$	Histone 3 methylated y-times at lysine x
HAEC	Human aortic endothelial cell
HAT	Histone acetyltransferase
HCAEC	Human coronary artery endothelial cells
HCl	Hydrogen chloride
HDAC	Histone deacetylase
HG	High glucose/ Hyperglycemia
HGEC	Human glomerular endothelial cells
HKP	Housekeeping protein
HMT	Histone methyltransferase
HMVEC	Human dermal microvasculature endothelial cell
HO-1	Heme oxygenase-1
HPLC	High performance liquid chromatography
HRP	Horse radish peroxidase
HUVEC	Human umbilical vein endothelial cells
ICDH	Isocitrate dehydrogenase
IFN-γ	Interferon-γ
IgG	Immunoglobulin G
IL-1β	Interleukin-1beta
iNOS (NOS2)	Inducible nitric oxide synthase
IOD	Integrated optical density
IP	Immunoprecipitation
JmjC	Jumonji C containing
JNK	c-Jun N-terminal kinase
kDa	Kilodalton
KDM	Lysine (K)-specific histone demethylase
KMT	Lysine (K) methyltransferase
KNO_2	Potassium nitrite
KO	Knock-out
LG	Low glucose
lncRNA	Long non-coding ribonucleic acid
LOX	Lipoxygenase
LPS	Lipopolysaccharide
LSD	Lysine-specific demethylase
MAPK	p38 mitogen-activated protein kinase
MDA	Malondialdehyde
METC	Mitochondrial electron transport chain
min	Minute
miRNA	Micro ribonucleic acid
Mito-HE	2-hydroxy-mito-ethidium
Mn	Manganese
mRNA	Messenger ribonucleic acid

MS	Mass spectrometry
NADH	Nicotinamide adenine dinucleotide
NADPH	Nicotinamide adenine dinucleotide phosphate
NaOH	Sodium hydroxide
ncRNA	Non-coding ribonucleic acid
NER	Nucleotide excision repair
NFkB	Nuclear factor kappa-light-chain-enhancer of activated B cells
NG	Normoglycemia
NMDA	N-methyl-D-aspartate
NMR	Nuclear magnetic resonance
nNOS (NOS1)	Neuronal nitric oxide synthase (type 1)
NO ($^\bullet$NO)	Nitric oxide
NOS1 (nNOS)	Neuronal nitric oxide synthase (type 1)
NOS2 (iNOS)	Inducible nitric oxide synthase
NOS3 (eNOS)	Endothelial nitric oxide synthase (type 3)
NOX	NADPH oxidase
Nrf2	Nuclear factor (erythroid-derived 2)-like 2
nt	nucleotide
O-GlcNAc	O-linked N-acetyl glucosamine
ONOO$^-$	Peroxynitrite
p.o.	Per os (oral administration)
p38 MAPK	p38 mitogen-activated protein kinases
PAGE	Polyacrylamide gel electrophoresis
PBS	Phosphate buffered saline
PBS-T	Phosphate-buffered saline with 0.1% Tween 20
PCR	Polymerase chain reaction
PenStrep	Penicillin-Streptomycin
PGC-1α	Peroxisome proliferator-activated receptor gamma coactivator 1α
piRNA	Piwi-interacting ribonucleic acid
PKC	Protein kinase C
PON	Peroxynitrite
PRMT	Protein arginine methyltransferase
Prx	Peroxiredoxin
PSNO	Protein-S-nitrosothiol
pThr495	Phosphorylated threonine 495
PTM	Posttranslational modification
qPCR	Quantitative polymerase chain reaction
RAGE	Receptor for advanced glycation end products
Rel. IOD	Relative integrated optical density
RNA	Ribonucleic acid
RONS	Reactive oxygen and nitrogen species
ROS	Reactive oxygen species
RT	Room temperature
SAH	S-adenosyl homocysteine
SAM	S-adenosyl methionine
SDS	Sodium dodecyl sulfate
SDS-PAGE	Sodium dodecyl sulfate – polyacrylamide gel electrophoresis
SEM	Standard error of the mean

SET	Suppressor of variegation, enhancer of zeste, trithorax
Set7	SET Domain-Containing Protein 7
SGLT2i	Sodium-glucose co-transporter 2 inhibitor
Sin-1	3-Morpholino-sydnonimine
siRNA	Short interfering ribonucleic acid
Sirt1	Sirtuin 1
SITA	Sitagliptin
skNAC	Skeletal nascent polypeptide-associated complex
SMC	Smooth muscle cell
SMYD1	SET and MYND domain-containing protein 1
SN	Supernatant
SNAP	S-nitroso-N-acetylpenicillamine
SNP	Sodium nitroprusside
SNVP	S-nitroso-N-valerylpenicillamine
SOD	Superoxide dismutase
SPENO	Spermine-NONOate
S-S	Disulfide bond
STZ	Streptozotocin
T2DM	Type 2 diabetes mellitus
TBS	Tris-buffered saline
TBS-T	Tris-buffered saline with 0.1% Tween 20
TDG	Thymine-DNA glycosylase
TEA	Triethanolamine
TET	Ten eleven translocation
THF	Tetrahydrofolate
Thr	Threonine
Top2α	DNA topoisomerase 2-alpha
Trx	Thioredoxin
TrxR	Thioredoxin reductase
TSS	Transcription start site
Tyr	Tyrosine
TZD	Thiazolidinedione
VASP	Vasodilator stimulated phosphoprotein
VPA	Valproic acid
WB	Western blot
XO	Xanthine oxidase
ZDF	Zucker diabetic fatty
Zn	Zinc
β-ME	β-mercaptoethanol

Histone 3 sequence (human, mouse, rat)

H3.1 (HIST1H3A)[*]

Mass: 15,404 kDa

```
          10          20          30          40          50
(M)ARTKQTARK  STGGKAPRKQ  LATKAARKSA  PATGGVKKPH  RYRPGTVALR
          60          70          80          90         100
EIRRYQKSTE    LLIRKLPFQR  LVREIAQDFK  TDLRFQSSAV  MALQEACEAY
         110         120         130
LVGLFEDTNL    CAIHAKRVTI  MPKDIQLARR  IRGERA
```

Histone 4 sequence (human, mouse, rat)

H4 (HIST1H4A)[*]

Mass: 11,367 kDa

```
          10          20          30          40          50
(M)SGRGKGGKG  LGKGGAKRHR  KVLRDNIQGI  TKPAIRRLAR  RGGVKRISGL
          60          70          80          90         100
IYEETRGVLK    VFLENVIRDA  VTYTEHAKRK  TVTAMDVVYA  LKRQGRTLYG  FGG
```

* Source: UniProt Consortium, T., *UniProt: the universal protein knowledgebase.* Nucleic Acids Research, 2018.

Mass spectrometry analysis

H3-IP from kidney lysate, GPx-1$^{-/-}$ young and old, 27 kDa band & 53 kDa band

1) GPx-1$^{-/-}$, 2mo, 27 kDa

Protein Group	Protein ID	Accession	-10lgP	Coverage (%)	#Peptides	#Unique	PTM	Avg. Mass	Description
30	190	P60710|ACTB_MOUSE	81.63	10	3	3	Oxidation (M); Hydroxylation	41737	Actin cytoplasmic 1 OS=Mus musculus GN=Actb PE=1 SV=1
30	189	P63260|ACTG_MOUSE	81.63	10	3	3	Oxidation (M); Hydroxylation	41793	Actin cytoplasmic 2 OS=Mus musculus GN=Actg1 PE=1 SV=1
147	1817	Q91VR2|ATPG_MOUSE	46.58	4	1	1		32886	ATP synthase subunit gamma mitochondrial OS=Mus musculus GN=Atp5c1 PE=1 SV=1
76	1858	Q69Z23|DYH17_MOUSE	21.51	0	1	1	Deamidation (N)	511609	Dynein heavy chain 17 axonemal OS=Mus musculus GN=Dnah17 PE=1 SV=2
2	1764	P00924|ENO1_YEAST	235.99	59	33	9	Oxidation (M); Deamidation (N); Deamidation (NQ); Formylation; Formylation (Protein N-term); 2 more	46802	Enolase 1 OS=Saccharomyces cerevisiae GN=ENO1 PE=1 SV=2
3	1765	P00925|ENO2_YEAST	228.28	51	29	5	Oxidation (M); Deamidation (N); Deamidation (NQ); Formylation; Formylation (Protein N-term); 2 more	46914	Enolase 2 OS=Saccharomyces cerevisiae GN=ENO2 PE=1 SV=2
97	1825	P22752|H2A1_MOUSE	38.97	7	1	1		14135	Histone H2A type 1 OS=Mus musculus GN=Hist1h2ab PE=1 SV=3
97	1829	Q8CGP5|H2A1F_MOUSE	38.97	7	1	1		14162	Histone H2A type 1-F OS=Mus musculus GN=Hist1h2af PE=1 SV=3
97	1820	Q8CGP6|H2A1H_MOUSE	38.97	7	1	1		13950	Histone H2A type 1-H OS=Mus musculus GN=Hist1h2ah PE=1 SV=3
97	1826	Q8CGP7|H2A1K_MOUSE	38.97	7	1	1		14150	Histone H2A type 1-K OS=Mus musculus GN=Hist1h2ak PE=1 SV=3
97	1827	Q6GSS7|H2A2A_MOUSE	38.97	7	1	1		14095	Histone H2A type 2-A OS=Mus musculus GN=Hist2h2aa1 PE=1 SV=3
97	1828	Q64522|H2A2B_MOUSE	38.97	7	1	1		14013	Histone H2A type 2-B OS=Mus musculus GN=Hist2h2ab PE=1 SV=3
97	1823	Q64523|H2A2C_MOUSE	38.97	7	1	1		13988	Histone H2A type 2-C OS=Mus musculus GN=Hist2h2ac PE=1 SV=3
97	1830	Q8BFU2|H2A3_MOUSE	38.97	7	1	1		14121	Histone H2A type 3 OS=Mus musculus GN=Hist3h2a PE=1 SV=3
97	1824	Q8R1M2|H2AJ_MOUSE	38.97	7	1	1		14045	Histone H2A.J OS=Mus musculus GN=H2afj PE=1 SV=1
97	1821	Q3THW5|H2AV_MOUSE	38.97	7	1	1		13509	Histone H2A.V OS=Mus musculus GN=H2afv PE=1 SV=3
97	1822	P0C0S6|H2AZ_MOUSE	38.97	7	1	1		13553	Histone H2A.Z OS=Mus musculus GN=H2afz PE=1 SV=2
97	1831	P27661|H2AX_MOUSE	38.97	6	1	1		15143	Histone H2AX OS=Mus musculus GN=H2afx PE=1 SV=2
63	1799	Q64475|H2B1B_MOUSE	43.15	15	2	2		13952	Histone H2B type 1-B OS=Mus musculus GN=Hist1h2bb PE=1 SV=3
63	1792	Q6ZWY9|H2B1C_MOUSE	43.15	15	2	2		13906	Histone H2B type 1-C/E/G OS=Mus musculus GN=Hist1h2bc PE=1 SV=3
63	1797	P10853|H2B1F_MOUSE	43.15	15	2	2		13936	Histone H2B type 1-F/J/L OS=Mus musculus GN=Hist1h2bf PE=1 SV=2
63	1796	Q64478|H2B1H_MOUSE	43.15	15	2	2		13920	Histone H2B type 1-H OS=Mus musculus GN=Hist1h2bh PE=1 SV=3
63	1794	Q8CGP1|H2B1K_MOUSE	43.15	15	2	2		13920	Histone H2B type 1-K OS=Mus musculus GN=Hist1h2bk PE=1 SV=3
63	1793	P10854|H2B1M_MOUSE	43.15	15	2	2		13936	Histone H2B type 1-M OS=Mus musculus GN=Hist1h2bm PE=1 SV=2
63	1798	Q8CGP2|H2B1P_MOUSE	43.15	15	2	2		13992	Histone H2B type 1-P OS=Mus musculus GN=Hist1h2bp PE=1 SV=3
63	1795	Q64525|H2B2B_MOUSE	43.15	15	2	2		13920	Histone H2B type 2-B OS=Mus musculus GN=Hist2h2bb PE=1 SV=3
56	1791	P62806|H4_MOUSE	58.13	17	2	2		11367	Histone H4 OS=Mus musculus GN=Hist1h4a PE=1 SV=2
98	218	P01869|IGH1M_MOUSE	32.54	3	1	1		43387	Ig gamma-1 chain C region membrane-bound form OS=Mus musculus GN=Ighg1 PE=1 SV=2
98	217	P01868|IGHG1_MOUSE	32.54	4	1	1		35705	Ig gamma-1 chain C region secreted form OS=Mus musculus GN=Ighg1 PE=1 SV=1
5	569	P01837|IGKC_MOUSE	100.82	50	6	6	Carbamidomethylation; Oxidation (M); Dehydration; Mutation	11778	Ig kappa chain C region OS=Mus musculus PE=1 SV=1
31	1774	P01631|KV2A7_MOUSE	90.61	30	4	2	Hydroxylation	12273	Ig kappa chain V-II region 26-10 OS=Mus musculus PE=1 SV=1
11	1804	P01658|KV3A6_MOUSE	119.91	19	5	2	Acetylation (Protein N-term); Deamidation (NQ); Carbamidomethylation (DHKE X@N-term); Deoxy; Trifluoroleucine; 2 more	14523	Ig kappa chain V-III region MOPC 321 OS=Mus musculus PE=1 SV=1
15	1814	P01657|KV3A5_MOUSE	102.08	24	4	2	Deamidation (NQ); Methyl ester; Trifluoroleucine; Mutation	11949	Ig kappa chain V-III region PC 2413 OS=Mus musculus PE=1 SV=1
28	1770	P01646|KV5AD_MOUSE	66.35	26	6	2	Deoxy; Mutation	11989	Ig kappa chain V-V region HP 123E6 OS=Mus musculus PE=1 SV=1
28	1769	P01647|KV5AE_MOUSE	66.35	26	6	2	Deoxy; Mutation	11965	Ig kappa chain V-V region HP 124E1 OS=Mus musculus PE=1 SV=1
28	1773	P01648|KV5AF_MOUSE	66.35	26	6	2	Deoxy; Mutation	11961	Ig kappa chain V-V region HP 91A3 OS=Mus musculus PE=1 SV=1
28	1772	P01645|KV5AC_MOUSE	66.35	26	6	2	Deoxy; Mutation	11954	Ig kappa chain V-V region HP 93G7 OS=Mus musculus PE=1 SV=1
28	1771	P01644|KV5AB_MOUSE	66.35	26	6	2	Deoxy; Mutation	11910	Ig kappa chain V-V region HP R16.7 OS=Mus musculus PE=1 SV=1
47	1780	P01635|KV5A3_MOUSE	77.74	20	2	2		12581	Ig kappa chain V-V region K2 (Fragment) OS=Mus musculus PE=1 SV=1
72	1790	P01642|KV5A9_MOUSE	70.53	26	2	2		12615	Ig kappa chain V-V region L7 (Fragment) OS=Mus musculus GN=Gm10881 PE=1 SV=1
74	1803	P01636|KV5A4_MOUSE	59.99	17	2	1		12030	Ig kappa chain V-V region MOPC 149 OS=Mus musculus PE=1 SV=1
71	1775	P01639|KV5A7_MOUSE	69.64	20	3	1		14311	Ig kappa chain V-V region MOPC 41 OS=Mus musculus GN=Gm5571 PE=1 SV=1
64	1859	P20764|IGLL1_MOUSE	20.47	4	1	1		22772	Immunoglobulin lambda-like polypeptide 1 OS=Mus musculus GN=Igll1 PE=2 SV=3
6	177	P13645|K1C10_HUMAN	173.83	22	14	8	Oxidation (M)	59511	Keratin type I cytoskeletal 10 (Cytokeratin-10) (CK-10) (Keratin-10) (K10)
7	191	P35527|K1C9_HUMAN	151.89	22	10	10	Oxidation (M); Hydroxylation	62129	Keratin type I cytoskeletal 9 (Cytokeratin-9) (CK-9) (K9)
42	233	Q9Z2T6|KRT85_MOUSE	53.94	6	2	1	Deamidation (NQ)	55759	Keratin type II cuticular Hb5 OS=Mus musculus GN=Krt85 PE=1 SV=2
4	176	P04264|K2C1_HUMAN	206.43	27	18	10	Oxidation (M); Pyro-glu from Q; Replacement of proton by lithium	66018	Keratin type II cytoskeletal 1 (Cytokeratin-1) (CK-1) (Keratin-1) (K1) (67 kDa cytokeratin) (Hair
12	179	P35908|K22E_HUMAN	172.22	16	8	4		65865	Keratin type II cytoskeletal 2 epidermal (Cytokeratin-2e) (K2e) (CK 2e) (keratin-2)
40	202	Q3UV17|K2O_MOUSE	48.99	2	1	1		62845	Keratin type II cytoskeletal 2 oral OS=Mus musculus GN=Krt76 PE=1 SV=1
8	178	P02769|ALBU_BOVIN	173.25	22	13	12	Carbamidomethylation; Oxidation (M); Dehydration	69294	Serum albumin OS=Bos taurus GN=ALB PE=1 SV=4
17	2	Q80VP2|SPAT7_MOUSE	21.14	1	1	1		65655	Spermatogenesis-associated protein 7 homolog OS=Mus musculus GN=Spata7 PE=1 SV=1
87	1855	Q8R4U0|STAB2_MOUSE	22.5	0	1	1		277531	Stabilin 2 OS=Mus musculus GN=Stab2 PE=1 SV=1
1	1	P00761|TRYP_PIG	163.88	41	12	12	Carbamidomethylation; Oxidation (M); Deamidation (N); Deamidation (NQ); Dehydration; 6 more	24409	Trypsin OS=Sus scrofa PE=1 SV=1

2) GPx-1$^{-/-}$, 12mo, 27 kDa

Protein Group	Protein ID	Accession	-10lgP	Coverage (%)	#Peptides	#Unique	PTM	Avg. Mass	Description
2	1764	P00924|ENO1_YEAST	216.98	57	31	7	Oxidation (M); Deamidation (N); Deamidation (NQ); Formylation; Formylation (Protein N-term); 2 more	46802	Enolase 1 OS=Saccharomyces cerevisiae GN=ENO1 PE=1 SV=2
3	1765	P00925|ENO2_YEAST	207.17	57	31	7	Oxidation (M); Deamidation (N); Deamidation (NQ); Formylation; Formylation (Protein N-term); 2 more	46914	Enolase 2 OS=Saccharomyces cerevisiae GN=ENO2 PE=1 SV=2
1	1	P00761|TRYP_PIG	157	50	20	19	Carbamidomethylation; Oxidation (M); Deamidation (N); Dehydration; Formylation; 7 more	24409	Trypsin OS=Sus scrofa PE=1 SV=1
4	1768	P01664|KV3AC_MOUSE	142.5	46	8	3	Carbamidomethylation; Acetylation (Protein N-term); Deamidation (NQ); Dehydration; Formylation (Protein N-term); 4 more	11964	Ig kappa chain V-III region CBPC 101 OS=Mus musculus PE=1 SV=1
6	1804	P01658|KV3A6_MOUSE	108.45	15	7	3	Acetylation (Protein N-term); Deamidation (NQ); Formylation; Carbamidomethylation (DHKE X@N-term); Deoxy; 2 more	14523	Ig kappa chain V-III region MOPC 321 OS=Mus musculus PE=1 SV=1
11	1788	P01662|KV3AA_MOUSE	102.52	26	3	1	Formylation (Protein N-term); Tri nitro benzene	12041	Ig kappa chain V-III region ABPC 22/PC 9245 OS=Mus musculus PE=1 SV=1
11	1789	P01661|KV3A9_MOUSE	102.52	22	3	1	Formylation; Tri nitro benzene	14291	Ig kappa chain V-III region MOPC 63 OS=Mus musculus PE=1 SV=1
14	191	P35527|K1C9_HUMAN	97.81	11	5	5	Oxidation (M); 2 5-dimethypyrrole	62129	Keratin type I cytoskeletal 9 (Cytokeratin-9) (CK-9) (Keratin-9) (K9)
7	1814	P01657|KV3A5_MOUSE	93.99	24	5	1	Acetylation (Protein N-term); Deamidation (NQ); Dehydration; Formylation (Protein N-term); Mutation	11949	Ig kappa chain V-III region PC 2413 OS=Mus musculus PE=1 SV=1
18	178	P02769|ALBU_BOVIN	90.4	6	3	3		69294	Serum albumin OS=Bos taurus GN=ALB PE=1 SV=4
17	176	P04264|K2C1_HUMAN	81.45	9	5	5	Deamidation (NQ); Methyl ester; Phosphorylation (STY)	66018	Keratin type II cytoskeletal 1 (Cytokeratin-1) (CK-1) (Keratin-1) (K1) (67 kDa cytokeratin) (Hair alpha prot
10	1769	P01647|KV5AE_MOUSE	64.88	40	3	2	Carbamidomethylation; Oxidation (M)	11965	Ig kappa chain V-V region HP 124E1 OS=Mus musculus PE=1 SV=1
10	1772	P01645|KV5AC_MOUSE	64.88	40	3	2	Carbamidomethylation; Oxidation (M)	11954	Ig kappa chain V-V region HP 93G7 OS=Mus musculus PE=1 SV=1
10	1771	P01644|KV5AB_MOUSE	64.88	40	3	2	Carbamidomethylation; Oxidation (M)	11910	Ig kappa chain V-V region HP R16.7 OS=Mus musculus PE=1 SV=1
21	177	P13645|K1C10_HUMAN	61.41	6	2	2		59511	Keratin type I cytoskeletal 10 (Cytokeratin-10) (CK-10) (Keratin-10) (K10)
15	1775	P01639|KV5A7_MOUSE	59.81	36	3	2	Carbamidomethylation; Amidation	14311	Ig kappa chain V-V region MOPC 41 OS=Mus musculus GN=Gm5571 PE=1 SV=1
5	569	P01837|IGKC_MOUSE	48.77	14	3	3	Carbamidomethylation; Deamidation (N)	11778	Ig kappa chain C region OS=Mus musculus PE=1 SV=1
19	4849	P01592|IGJ_MOUSE	37.88	9	1	1		18014	Immunoglobulin J chain OS=Mus musculus GN=Jchain PE=1 SV=4
44	1790	P01642|KV5A9_MOUSE	37.12	16	1	1		12615	Ig kappa chain V-V region L7 (Fragment) OS=Mus musculus GN=Gm10881 PE=1 SV=1

3) GPx-1⁻ᐟ⁻, 2mo, 53 kDa

Protein Group	Protein ID	Accession	-10lgP	Coverage (%)	#Peptides	#Unique	PTM	Avg. Mass	Description
9	190	P60710|ACTB_MOUSE	215.12	58	20	13	Carbamidomethylation; Oxidation (M); Deamidation (N); Acetylation (Protein N-term); Deamidation (NQ); Dethiomethyl	41737	Actin cytoplasmic 1 OS=Mus musculus GN=Actb PE=1 SV=1
54	1840	P17182|ENOA_MOUSE	45.65	3	2	1		47141	Alpha-enolase OS=Mus musculus GN=Eno1 PE=1 SV=3
51	192	P16460|ASSY_MOUSE	134.85	18	7	7	Carbamidomethylation; Oxidation (M); Pyro-glu from Q	46585	Argininosuccinate synthase OS=Mus musculus GN=Ass1 PE=1 SV=1
23	3361	Q03265|ATPA_MOUSE	188.17	25	11	11		59753	ATP synthase subunit alpha mitochondrial OS=Mus musculus GN=Atp5a1 PE=1 SV=1
18	226	P56480|ATPB_MOUSE	171.35	22	9	9	Oxidation (M); Formylation; Methyl ester; Sulphone	56301	ATP synthase subunit beta mitochondrial OS=Mus musculus GN=Atp5b PE=1 SV=2
86	3373	Q8BIQ5|CSTF2_MOUSE	40.25	2	2	1		61341	Cleavage stimulation factor subunit 2 OS=Mus musculus GN=Cstf2 PE=1 SV=2
81	238	P10126|EF1A1_MOUSE	43.06	2	1	1		50114	Elongation factor 1-alpha 1 OS=Mus musculus GN=Eef1a1 PE=1 SV=3
81	239	P62631|EF1A2_MOUSE	43.06	2	1	1		50454	Elongation factor 1-alpha 2 OS=Mus musculus GN=Eef1a2 PE=1 SV=1
85	228	Q8BFR5|EFTU_MOUSE	67.08	6	2	2		49508	Elongation factor Tu mitochondrial OS=Mus musculus GN=Tufm PE=1 SV=1
2	1764	P00924|ENO1_YEAST	265.31	68	41	11	Oxidation (M); Deamidation (N); Deamidation (NQ); Dehydration; Formylation; 2 more	46802	Enolase 1 OS=Saccharomyces cerevisiae GN=ENO1 PE=1 SV=2
4	1765	P00925|ENO2_YEAST	253.92	60	37	7	Oxidation (M); Deamidation (N); Deamidation (NQ); Dehydration; Formylation; Ethylation	46914	Enolase 2 OS=Saccharomyces cerevisiae GN=ENO2 PE=1 SV=2
43	218	P01869|IGH1M_MOUSE	127.58	14	4	4	Oxidation (M); Deamidation (N)	43387	Ig gamma-1 chain C region membrane-bound form OS=Mus musculus GN=Ighg1 PE=1 SV=1
43	217	P01868|IGHG1_MOUSE	127.58	17	4	4	Oxidation (M); Deamidation (N)	35705	Ig gamma-1 chain C region secreted form OS=Mus musculus GN=Ighg1 PE=1 SV=1
31	235	P01863|GCAA_MOUSE	105.47	17	5	3	Carbamidomethylation; Oxidation (M); Ethylation	36389	Ig gamma-2A chain C region A allele OS=Mus musculus GN=Ighg PE=1 SV=1
31	236	P01865|GCAM_MOUSE	105.47	14	5	3	Carbamidomethylation; Oxidation (M); Ethylation	43949	Ig gamma-2A chain C region membrane-bound form OS=Mus musculus GN=Igh-1a PE=1 SV=3
121	3381	P01864|GCAB_MOUSE	46.41	5	1	1	Oxidation (M)	36596	Ig gamma-2A chain C region secreted form OS=Mus musculus PE=1 SV=1
47	237	P01867|IGG2B_MOUSE	80.7	13	5	4	Carbamidomethylation; Methyl ester; Ethylation	44259	Ig gamma-2B chain C region OS=Mus musculus GN=Igh-3 PE=1 SV=3
123	247	P03987|IGHG3_MOUSE	32.64	3	1	1	Oxidation (M)	43929	Ig gamma-3 chain C region OS=Mus musculus PE=1 SV=2
96	3374	P18527|HVM56_MOUSE	28.17	11	1	1	Oxidation (M); Deamidation (N)	10661	Ig heavy chain V region 914 OS=Mus musculus PE=1 SV=1
52	3366	P06330|HVMS1_MOUSE	100.11	36	3	1	Carbamidomethylation; Oxidation (M)	12934	Ig heavy chain V region AC38 205.12 OS=Mus musculus PE=1 SV=1
75	569	P01837|IGKC_MOUSE	46.72	22	3	3	Carbamidomethylation	11778	Ig kappa chain C region OS=Mus musculus PE=1 SV=1
5	177	P13645|K1C10_HUMAN	272.43	56	33	26	Carbamidomethylation; Oxidation (M); Deamidation (N); Pyro-glu from Q; Sulphone; 2 more	59511	Keratin type I cytoskeletal 10 (Cytokeratin-10) (CK-10) (Keratin-10) (K10)
10	188	P02533|K1C14_HUMAN	179.38	42	19	4	Carbamidomethylation; Oxidation (M); Pyro-glu from Q; Sulphone	51622	Keratin type I cytoskeletal 14 (Cytokeratin-14) (CK-14) (Keratin-14) (K14)
11	187	P08779|K1C16_HUMAN	163.41	32	16	4	Carbamidomethylation; Oxidation (M); Sulphone	51268	Keratin type I cytoskeletal 16 (Cytokeratin-16) (CK-16) (Keratin-16) (K16)
6	191	P35527|K1C9_HUMAN	251.91	49	24	23	Oxidation (M); Deamidation (N); Dehydration; Sulphone; Carbamidomethylation (DHKE X@N-term); Dihydroxy	62129	Keratin type I cytoskeletal 9 (Cytokeratin-9) (CK-9) (Keratin-9) (K9)
3	176	P04264|K2C1_HUMAN	286.72	51	44	30	Carbamidomethylation; Oxidation (M); Deamidation (N); Pyro-glu from Q; Sulphone; 4 more	66018	Keratin type II cytoskeletal 1 (Cytokeratin-1) (CK-1) (Keratin-1) (K1) (67 kDa cytokeratin) (Hair alpha protein)
13	224	P04104|K2C1_MOUSE	129.65	8	5	1		65606	Keratin type II cytoskeletal 1 OS=Mus musculus GN=Krt1 PE=1 SV=4
26	227	Q6IFZ6|K2C1B_MOUSE	115.02	8	5	1	Deamidation (N)	61359	Keratin type II cytoskeletal 1b OS=Mus musculus GN=Krt77 PE=1 SV=1
12	179	P35908|K22E_HUMAN	206.32	37	20	11	Carbamidomethylation	65865	Keratin type II cytoskeletal 2 epidermal (Cytokeratin-2e) (K2e) (CK 2e) (keratin-2)
46	202	Q3UV17|K22O_MOUSE	103.8	8	6	1	Carbamidomethylation; Deamidation (NQ); Dehydration	62845	Keratin type II cytoskeletal 2 oral OS=Mus musculus GN=Krt76 PE=1 SV=1
22	180	P13647|K2C5_HUMAN	152.48	22	15	2	Carbamidomethylation; Dehydration	62378	Keratin type II cytoskeletal 5 (Cytokeratin-5) (CK-5) (Keratin-5) (K5) (58 kDa cytokeratin)
19	184	P02538|K2C6A_HUMAN	164.19	28	17	3	Carbamidomethylation; Dehydration	60045	Keratin type II cytoskeletal 6A (Cytokeratin-6A) (CK 6A) (K6a keratin)
58	3368	P11679|K2C8_MOUSE	75.82	6	5	1		54565	Keratin type II cytoskeletal 8 OS=Mus musculus GN=Krt8 PE=1 SV=4
7	185	P53395|ODB2_MOUSE	220.82	54	29	29	Carbamidomethylation; Oxidation (M); Dethiomethyl	53247	Lipoamide acyltransferase component of branched-chain alpha-keto acid dehydrogenase complex mitochondrial OS=…
8	178	P02769|ALBU_BOVIN	223.7	32	21	20	Carbamidomethylation; Oxidation (M); Dehydration	69294	Serum albumin OS=Bos taurus GN=ALB PE=1 SV=4
65	2	Q80VP2|SPAT7_MOUSE	22.52	1	1	1		65655	Spermatogenesis-associated protein 7 homolog OS=Mus musculus GN=Spata7 PE=1 SV=1
122	3382	Q9R112|SQRD_MOUSE	47.18	2	1	1	Carbamidomethylation; Oxidation (M); Deamidation (N); Dehydration	50282	Sulfide:quinone oxidoreductase mitochondrial OS=Mus musculus GN=Sqrdl PE=1 SV=3
1	1	P00761|TRYP_PIG	183.22	50	18	18	Deamidation (NQ); Dehydration; 10 more	24409	Trypsin OS=Sus scrofa PE=1 SV=1
40	3362	P05213|TBA1B_MOUSE	128.1	20	6	2	Carbamidomethylation	50152	Tubulin alpha-1B chain OS=Mus musculus GN=Tuba1b PE=1 SV=2
61	3364	P68368|TBA4A_MOUSE	110.53	15	5	1	Carbamidomethylation	49924	Tubulin alpha-4A chain OS=Mus musculus GN=Tuba4a PE=1 SV=1
27	220	P68372|TBB4B_MOUSE	147.24	23	8	2	Oxidation (M)	49831	Tubulin beta-4B chain OS=Mus musculus GN=Tubb4b PE=1 SV=1
36	240	P99024|TBB5_MOUSE	136.75	17	6	1	Oxidation (M)	49671	Tubulin beta-5 chain OS=Mus musculus GN=Tubb5 PE=1 SV=1
44	243	Q922F4|TBB6_MOUSE	116.29	15	5	1	Oxidation (M)	50090	Tubulin beta-6 chain OS=Mus musculus GN=Tubb6 PE=1 SV=1
74	1882	P20152|VIME_MOUSE	72.04	8	3	2		53688	Vimentin OS=Mus musculus GN=Vim PE=1 SV=3

4) GPx-1⁻ᐟ⁻, 12mo, 53 kDa

Protein Group	Protein ID	Accession	-10lgP	Coverage (%)	#Peptides	#Unique	PTM	Avg. Mass	Description
8	190	P60710|ACTB_MOUSE	166.65	37	14	1	Carbamidomethylation; Oxidation (M); Acetylation (Protein N-term); Deamidation (NQ); Carbamidomethylation (DHKE X@N-term); Dethiomethyl	41737	Actin cytoplasmic 1 OS=Mus musculus GN=Actb PE=1 SV=1
10	189	P63260|ACTG_MOUSE	166.05	37	14	1	Carbamidomethylation; Oxidation (M); Acetylation (Protein N-term); Dethiomethyl	41793	Actin cytoplasmic 2 OS=Mus musculus GN=Actg1 PE=1 SV=1
81	3361	Q03265|ATPA_MOUSE	68.66	6	2	2		59753	ATP synthase subunit alpha mitochondrial OS=Mus musculus GN=Atp5a1 PE=1
26	226	P56480|ATPB_MOUSE	102.4	14	7	7	Oxidation (M); Formylation; Methyl ester; Mutation	56301	ATP synthase subunit beta mitochondrial OS=Mus musculus GN=Atp5b PE=1 SV
39	5378	Q9QWK4|CD5L_MOUSE	106.58	12	4	4	Carbamidomethylation; Oxidation (M)	38863	CD5 antigen-like OS=Mus musculus GN=Cd5l PE=1 SV=1
126	238	P10126|EF1A1_MOUSE	22.43	2	1	1		50114	Elongation factor 1-alpha 1 OS=Mus musculus GN=Eef1a1 PE=1 SV=3
2	1764	P00924|ENO1_YEAST	232.35	68	39	11	Oxidation (M); Deamidation (N); Deamidation (NQ); Formylation	46802	Enolase 1 OS=Saccharomyces cerevisiae GN=ENO1 PE=1 SV=2
3	1765	P00925|ENO2_YEAST	227.89	63	36	8	Oxidation (M); Deamidation (N); Deamidation (NQ); Formylation	46914	Enolase 2 OS=Saccharomyces cerevisiae GN=ENO2 PE=1 SV=2
14	218	P01869|IGH1M_MOUSE	123	16	6	6	Carbamidomethylation; Oxidation (M); Deamidation (N); Deamidation (NQ); Dehydration; 2 more	43387	Ig gamma-1 chain C region membrane-bound form OS=Mus musculus GN=Ighg…
14	217	P01868|IGHG1_MOUSE	123	20	6	6	Carbamidomethylation; Oxidation (M); Deamidation (N); Deamidation (NQ); Dehydration; 2 more	35705	Ig gamma-1 chain C region secreted form OS=Mus musculus GN=Ighg1 PE=1 SV
35	235	P01863|GCAA_MOUSE	68.76	10	3	2	Carbamidomethylation; Oxidation (M); Ethylation	36389	Ig gamma-2A chain C region A allele OS=Mus musculus GN=Ighg PE=1 SV=1
35	236	P01865|GCAM_MOUSE	68.76	8	3	2	Carbamidomethylation; Oxidation (M); Ethylation	43949	Ig gamma-2A chain C region membrane-bound form OS=Mus musculus GN=Igh…
20	3381	P01864|GCAB_MOUSE	94.36	17	5	3	Carbamidomethylation; Oxidation (M); Ethylation	36596	Ig gamma-2A chain C region secreted form OS=Mus musculus PE=1 SV=1
7	237	P01867|IGG2B_MOUSE	133.91	25	14	12	Carbamidomethylation; Deamidation (NQ); Dehydration; Methyl ester; Carbamidomethylation (DHKE X@N-term); 3 more	44259	Ig gamma-2B chain C region OS=Mus musculus GN=Igh-3 PE=1 SV=3
61	247	P03987|IGHG3_MOUSE	48.09	4	2	2	Oxidation (M)	43929	Ig gamma-3 chain C region OS=Mus musculus PE=1 SV=2
53	3376	P01749|HVM05_MOUSE	71.83	25	2	1	Carbamidomethylation; Mutation	13016	Ig heavy chain V region 3 OS=Mus musculus GN=Ighv1-61 PE=1 SV=1
52	5379	P01747|HVM03_MOUSE	52.96	12	1	1	Carbamidomethylation	13307	Ig heavy chain V region 36-65 OS=Mus musculus PE=1 SV=1
52	5380	P01746|HVM02_MOUSE	52.96	10	1	1	Carbamidomethylation	15514	Ig heavy chain V region 93G7 OS=Mus musculus PE=2 SV=1
19	3366	P06330|HVMS1_MOUSE	115.83	55	5	4	Carbamidomethylation; Oxidation (M); Mutation	12934	Ig heavy chain V region AC38 205.12 OS=Mus musculus PE=1 SV=1
82	569	P01837|IGKC_MOUSE	43.53	14	2	2	Carbamidomethylation	11778	Ig kappa chain C region OS=Mus musculus PE=1 SV=1
64	1785	P03977|KV3A4_MOUSE	62.58	16	1	1		12042	Ig kappa chain V-III region 50S10.1 OS=Mus musculus PE=1 SV=1
64	1782	P01656|KV3A3_MOUSE	62.58	16	1	1		11904	Ig kappa chain V-III region MOPC 70 O OS=Mus musculus PE=1 SV=1
64	1786	P01654|KV3A1_MOUSE	62.58	16	1	1		11980	Ig kappa chain V-III region PC 2880/PC 1229 OS=Mus musculus PE=1 SV=1
64	1787	P01655|KV3A2_MOUSE	62.58	16	1	1		12054	Ig kappa chain V-III region PC 7132 OS=Mus musculus PE=1 SV=1
18	727	P01872|IGHM_MOUSE	131.89	20	8	8	Carbamidomethylation	49972	Ig mu chain C region OS=Mus musculus GN=Ighm PE=1 SV=2
6	177	P13645|K1C10_HUMAN	202.63	41	22	17	Carbamidomethylation; Oxidation (M); Deamidation (N); Carbamidomethylation (DHKE X@N-term)	59511	Keratin type I cytoskeletal 10 (Cytokeratin-10) (CK-10) (Keratin-10) (K10)
17	188	P02533|K1C14_HUMAN	112.03	15	9	3	Carbamidomethylation; Oxidation (M)	51622	Keratin type I cytoskeletal 14 (Cytokeratin-14) (CK-14) (Keratin-14) (K14)
9	191	P35527|K1C9_HUMAN	180.26	32	11	11	Oxidation (M); Carbamidomethylation (DHKE X@N-term)	62129	Keratin type I cytoskeletal 9 (Cytokeratin-9) (CK-9) (Keratin-9) (K9)
84	2360	Q99M73|KRT84_MOUSE	34.73	3	2	1	Deamidation (N)	64983	Keratin type I cuticular Hb4 OS=Mus musculus GN=Krt84 PE=2 SV=2
5	176	P04264|K2C1_HUMAN	222.42	40	26	19	Carbamidomethylation; Oxidation (M); Deamidation (N); Deamidation (NQ); Dehydration; 3 more	66018	Keratin type II cytoskeletal 1 (Cytokeratin-1) (CK-1) (Keratin-1) (K1) (67 kDa cyt…
13	224	P04104|K2C1_MOUSE	117.53	7	6	1		65606	Keratin type II cytoskeletal 1 OS=Mus musculus GN=Krt1 PE=1 SV=4
34	227	Q6IFZ6|K2C1B_MOUSE	86.14	5	3	1	Deamidation (N)	61359	Keratin type II cytoskeletal 1b OS=Mus musculus GN=Krt77 PE=1 SV=1
11	179	P35908|K22E_HUMAN	157.48	24	11	7	Carbamidomethylation	65865	Keratin type II cytoskeletal 2 epidermal (Cytokeratin-2e) (K2e) (CK 2e) (kerati…
50	202	Q3UV17|K22O_MOUSE	87.92	9	5	1	Formylation	62845	Keratin type II cytoskeletal 2 oral OS=Mus musculus GN=Krt76 PE=1 SV=1
23	180	P13647|K2C5_HUMAN	101.5	11	7	1		62378	Keratin type II cytoskeletal 5 (Cytokeratin-5) (CK-5) (Keratin-5) (K5) (58 kDa cy…
15	184	P02538|K2C6A_HUMAN	113.06	13	8	1		60045	Keratin type II cytoskeletal 6A (Cytokeratin-6A) (CK 6A) (K6a keratin)
22	198	P50446|K2C6A_MOUSE	102	11	7	1	Carbamidomethylation (DHKE X@N-term); Mutation	59335	Keratin type II cytoskeletal 6A OS=Mus musculus GN=Krt6a PE=1 SV=3
49	234	Q8VED5|K2C79_MOUSE	64.92	7	4	1		57552	Keratin type II cytoskeletal 79 OS=Mus musculus GN=Krt79 PE=1 SV=2
51	232	P05787|K2C8_HUMAN	61.7	6	3	1	Dehydration; Methyl ester	53704	Keratin type II cytoskeletal 8 (Cytokeratin-8) (CK-8) (K8)
84	2261	Q9NSB2|KRT84_HUMAN	34.73	3	2	1	Deamidation (N)	64895	Keratin type II cuticular Hb4 (Type II hair keratin Hb4) (Keratin-84) (K84)
21	185	P53395|ODB2_MOUSE	114.72	16	7	7	Oxidation (M)	53247	Lipoamide acyltransferase component of branched-chain alpha-keto acid dehy…
124	5381	O08638|MYH11_MOUSE	31.18	1	1	1		227026	Myosin-11 OS=Mus musculus GN=Myh11 PE=1 SV=1
124	5382	Q6URW6|MYH14_MOUSE	31.18	1	1	1		228584	Myosin-14 OS=Mus musculus GN=Myh14 PE=1 SV=1
124	2321	Q8VDD5|MYH9_MOUSE	31.18	1	1	1		226370	Myosin-9 OS=Mus musculus GN=Myh9 PE=1 SV=4
4	178	P02769|ALBU_BOVIN	210.39	36	26	25	Carbamidomethylation; Oxidation (M); Dehydration; Sulphone; Mutation	69294	Serum albumin OS=Bos taurus GN=ALB PE=1 SV=4
12	2	Q80VP2|SPAT7_MOUSE	21.01	1	1	1		65655	Spermatogenesis-associated protein 7 homolog OS=Mus musculus GN=Spata7…
1	1	P00761|TRYP_PIG	169.16	54	20	20	Carbamidomethylation; Oxidation (M); Deamidation (N); Dehydration; Formylation; 9 more	24409	Trypsin OS=Sus scrofa PE=1 SV=1
43	3362	P05213|TBA1B_MOUSE	86.48	13	5	5	Carbamidomethylation	50152	Tubulin alpha-1B chain OS=Mus musculus GN=Tuba1b PE=1 SV=2
27	241	Q7TMM9|TBB2A_MOUSE	93.01	12	5	1	Oxidation (M); Acetylation (K); Phosphorylation (STY)	49907	Tubulin beta-2A chain OS=Mus musculus GN=Tubb2a PE=1 SV=1
27	242	Q9CWF2|TBB2B_MOUSE	93.01	12	5	1	Oxidation (M); Acetylation (K); Phosphorylation (STY)	49953	Tubulin beta-2B chain OS=Mus musculus GN=Tubb2b PE=1 SV=1
16	220	P68372|TBB4B_MOUSE	120.28	16	7	3	Oxidation (M); Acetylation (K); Phosphorylation (STY)	49831	Tubulin beta-4B chain OS=Mus musculus GN=Tubb4b PE=1 SV=1
83	1882	P20152|VIME_MOUSE	52.32	5	2	1		53688	Vimentin OS=Mus musculus GN=Vim PE=1 SV=3

Histone extracts from kidney lysates, GPx-1$^{-/-}$ young and old, 27 kDa band & 53 kDa band

*Only excerpts containing histones are shown!

1) GPx-1$^{-/-}$, 2mo, 17 kDa

Protein Group	Protein ID	Accession	-10lgP	Coverage (%)	#Peptides	#Unique	PTM	Avg. Mass	Description
73	6877	P16858|G3P_MOUSE	25.89	5	1	1	Deamidation (N)	35810	Glyceraldehyde-3-phosphate dehydrogenase OS=Mus musculus GN=Gapdh PE=1 SV=2
37	6847	Q9DCY0|KEG1_MOUSE	64.25	8	3	3	Oxidation (M)	33723	Glycine N-acyltransferase-like protein Keg1 OS=Mus musculus GN=Keg1 PE=1 SV=2
40	6839	P01942|HBA_MOUSE	73.9	25	4	4	Oxidation (M)	15085	Hemoglobin subunit alpha OS=Mus musculus GN=Hba PE=1 SV=2
53	6836	P02088|HBB1_MOUSE	86.47	25	3	1	Oxidation (M)	15840	Hemoglobin subunit beta-1 OS=Mus musculus GN=Hbb-b1 PE=1 SV=2
54	6850	P02089|HBB2_MOUSE	68.65	21	3	1	Mutation	15878	Hemoglobin subunit beta-2 OS=Mus musculus GN=Hbb-b2 PE=1 SV=2
25	6827	P15864|H12_MOUSE	130	33	8	1	Acetylation (Protein N-term)	21267	Histone H1.2 OS=Mus musculus GN=Hist1h1c PE=1 SV=2
23	6826	P43274|H14_MOUSE	134.53	36	10	3	Acetylation (Protein N-term)	21977	Histone H1.4 OS=Mus musculus GN=Hist1h1e PE=1 SV=2
32	6828	P43276|H15_MOUSE	104.66	21	6	3		22576	Histone H1.5 OS=Mus musculus GN=Hist1h1b PE=1 SV=2
22	1827	Q6GSS7|H2A2A_MOUSE	113.42	39	9	1	Deamidation (N); Deamidation (NQ); Carbamidomethylation (DHKE X@N-term)	14095	Histone H2A type 2-A OS=Mus musculus GN=Hist2h2aa1 PE=1 SV=3
22	1823	Q64523|H2A2C_MOUSE	113.42	40	9	1	Deamidation (N); Deamidation (NQ); Carbamidomethylation (DHKE X@N-term)	13988	Histone H2A type 2-C OS=Mus musculus GN=Hist2h2ac PE=1 SV=3
22	1824	Q8R1M2|H2AJ_MOUSE	113.42	40	9	1	Deamidation (N); Deamidation (NQ); Carbamidomethylation (DHKE X@N-term)	14045	Histone H2A.J OS=Mus musculus GN=H2afj PE=1 SV=1
19	1831	P27661|H2AX_MOUSE	131.4	48	12	4	Deamidation (N); Deamidation (NQ); Carbamidomethylation (DHKE X@N-term)	15143	Histone H2AX OS=Mus musculus GN=H2afx PE=1 SV=2
3	1799	Q64475|H2B1B_MOUSE	215.08	83	40	1	Oxidation (M); Deamidation (N); Carbamylation; Deamidation (NQ); Dehydration; 12 more	13952	Histone H2B type 1-B OS=Mus musculus GN=Hist1h2bb PE=1 SV=3
5	1793	P10854|H2B1M_MOUSE	213.8	83	39	1	Oxidation (M); Deamidation (N); Carbamylation; Deamidation (NQ); Dehydration; 12 more	13936	Histone H2B type 1-M OS=Mus musculus GN=Hist1h2bm PE=1 SV=2
4	1795	Q64525|H2B2B_MOUSE	213.95	83	39	1	Oxidation (M); Deamidation (N); Acetylation (Protein N-term); Carbamylation; Deamidation (NQ); 13 more	13920	Histone H2B type 2-B OS=Mus musculus GN=Hist2h2bb PE=1 SV=3
12	6818	P68433|H31_MOUSE	153.78	68	26	1	Carbamidomethylation; Oxidation (M); Acetylation (K); Acetylation (Protein N-term); Deamidation (NQ); 10 more	15404	Histone H3.1 OS=Mus musculus GN=Hist1h3a PE=1 SV=2
12	6820	P84228|H32_MOUSE	153.78	68	26	1	Carbamidomethylation; Oxidation (M); Acetylation (K); Acetylation (Protein N-term); Deamidation (NQ); 10 more	15388	Histone H3.2 OS=Mus musculus GN=Hist1h3b PE=1 SV=2
14	6821	P02301|H3C_MOUSE	148.7	68	25	1	Carbamidomethylation; Oxidation (M); Acetylation (K); Acetylation (Protein N-term); Deamidation (NQ) 9 more	15315	Histone H3.3C OS=Mus musculus GN=H3f3c PE=3 SV=3
61	177	P13645|K1C10_HUMAN	68.46	6	2	2		59511	Keratin type I cytoskeletal 10 (Cytokeratin-10) (CK-10) (Keratin-10) (K10)
94	191	P35527|K1C9_HUMAN	37.82	2	1	1		62129	Keratin type I cytoskeletal 9 (Cytokeratin-9) (CK-9) (Keratin-9) (K9)
46	176	P04264|K2C1_HUMAN	99.61	8	4	3	Deamidation (NQ); Methyl ester; Phosphorylation (STY)	66018	Keratin type II cytoskeletal 1 (Cytokeratin-1) (CK-1) (Keratin-1) (K1) (67 kDa cytokeratin) (Hair alpha protein)

2) GPx-1$^{-/-}$, 12mo, 17 kDa

Protein Group	Protein ID	Accession	-10lgP	Coverage (%)	#Peptides	#Unique	PTM	Avg. Mass	Description
22	6825	P43277|H13_MOUSE	126.86	23	6	2		22100	Histone H1.3 OS=Mus musculus GN=Hist1h1d PE=1 SV=2
24	6826	P43274|H14_MOUSE	120.73	23	6	2		21977	Histone H1.4 OS=Mus musculus GN=Hist1h1e PE=1 SV=2
16	1831	P27661|H2AX_MOUSE	132.87	42	12	12	Deamidation (N); Deamidation (NQ); Hydroxylation; Carbamidomethylation (DHKE X@N-term); Mutation	15143	Histone H2AX OS=Mus musculus GN=H2afx PE=1 SV=2
4	1799	Q64475|H2B1B_MOUSE	208.76	78	29	1	Oxidation (M); Deamidation (N); Acetylation (K); Biotinylation; Carbamylation; 14 more	13952	Histone H2B type 1-B OS=Mus musculus GN=Hist1h2bb PE=1 SV=3
2	1795	Q64525|H2B2B_MOUSE	209.56	83	30	1	Oxidation (M); Deamidation (N); Acetylation (K); Biotinylation; Carbamylation; 14 more	13920	Histone H2B type 2-B OS=Mus musculus GN=Hist2h2bb PE=1 SV=3
6	1836	Q8CGP0|H2B3B_MOUSE	183.98	71	20	1	Oxidation (M); Deamidation (N); Acetylation (K); Biotinylation; Carbamylation; 13 more	13908	Histone H2B type 3-B OS=Mus musculus GN=Hist3h2bb PE=1 SV=3
10	6818	P68433|H31_MOUSE	141.23	57	20	1	Oxidation (M); Acetylation (K); Acetylation (Protein N-term); Deamidation (NQ); Dehydration; 9 more	15404	Histone H3.1 OS=Mus musculus GN=Hist1h3a PE=1 SV=2
10	6820	P84228|H32_MOUSE	141.23	57	20	1	Oxidation (M); Acetylation (K); Acetylation (Protein N-term); Deamidation (NQ); Dehydration; 9 more	15388	Histone H3.2 OS=Mus musculus GN=Hist1h3b PE=1 SV=2
12	6821	P02301|H3C_MOUSE	134.68	57	19	1	Oxidation (M); Acetylation (K); Acetylation (Protein N-term); Deamidation (NQ); Dehydration; 6 more	15315	Histone H3.3C OS=Mus musculus GN=H3f3c PE=3 SV=3
25	177	P13645|K1C10_HUMAN	125.24	13	6	6		59511	Keratin type I cytoskeletal 10 (Cytokeratin-10) (CK-10) (Keratin-10)
69	203	Q04695|K1C17_HUMAN	41.85	2	1	1		48106	Keratin type I cytoskeletal 17 (Cytokeratin-17) (CK-17) (Keratin-17)
69	211	P19001|K1C19_MOUSE	41.85	2	1	1		44542	Keratin type I cytoskeletal 19 OS=Mus musculus GN=Krt19 PE=1 SV=1
26	191	P35527|K1C9_HUMAN	106.79	14	6	6	Oxidation (M)	62129	Keratin type I cytoskeletal 9 (Cytokeratin-9) (CK-9) (Keratin-9) (K9)
20	176	P04264|K2C1_HUMAN	148.92	14	9	8	Carbamidomethylation	66018	Keratin type II cytoskeletal 1 (Cytokeratin-1) (CK-1) (Keratin-1) (K1)
23	179	P35908|K22E_HUMAN	132.24	17	8	6	Carbamidomethylation	65865	Keratin type II cytoskeletal 2 epidermal (Cytokeratin-2e) (K2e) (CK-2e)
79	202	Q3UV17|K22O_MOUSE	35.99	2	1	1		62845	Keratin type II cytoskeletal 2 oral OS=Mus musculus GN=Krt76 PE=1 SV=1
57	180	P13647|K2C5_HUMAN	61.17	4	2	1		62378	Keratin type II cytoskeletal 5 (Cytokeratin-5) (CK-5) (Keratin-5) (K5)

3) GPx-1$^{-/-}$, 2mo, 27 kDa

Protein Group	Protein ID	Accession	-10lgP	Coverage (%)	#Peptides	#Unique	PTM	Avg. Mass	Description
245	8129	P63158|HMGB1_MOUSE	21.77	4	1	1		24894	High mobility group protein B1 OS=Mus musculus GN=Hmgb1 PE=1 SV=2
94	7965	P10922|H10_MOUSE	103.54	16	3	3	Oxidation (M)	20861	Histone H1.0 OS=Mus musculus GN=H1f0 PE=2 SV=4
15	6827	P15864|H12_MOUSE	161.93	31	13	1		21267	Histone H1.2 OS=Mus musculus GN=Hist1h1c PE=1 SV=2
13	6826	P43274|H14_MOUSE	155.75	31	14	2		21977	Histone H1.4 OS=Mus musculus GN=Hist1h1e PE=1 SV=2
33	6828	P43276|H15_MOUSE	120.85	24	10	3		22576	Histone H1.5 OS=Mus musculus GN=Hist1h1b PE=1 SV=2
63	1827	Q6GSS7|H2A2A_MOUSE	93.85	27	3	3	Deamidation (N)	14095	Histone H2A type 2-A OS=Mus musculus GN=Hist2h2aa1 PE=1 SV=3
63	1828	Q64522|H2A2B_MOUSE	93.85	27	3	3	Deamidation (N)	14013	Histone H2A type 2-B OS=Mus musculus GN=Hist2h2ab PE=1 SV=3
63	1823	Q64523|H2A2C_MOUSE	93.85	27	3	3	Deamidation (N)	13988	Histone H2A type 2-C OS=Mus musculus GN=Hist2h2ac PE=1 SV=3
63	1824	Q8R1M2|H2AJ_MOUSE	93.85	27	3	3	Deamidation (N)	14045	Histone H2A.J OS=Mus musculus GN=H2afj PE=1 SV=1
39	1799	Q64475|H2B1B_MOUSE	131.79	48	7	7	Oxidation (M)	13952	Histone H2B type 1-B OS=Mus musculus GN=Hist1h2bb PE=1 SV=3
39	1792	Q9ZWY9|H2B1C_MOUSE	131.79	48	7	7	Oxidation (M)	13906	Histone H2B type 1-C/E/G OS=Mus musculus GN=Hist1h2bc PE=1 SV=3
39	1797	P10853|H2B1F_MOUSE	131.79	48	7	7	Oxidation (M)	13936	Histone H2B type 1-F/J/L OS=Mus musculus GN=Hist1h2bf PE=1 SV=3
39	1796	Q64478|H2B1H_MOUSE	131.79	48	7	7	Oxidation (M)	13920	Histone H2B type 1-H OS=Mus musculus GN=Hist1h2bh PE=1 SV=3
39	1793	P10854|H2B1M_MOUSE	131.79	48	7	7	Oxidation (M)	13936	Histone H2B type 1-M OS=Mus musculus GN=Hist1h2bm PE=1 SV=2
39	1798	Q8CGP2|H2B1P_MOUSE	131.79	48	7	7	Oxidation (M)	13992	Histone H2B type 1-P OS=Mus musculus GN=Hist1h2bp PE=1 SV=3
39	1795	Q64525|H2B2B_MOUSE	131.79	48	7	7	Oxidation (M)	13920	Histone H2B type 2-B OS=Mus musculus GN=Hist2h2bb PE=1 SV=3
93	6818	P68433|H31_MOUSE	43.54	21	4	4	Oxidation (M)	15404	Histone H3.1 OS=Mus musculus GN=Hist1h3a PE=1 SV=2
93	6820	P84228|H32_MOUSE	43.54	21	4	4	Oxidation (M)	15388	Histone H3.2 OS=Mus musculus GN=Hist1h3b PE=1 SV=2
93	6819	P84244|H33_MOUSE	43.54	21	4	4	Oxidation (M)	15328	Histone H3.3 OS=Mus musculus GN=H3f3a PE=1 SV=2
93	6821	P02301|H3C_MOUSE	43.54	21	4	4	Oxidation (M)	15315	Histone H3.3C OS=Mus musculus GN=H3f3c PE=3 SV=3
213	1791	P62806|H4_MOUSE	36.83	10	1	1		11367	Histone H4 OS=Mus musculus GN=Hist1h4a PE=1 SV=2
88	7957	Q61425|HCDH_MOUSE	83.77	12	4	4	Carbamidomethylation	34464	Hydroxyacyl-coenzyme A dehydrogenase mitochondrial OS=Mus musculus GN=Hadh PE=1 SV=2
199	8074	Q99K88|GLO2_MOUSE	42.15	4	1	1		34084	Hydroxyacylglutathione hydrolase mitochondrial OS=Mus musculus GN=Hagh PE=1 SV=2
117	7991	P40936|INMT_MOUSE	73.98	11	3	3	Carbamidomethylation	29460	Indolethylamine N-methyltransferase OS=Mus musculus GN=Inmt PE=1 SV=1
108	7994	Q9DB29|IAH1_MOUSE	81.99	10	3	3	Carbamidomethylation	27974	Isoamyl acetate-hydrolyzing esterase 1 homolog OS=Mus musculus GN=Iah1 PE=1 SV=1

4) GPx-1⁻ᐟ⁻, 12mo, 27 kDa

Protein Group	Protein ID	Accession	-10lgP	Coverage (%)	#Peptides	#Unique	PTM	Avg. Mass	Description
	29	7923 Q8BH95|ECHM_MOUSE	31.44	4		1	1		31474 Enoyl-CoA hydratase mitochondrial OS=Mus musculus GN=Echs1 PE=1 SV=1
	32	7927 P10649|GSTM1_MOUSE	31.43	4		1	1		25970 Glutathione S-transferase Mu 1 OS=Mus musculus GN=Gstm1 PE=1 SV=2
	31	6839 P01942|HBA_MOUSE	31.7	6		1	1	Oxidation (M)	15085 Hemoglobin subunit alpha OS=Mus musculus GN=Hba PE=1 SV=2
	28	6827 P15864|H12_MOUSE	31.95	6	1	1		21267 Histone H1.2 OS=Mus musculus GN=Hist1h1c PE=1 SV=2
	28	6825 P43277|H13_MOUSE	31.95	5	1	1		22100 Histone H1.3 OS=Mus musculus GN=Hist1h1d PE=1 SV=2
	38	6826 P43274|H14_MOUSE	24.98	5	1	1		21977 Histone H1.4 OS=Mus musculus GN=Hist1h1e PE=1 SV=2
	27	1825 P22752|H2A1_MOUSE	34.56	7	1	1		14135 Histone H2A type 1 OS=Mus musculus GN=Hist1h2ab PE=1 SV=3
	27	1829 Q8CGP5|H2A1F_MOUSE	34.56	7	1	1		14162 Histone H2A type 1-F OS=Mus musculus GN=Hist1h2af PE=1 SV=3
	27	1820 Q8CGP6|H2A1H_MOUSE	34.56	7	1	1		13950 Histone H2A type 1-H OS=Mus musculus GN=Hist1h2ah PE=1 SV=3
	27	1826 Q8CGP7|H2A1K_MOUSE	34.56	7	1	1		14150 Histone H2A type 1-K OS=Mus musculus GN=Hist1h2ak PE=1 SV=3
	27	1827 Q6GSS7|H2A2A_MOUSE	34.56	7	1	1		14095 Histone H2A type 2-A OS=Mus musculus GN=Hist2h2aa1 PE=1 SV=3
	27	1828 Q64522|H2A2B_MOUSE	34.56	7	1	1		14013 Histone H2A type 2-B OS=Mus musculus GN=Hist2h2ab PE=1 SV=3
	27	1823 Q64523|H2A2C_MOUSE	34.56	7	1	1		13988 Histone H2A type 2-C OS=Mus musculus GN=Hist2h2ac PE=1 SV=1
	27	1830 Q8BFU2|H2A3_MOUSE	34.56	7	1	1		14121 Histone H2A type 3 OS=Mus musculus GN=Hist3h2a PE=1 SV=3
	27	1824 Q8R1M2|H2AJ_MOUSE	34.56	7	1	1		14045 Histone H2A.J OS=Mus musculus GN=H2afj PE=1 SV=1
	27	1821 Q3THW5|H2AV_MOUSE	34.56	7	1	1		13509 Histone H2A.V OS=Mus musculus GN=H2afv PE=1 SV=3
	27	1822 P0C0S6|H2AZ_MOUSE	34.56	7	1	1		13553 Histone H2A.Z OS=Mus musculus GN=H2afz PE=1 SV=2
	27	1831 P27661|H2AX_MOUSE	34.56	6	1	1		15143 Histone H2AX OS=Mus musculus GN=H2afx PE=1 SV=2
	15	1839 P70696|H2B1A_MOUSE	42.1	14	2	2		14237 Histone H2B type 1-A OS=Mus musculus GN=Hist1h2ba PE=1 SV=3
	15	1799 Q64475|H2B1B_MOUSE	42.1	14	2	2		13952 Histone H2B type 1-B OS=Mus musculus GN=Hist1h2bb PE=1 SV=3
	15	1792 Q6ZWY9|H2B1C_MOUSE	42.1	14	2	2		13906 Histone H2B type 1-C/E/G OS=Mus musculus GN=Hist1h2bc PE=1 SV=3
	15	1797 P10853|H2B1F_MOUSE	42.1	14	2	2		13936 Histone H2B type 1-F/J/L OS=Mus musculus GN=Hist1h2bf PE=1 SV=2
	15	1796 Q64478|H2B1H_MOUSE	42.1	14	2	2		13920 Histone H2B type 1-H OS=Mus musculus GN=Hist1h2bh PE=1 SV=3
	15	1793 P10854|H2B1M_MOUSE	42.1	14	2	2		13936 Histone H2B type 1-M OS=Mus musculus GN=Hist1h2bm PE=1 SV=2
	15	1798 Q8CGP2|H2B1P_MOUSE	42.1	14	2	2		13992 Histone H2B type 1-P OS=Mus musculus GN=Hist1h2bp PE=1 SV=3
	15	1795 Q64525|H2B2B_MOUSE	42.1	14	2	2		13920 Histone H2B type 2-B OS=Mus musculus GN=Hist2h2bb PE=1 SV=3
	15	1835 Q9D2U9|H2B3A_MOUSE	42.1	14	2	2		13994 Histone H2B type 3-A OS=Mus musculus GN=Hist3h2ba PE=1 SV=3
	15	1836 Q8CGP0|H2B3B_MOUSE	42.1	14	2	2		13908 Histone H2B type 3-B OS=Mus musculus GN=Hist3h2bb PE=1 SV=3
	13	569 P01837|IGKC_MOUSE	42.35	14	2	2	Carbamidomethylation	11778 Ig kappa chain C region OS=Mus musculus PE=1 SV=1

5) GPx-1⁻ᐟ⁻, 2mo, 53 kDa

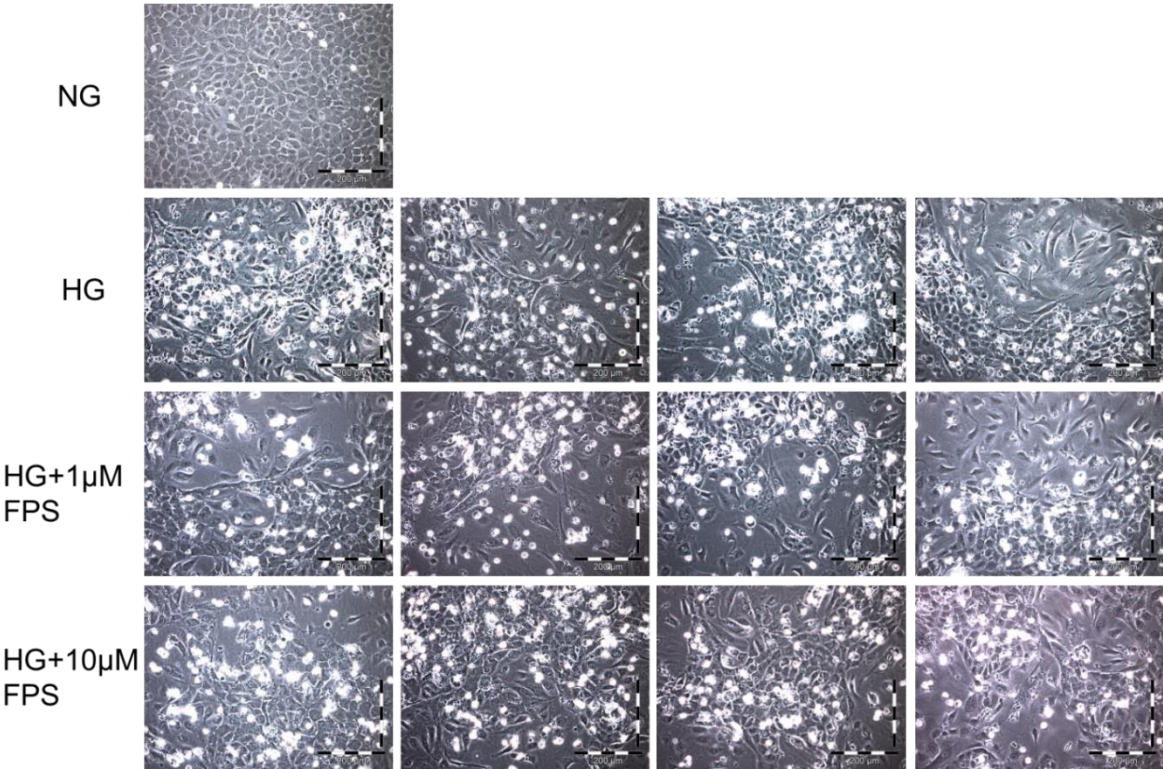| Protein Group	Protein ID	Accession	-10lgP	Coverage (%)	#Peptides	#Unique	PTM	Avg. Mass	Description
	81	8023 P61979|HNRPK_MOUSE	171.84	36	15	15	Carbamidomethylation; Dethiomethyl	50976 Heterogeneous nuclear ribonucleoprotein K OS=Mus musculus GN=Hnrnpk PE=1 SV=1
	243	8928 Q8R081|HNRPL_MOUSE	95.82	10	5	5	Carbamidomethylation; Deamidation (N)	63964 Heterogeneous nuclear ribonucleoprotein L OS=Mus musculus GN=Hnrnpl PE=1 SV=2
	322	8963 Q8VEK3|HNRPU_MOUSE	79.95	5	3	3		87918 Heterogeneous nuclear ribonucleoprotein U OS=Mus musculus GN=Hnrnpu PE=1 SV=1
	175	6827 P15864|H12_MOUSE	109.08	20	5	2		21267 Histone H1.2 OS=Mus musculus GN=Hist1h1c PE=1 SV=2
	175	6825 P43277|H13_MOUSE	109.08	19	5	2		22100 Histone H1.3 OS=Mus musculus GN=Hist1h1d PE=1 SV=2
	166	6826 P43274|H14_MOUSE	123.74	27	6	3	Acetylation (Protein N-term)	21977 Histone H1.4 OS=Mus musculus GN=Hist1h1e PE=1 SV=2
	340	6828 P43276|H15_MOUSE	65.59	9	2	1		22576 Histone H1.5 OS=Mus musculus GN=Hist1h1b PE=1 SV=2
	251	1825 P22752|H2A1_MOUSE	85.59	27	3	3		14135 Histone H2A type 1 OS=Mus musculus GN=Hist1h2ab PE=1 SV=3
	251	1829 Q8CGP5|H2A1F_MOUSE	85.59	27	3	3		14162 Histone H2A type 1-F OS=Mus musculus GN=Hist1h2af PE=1 SV=3
	251	1820 Q8CGP6|H2A1H_MOUSE	85.59	27	3	3		13950 Histone H2A type 1-H OS=Mus musculus GN=Hist1h2ah PE=1 SV=3
	251	1826 Q8CGP7|H2A1K_MOUSE	85.59	27	3	3		14150 Histone H2A type 1-K OS=Mus musculus GN=Hist1h2ak PE=1 SV=3
	251	1827 Q6GSS7|H2A2A_MOUSE	85.59	27	3	3		14095 Histone H2A type 2-A OS=Mus musculus GN=Hist2h2aa1 PE=1 SV=3
	251	1823 Q64523|H2A2C_MOUSE	85.59	27	3	3		13988 Histone H2A type 2-C OS=Mus musculus GN=Hist2h2ac PE=1 SV=1
	251	1830 Q8BFU2|H2A3_MOUSE	85.59	27	3	3		14121 Histone H2A type 3 OS=Mus musculus GN=Hist3h2a PE=1 SV=3
	251	1824 Q8R1M2|H2AJ_MOUSE	85.59	27	3	3		14045 Histone H2A.J OS=Mus musculus GN=H2afj PE=1 SV=1
	251	1831 P27661|H2AX_MOUSE	85.59	24	3	3		15143 Histone H2AX OS=Mus musculus GN=H2afx PE=1 SV=2
	233	1799 Q64475|H2B1B_MOUSE	112.1	36	5	5	Oxidation (M)	13952 Histone H2B type 1-B OS=Mus musculus GN=Hist1h2bb PE=1 SV=3
	167	6818 P68433|H31_MOUSE	61.95	20	3	3	Pyro-glu from E	15404 Histone H3.1 OS=Mus musculus GN=Hist1h3a PE=1 SV=2
	167	6820 P84228|H32_MOUSE	61.95	20	3	3	Pyro-glu from E	15388 Histone H3.2 OS=Mus musculus GN=Hist1h3b PE=1 SV=2
	167	6819 P84244|H33_MOUSE	61.95	20	3	3	Pyro-glu from E	15328 Histone H3.3 OS=Mus musculus GN=H3f3a PE=1 SV=2
	167	6821 P02301|H3C_MOUSE	61.95	20	3	3	Pyro-glu from E	15315 Histone H3.3C OS=Mus musculus GN=H3f3c PE=3 SV=3
	246	1791 P62806|H4_MOUSE	86.52	39	4	4		11367 Histone H4 OS=Mus musculus GN=Hist1h4a PE=1 SV=2
	339	7957 Q61425|HCDH_MOUSE	52.99	9	3	3	Carbamidomethylation	34464 Hydroxyacyl-coenzyme A dehydrogenase mitochondrial OS=Mus musculus GN=Hadh PE=1 SV=2

6) GPx-1⁻ᐟ⁻, 12mo, 53 kDa

| Protein Group	Protein ID	Accession	-10lgP	Coverage (%)	#Peptides	#Unique	PTM	Avg. Mass	Description
	384	15046 Q7TMK9|HNRPQ_MOUSE	83.2	6	3	3		69633 Heterogeneous nuclear ribonucleoprotein Q OS=Mus musculus GN=Syncrip P
	284	8963 Q8VEK3|HNRPU_MOUSE	104.33	9	6	6	Carbamidomethylation	87918 Heterogeneous nuclear ribonucleoprotein U OS=Mus musculus GN=Hnrnpu P
	286	15032 P17710|HXK1_MOUSE	100.23	7	6	6	Carbamidomethylation; Pyro-glu from Q	108303 Hexokinase-1 OS=Mus musculus GN=Hk1 PE=1 SV=3
	220	7965 P10922|H10_MOUSE	119.81	31	7	6	Oxidation (M); Deamidation (N); Acetylation (Protein N-term); Deamidation (NQ)	20861 Histone H1.0 OS=Mus musculus GN=H1f0 PE=2 SV=4
	61	6827 P15864|H12_MOUSE	159.14	38	12	2	Deamidation (N); Acetylation (Protein N-term); Methyl ester; Carbamidomethylation (DHKE X@N-2 term)	21267 Histone H1.2 OS=Mus musculus GN=Hist1h1c PE=1 SV=2
	65	6825 P43277|H13_MOUSE	157.53	38	13	1	Deamidation (N); Acetylation (Protein N-term); Methyl ester; Carbamidomethylation (DHKE X@N-1 term)	22100 Histone H1.3 OS=Mus musculus GN=Hist1h1d PE=1 SV=2
	50	6826 P43274|H14_MOUSE	169.26	42	15	3	Deamidation (N); Acetylation (Protein N-term); Methyl ester; Carbamidomethylation (DHKE X@N-3 term)	21977 Histone H1.4 OS=Mus musculus GN=Hist1h1e PE=1 SV=2
	394	1825 P22752|H2A1_MOUSE	78.22	27	3	3		14135 Histone H2A type 1 OS=Mus musculus GN=Hist1h2ab PE=1 SV=3
	394	1829 Q8CGP5|H2A1F_MOUSE	78.22	27	3	3		14162 Histone H2A type 1-F OS=Mus musculus GN=Hist1h2af PE=1 SV=3
	394	1820 Q8CGP6|H2A1H_MOUSE	78.22	27	3	3		13950 Histone H2A type 1-H OS=Mus musculus GN=Hist1h2ah PE=1 SV=3
	394	1826 Q8CGP7|H2A1K_MOUSE	78.22	27	3	3		14150 Histone H2A type 1-K OS=Mus musculus GN=Hist1h2ak PE=1 SV=3
	394	1827 Q6GSS7|H2A2A_MOUSE	78.22	27	3	3		14095 Histone H2A type 2-A OS=Mus musculus GN=Hist2h2aa1 PE=1 SV=3
	394	1823 Q64523|H2A2C_MOUSE	78.22	27	3	3		13988 Histone H2A type 2-C OS=Mus musculus GN=Hist2h2ac PE=1 SV=1
	394	1830 Q8BFU2|H2A3_MOUSE	78.22	27	3	3		14121 Histone H2A type 3 OS=Mus musculus GN=Hist3h2a PE=1 SV=3
	394	1824 Q8R1M2|H2AJ_MOUSE	78.22	27	3	3		14045 Histone H2A.J OS=Mus musculus GN=H2afj PE=1 SV=1
	394	1831 P27661|H2AX_MOUSE	78.22	24	3	3		15143 Histone H2AX OS=Mus musculus GN=H2afx PE=1 SV=2
	298	1799 Q64475|H2B1B_MOUSE	126.04	33	5	5	Oxidation (M)	13952 Histone H2B type 1-B OS=Mus musculus GN=Hist1h2bb PE=1 SV=3
	298	1792 Q6ZWY9|H2B1C_MOUSE	126.04	33	5	5	Oxidation (M)	13906 Histone H2B type 1-C/E/G OS=Mus musculus GN=Hist1h2bc PE=1 SV=3
	298	1797 P10853|H2B1F_MOUSE	126.04	33	5	5	Oxidation (M)	13936 Histone H2B type 1-F/J/L OS=Mus musculus GN=Hist1h2bf PE=1 SV=2
	298	1796 Q64478|H2B1H_MOUSE	126.04	33	5	5	Oxidation (M)	13920 Histone H2B type 1-H OS=Mus musculus GN=Hist1h2bh PE=1 SV=3
	298	1794 Q8CGP1|H2B1K_MOUSE	126.04	33	5	5	Oxidation (M)	13920 Histone H2B type 1-K OS=Mus musculus GN=Hist1h2bk PE=1 SV=3
	298	1793 P10854|H2B1M_MOUSE	126.04	33	5	5	Oxidation (M)	13936 Histone H2B type 1-M OS=Mus musculus GN=Hist1h2bm PE=1 SV=2
	298	1798 Q8CGP2|H2B1P_MOUSE	126.04	33	5	5	Oxidation (M)	13992 Histone H2B type 1-P OS=Mus musculus GN=Hist1h2bp PE=1 SV=3
	298	1795 Q64525|H2B2B_MOUSE	126.04	33	5	5	Oxidation (M)	13920 Histone H2B type 2-B OS=Mus musculus GN=Hist2h2bb PE=1 SV=3
	190	6818 P68433|H31_MOUSE	74.98	29	6	6	Oxidation (M); Pyro-glu from E	15404 Histone H3.1 OS=Mus musculus GN=Hist1h3a PE=1 SV=2
	190	6820 P84228|H32_MOUSE	74.98	29	6	6	Oxidation (M); Pyro-glu from E	15388 Histone H3.2 OS=Mus musculus GN=Hist1h3b PE=1 SV=2
	190	6819 P84244|H33_MOUSE	74.98	29	6	6	Oxidation (M); Pyro-glu from E	15328 Histone H3.3 OS=Mus musculus GN=H3f3a PE=1 SV=2
	190	6821 P02301|H3C_MOUSE	74.98	29	6	6	Oxidation (M); Pyro-glu from E	15315 Histone H3.3C OS=Mus musculus GN=H3f3c PE=3 SV=3
	237	1791 P62806|H4_MOUSE	108.38	55	6	6	Oxidation (M)	11367 Histone H4 OS=Mus musculus GN=Hist1h4a PE=1 SV=2
	566	15084 Q9NYQ2|HAOX2_MOUSE	33.9	4	1	1		38700 Hydroxyacid oxidase 2 OS=Mus musculus GN=Hao2 PE=1 SV=1
	283	7957 Q61425|HCDH_MOUSE	85.11	12	4	4	Carbamidomethylation	34464 Hydroxyacyl-coenzyme A dehydrogenase mitochondrial OS=Mus musculus G
	562	15078 P01878|IGHA_MOUSE	34.73	8	2	2		36876 Ig alpha chain C region OS=Mus musculus PE=1 SV=1

Protective effects of empagliflozin (EMPA), the DPP-4 inhibitor sitagliptin (SITA) and the RAGE inhibitor FPS-ZM1 on cultured hyperglycemic human umbilical vein endothelial cells (HUVECs)
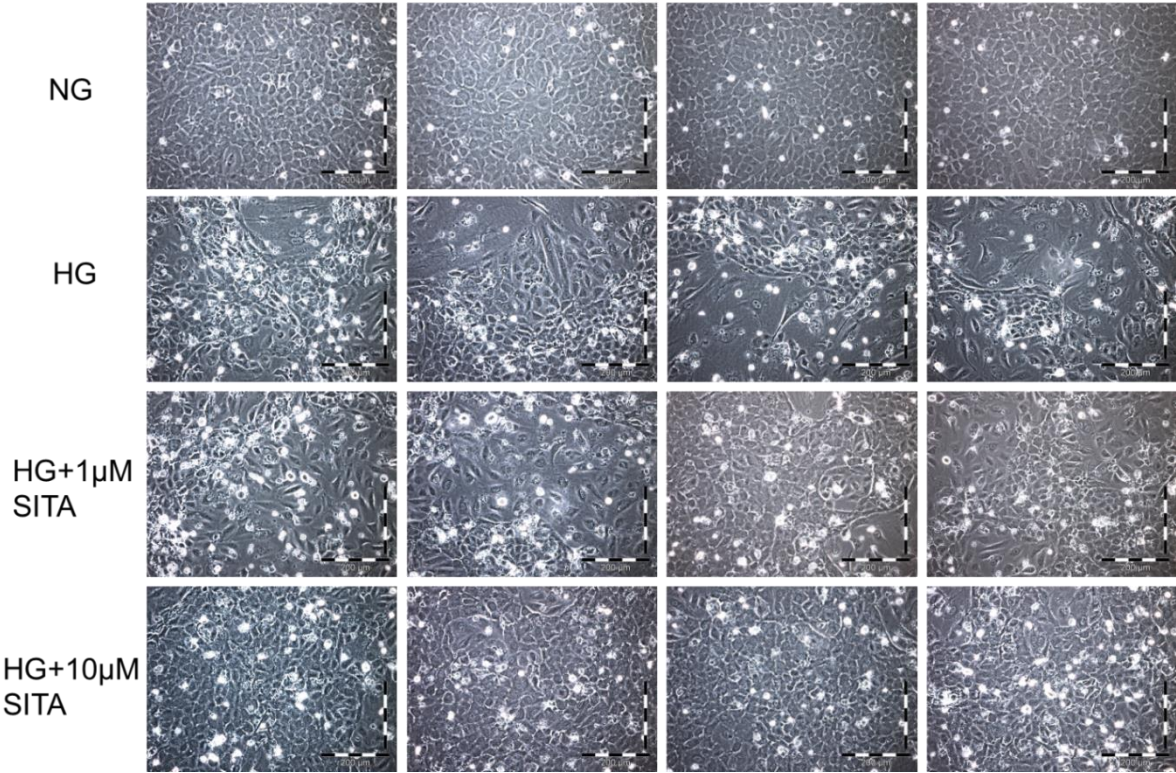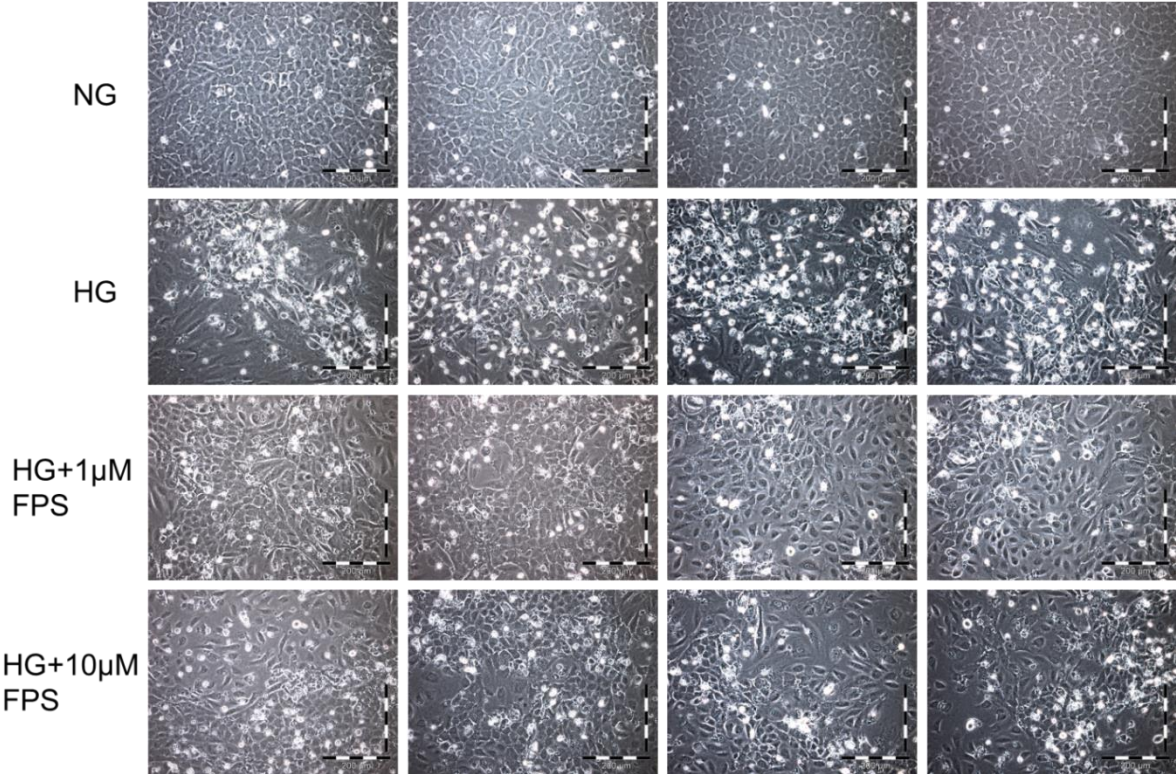
Day 5 = 2 days FPS-ZM1 treatment

NG

HG

HG+1µM
FPS

HG+10µM
FPS
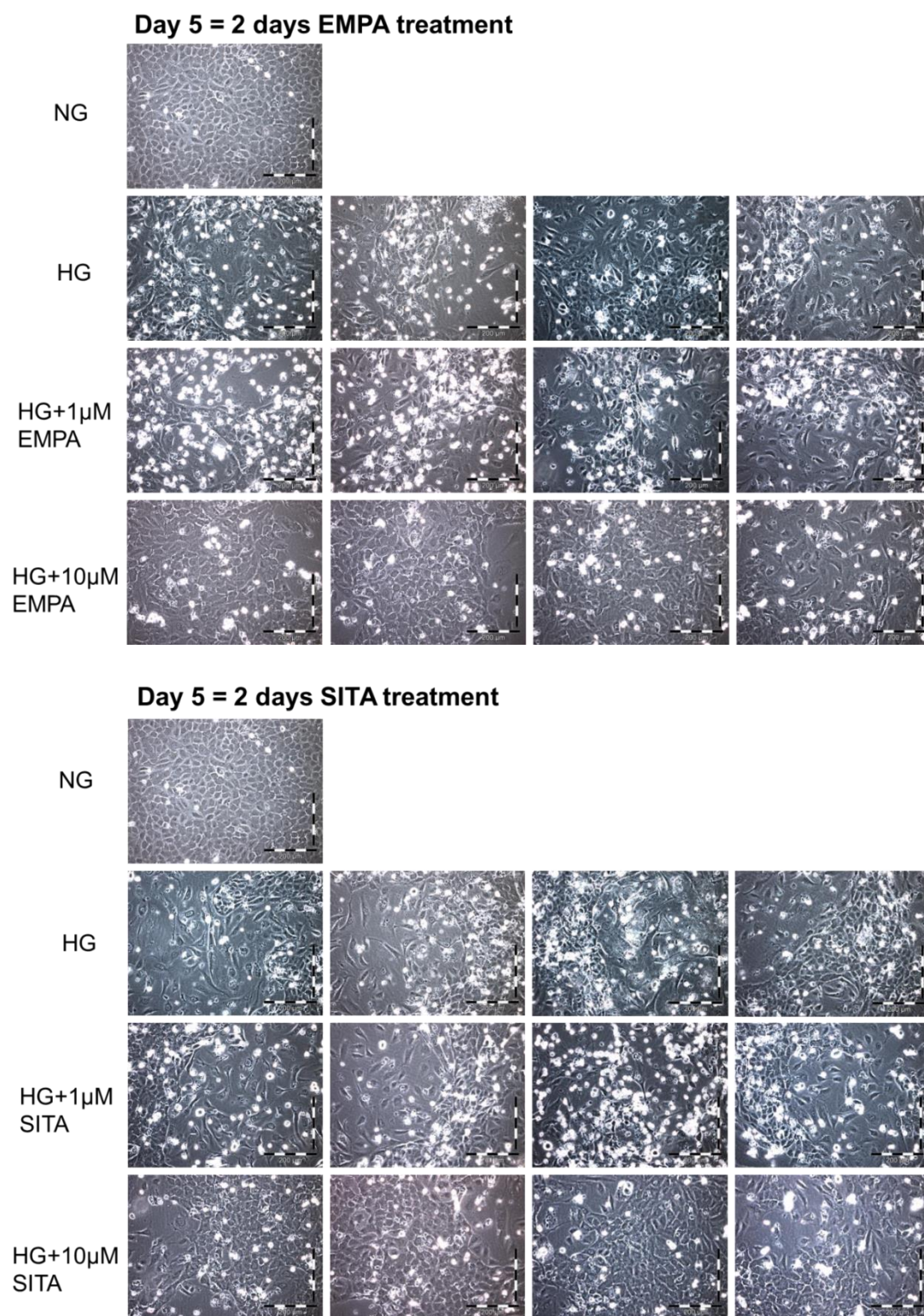
Day 6 = 3 days EMPA treatment

NG

HG

HG+1µM
EMPA

HG+10µM
EMPA
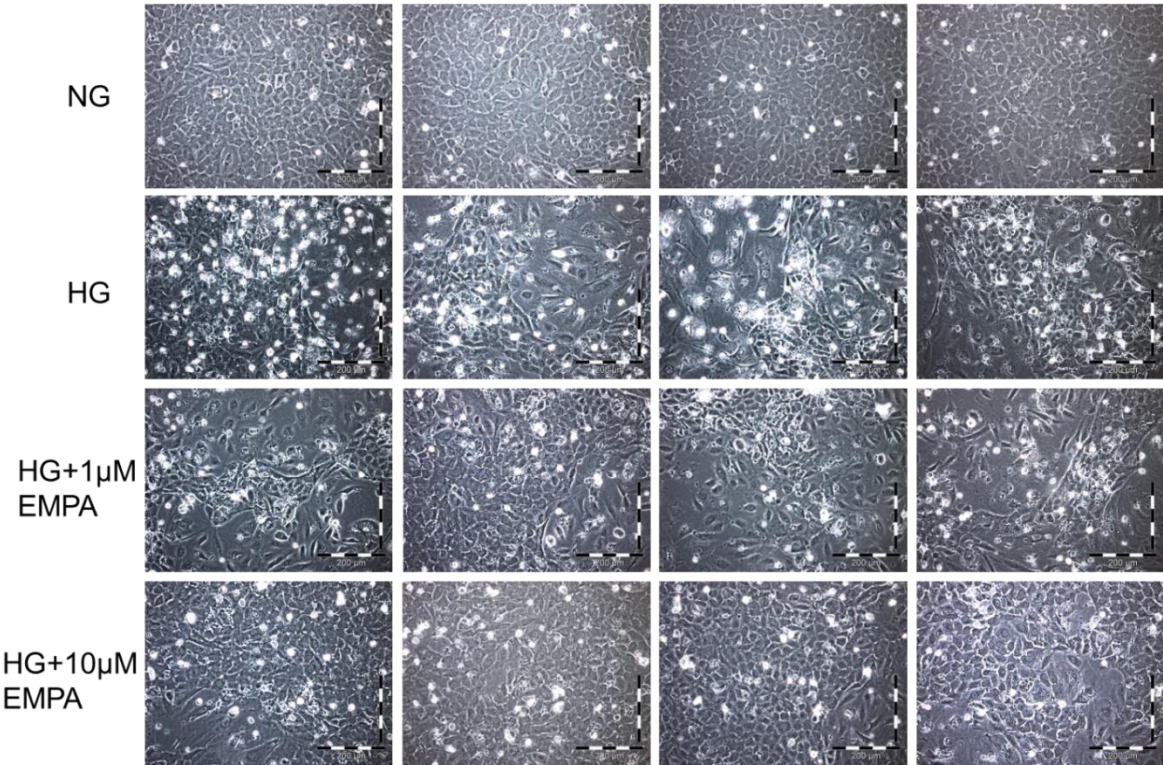
Day 6 = 3 days SITA treatment

NG	
HG	
HG+1μM SITA	
HG+10μM SITA	

Day 6 = 3 days FPS-ZM1 treatment

NG	
HG	
HG+1μM FPS	
HG+10μM FPS	

Curriculum Vitae

- Aus Datenschutzgründen entfernt

Danksagung

- Aus Datenschutzgründen entfernt